Antonella Lupica

Mathematical modeling, analysis and control of some infectious diseases

Dottorato in Matematica ed Informatica, Catania (2020).

<http://www.bdim.eu/item?id=tesi_2020_LupicaAntonella_1>

UNIVERSITY OF CATANIA

DEPARTMENT OF MATHEMATICS AND COMPUTER SCIENCE

DOCTORAL THESIS
SSD:MAT/07

MATHEMATICAL MODELING, ANALYSIS AND CONTROL OF SOME INFECTIOUS DISEASES

AUTHOR:
ANTONELLA LUPICA

SUPERVISOR:
PROF. ANNUNZIATA PALUMBO

HEAD OF PH.D. SCHOOL:
PROF. GIOVANNI RUSSO

A THESIS SUBMITTED IN FULFILLMENT OF THE REQUIREMENTS
FOR THE DEGREE OF DOCTOR OF PHILOSOPHY

IN THE PARTNER INSTITUTION

UNIVERSITY OF MESSINA

DEPARTMENT OF MATHEMATICAL AND COMPUTER SCIENCE, PHYSICAL SCIENCE AND EARTH SCIENCE

The first time I solved a real problem was a moment that I will remember and I will cherish forever. It was an incredible feeling of inebriation: for the first time I had something that no one else in the world had. I could say something new about the Universe. It is true: it was not a new cure for cancer, but it still had value, and no one could ever take it away from me. It was the first time that happened to me, and as with the first kiss, it was a very special thing. Since then, I have been unable to stop.

(Edward Frenkel)

Cominciate col fare ciò che è necessario, poi ciò che è possibile. E all'improvviso vi sorprenderete a fare l'impossibile.

(San Francesco d'Assisi)

DECLARATION OF AUTHORSHIP

I, ANTONELLA LUPICA, declare that this thesis entitled "Mathematical Modeling, Analysis and Control of Some Infectious Diseases" and the work presented in it are my own. This work was carried out entirely during the candidature for a research degree at this University and where I consulted the published work of others, this is always clearly attributed.

Messina, November 2019

ACKNOWLEDGEMENT

I would like to thank all the people who, for various reasons, have accompanied me in this journey.
First of all, special mention goes to my supervisor, Prof. Annunziata Palumbo, who has followed me with great dedication during these years. She introduced me to the study of Mathematical Physics and during her first lesson, I realized that this could have been my way. Much of what I know, is thanks to her. Being my advisor during the degree course in Mathematics, she accompanied me from the early years of University until this important goal was achieved.
I would like to acknowledge two co-authors, who supported me during my research visit in Lyon, Prof. Alberto d'Onofrio and Prof. Vitaly Volpert. Prof. Alberto d'Onofrio, being my advisor during the first two months in Lyon at *International Prevention Research Institut*, gave me scientific confidence and taught me a lot. He was always very helpful with me and treated me like a scientific peer. He is very friendly and a big personality. Prof. Vitaly Volpert, my advisor for 4 months in Lyon at the *Université Claude Bernard Lyon 1*, has discussed with me about science many times, he is very patient, a great guide and for me it was a joy to know and learn by one of the greatest Traveling Waves experts. He gave me the freedom I needed to move on and to grow as a young research scientist.
I want to say thanks to another co-author, Prof. Abba B. Gumel, whom I met for the first time at a conference in Erice. There, an important scientific collaboration was born, from which I learned many lessons. He taught me to look at math as an art. It was a joy to work and learn from him. The enthusiasm he has for the research was contagious and motivational for me.
Thanks also to Prof. Rosanna Utano, who has always involved me in various educational experiences and for having always a kind word towards me.
A special thanks goes to all my family, especially my parents, Luigi and Maria Benuccia, who have supported me morally and materially, always providing good advice. They have been a source of energy and encouragement especially during the period in Lyon. They have been beside me both in good and in bad times. Many thanks also to my brother Paolo.
Many thanks also to my friends Mariagrazia and Rosalia, for always supporting me in every possible situation. They have always been there for me.
I would like to thank my colleague and friend Carmelo, with whom I share the office, for the many moments we spent together during the years of University and during the Ph.D. course. Thanks for the good advice he always gave me: our scientific discussions have always been helpful. I am very happy that our friendship

was born from the first year of University and to reach this result together with him.

DEDICATION

To my father, Luigi, and to my mother, Maria Benuccia,
without whom this dissertation would not exist.

ABSTRACT

Mathematical models are useful in epidemiological research to describe, explain or predict the development and spread of infectious diseases. In addition they play a critical role in disease control, indicating intervention strategies concerning public health such as vaccinations, isolation, treatments and so on.
The underlying theme of this Ph.D. thesis is the mathematical modeling and analysis of some aspects concerning infectious diseases, in the absence and presence of infection. In fact, the control of a possible epidemic can be carried out both by investigating aspects external to the infection, such as vaccination (as was done in chapter 1) or alternative prevention methods, such as controlling the life cycle of carriers of the virus (as presented in chapter 4) and by analyzing and studying models that describe the dynamics of the infection itself (as we will see in chapters 2 and 3). Chapter 1 models epidemiological aspects when the disease is not present in the population. Indeed it focuses mainly on the decision of individuals to be vaccinated or not, in the absence of infection and based on information they receive from the outside on the state of the disease and the side effects of the vaccine. This information is modeled through the introduction of a spatial kernel that weighs the distance from which the information comes. The proposed new model is based on the theory of the *Imitation Game*, in which the exchanges of opinions and contacts between individuals are taken into consideration. The model is parabolic, since the Fickian diffusion is assumed to be valid. In chapters 2 and 3 we investigate on the spread of two infectious diseases, which differ from each other via different transmission vehicles of the virus. In particular, chapter 2 deals with a new model for the transmission of cholera, a water-borne disease that involves host-environment interaction. The model extends works featured in the published literature on the subject, including the possibility of water exchange between two different aquatic environments, then the cohabitation of two populations of bacteria, different from each other due to the position occupied within the aquatic system, is incorporated in the model. Instead, chapter 3 is concerned with proposing a new model for host-vector diseases. The modeling carried out takes into account the possible vertical transmission in the vector population, in addition to the presence of two different types of host population. Furthermore, a maximum capacity is placed on the growth of the vector population. In order to investigate the spatial dynamics of disease, both models presented in chapters 2 and 3 are extended to a PDE systems, considering the diffusion of the populations described by Fick's law. For both models an estimate of the Basic Reproductive Number $\mathcal{R}_0^{PDE}$ related to the spatial case is provided, comparing it later with the one corresponding to the non-spatial model. The conditions are given for which $\mathcal{R}_0^{PDE}$ constitutes a threshold value for the eradication of the infection also in the spatial case. Furthermore,

for the PDE model presented in the chapter 2, traveling waves are studied. Finally, chapter 4, in order to provide a possible prevention method against host-vector type diseases, proposes a new model for vector population dynamics, in which slow and fast diffusion processes coexist, assuming that the diffusion flux is consisting of a Fickian type part and a satisfactory part of an evolution equation of Maxwell-Cattaneo-Vernotte type. The analysis of the corresponding ODE model is carried out, and traveling Wave solutions are investigated. A section of the chapter is devoted to the limit case analysis of the presented model, in which the Fickian diffusion is neglected, thus obtaining a strictly hyperbolic system. Numerical simulations compare the model characterized by the coexistence of both diffusion processes (slow and fast), the hyperbolic model characterized by slow diffusion only and the parabolic model, present in literature [151], characterized by fast diffusion only.

CONTENTS

INTRODUCTION

This Ph.D. thesis deals with the modeling and mathematical analysis of some ODEs and PDEs systems, deduced in the context of controlling the spread of some infectious diseases in humans. Mathematical epidemiology is an important tool, through which one can predict the evolution of a system in situations that cannot be experimentally verified. It is also possible to reconstruct real situations starting from experimental data: think for example of the reconstruction of three-dimensional objects starting from cross-sections (CT scan). Mathematical approaches can provide good knowledge of the biological or medical problem, since they are simplified descriptions of reality and, if reasonably faithful, they have yielded the desired control parameters. Mathematical modeling is today the basis of public health decisions regarding the control of traditional and endemic diseases, emerging and re-emerging infections as well as the basis of the preventive evaluation of the impact of diseases completely new. The mathematical models that describe the dynamics of transmissible and epidemiological diseases certainly have a direct relationship with the choice of an immunization program, the optimal allocation of scarce resources or the best combination of control or eradication techniques, such as points out Bailey in the second edition of his book [11].

The first to use a mathematical model in the medical field was Daniel Bernoulli in 1760. He used it to evaluate the effects of inoculation against smallpox. This episode can be considered the beginning of the "Mathematics of epidemics". In fact, the decisive step is accomplished around 1920, with the modeling of malaria by Ronald Ross (Nobel Prize for Medicine) and with the model of Kermack and McKendrick, which is at the base of all the subsequent development of the theory.

This Ph.D. thesis presents several mathematical models, in order to control possible outbreak of infectious epidemics. It is divided into 4 main chapters.

Chapter 1 investigates the problem of interplay between vaccination dynamics, spatial mobility and information, when the disease is not present in the population. Under voluntary vaccination, a critical role in shaping the level and trends of vaccine uptake is played by the type and structure of information that is received and used by parents of children eligible for vaccination. The chapter deals with the feedbacks of spatial mobility and the spatial structure of information on vaccination dynamics, by extending to a continuous spatially structured setting existing behavioral epidemiology models for the impact of vaccine adverse events (VAEs) on vaccination choices. The simplest spatial setting is considered, namely the classical "Fickian" diffusion, and focused on the noteworthy case where the infection is absent, for example imitating the case of a population in which an infection previously preventable with a vaccine, it has been successfully

eliminated, but for which it is necessary to maintain high-level immune coverage to prevent the risk of re-emergence, as is the case of poliomyelitis in most countries wordwide. In such a situation, the dynamics of VAEs and of the related information arguably become the key determinant of vaccination decision and of collective coverage. It was considered a problem of binary decision, that is a problem for which only two mutually exclusive strategies are played: the first strategy, adopted by the subjects in favor of vaccination and the second strategy, adopted by individuals against vaccination. It has also been assumed that individuals can move from the strategy they are currently adopting to the alternative one by learning and imitating after social encounters with subjects who adhere to the other strategy. The dynamics of individuals of a certain population who are likely to be vaccinated in the absence of infection and in three cases that differ from each other due to the origin of the information received by individuals, has been described. In relation to this "information issue", the effects of three main cases are compared: (i) the case of purely local information, where agents react only to locally occurred events; (ii) a mix of purely local and global, country-wide, information due e.g., to countrywide media and the internet; (iii) a mix of local and non-local information. By representing these different information options through a range of different spatial information kernels, we supplied the conditions for the presence and stability of space-homogeneous, nontrivial, behavioral equilibria; the existence of bifurcations; the existence of classical and generalized traveling waves; and the effects of awareness campaigns enacted by the Public Health System to sustain vaccine uptake.

Chapter 2 presents a new model for the environment-host-environment transmission dynamics of *V. cholerae* in a community with an interconnected pond-river water network. Some of the notable key features of the model include accounting for the back-and-forth flow of water within the pond-river network, in addition to sub-dividing the bacterial population based on location of residence (i.e., we allow different ecological compartments for *V. cholerae* concentration in the pond and in the river) and monitoring the temporal dynamics of the local interactions between the human host and the two *V.cholerae* populations. Rigorous analysis of the resulting ecology-epidemiology-hydrology model shows that, for the case when the human host is the sole target of anti-cholera control and the volume of water in the pond is maximum, the disease-free equilibrium (DFE) of the model is globally-asymptotically stable whenever a certain epidemiological threshold, known as the basic reproduction number (denoted by $\mathcal{R}_0$) is less than unity. The epidemiological implication of this result is that cholera can be eliminated from the community if the control strategies implemented can bring (and maintain) $\mathcal{R}_0$ to a value less than unity, reducing for example the transmission rates of the virus from bacteria in the aquatic environment to the host, the shedding rates of virus in the water or increasing the mortality rate of the bacteria. Four scenarios were studied, that represent four different interpretations of the role of the *V. cholerea* pathogen within the environment, i.e. bacterial (*V. cholerea*) growth and shedding can, certainly, be interpreted both as new infections or as transitions into the bacterial class. This is routinely done in models for the transmission dynamics of cholera in human-environment systems. For example, in the model in [166], shedding and bacterial growth are interpreted as new infections; similarly, in the model in [155], the authors considered bacterial shedding as a transition into the bacterial class. The corresponding basic reproduction numbers were shown to exhibit the same threshold property with respect to the value unity (i.e., if one is less (equal, greater) than unity, then the three others are also less (equal, greater) than unity. Further, it was shown that for the case where anti-cholera control is focused on the human host population, the associated type reproduction number of the model (corresponding to each

of the four transmission scenarios considered) is unique. The implication of this result is that the estimate of the effort needed for disease elimination (i.e., the required herd immunity threshold) is unique, regardless of which of the four transmission scenarios is considered. However, when any of the other two bacteria populations (i.e., in the pond or in the river) is the focus of the control efforts, this study shows that the associated type reproduction number is not unique. Extensive numerical simulations of the model, using a realistic set of parameters from the published literature, show that, the community-wide implementation of a strategy that focus on improved water, sanitation and hygiene (known as WASH-only strategy) is unable to lead to the elimination of the disease (owing to its low estimated coverage of 50% and efficacy of 60%). However, if the coverage and efficacy can be increased (e.g., to 80% coverage and 90% efficacy), such elimination is indeed feasible using the WASH-only strategy. It was further shown that such elimination can also be achieved using a strategy that focus on oral rehydration therapy and the use of antibiotics to treat infected humans (i.e., treatment-only strategy), using a moderate and high effective levels of this strategy, for low coverage in the range 50% to 70%. As expected, of course, the combined hybrid WASH-treatment strategy provides far better population-level impact *vis a vis* disease elimination. This study ranks the three intervention in the following order of population-level effectiveness: combined WASH-treatment, followed by treatment-only and then WASH-only strategy. Overall, this study suggests that the prospect for the effective control or elimination of cholera in a population is promising using relatively modest (and realistically-attainable) coverages and efficacies of singular and combined anti-cholera control strategies. Moreover, traveling wave solutions are investigated, providing an estimate of the minimal speed for which there can be monotone waves that connect two constant states. Finally, By choosing one of the 4 scenarios studied, an estimate of the threshold parameter, known as $\mathcal{R}_0^{PDE}$, was provided in the spatially heterogeneous case. It has been shown that this quantity, under appropriate hypotheses, coincides with the basic reproductive number $\mathcal{R}_0$ associated with the corresponding spatially homogeneous case. Furthermore, if $\mathcal{R}_0^{PDE}$ appears to be below 1, then it is possible to eradicate the infection even in the spatial case, when the initial data are sufficiently small.

Chapter 3, is concerned with a novel mathematical model of vector-borne infectious diseases. The system, which generalizes the models present in the published literature, is characterized by 13 ordinary differential equations and takes into account the local interactions between reservoirs and vectors, as well as the transmission from vectors to dilution hosts. For both host populations, birds and humans, all the epidemiological classes of a SEIR model are considered, in order to take into account incubation period of virus and healing from the disease. The vector population is in turn divided into two sub-populations: the aquatic phase, which includes eggs, larvae and pupae, and anchored in marshy and stagnant areas, and the adult phase, capable of moving and spreading the virus. For the vectors of the aquatic phase a SI model is adopted, while for the vectors in the adult phase it is assumed in the SEI model. In the model, vectors possess the ability to keep the virus within their own population through vertical transmission. In addition, due to the lack of the breeding sites for eggs, a carrying capacity was assumed for the aquatic phase; moreover, a different carrying capacity was supposed for adult stage, since mosquitoes cannot survive at high temperatures or altitudes. The analysis of the model shows the local stability of the DFE, if the threshold parameter $\mathcal{R}_0$ is less than 1, in addition to the possibility of a bifurcation backwards, under appropriate conditions. 3 sets of simulations were compiled to validate the analytical results. After having simplified

the model, the simplest approximation for spatial diffusion, ie the Fickian one, is assumed: for the inferred model, an estimate of the Basic Reproductive Number $\mathcal{R}_0^{PDE}$, related to the spatial case is given. It provides a threshold for the local stability of the DFE in the spatial case and is compared with the basic Reproductive Number $\mathcal{R}_0$ associated with the non-spatial case.

In order to provide a control policy and an alternative prevention strategy to vaccines, Chapter 4 presents a model for the control of the infestation of mosquitoes of the species *Aedes Aegypty*, main carriers of vector-borne diseases. The system includes two main partial differential equations that describe the dynamics of mosquitoes in the aquatic phase and in the adult phase. Adult mosquitoes are assumed to be carried by the wind and diffuse. In the published literature the diffusive flux of adult mosquitoes satisfies Fick's constitutive law. The novelty of this chapter consists in proposing the coexistence of fast and slow diffusion fluxes, then the total diffusion flux of adult mosquitoes is the sum of two contributions: one that obeys the classical Fick's law, the other satisfies an evolution equation of Cattaneo type. In the dissertation, a parameter plays an important role, indicated by F_D, which involves the two diffusion coefficients, corresponding to the two independent diffusion processes. By its definition, it has to strictly satisfy the bounds $F_D \in [0, 1]$. The limit value 0 leads to a hyperbolic model, characterized by slow diffusion and whose diffusive flow satisfies a Maxwell-Cattaneo-Vernotte evolution equation. The limit value 1, leads to the parabolic model studied in [151], characterized by fast diffusion and whose diffusion flow obeys Fick's law. A detailed analysis of the corresponding ODE system was carried out, showing the global stability of the Disease-Free Equilibrium, if a threshold parameter $\mathcal{Q}_0$, remains below 1. $\mathcal{Q}_0$ is the product between the average number of female mosquitoes produced by one fertile mosquitoto survive the entire aquatic phase and the average number of viable eggs laid by the emerging female mosquito during its entire lifespan. Traveling Wave type solutions have been investigated, providing an estimate of the minimal speed for which there are monotone waves that connect constant equilibria. The presented system admits as a special case the hyperbolic model obtained by neglecting the contribution of the fast diffusion flow described by Fick's law, which is analyzed in detail in a particular section. This hyperbolic special system is able to overcome the paradox of infinite speed propagation, typical of parabolic systems. Several numerical simulations compare the Fickian model present in the literature with those presented in this chapter, i.e. the hyperbolic model obtained when fickian diffusion is neglected, and the more general model in which the coexistence of both contributions is proposed.

Chapter 1

SPATIO-TEMPORAL GAMES OF VOLUNTARY VACCINATION IN THE ABSENCE OF THE INFECTION: THE INTERPLAY OF LOCAL VERSUS NON-LOCAL INFORMATION ABOUT VACCINE ADVERSE EVENTS

This chapter has materialized in the following paper:

A. Lupica, P. Manfredi, V. Volpert, A. Palumbo and A. d'Onofrio. Spatio-temporal games of voluntary vaccination in the absence of the infection: the interplay of local versus non-local information about vaccine adverse events, *Mathematical Biosciences and Engineering*, Vol 17, n. mbe-17-02-058, pp. 1090, 2020.

1.1 Introduction

Mathematical epidemiology (ME), as the study of the transmission dynamics and control of infectious diseases, not only represents one of the oldest and richest areas of mathematical biology [11, 35], but it is also the area that probably had the largest impact on actual policy. Indeed, mathematical models of infections are nowadays routinely applied by international and national public health institutions, ranging from the design of immunization programs against vaccine preventable infectious diseases of childhood, up to the preparedness plans against the threats from possible future influenza pandemics, see [115] and references therein.
A limitation of classical ME is that its key assumptions are the legacy of classical Statistical mechanics. As a consequence, the social contacts between agents at risk of spreading or acquiring the infection are treated

as "encounters of particles" of a perfect gas. Pairwise, the contagion process is abstracted as it were a chemical reaction. Consequently, transmission processes have been traditionally modelled by means of the mass action law.

Treating human beings as "gas particles" implies that the spread of infectious diseases is totally unaffected by the agents' behaviour, and *vice-versa*, simply because behaviour is absent from the models of classical ME. This means that e.g., models used to evaluate the impact and cost-effectiveness of vaccination programs under voluntary immunization did not include neither the individuals risk perceptions about the disease nor those about vaccine-related adverse events (VAEs). Similarly, ME models treat the social contact process between individuals as a physical constant, implying that individuals continue contacting each other at the same rate independently of the magnitude they perceived of the risk of contracting the infection.

Nowadays we know well that the above assumption are quite coarse, possible useful to depict "normal" situations but totally inadequate to describe scenarios such as vaccine scares, where the perceived risk of VAEs blows up for a while, or the course of a deadly epidemics [110, 167].

The pioneering work that first included the human behaviour in a simple ME model was [38], which extended the classical Kermack and McKendrick's ODE epidemic model to account for behavioural responses. However, this paper remained relatively isolated until the need of embedding human behaviour in ME models became increasingly urgent due to the onset of a range of new phenomena such as the increasing mistrust and opposition towards vaccines [40, 68, 88, 126]. In [110, 167] it was argued that such phenomena are characteristic of the current landscape of infection and public health in modern industrialised countries. Notably, mistrust towards vaccination can be considered as part of the more global phenomenon known as *post-trust society* [101].

This led in the last two decades to the birth of a new branch of ME that was termed the Behavioural Epidemiology of Infectious Diseases (BEID) [110, 167]. The very core of BEID aims at the proper modelling of human behaviour in the transmission and control of infectious diseases integrating the classical mathematical epidemiology tools with models and ideas from behavioral disciplines, ranging from psychology to neural sciences, and from economics to sociology.

Most BEID models of vaccination behavior include the strategic behavior of agents, and therefore extensively use Game Theory. In particular, Bauch [17] pioneered the applications of evolutionary games to describe the dynamics of the vaccine propensity in a population by using what we will call *Imitation Game Dynamics* (IGD) i.e., a model where the strategy perceived as better at a given time spreads in the population through imitation. In his work [17], the perceived risk of infection is taken as linearly increasing with the infection prevalence, whereas the perceived risk of VAE is assumed constant. Instead, in [64] the perceived risk of suffering a vaccine side effect is modelled as an increasing function of the *information* of the present and past incidence of VAEs.

As expected, in BEID a key role is played by the information that agents can access and use for evaluating risks upon which to base their actions. The importance of both present and past information on infection and vaccines, including VAEs, for BEID models was first stressed in [66, 110]. In [65], the first amendment of the basic IGD vaccination model to include the effect of public intervention in communicating perceived risks from vaccines and infection, was proposed.

Most previously cited BEID models [17, 31, 64, 65], and other works in the same line, are "simple" i.e.,

they are based on simple ordinary differential equation (ODE) models, and disregard any type of structural heterogeneity. In particular, they are "spatially homogeneous", which is a crude approximation from at least two standpoints namely, (i) the wide and complicate population mobility patterns in both industrialised countries and worldwide, (ii) the complicate role played by the spatial information network for behavior in relation to health.

In relation to this, a still unexplored area in the BEID literature regards the incorporation of behavioral hypotheses within classical PDE models of spatial dynamics of the reaction-diffusion type. This represent a worthwhile effort for two main reasons. The first one is substantive and relates to the critical role played by information in behavioral epidemiology models. From this standpoint classical diffusion allows to subdivide the type of information that can be accessed by vaccination decision makers into a few sharply distinct types namely, "local" vs "global" vs "non-local" based on simple hypotheses on the underlying *spatial information kernels*. The second reason is technical and relates to the robust analytic techniques that classical diffusion mathematics makes it available for the understanding of real world processes. And indeed, since the sixties mathematical reaction-diffusion theory was extensively applied in ME models [35, 109, 122], such as the pioneering paper by Noble [125] on European plague epidemics in the 14th century. Ducrot and Giletti [69] showed that, under Fickian diffusion hypothesis, the Kermack-McKendrick epidemic model with non-diffusive susceptible population can have pulsating travelling wave solutions. Very recently Magal and coworkers [103] adopted Fickian diffusion with anysotropic diffusion coefficents to model the spread of infectious diseases, with focus on the impact of diffusion on the basic reproduction number. They adopted a similar approach [102] to model the spread of influenza in Puerto Rico, including also behavioural effects. They obtained a good match between their simulations and available spatiotemporal data. As far as vector-borne infectious diseases are concerned, recently Fitzgibbon et al [76] proposed a model, where the diffusion of hosts was described by Fickian diffusion. Zhao and colleagues [182] again adopted Fickian diffusion to model the spread of a two–groups infectious diseases of SIR type, focusing in particular on the onset of traveling waves.

Therefore, the aim in this chapter is to investigate the interplay between vaccination dynamics, spatial mobility and information. To do so, the behavioral epidemiology models for the impact of vaccine adverse events (VAEs) on vaccination choices has been extended to a continuous spatially structured setting, that were first introduced in [64, 65] and reformulated as a process of double *ideational contagion* in [31, 32, 167]. In particular, voluntary immunization decisions were considered and the work is focused on the simplest but important case in which the disease is absent in the population studied This case is not special at all as, e.g., it represents the case of a population where a previously endemic vaccine preventable infectious disease of childhood has been successfully eliminated, so that prevalence is equal to zero, but there is the need to maintain a high-coverage immunization policy in the post-elimination period to prevent the risk of infection re-emergence. A major instance is that of poliomyelitis in industrialized countries, where herd immunity, which was already achieved the 1970s, needed however to be sustained for several further decades until (global) eradication will be achieved. In such a context, where the absence of the infection will remarkably reduce the incentive to immunize thereby weakening the probability of switching from the "non-vaccinator" to the "vaccinator" strategy , the dynamics of VAEs will arguably become the key determinant of vaccination decision and collective coverage. To investigate the interplay with spatial mobility the resulting vaccination

dynamics is set into the simplest possible framework for spatial mobility, namely classical diffusion based on Fick's law.
The consideration of the spatial effects i.e., the spatial distribution of VAEs, requires to carefully take into account the information on VAEs that is handled by parents of children eligible for vaccination while forming their perceptions of risk, that they will subsequently use to take their immunization decisions.
In relation to this "information issue", three scenarios were considered. In the first scenario, the information that individuals access and use uniquely concerns VAEs occurred locally. In the second case, the information used is both the local one and a global, nation-wide, average. Roughly speaking, this scenario corresponds to the the case where agents take their decisions also based on national media such as national news or the internet. The third scenario is an intermediate one and aims at taking into the account both the known phenomenon of information attenuation [80], and the reasonable assumption that agents give less weight to events occurred at far distant locations. We represented the latter scenario, where the information used is not purely local but it is also not global, by resorting to a range of different *spatial information kernels*.
Of the vast resulting collection of inferred problems, we have examined (also distinguishing the nature of space as limited by non-limited) (i) the presence and stability of homogeneous space balances, focusing on non-trivial behavioral equilibrium; (ii) conditions for bifurcations; (iii) existence of mobile waves; (iv) effects of awareness campaigns promoted by the public health system to effectively support the absorption of the vaccine, as proposed for the first time by [65]. The chapter is organized as follow: the main model is presented in section 1.2 while a list of possible kernels is given in section 1.3. Some key features of the non-spatial model are exploded in section 1.4. Stability of homogeneous steady states and bifurcation analysis are placed in section 1.5 and 1.6, respectively. Traveling Wave and Generalized Traveling Wave of the main model are investigated in section 1.7. The role of memory within the main model is studied in section 1.8, while intervention of public health campaigns is investigad in 1.9. Section 1.10 is constituted by a preliminary simulation on the main model containing both memory and public health departmente intervation, finally conclusions are placed in section 1.12.

1.2 The spatio-temporal imitation game for vaccination

To model the impact of human responses to VAEs on the overall dynamics of vaccine uptake in the newborn, following [17, 64, 65], is assumed that vaccination is a binary decision problem, i.e. one for which only two mutually exclusive strategies are played by parents: "vaccinator" (strategy 1) and "non-vaccinator" (strategy 2). Let us consequently denote by $P(x,t)$ and $A(x,t)$ the fractions of vaccination decision makers (e.g., parents of children eligible for vaccination) at location x and time t that follow, respectively, strategy 1 and 2. The previously cited models of IGD [17, 64, 65] all relied on the concept of payoff. However, it was noted [78] that many evolutionary game models belong to the class of urn models, a remarkably wide family that includes both chemical kinetcs models as well as classical ME models. Thus, follow here [31, 33, 167], where the vaccination IGD was derived as a model of "double contagion" of ideas between the two involved groups namely, the group playing the "vaccinator" strategy and the one playing the "non-vaccinator" strategy).
Thus, by extending to the present spatio-temporal setting the IGD in [33, 167], the following model is

obtained:

$$\begin{aligned} \partial_t P &= D\nabla^2 P + \vartheta(M_i)AP - \alpha(M_{se})AP, \\ \partial_t A &= D\nabla^2 A - \vartheta(M_i)AP + \alpha(M_{se})AP, \end{aligned} \tag{1.2.1}$$

where $t > 0$, $x \in \Omega$, with Ω a bounded subset of $\mathbb{R}^n$, $n = 1, 2$. If $n = 1$, then we assume that $\Omega = [-L, L]$, $L > 0$, while, if $n = 2$, then we assume that boundary of Ω (i.e. $\partial\Omega$) is sufficiently smooth.
In particular, $\vartheta(M_i)$ and $\alpha(M_{se})$ represent the strategy-specific "transmission rates" following social contacts with individuals playing the other strategy. They are assumed to be non-decreasing functions of the variables M_i and M_{se}. The latter are information indices summarizing the available information about the (current or past) state of the infection (M_i) and of VAEs (M_{se}), respectively, that are used by parents to formulate evaluations of related risks.
Assuming a stationary population and normalizing with respect to its steady state, since $A = 1 - P$, system (1.2.1) collapses into the following single equation:

$$\partial_t P = D\nabla^2 P + P(1 - P)(\vartheta(M_i) - \alpha(M_{se})). \tag{1.2.2}$$

Regarding the key quantities M_i and M_{se}, given the assumption according to which the infection was eliminated, it is stated that the perceived risk related to the infection is only constant:

$$\vartheta(M_i(I)) = \vartheta_0. \tag{1.2.3}$$

The previous formulation mimics the situation where the infection is absent, so the corresponding perceived risk is prevalence- independent. It is assumed that $\vartheta_0 > 0$ to reflect a positive perceived risk of infection even in the absence of infection. This can be justified by the continued activity of an active public health system that aims to keep a high degree of population awareness on the risk of reintroduction which is perceived as homogeneous throughout the entire space. Moreover, it is assumed that the perceived risk of VAEs depends on information on vaccine side effects occurring both locally but also non-locally, as follows:

$$\alpha(M_{se}(P)) = \alpha_0 + \alpha_1 P + \alpha_2 J(P), \tag{1.2.4}$$

where

$$J(P) = \int_\Omega \phi(x - y)P(y, t)dy. \tag{1.2.5}$$

The function $\phi(x)$ is non-negative with

$$\int_\Omega \phi(x)dx = 1, \tag{1.2.6}$$

and even

$$\phi(x) = \phi(-x), \text{ for all } x \in \Omega. \tag{1.2.7}$$

To sum up, the perceived risk of VAEs $\alpha(M_{se})$, has three components: (i) a baseline value α_0 possibly constant over space, mirroring a true underlying risk of VAEs, (ii) a strictly local component $\alpha_1 P$, possibly reflecting local deviations in vaccine coverage and ensuing deviations in the local number of VAEs (as in [64]), and (iii) a non-local component $\alpha_2 J(P)$ tuning risk perceptions arising from differences in VAEs at

different geographic sites, according to a suitable *spatial information kernel*. In particular, the functional $J(P)$ describes two mathematically equivalent scenarios, where individuals located at position x can: i) receive information concerning the value of P at the space point y with a weight/attenuation $\phi(x-y)$; ii) receive full spatial information but, in taking their decisions, they assign a weight $\phi(x-y)$ to $P(y,t)$.
Setting $\vartheta_* = \vartheta_0 - \alpha_0 > 0$, brings to the following model

$$\partial_t P = D\nabla^2 P + P(1-P)(\vartheta_* - \alpha_1 P - \alpha_2 J(P)), \tag{1.2.8}$$

with $x \in \Omega$ and $t > 0$.
Let l be a characteristic length of the domain Ω; to mathematically simplify the analysis, the model is reformulated in terms of the following variables:

$$t^* = \vartheta_* t,\ x^* = x l^{-1},\ D^* = D\vartheta_*^{-1} l^{-2},$$

$$\alpha_1^* = \alpha_1 \vartheta_*^{-1},\ \alpha_2^* = \alpha_2 \vartheta_*^{-1}, \tag{1.2.9}$$

where $1/\vartheta_*$ is time unit. The set derived from Ω by adimensionalization will be denoted as Ω^* (e.g. in 1D $\Omega^* = [-L/l, L/l]$).
Thus, the model (1.2.8) becomes (for the sake of simplicity we omit the stars):

$$\partial_t P = D\nabla^2 P + P(1-P)(1 - \alpha_1 P - \alpha_2 J(P)), \tag{1.2.10}$$

with $x \in \Omega$ and $t > 0$.
Moreover, by imposing Neumann boundary conditions:

$$\partial_x P = 0,\ \text{on } \partial\Omega,\ \text{if } \Omega \subset \mathbb{R},\ \text{or } \partial_n P = 0,\ \text{on } \partial\Omega, \text{if } \Omega \subset \mathbb{R}^2, \tag{1.2.11}$$

where n is the outer normal vector with respect to $\partial\Omega$.
In the case in which the characteristic size of Ω is larger than the unit (for example in one dimension, $L/l \gg 1$), then we can assume that the domain is unbounded, i.e. $\Omega = \mathbb{R}^n$, $n = 1, 2$.

1.2.1 The Fisher-Kolmogorov model as a particular case of (1.2.10)

In the special case where people do not take into account the spatial variation in VAEs, i.e. $\alpha(M_{se}(P)) = \alpha_0$, model (1.2.10) reduces to the well-known Fisher-Kolmogorov (FK) equation

$$\partial_t P = D\nabla^2 P + P(1-P), \tag{1.2.12}$$

introduced in [75, 94]. The FK equation (1.2.12) in this case describes the spread (via traveling waves [122]) of the idealized state $P = 1$, where all people are in favor of the vaccination and the "recession" of the state $P = 0$, where no subjects are in favor of vaccination.

1.3 Modelling risk perceptions: global vs local vs non-local information

Arguably, the behaviour of (1.2.10) critically depends on the specific functional form of the spatial information kernel $\phi(x)$. Below, a list of relevant forms.
The simplest case is when the available information is purely local, that is

$$\phi(x) = \delta(x),$$

where $\delta(x)$ is the Dirac funtion. Then, equation (1.2.10) reads as:

$$\partial_t P = D\nabla^2 P + P(1-P)(1-\alpha P), \tag{1.3.1}$$

where, with slight abuse of notation, we set

$$\alpha = \alpha_1 + \alpha_2.$$

As mentioned in the introduction, by far the most important specific form for $\phi(x)$ is the constant one, namely

$$\phi(x) = \frac{1}{\mu(\Omega)},$$

where $\mu(\Omega)$ is the measure of Ω; thus, the non–local term (1.2.5) yields:

$$J(P) = \frac{1}{\mu(\Omega)} \int_\Omega P(y,t)dt. \tag{1.3.2}$$

This specific form models the noteworthy scenario where people are exposed to a global (average) information e.g., by the media (including the internet) and the Public Health system, about the current state of vaccine-side effects coming from the whole domain Ω. Model (1.2.10) becomes

$$\partial_t P = D\nabla^2 P + P(1-P)\left(1 - \alpha_1 P - \alpha_2 \frac{1}{\mu(\Omega)} \int_\Omega P(y,t)dy\right). \tag{1.3.3}$$

Another important scenario is when the information about VAEs comes from the whole Ω but it is either attenuated with the distance (this was possibly true for diseases in historical epochs) or it is the individual receiving the information that pays lesser and lesser weight depending on the distance.
Two reasonable functional forms that might well represent this scenario are:
i) Gaussian decay

$$\phi_1(x) = C_g e^{-ax^2},$$

where $a > 0$ and $1/\sqrt{a}$ is the characteristic *attenuation length*. In R^n $(n = 1, 2)$ the normalization constant C_g is:

$$C_g = \left(\frac{a}{\pi}\right)^{\frac{n}{2}}.$$

In this case, model (1.2.10) becomes:

$$\partial_t P = D\nabla^2 P + P(1-P)\left(1 - \alpha_1 P - \alpha_2 \int_\Omega C_g e^{-ay^2} P(y,t)dy\right);$$

ii) Exponential decay,

$$\phi_2(x) = C_e e^{-a|x|},$$

where $a > 0$ and in R^n $(n = 1, 2)$ the constant C_e reads as follows

$$C_e = \frac{a}{2}, \text{ in } \mathbb{R}, \text{ and } C_e = \frac{a^2}{2\pi}, \text{ in } \mathbb{R}^2.$$

In this case, model (1.2.10) becomes:

$$\partial_t P = D\nabla^2 P + P(1-P)\left(1 - \alpha_1 P - \alpha_2 \int_\Omega C_e e^{-a|y|} P(y,t)dy\right).$$

Another important class of spatial kernels is represent by non–local kernels boundedly supported, i.e. that are null beyond a given distance. An example is:

$$\phi_3(x) = C_N \left(1 - \left|\frac{x}{N}\right|^2\right) Hev(N - |x|)$$

where $Hev(.)$ is the Heaviside function and

$$C_N = \frac{3}{4N}, \text{ in } \mathbb{R}, \text{ and } C_N = \frac{2}{\pi N^2}, \text{ in } \mathbb{R}^2.$$

In this case, model (1.2.10) becomes:

$$\partial_t P = D\nabla^2 P + P(1-P)\left(1 - \alpha_1 P - \alpha_2 \int_\Omega C_N \left(1 - \left|\frac{y}{N}\right|^2\right) Hev(N - |y|)P(y,t)dy\right).$$

Another example in $\mathbb{R}$ is

$$\phi_4(x) = \frac{1}{2h} Hev(h - |x|),$$

and in $\mathbb{R}^2$

$$\phi_4(x) = (1/(\pi h^2)) Hev(h - |x|).$$

In this case, model (1.2.10) becomes:

$$\partial_t P = D\nabla^2 P + P(1-P)\left(1 - \alpha_1 P - \alpha_2 \int_\Omega (1/(2h)) Hev(h - |y|)P(y,t)dy\right), \text{ in } \mathbb{R}.$$

As it is to be expected in the problem in study, the Fourier transform will be important in the mathematical analysis of the problem.

We use the following definition of Fourier transform for a generic function $f(x) : \mathbb{R}^n \longrightarrow \mathbb{R}$ $(n = 1, 2)$:

$$\widetilde{f}(\xi) = \int_{\mathbb{R}^n} f(x) e^{-i\xi x} dx, \tag{1.3.4}$$

where ξ is the Fourier's vector, $\xi x = \xi_1 x$ in $\mathbb{R}$ or $\xi x = \xi_1 x_1 + \xi_2 x_2$ in $\mathbb{R}^2$. Here and further down $\xi^2 = \xi_1^2$ in $\mathbb{R}$ or $\xi^2 = \xi_1^2 + \xi_2^2$ in $\mathbb{R}^2$.

We have that:

$$\widetilde{\phi}_1(\xi) = e^{-\frac{\xi^2}{4a}}, \text{ in } \mathbb{R}^n, \ n = 1, 2;$$

$$\widetilde{\phi}_2(\xi) = \left(\frac{a^2}{a^2 + \xi^2}\right)^{(n+1)/2}, \text{ in } \mathbb{R}^n, \ n = 1, 2;$$

$$\widetilde{\phi}_3(\xi) = \frac{3}{N^3 \xi^3} \left(\sin[N\xi] - N\xi \cos[N\xi]\right), \text{ in } \mathbb{R};$$

$$\widetilde{\phi}_4(\xi) = \frac{1}{h\xi} \sin(h\xi), \text{ in } \mathbb{R}.$$

1.4 Properties of the spatially homogeneous model

In this section, it is briefly summarized the results in [64], concerning the behaviour of the spatially homogenous model corresponding to (1.3.1). This is described by the ordinary differential equation (ODE)

$$P'(t) = P(1-P)(1-\alpha P). \tag{1.4.1}$$

A first equilibrium $P_0 = 0$ corresponds to the no vaccination scenario where no parent is favorable to immunization. This *non-vaccinator equilibrium, NVE* is always unstable. If $1 < \alpha$, then there exists a non-trivial *behavioral equilibrium*

$$P_2 = \frac{1}{\alpha}, \tag{1.4.2}$$

that is globally attractive in (0,1). P_2 is termed a behavioral equilibrium (BE) because its level is tuned by the balance between the parents' perceptions of risks based on the handling of available information. Finally, there is a *pure vaccinator equilibrium, PVE* $P_1 = 1$ [17, 64], corresponding to the unrealistic scenario where all parents are unanimously favorable to immunization. The PVE is unstable if $1 < \alpha$, and globally attractive if $0 \leq \alpha \leq 1$.
Arguably, in the case of an infection that has been eliminated, one expects that at least in an initial phase it holds $P_2 > p_C$ where $p_C = 1 - 1/\mathcal{R}_0$ is the critical vaccination threshold allowing infection elimination, and $\mathcal{R}_0$ is the basic reproduction number of infection. However, this does not need to be true at subsequent times, and this is why it is important for the public health system to monitor the evolution of VAEs and related information. Finally, if $\alpha = 0$ then the model reduces to the well-known logistic model (see also next section).

1.5 Stability Analysis of Homogeneous Steady State

The equilibria of the ODE model (1.4.1) described in section 1.4 are also homogenous equilibria of the spatially structured model (1.3.1). In this section will be investigated their stability, focusing primarily on the behavioral equilibrium P_2 defined in (1.4.2), since the other two equilibria ($P_0 = 0$, i.e. no vaccinators, and $P_1 =$, i.e. all vacciantors) do not correspond to realistic situations.
Will be explored multiple relevant cases depending on: i) the nature of the information used to make the vaccination decision: local, global or non–local i.e., on the structure of the spatial information kernel; ii) the nature of Ω: bounded vs unbounded.

1.5.1 Local Information

Under purely local information i.e., equation (1.3.1) with boundary condition (1.2.11), the structure of the local stability of the homogeneous equilibria is similar to the one characteristic of the ODE model (1.4.1). We proved the following:

Theorem 1.5.1 *The non-vaccinator equilibrium P_0 is always unstable.*
If $\alpha > 1$, the behavioral equilibrium P_2 is locally asymptotically stable (LAS) and the PVE P_1 is unstable.

Moreover, if Ω is bounded then P_2 is also globally asymptotically stable (GAS).
If $0 \leq \alpha \leq 1$, P_2 is not an admissible equilibrium and the PVE P_1 is LAS. Moreover, if Ω is bounded then P_1 is also globally asymptotically stable (GAS).

Proof. It is reported the proof for the non-trivial parts. If Ω is bounded, from the linearized equation around the behavioral equilibrium $P_2 = 1/\alpha$,

$$\partial_t w = D\nabla^2 w - (1 - P_2)w, \tag{1.5.1}$$

it follows that the the m–th eigenvalue is given by:

$$\lambda_m = -D\xi_m^2 - (1 - P_2) < 0, \tag{1.5.2}$$

where $\nu_m = -\xi_m^2$ is the m–th eigenvalue of the heat equation with Neumann conditions (1.2.11) in Ω. For example, if $\Omega = [-L, L]$, then $\xi_m = m\pi/L$, $m \in \mathbb{N}$.
Similarly, if Ω is unbounded, then by applying the Fourier's Trasform (1.3.4), we obtain the following expression for the spectrum:

$$\lambda(\xi) = -D\xi^2 - (1 - P_2) < 0. \tag{1.5.3}$$

The global stability of P_2 and P_1 respectively, can both be demonstrated by adopting as Liapunov functional the free energy:

$$Li(t) = \int_\Omega \left(D|\nabla P|^2 + U(P)\right) dx, \tag{1.5.4}$$

where $U(P)$ is the "potential" *(associated to the "force" $P(1 - P)(1 - \alpha P)$)*, given by:

$$U(P) = -\int \left(P(1 - P)(1 - \alpha P)\right) dP,$$

from which the claim easily follows. □

1.5.2 Global Information

Under global information i.e., when people are exposed to the average information on VAEs coming from the whole domain (note this scenario only concerns the case where Ω is bounded):

$$J(P) = \langle P(x, t)\rangle = \frac{1}{\mu(\Omega)} \int_\Omega P(y, t)dy,$$

then the model (1.2.10) becomes:

$$\partial_t P = D\nabla^2 P + P(1 - P)\left(1 - \alpha_1 P - \alpha_2 \frac{1}{\mu(\Omega)} \int_\Omega P(y, t)dy\right), \tag{1.5.5}$$

with Neumann conditions (1.2.11).
The linearized equation at $P_2 = 1/\alpha$ reads as follows

$$\partial_t w = D\nabla^2 w - P_2(1 - P_2)\left(\alpha_1 w + \alpha_2 \frac{1}{\mu(\Omega)} \int_\Omega w(y, t)dy\right). \tag{1.5.6}$$

Setting $w(x) = \cos(\xi_m x)$ as eigenfunction, it is straightforward to show that the m–th corresponding eigenvalue is given by

$$\widetilde{\lambda}_0 = -(1 - P_2) < 0, \text{ if } m = 0, \ \widetilde{\lambda}_m = -D\xi_m^2 - \alpha_1 P_2 (1 - P_2) < 0, \text{ if } m \geq 1. \tag{1.5.7}$$

Thus P_2 is LAS.
Interestingly, if $m = 0$, referring to expreessions (1.5.2) and (1.5.7), then $\lambda_0 = \widetilde{\lambda}_0$. On the contrary, if $m \geq 1$, comparing eigenvalues in (1.5.2) and (1.5.7), we can deduce that $\widetilde{\lambda}_m > \lambda_m$: therefore eigenvalues in (1.5.7) are "less negative" than their counterparts for the local information model in (1.5.2). This indicates a slower convergence to P_2 in equation (1.5.5) compared to equation (1.3.1) for all modes $m \geq 1$.
As for the NVE $P_0 = 0$, the eigenvalues obey

$$\widetilde{\lambda}_m = -D\xi_m^2 + 1,$$

i.e. at least the mode 0 is unstable. Moreover, the linearized equation of (1.5.5) around the PVE $P_1 = 1$ gives the eigenvalues:

$$\widetilde{\lambda}_m = -D\xi_m^2 + \alpha - 1.$$

Thus P_1 is unstable, unless the unlikely event $0 \leq \alpha \leq 1$ holds, implyig the LAS of P_1.

1.5.3 Non–Local Information

At variance with the global information scenario, under non-local information it is necessary to distinguish the case where Ω is unbounded from the one where it is bounded.

Stability of homogeneous equilibria: Ω unbounded

As noted above, assuming that $L/l \gg 1$, we can study the following equation deduced from (1.2.10)

$$\partial_t P = D\nabla^2 P + P(1 - P)\left(1 - \alpha_1 P - \alpha_2 \int_\Omega \phi(x - y)P(y, t)dy\right), \tag{1.5.8}$$

with $x \in \Omega = \mathbb{R}^n$, $n = 1, 2$, $t > 0$ and Neumann condition (1.2.11) on the boundary (i.e. at infinity).
The associated linearized equation at a generic homogeneous steady state P^* is:

$$\partial_t w = D\nabla^2 w + [(1 - 2P^*)(1 - \alpha P^*) - \alpha_1 P^*(1 - P^*)]\, w - \alpha_2 P^*(1 - P^*) \int_\Omega \phi(x - y)w(y, t)dy. \tag{1.5.9}$$

The associated eigenvalue problem has the form:

$$D\nabla^2 W + [(1 - 2P^*)(1 - \alpha P^*) - \alpha_1 P^*(1 - P^*)]\, W - \alpha_2 P^*(1 - P^*) \int_\Omega \phi(x - y)W(y)dy = \lambda W. \tag{1.5.10}$$

Let us now focus on the case of primary interest here namely when P^* is given by the behavioral equilibrium i.e. P_2 defined in (1.4.2). This yields:

$$D\nabla^2 W - P_2 (1 - P_2) (\alpha_1 W + \alpha_2 J(W)) = \lambda W. \tag{1.5.11}$$

We consider the linearized operator $\mathcal{L}$ on $L^2(\mathbb{R}^n)$ (n=1,2), such that

$$\mathcal{L}W := -D\nabla^2 W + P_2\left(1-P_2\right)\left(\alpha_1 W + \alpha_2 J(W)\right). \tag{1.5.12}$$

The spectrum of this operator is denoted by $\sigma(\mathcal{L})$. The eigenvalue problem

$$\mathcal{L}W = \lambda W$$

is called *spectrally stable* if $\sigma(\mathcal{L}) \subset [0, +\infty)$ and *spectrally unstable* if there exists $\lambda < 0 \mid \lambda \in \sigma(\mathcal{L})$, as reported in [8]. Moreover, $\sigma(\mathcal{L})$ is spectrally stable iff the operator $\mathcal{L}$ is positive, i.e. $(\mathcal{L}W, W) > 0$ for any W [8]. Let us introduce the function

$$\Phi(\xi) = D\xi^2 + P_2\left(1-P_2\right)\left(\alpha_1 + \alpha_2\tilde{\phi}(\xi)\right),$$

where $\tilde{\phi}(\xi)$ is the Fourier transform (defined in formula (1.3.4)) of $\phi(x)$, which is real since we assumed symmetric $\phi(x)$.
Noting that

$$\tilde{\phi}(0) = \int_\Omega \phi(y)dy = 1, \tag{1.5.13}$$

we can state the following:
i) function $\Phi(\xi)$ evaluated at $\xi = 0$ is always positive, i.e.

$$\Phi(0) = P_2\left(1-P_2\right)\left(\alpha_1+\alpha_2\right) = 1 - P_2 > 0;$$

ii) for any given continuous and bounded function $\tilde{\phi}$, $\Phi(\xi)$ becomes strictly positive if D is sufficiently large.
Thus, for sufficiently large values of the diffusion coefficient the behavioral equilibrium P_2 will be stable irrespective of the shape of the spatial information kernel.
On the contrary, if $\phi(x)$ has bounded support, then its Fourier transform can take negative values that can destabilize P_2.
Consider now the special cases of the spatial information kernel $\phi(x)$ considered in section 1.3.
If $\phi(x) = \phi_1(x) = C_g e^{-ax^2}$ then function Φ takes the form:

$$\Phi(\xi) = D\xi^2 + \frac{1}{\alpha}\left(1-\frac{1}{\alpha}\right)\left(\alpha_1 + \alpha_2 e^{-\frac{\xi^2}{4a}}\right). \tag{1.5.14}$$

As the latter expression is strictly positive, the behavioral equilibrium P_2 is always locally stable.
Similarly, under the exponential kernel $\phi(x) = \phi_2(x) = C_e e^{-a|x|}$, $x \in \mathbb{R}^n$ ($n = 1$ or 2):

$$\Phi(\xi) = D\xi^2 + \frac{1}{\alpha}\left(1-\frac{1}{\alpha}\right)\left(\alpha_1 + \alpha_2\left(\frac{a^2}{a^2+\xi^2}\right)^{(n+1)/2}\right). \tag{1.5.15}$$

Therefore, also in this case function $\Phi(\xi)$ is strictly positive and P_2 is locally asymptotically stable.
These two examples suggest that kernels that are non-null over the whole space, and have a realistic shape (i.e., are decreasing in the distance from the current site), always promote the local stability of the behavioral equilibrium P_2.
To analyse the effects of the two proposed kernels with bounded support, we will only consider, for sake of

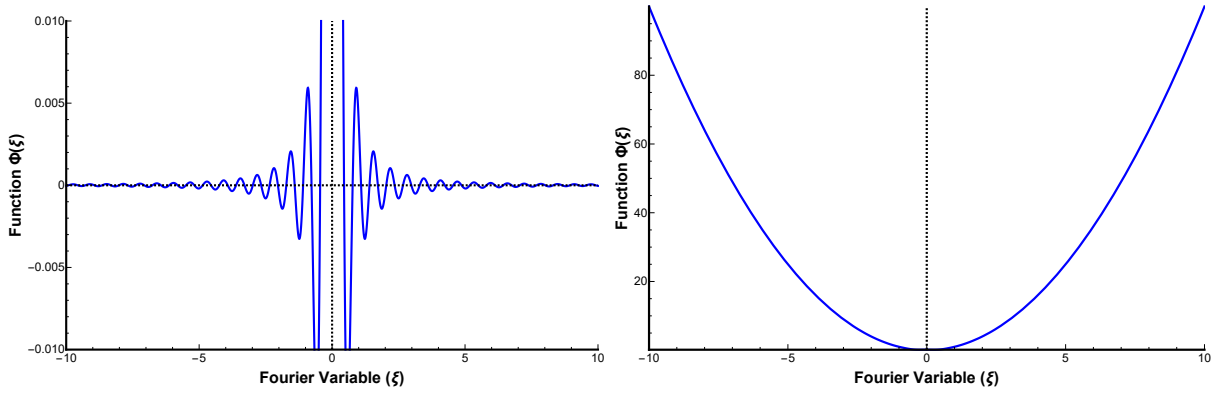

(a) (b)

Figure 1.1: Representation of function $\Phi(\xi)$ in the event $\phi(x) = \phi_3(x)$ with $\alpha_1 = 0$, $\alpha_2 = 1.2$ and $N = 10$. Here $D = 10^{-7}$ in (a) and $D = 1$ in (b).

notation simplicity, the case $\Omega = \mathbb{R}$.

Under the kernel $\phi(x) = \phi_3(x) = C_N(N^2 - x^2)Hev(N - |x|)$, with $N > 0$, function Φ is as follows:

$$\Phi(\xi) = D\xi^2 + \frac{1}{\alpha}\left(1 - \frac{1}{\alpha}\right)\left(\alpha_1 + \alpha_2 \frac{3}{N^3\xi^3}\left(\sin[N\xi] - N\xi\cos[N\xi]\right)\right). \tag{1.5.16}$$

Depending on N and on the other parameters, $\Phi(\xi)$ can be strictly positive or can change sign. As noted before, $\Phi(0) = 1 - 1/\alpha > 0$. Also in this case, if ξ is large enough, the function $\Phi(\xi)$ is positive and the equilibrium P_2 is locally stable. When the diffusion coefficient is large enough, the local stability in ensured. The instability can appear if D is small enough and if the ratio $\rho = \alpha_2/\alpha_1$ is large enough.

This type of behavior is illustrated in the Figure 1.1 in the particular case in which $\alpha_1 = 0$.

We finally consider $\phi(x) = \phi_4(x) = 1/(2h)Hev(h - |x|)$, with $h > 0$. The function $\Phi(\xi)$ reads as follows:

$$\Phi(\xi) = D\xi^2 + \frac{1}{\alpha}\left(1 - \frac{1}{\alpha}\right)\left(\alpha_1 + \alpha_2 \frac{\sin[h\xi]}{h\xi}\right). \tag{1.5.17}$$

Depending on h and the other parameters, this function can be strictly positive or can change sign. Moreover, $\Phi(\xi)$ is positive for $|\xi|$ sufficiently large. If the diffusion coefficient is large, then $\Phi(\xi)$ is positive for all ξ, and the behavioral equilibrium P_2 is locally stable. The instability can appear if D is small enough and $\rho = \alpha_2/\alpha_1$ is large enough.

A possible form of function $\Phi(\xi)$ is given in Figure 1.2, in the special case in which $\alpha_1 = 0$. So you can say that in the examined examples, the stability of P_2 depends on whether or not the support of $\phi(x)$ is bounded. If it is bounded, then P_2 can become unstable depending on the parameters characterizing the kernel $\phi(x)$, i.e. on the features of the kernel. In this case some spatially heterogeneous solutions can appear.

Proceeding as above, it is an easy matter to show that replacing $P^* = P_0 = 0$ (the "no-vaccinators" scenario) in eigenvalue problem (1.5.10), we obtain instability (since $\Phi(\xi) = D\xi^2 - 1$); moreover if $\alpha > 1$ (that correspond to biological existence of P_2), also $P_1 = 1$ is unstable:

$$\Phi(\xi) = D\xi^2 + 1 - \alpha. \tag{1.5.18}$$

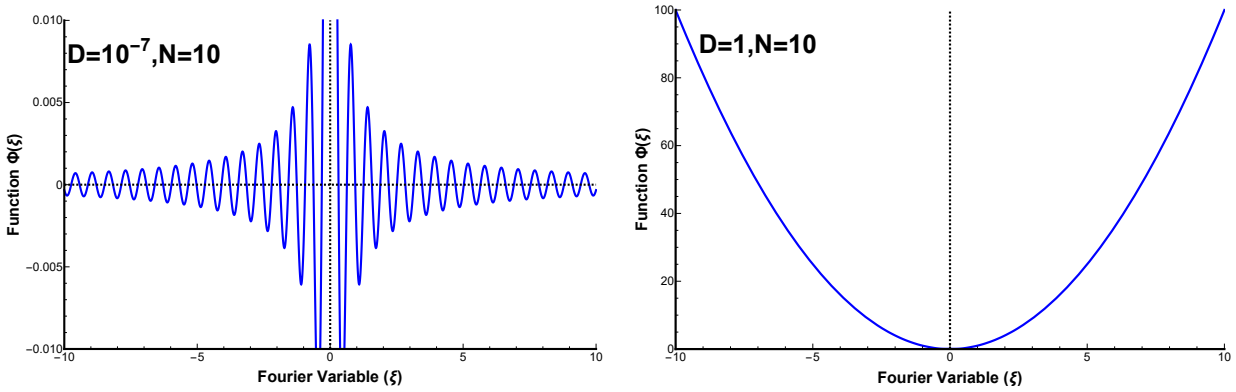

(a) (b)

Figure 1.2: Representation of function $\Phi(\xi)$ in the event $\phi(x) = \phi_4(x)$ with parameters listed in Fig. 1.1 and $h = 10$.

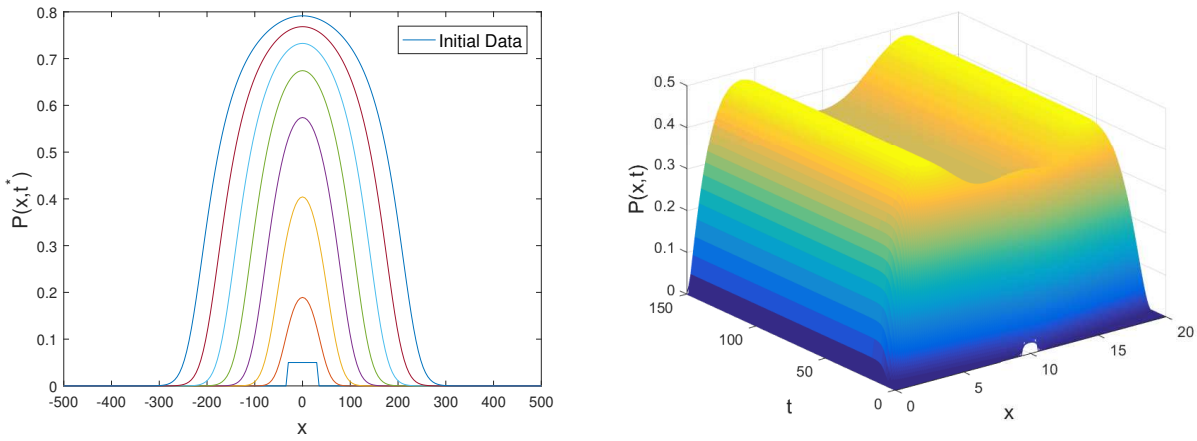

(a) (b)

Figure 1.3: Illustration of stability character of equilibrium P_2 in equation (1.2.10), with $\phi(x) = \phi_4(x)$. In (a) $\alpha_1 = 0.6$, $\alpha_2 = 0.7$, $D = 100$ and $h = 3$. In (b) $\alpha_1 = 0.9$, $\alpha_2 = 1.7$, $D = 0.6$ and $h = 7$

In the unlikely event that $\alpha \leq 1$, instead, the all-vaccinator homogeneous equilibrium $P_1 = 1$ is LAS.
In Figure 1.3 an illustration of stability analysis of equilibrium P_2 is given for equation (1.5.8). The equation (1.2.10) is simulated with the step function $\phi_4(x) = 1/(2h)Hev(h - |x|)$ as kernel. Choosing a small perturbation as initial data, in Figure 1.3-(a), the solution evolves in time approaching to the stable equilibrium P_2; while in Figure 1.3-(b) the loss of stability of the constant equilibrium point P_2 and the convergence to a periodic spatial structure is shown. The numerical results confirm the analytical ones: in the case where D is sufficiently large and the step h small, P_2 is LAS, if D is small and h increases, we see convergence to non-constant structures.

Stability of uniform equilibria: Ω bounded

Assuming now that Ω is bounded, we obtain the following equation from (1.2.10)

$$\partial_t P = D\nabla^2 P + P(1-P)\left(1 - \alpha_1 P - \alpha_2 \int_\Omega \phi(x-y)P(y,t)dy\right), \tag{1.5.19}$$

with $t > 0$, $x \in \Omega$ and Neumann conditions (1.2.11).
For the sake of notation simplicity we will consider here $\Omega = [-L, L]$.
The eigenvalues problem obtained as a result of the linearization about a generic steady state P^* is given by the equality

$$DW'' + \left[(1-2P^*)(1-\alpha P^*) - \alpha_1 P^*(1-P^*)\right] W - \alpha_2 P^*(1-P^*)\int_{-L}^{L} \phi(x-y)W(y)dy = \lambda W. \tag{1.5.20}$$

Since for both the NVE and the PVE equilibria $P^* = P_0 = 0$ and $P^* = P_1 = 1$ the non–local term disappears, the resulting local stability analisys is straightforward and it is omitted. Therefore, we will only focus on the behavioral equilibrium $P_2 = 1/\alpha$.
Here, we make some assumptions. We will suppose that the function $\phi(x)$ is defined on the whole axis and that it is periodic with the period $2L$:

$$\phi(x + 2Lm) = \phi(x), \quad -L \le x \le L, \quad m = \pm 1, \pm 2, ... \tag{1.5.21}$$

Taking $P^* = P_2$, brings to the eigenvalue problem

$$DW'' - P_2(1-P_2)\left(\alpha_1 W + \alpha_2 \int_{-L}^{L} \phi(x-y)W(y)dy\right) = \lambda W,$$

in the form

$$w(x) = \cos(\xi_m x), \ \xi_m = \frac{m\pi}{L}, \ m = 0, 1, 2, ...$$

Note that the boundary conditions (1.2.11) are satisfied. Taking into account that function ϕ is periodic and even, we obtain

$$\int_{-L}^{L} \phi(x-y)\cos(\xi_m y)\, dy = \cos(\xi_m x)\int_{-L}^{L} \phi(z)\cos(\xi_m z)\, dz.$$

Thus, we have that the m–th eigenvalue reads as follows:

$$\lambda_m^* = -D\xi_m^2 - P_2(1-P_2)(\alpha_1 + \alpha_2\phi_m), \tag{1.5.22}$$

where

$$\phi_m = \int_{-L}^{L} \phi(z)\cos(\xi_m z)\, dz. \tag{1.5.23}$$

We note that λ_m^* is negative for $m = 0$, while, for m sufficiently large, it can be positive for some intermediate values of m depending on the function ϕ and on the values of parameters, similarly to what we observed in the continuous spectrum analysis.
Let us now consider $\phi(x) = \phi_3(x) = (1/(2h))Hev(h - |x|)$, $0 < h < L$. Then

$$\phi_m = \frac{1}{\xi_m h}\sin(\xi_m h). \tag{1.5.24}$$

Consider the functions

$$\Phi_m(h) = -D\xi_m^2 - P_2\left(1 - P_2\right)\left(\alpha_1 + \alpha_2 \frac{1}{\xi_m h}\sin\left(\xi_m h\right)\right),\ m = 1, 2, ...$$

If $\Phi_m(h)$ is a positive function, then the corresponding eigenvalue λ_m^* is also positive. Let us find the conditions on parameters when the maximal eigenvalue is zero (stability boundary). From the conditions

$$\Phi_m(h) = 0, \quad \Phi_m^{'}(h) = 0,$$

where prime denotes the derivative with respect to h, we obtain

$$\nu = \tan\nu, \quad m^2 P_2(1 - P_2)(\alpha_1 + \frac{\alpha_2}{\nu}\sin\nu) = 0, \tag{1.5.25}$$

where $\nu = \xi_m h$. The first relation in (1.5.25) allows us to find ν, and the second relation determines the stability boundary.

1.6 Bifurcation Analysis for nonlocal information in case of bounded Ω

In the case of nonlocal information and bounded one-dimensional Ω, it is possible to carry out the bifurcation analysis (a.k.a. weakly nonlinear analysis) for equation (1.5.19) under the assumption that D is the bifurcation parameter [163].
The stationary non-homogenus solutions of the model solve

$$DP'' + P(1 - P)\left(1 - \alpha_1 P - \alpha_2 \int_{-L}^{L} \phi(x - y)P(y, t)dy\right) = 0, \tag{1.6.1}$$

with $P'(-L) = P'(L) = 0$ and assuming that conditions (1.5.21) for the kernel $\phi(x)$ hold.
The equilibrium state $P(x) = P_2 = 1/\alpha$ is a solution of (1.6.1), independently from the values assumed by D.
If D crosses a bifurcation value D_0, a simple real eigenvalue of the linearized problem crosses zero. In order to study this bifurcation, we look for solutions of (1.6.1) in the form of the expansion

$$P(x) = P_2 + \varepsilon p_1(x) + \varepsilon^2 p_2(x) + ...$$

where ε is a small parameter. We set

$$D = D_0 + \varepsilon D_1 + \varepsilon^2 D_2 + ...$$

Substituting these expansions into equation (1.6.1) and equating the terms in ε^1, we get

$$D_0 p_1''(x) - \alpha_1 P_2(1 - P_2)p_1(x) - \alpha_2 P_2(1 - P_2)\int_{-L}^{L} \phi(x - y)p_1(y)dy = 0, \tag{1.6.2}$$

with $p_1(-L) = p_1(L) = 0$. This problem coincides with eigenvalue problem (1.5.20) with $P^* = P_2$ and $\lambda = 0$. Hence the value D_0 should be chosen in such a way that this eigenvalue problem has a zero

eigenvalue, $p_1(x) = \cos(\xi_m x)$ is the corresponding eigenfunction, with m an integer, $m \neq 0$.
Next, we equate the terms with ε^2:

$$D_0 p_2''(x) - \alpha_1 P_2(1-P_2)p_2(x) - \alpha_2 P_2(1-P_2)\int_{-L}^{L}\phi(x-y)p_2(y)dy = f, \tag{1.6.3}$$

where $p_2(-L) = p_2(L) = 0$ and

$$\begin{aligned} f &= -D_1 p_1''(x) + (1+\alpha_1 - 3\alpha_1 P_2 - \alpha_2 P_2)\, p_1(x)^2 + \alpha_2(1-2P_2)\, p_1(x)\int_{-L}^{L}\phi(x-y)p_1(y)dy = \\ &= \left(-D_1 + \frac{1-2P_2}{P_2(1-P_2)} D_0 p_1(x)\right) p_1''(x) + (1+\alpha_1 - 3\alpha_1 P_2 - \alpha_2 P_2 + \alpha_1(2P_2-1))\, p_1^2(x). \end{aligned}$$

In order to obtain solvability conditions for problem (1.6.3), let us note that problem (1.6.2) is self-adjoint since the kernel ϕ is an even function. Indeed, it can be directly verified that [163]

$$\int_{-L}^{L} v(x)(\mathcal{L}_{\mathcal{H}}P)(x)dx = \int_{-L}^{L} P(x)(\mathcal{L}_{\mathcal{H}}v)(x)dx,$$

where $\mathcal{L}_{\mathcal{H}}$ is the operator which corresponds to the left-hand side of (1.6.2) and which acts on C^2 functions satisfying the boundary conditions. Hence problem (1.6.3) is solvable if and only if [163]

$$\int_{-L}^{L} f(x)p_1(x)dx = 0.$$

Therefore

$$D_1 = \frac{D_0(1-2P_2)}{P_2(1-P_2)} \frac{\displaystyle\int_{-L}^{L} p_1^3(x)dx}{\displaystyle\int_{-L}^{L} p_1^2(x)dx} = 0,$$

and

$$p_2(x) = A\left(1 + B\cos(2\xi_m x)\right),$$

where

$$A = \frac{D_0\xi_m^2(2P_2-1)}{2P_2(P_2-1)^2}, \quad B = \frac{(1-P_2)}{4D_0\xi_m^2 + P_2(1-P_2)(\alpha_1 + \alpha_2\phi_{2m})}.$$

The terms with ε^3 give the problem

$$D_0 p_3''(x) - \alpha_1 P_2(1-P_2)p_3(x) - \alpha_2 P_2(1-P_2)\int_{-L}^{L}\phi(x-y)p_3(y)dy = f_1, \tag{1.6.4}$$

where

$$\begin{aligned} f_1 &= -D_2 p_1'' - \alpha_1 p_1^3 + (2 + 2\alpha_1 - 6\alpha_1 P_2 - 2\alpha_2 P_2)p_1(x)p_2(x) + \alpha_2\left[(1-2P_2)p_2(x) - p_1^2(x)\right] + \\ &+ \int_{-L}^{L}\phi(x-y)p_1(y)dy + \alpha_2(1-2P_2)p_1(x)\int_{-L}^{L}\phi(x-y)p_2(y)dy = \\ &= \left(-D_2 + D_0\frac{(1-2P_2)p_2(x)}{P_2(1-P_2)} - D_0\frac{3P_2^2 - 3P_2 + 1}{P_2^2(1-P_2)^2}p_1(x)^2\right)p_1'' + D_0\frac{1-2P_2}{P_2(1-P_2)}p_1(x)p_2''. \end{aligned}$$

From the solvability condition [163]

$$\int_{L}^{-L} f_1(x)p_1(x)dx = 0,$$

we obtain

$$D_2 = D_0 \frac{4A(2+5B)P_2^3 - 3[3+2A(2+5B)]P_2^2 + [9+2A(2+5B)]P_2 - 3}{4P_2^2(1-P_2)^2}.$$

If $D_2 \neq 0$, then from the expansion for D we obtain

$$\varepsilon = \pm\sqrt{\frac{D-D_0}{D_2}},$$

and up to the second-order terms,

$$P(x) = P_2 + \varepsilon P_1(x) + \varepsilon^2 P_2(x). \tag{1.6.5}$$

The bifurcation is supercritical ($D > D_0$) for $D_2 > 0$ and $P_2 > \frac{1}{2}$. The bifurcation is subcritical ($D < D_0$) if the ratio $(2P_2 - 1)/D_2$ is negative.

1.7 Traveling Waves and Generalized Traveling Waves

Preliminarly, recall that in section 1.2, has been emphasized that in case of constant rate of transfer from the strategy "vaccine" to the strategy "no–vaccine" ($\alpha(M_{se})$), the model is equivalent to the most prototypical equation generating *traveling waves*, the Fisher-Kolmogorov equation (1.2.12). However, this case can more be considered as pathological than a realistic scenario.
In this section, it is investigated the non-pathological cases (from the epidemiological viewpoint) for the onset of possible traveling waves [122, 123], i.e. heteroclinic connections between two equilibria.
In this section, we restrict the analysis to the case in which the domain Ω is one-dimensional and unbounded, i.e. $\Omega = \mathbb{R}$.

1.7.1 Local Information

Wave solutions for equation (1.3.1)

$$\partial_t P = \nabla^2 P + P(1-P)(1-\alpha P),$$

are function of the form $P(x-ct) = p(z)$, bounded on the whole axis and twice continuously differentiable. The constant c is the speed of the wave, $z = x - ct$ is the moving coordinate frame and

$$\lim_{x\to\pm\infty} P(x) = P_{\pm} \tag{1.7.1}$$

with P_- and P_+ homogeneous in space equilibria of equation (1.3.1). After substitution of variable z in equation (1.3.1), the following ordinary differential equation is obtained:

$$Dp'' + cp' + p(1-p)(1-\alpha p) = 0. \tag{1.7.2}$$

It is known that, a necessary condition for the existence of the solution is that the P_- must have an unstable (departing) manifold and P_+ a stable (incoming) manifold. The following result holds [162]:

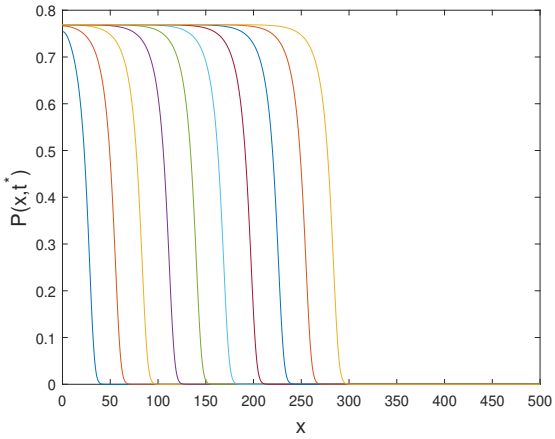

(a)

Figure 1.4: Traveling wave for equation (1.3.1) with $\alpha_1 = 0.6$, $\alpha_2 = 0.7$, $D = 2$ and $c = 2\sqrt{2}$.

Theorem 1.7.1 *If $\alpha > 1$, there exists a constant $c^{(1)} = 2\sqrt{D}$ such that $\forall\ c \in [c^{(1)}, +\infty[$, there exists a travelling wave solution of velocity c connecting equilibrium $P_2 = 1/\alpha$ and equilibrium $P_0 = 0$, i.e. a function $P(x - ct)$, solution of equation (1.7.2) on the real line $]-\infty, +\infty[$ and satisfying equation (1.7.1) with $P_- = P_2$ and $P_+ = P_0$. This solution is monotone decreasing and the derivatives $P''(z)$ and $P'(z)$ tend to zero as $x \to \pm\infty$. Moreover, a traveling wave solution of velocity c conncecting equilibria P_1 and P_0 cannot exist.*

For bounded Ω,it has been shown that the spatially homogenous equilibrium P_2 is GAS. In the above theorem it is shown, roughly speaking, that the TW are such that the scenario where the value $P = P_2$ spreads until it invades all the space.
The case $0 < \alpha < 1$ has here some further mathematical interest, since the equation can be read as a modification of the Fisher-Kolmogorov equation. The following result holds [162]

Theorem 1.7.2 *If $0 < \alpha < 1$, there exists a constant $c^{(1)}$ such that $\forall\ c \in [c^{(1)}, +\infty[$, there exists a travelling wave solution of velocity c connecting equilibrium $P_1 = 1$ and equilibrium $P_0 = 0$, i.e. a function $P(x-ct)$, solution of equation (1.7.2) on the real line $]-\infty, +\infty[$ and satisfying equation (1.7.1) with $P_- = P_1$ and $P_+ = P_0$. This solution is monotone decreasing and the derivatives $P''(z)$ and $P'(z)$ tend to zero as $x \to \pm\infty$.*

Traveling wave solutions for the equation (1.3.1) are shown in Figure 1.4 in the case in which $\alpha > 1$. They connect the constant state P_2 at $-\infty$ and the constant state P_0 at $+\infty$, with the minimal speed $c = c^{(1)} = 2\sqrt{D}$.

1.7.2 Non–local information

In previous section, it was demonstrated that, in the case of non–local information, the spatially homogeneous equilibrium solution $P_2 = 1/\alpha$ can lose its stability. Then some spatial structures can bifurcate from it. Therefore, instead of travelling waves connecting P_0 and P_2, we can expect the existence of some other

solutions connecting P_0 at $+\infty$ with some structures at $-\infty$. Such solutions are called *generalized travelling waves* (GTW) and were first introduced in [160] for reaction-diffusion systems. Such solutions can be characterized by two main properties:
(1) They exist for all $t \in \mathbb{R}$. Moreover, under some conditions, such solution can be unique and stable.
(2) They are propagating solutions, which can be explained as follows: let q be a constant, $P_+ < q < P_-$. For each t fixed consider the equation $P(x,t) = q$ with respect to x. Denote by $m_q^+(t)$ its maximal solution (if it exists) and by $m_q^-(t)$ its minimal solution. If $\frac{m_q^{\pm}(t)}{t} \to c$ as $t \to \infty$, then we say that this solution propagates with the speed c. Thus, GTW are global propagating solutions.
Thus, we want to study GTW solution for the equation

$$\partial_t P = D\nabla^2 P + P(1-P)\left(1 - \alpha_1 P - \alpha_2 \int_{-\infty}^{\infty} \phi(x-y)P(y,t)dy\right). \tag{1.7.3}$$

Consider the Cauchy problem for the equation

$$\partial_t P = D\nabla^2 P + c\frac{\partial P}{\partial x} + P(1-P)\left(1 - \alpha_1 P - \alpha_2 \int_{-\infty}^{\infty} \phi(x-y)P(y,t)dy\right), \tag{1.7.4}$$

with $c \geq 2\sqrt{D}$ a given constant. Assume that the initial condition $P(x,0) = P^0(x)$ is non-negative and less than 1. Then the solution $P(x,t)$ exists and is also non-negative and less than 1 for all $t \geq 0$. Consider

$$J(x,t) \equiv \int_{-\infty}^{\infty} \phi(x-y)P(y,t)dy \geq 0.$$

Hence

$$d(x,t) \equiv 1 - \alpha_1 P - \alpha_2 J(x,t) \leq 1.$$

Equation (1.7.4) becames

$$\partial_t P = D\nabla^2 P + c\frac{\partial P}{\partial x} + P(1-P)d(x,t). \tag{1.7.5}$$

Consider also the equation

$$\partial_t v = D\nabla^2 v + c\frac{\partial v}{\partial x} + v(1-v). \tag{1.7.6}$$

The following result holds:

Lemma 1 *If $c \geq 2\sqrt{D}$, there exists a stationary solution $v_c(x)$ of (1.7.6) such that*

$$P(x,0) < v_c(x),\ x \in \mathbb{R} \ \Rightarrow\ P(x,t) < v_c(x),\ x \in \mathbb{R},\ t > 0. \tag{1.7.7}$$

Proof. Denoting $z = v - P$ and taking the difference of equations (1.7.6) and (1.7.5), we obtain

$$\partial_t z = D\nabla^2 z + c\frac{\partial z}{\partial x} + z(1-v-P) + P(1-P)\left(1 - d(x,t)\right). \tag{1.7.8}$$

Since the last term in the right-hand side of equation (1.7.8) is non-negative, then from the inequality $z(x,0) > 0$ for all $x \in \mathbb{R}$, it follows that $z(x,t) > 0$ for all $t > 0$ and $x \in \mathbb{R}$. Hence,

$$P(x,0) < v(x,0),\ x \in \mathbb{R} \ \Rightarrow\ P(x,t) < v(x,t),\ x \in \mathbb{R},\ t > 0. \tag{1.7.9}$$

Stationary solutions of equation (1.7.6) correspond to traveling waves for the KPP-equation [75, 94]. If $c \geq 2\sqrt{D}$, then they are monotone in space and stable, while for $0 < c < 2\sqrt{D}$ they are nonmonotone and unstable ([94]-[162]). These waves have limits at infinity: $v(-\infty) = 1$, $v(+\infty) = 0$.
Denoting by $v_c(x)$ a stationary solution of equation (1.7.6) for $c \geq 2\sqrt{D}$, the claim is proved. □
Thus, this is estimate from above of the solution of the Cauchy problem associated to (1.7.5). An estimate is now provided from below. From the inequality (1.7.9),

$$J(x,t) \leq \int_{-\infty}^{+\infty} \phi(x-y)v_c(y)dy \equiv K(x). \tag{1.7.10}$$

Assuming $w < 1$, consider the equation

$$\partial_t w = D\nabla^2 w + c\frac{\partial w}{\partial x} + w(1-w)(1-\alpha_1 v_c - \alpha_2 K(x)). \tag{1.7.11}$$

Denoting $s = P - w$ and taking the difference between equations (1.7.5) and (1.7.11), you obtain

$$\partial_t s = D\nabla^2 s + c\frac{\partial s}{\partial x} + s(1-P-w)(1-\alpha_1 v_c - \alpha_2 J(x)) + \alpha_1 P(1-P)(v_c - P) + \alpha_2 P(1-P)(K(x) - J(x,t)). \tag{1.7.12}$$

Since the last two terms in the right-hand side of this equation are non-negative, then

$$w(x,0) \leq P(x,0),\ x \in \mathbb{R},\ \Rightarrow\ w(x,t) \leq P(x,t),\ x \in \mathbb{R},\ t > 0. \tag{1.7.13}$$

The following result holds:

Lemma 2 *If $c \geq 2\sqrt{D}$, there exists a stationary solution $w_c(x)$ of (1.7.11) such that $w_c(x_0) = 0$ for some x_0, $w_c(x) > 0$ for $x > x_0$, $w_c(x) < 0$ for $x < x_0$ and $w_c(x) \sim v_c(x)$, when $x \to \infty$*

Proof. Stationary solution of equation (1.7.11) are sought, i.e.

$$Dw'' + cw' + w(1-w)(1-\alpha_1 v_c - \alpha_2 K(x)) = 0. \tag{1.7.14}$$

Since v_c and $K(x)$ tend to zero when $x \to \infty$, then $1 - \alpha_1 v_c - \alpha_2 K(x)$ is close to 1 in some right half-axis. Then, for $c \geq 2\sqrt{D}$, solutions of (1.7.14) are close to functions $v_c(x)$ when $x \to \infty$.
Let us prove the existence of a solution which has a zero. Denote $g(x) = 1 - \alpha_1 v_c - \alpha_2 K(x)$ and let $I = (-\infty, \omega)$ be the interval where $g(x) < 0$: then any non-zero solution of (1.7.14) has at most one zero in I. Indeed, let $w(x)$ be solution of (1.7.14) and x_0 one of its zeros. Put

$$W(x) = e^{\frac{c}{D}(x-x_0)} w(x)w'(x),\ x \in I. \tag{1.7.15}$$

Taking into account equation (1.7.14), we have

$$W'(x) = e^{\frac{c}{D}(x-x_0)} \left((w')^2 - \frac{w^2}{D}(1-w)g(x) \right) \geq 0. \tag{1.7.16}$$

So W is nondecreasing on I. If W has another zero $x_1 \in I$, then $W(x) = 0$ on $[x_0, x_1]$. Thus w is constant on $[x_0, x_1]$, namely $w = 0$ (from (1.7.14)) on $[x_0, x_1]$ and consequently on I. The contradiction shows that w has at most one zero in I.

Since $w(x)$ converges to zero when $x \to \infty$, there exists x^* large enough such that we can assum that equation (1.7.14) becomes:

$$Dw'' + cw' + g(x)w = 0. \tag{1.7.17}$$

Let $c > 2\sqrt{D}$. Since $g(x) \to 1$ at infinity, there exist two linearly independent solutions of equation (1.7.17) given by [130]

$$w_1(x) \sim e^{-\lambda_1 x}, \quad w_2(x) \sim e^{-\lambda_2 x}, \tag{1.7.18}$$

where λ_1 and λ_2 are solution of the algebraic equation

$$D\lambda^2 - c\lambda + 1 = 0.$$

If $\lambda_1 > \lambda_2$, then the general solution of (1.7.17) can be written as

$$w(x) = k_1 w_1(x) + k_2 w_2(x), \ x \in \mathbb{R},$$

where k_1 and k_2 are real constants. $k_1 < 0$ and $k_2 > 0$ can be choosen such that $w(x)$ has an only zero x_0 and $w(x) < 0$ for $x < x_0$, $w(x) > 0$ for $x > x_0$. In addition, $w(x)$ behaves as $v_c(x)$ if $c > 2\sqrt{D}$: so that, it can possible the estimation $w(x) \leq P(x,0) \leq v_c(x)$ for the initial condition.
If $c = 2\sqrt{D}$, then $\lambda_1 = \lambda_2$. Then the qualitative behavior of the solutions of equation (1.7.17) as $x \to \infty$ is determined by

$$w(x) = w_1(x)\left(k_1 + k_2 x\right), \tag{1.7.19}$$

with k_1 and k_2 real constants. $k_1 < 0$ and $k_2 > 0$ can be choosen such that $w(x)$ has an only zero x_0 and $w(x) < 0$ for $x < x_0$, $w(x) > 0$ for $x > x_0$. This result can be achieved choosing both the constants k_1 and k_2 positive. In addition, $w(x)$ behaves as $v_c(x)$ if $c = 2\sqrt{D}$: so that, it is possible the estimation $w(x) \leq P(x,0) \leq v_c(x)$ for the initial condition. □

Lemma 3 *Let $z_1(x) = \max(0, w_c(x))$, and $z_2(x) = v_c(x)$. If*

$$z_1(x) < P^0(x) < z_2(x), \ x \in \mathbb{R}$$

then the solution of the Cauchy problem for equation (1.7.4) with the initial condition $P^0(x)$ satisfies the estimate

$$z_1(x) < P(x,t) < z_2(x), \ x \in \mathbb{R}$$

for all $t > 0$.

Theorem 1.7.3 *There exist positive GTW solutions of equation (1.7.3) for all $c \geq 2\sqrt{D}$. Positive GTW converging to zero as $x \to \infty$ do not exist for $c < 2\sqrt{D}$.*

Proof. The existence of GTWs for all $c \geq 2\sqrt{D}$ follows from the previous lemma. Indeed, consider solution of equation (1.7.3) in the form $P(x,t) = P(x - ct, t)$. Then

$$\partial_t P = D\nabla^2 P + c\nabla P + P(1-P)\left(1 - \alpha_1 P - \alpha_2 \int_{-\infty}^{\infty} \phi(x-y)P(y,t)dy\right). \tag{1.7.20}$$

It follows from Lemma 3 that there exists an ω-limit solution $P_c(x,t)$ of equation (1.7.20) such that

$$z_1(x) \le P_c(x,t) \le z_2(x), \tag{1.7.21}$$

for all $t \in \mathbb{R}$. In order to construct this solution, consider the solution $P(x,t)$ of equation (1.7.20) with an initial condition $P^0(x)$ which satisfies the inequality $z_1(x) \le P^0(x) \le z_2(x)$ for all x. Let $t_n \to \infty$ as $n \to \infty$. Consider next solutions $P_n(x,t)$ with the initial conditions $P_n^0 = P(x,t_n)$. Obviously, each of them is defined for $t > -t_n$. A locally convergent subsequence of the sequence of functions $P_n(x,t)$ is a solution of equation (1.7.20) defined for all $t \in \mathbb{R}$. It satisfies inequality (1.7.21). It can be easily verified that it is a GTW with the speed c.

Suppose now that there exists a positive GTW $P_c(x,t)$, converging to 0 as $x \to \infty$, with a speed $c < 2\sqrt{D}$. Then $P_c(x-ct,t)$ satisfies equation (1.7.20). Let us take $c < c_0 < 2\sqrt{D}$ and consider the equation

$$DP'' + c_0 P' + P(1-P) = 0. \tag{1.7.22}$$

It has a solution $P_0(x)$ that is non-monotone and unstable [94]. Moreover, when x tends to infinity, then $P_0(x) \sim exp(-c_0 x/2)\sin(ax)$, where $a = \sqrt{D|c_0^2/4 - 1|}$. Therefore, equation

$$\partial_t P = D\nabla^2 P + c\nabla P + P(1-P), \tag{1.7.23}$$

has a solution $P^*(x,t) = \varepsilon P_0(x - (c_0 - c)t)$, where ε is a positive constant. Let $x = N_1$ and $x = N_2$ be two consecutive zeros of the function $P_0(x)$ such that $P_0(x)$ is positive between them. Then $P^*(x,t)$ is a solution of the boundary value problem for equation (1.7.23) in the domain

$$N_1 + (c_0 - c)t \le x \le N_2 + (c_0 - c)t$$

with the zero boundary conditions. For ε small enough, similarly to (1.7.9) we can obtain the inequality

$$P^*(x,t) < P_c(x-ct,t), \quad N_1 + (c_0 - c)t \le x \le N_2 + (c_0 - c)t. \tag{1.7.24}$$

If $m_a(t)$ is the maximal solution of the equation

$$P_c(x,t) = a, \quad 0 < a < \max_{N_1 + (c_0 - c)t \le x \le N_2 + (c_0 - c)t} P^*(x,t), \tag{1.7.25}$$

then

$$\overline{\lim_{t\to\infty}} \frac{m_a(t)}{t} \ge c_0. \tag{1.7.26}$$

Since $c_0 > c$ and $P_c(x,t)$ converges to zero as $x \to \infty$, then the last inequality contradicts the assumption that $P_c(x,t)$ is a GTW with the speed c.

This contradiction proves the theorem. □

Numerical Simulations

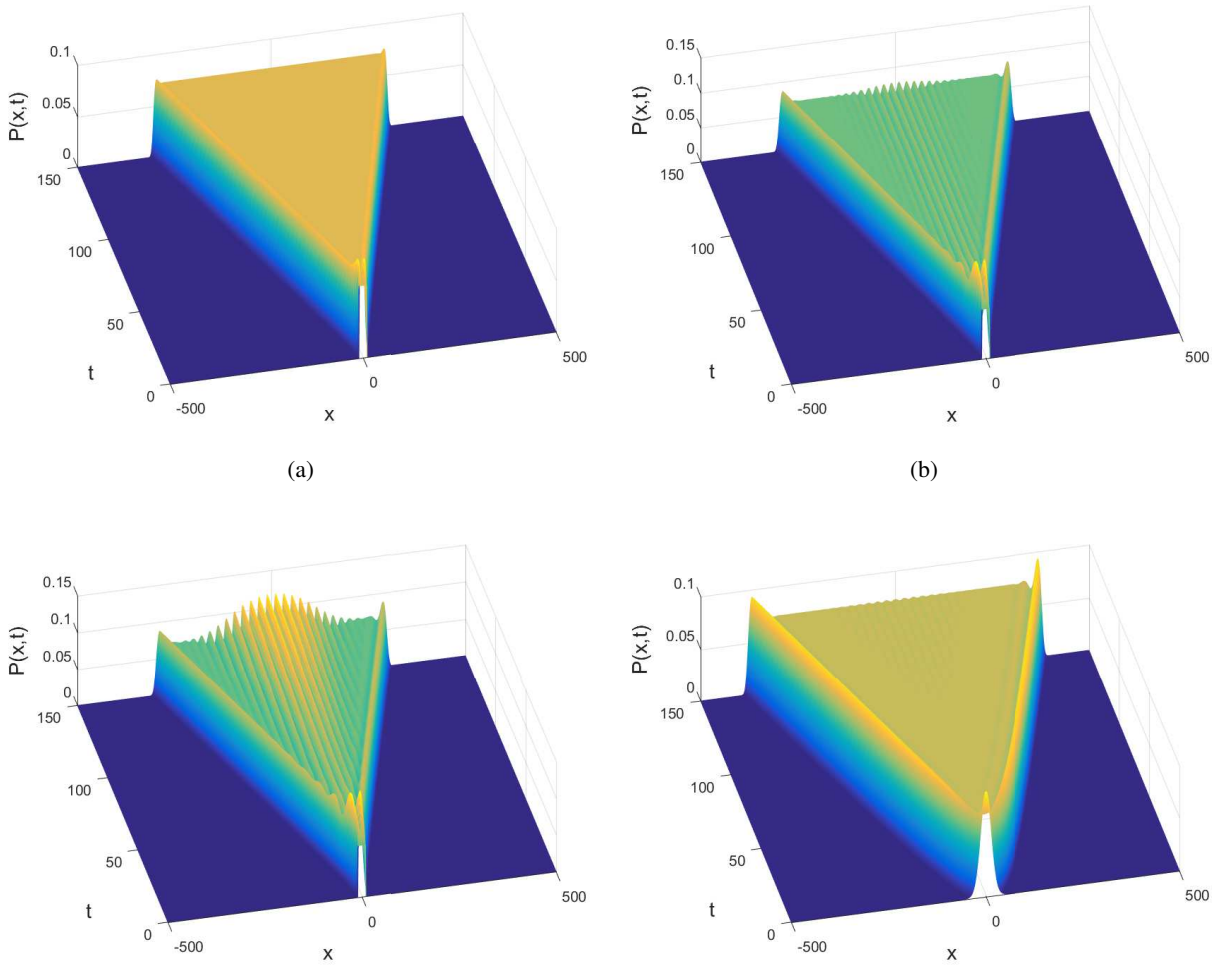

Figure 1.5: Propagation of waves (a) and periodic wave (b)-(c)-(d) for equation (1.2.10). Solution $P(x,t)$ as a function of two variables. Here $\alpha_1 = 1.1$, $\alpha_2 = 13.1$, $D = 1$. Moreover $h = 7$ in (a), $h = 13$ in (b), $h = 14$ in (c) and $h = 16$ in (d).

In Figure 1.5 the results of numerical simulations of equation (1.2.10) in one space dimensions are presented. The kernel is the function $\phi_4(x)$. If the support of ϕ is suffciently small, then there is a usual travelling wave propagating with a constant speed. Figure 1.5-(a) shows the solution $P(x,t)$ of equation (1.2.10) with the initial condition which has a bounded support. The solution represents two waves propagating in the opposite directions. It is interesting to note that the wave is not monotone with respect to x. If you increase the support of the function ϕ, then the homogeneous in space stationary solution P_2 loses its stability and a periodic in space structure appears. In this case it is easy to observe propagation of a periodic wave (Figure 1.5, (b)-(c)). Figure 1.5-(d) shows the solution $P(x,t)$ with the exponentially decaying initial conditions. Therefore, depending on the values of parameters equation (1.2.10) can have solutions of different types. For all other parameters fixed, usual traveling waves (with a constant speed and profile) are observed for sufficiently small values of h. Periodic traveling waves exist for sufficiently large h. Transition from simple

to periodic waves occurs due to the essential spectrum crossing the imaginary axis. The stationary solution homogeneous in space P_2 loses its stability resulting in the appearance of a stationary periodic solution. The traveling wave connects the constant value P_0 for $x = +\infty$ with this periodic solution for $x \longrightarrow -\infty$. The waves in (a)-(b)-(c) (in which the initial data has a bounded support) move at their minimal speed $c = 2\sqrt{D} = 2$ and this speed doesn't depends on h; while, the speed of the wave (d) is greater than the minimal speed $c > 2\sqrt{D}$ and depends on h. Though in numerical simulations a finite interval is considered, if it is suffciently large, then the solution can approach the corresponding GTW.

1.8 The role of the memory of past information

Here it is assumed that the information is not only spatially and but also temporally non–local: the subjects take their decisions not only on the information on the current state of the system but also on the past states. In other words, the memory of the subjects concerning the past information about vaccine side-effects is included. We consider in this section the 1D unbounded domain, i.e. $\Omega = \mathbb{R}$.
These assumptions yield:

$$\alpha(M_{se}(P)) = \alpha_0 + \alpha_1 \int_0^{+\infty} W(\tau)P(x, t-\tau)d\tau + \alpha_2 \int_\Omega \int_0^{+\infty} \phi(x-y)W(\tau)P(y, t-\tau)d\tau dy, \quad (1.8.1)$$

with $W(\tau)$ a delaying kernel, i.e. a positive function such that $\int_0^{+\infty} W(\tau)d\tau = 1$. Using scaling (1.2.9), previous equation becomes:

$$\partial_t P = D\nabla^2 P + P(1-P)\left(1 - \alpha_1 \int_0^{+\infty} W(\tau)P(x, t-\tau)d\tau - \alpha_2 \int_\Omega \int_0^{+\infty} \phi(x-y)W(\tau)P(y, t-\tau)d\tau dy\right), \quad (1.8.2)$$

with $t > 0$, $x \in \Omega$.
Here, the so called acquisition–fading kernel (AFK) [67] is given:

$$W(\tau) = \frac{bd}{d-b}\left(e^{-b\tau} - e^{-d\tau}\right), \quad (1.8.3)$$

with $0 < b < d$. This memory kernel, which is such that $W(0) = 0$ (i.e. absence of information of the current state of the process), models the process of temporal acquisition of information (with a rapid timescale $1/d$) followed by a fading of the memory (with a "slow" timescale $1/b$).
By applying the linear chain trick (see the Appendix A) one gets the following equivalent system:

$$\begin{aligned} \partial_t P &= D\nabla^2 P + P(1-P)(1 - \alpha_1 M - \alpha_2 J(M)), \\ \partial_t Z &= b(P - Z), \\ \partial_t M &= d(Z - M). \end{aligned} \quad (1.8.4)$$

1.8.1 Stability of Stationary Solutions

Model (1.8.4) is remindful of systems generating complex self-organized patterns in biochemistry and in population biology [116, 122], since only one of the involved state densities is endowed of diffusion. The

aim of this section is to investigate the possible bifurcation from the homogenous equilibria of (1.8.4) of such self-organized structures.
It is easy to verify that model (1.8.4) admits the following homogeneous in space stationary solutions

$$\mathbf{E}_0 = (0,0,0), \quad \mathbf{E}_1 = (1,1,1), \quad \mathbf{E}_2 = \left(\frac{1}{\alpha}, \frac{1}{\alpha}, \frac{1}{\alpha}\right).$$

Also here, is the most significant is $\mathbf{E}_2$. Considering the case where Ω is unbounded and linearizing (1.8.4) at $\mathbf{E}_2$ yields the following eigenvalue problem:

$$\begin{aligned} D\nabla^2 P - \frac{1}{\alpha}\left(1-\frac{1}{\alpha}\right)(\alpha_1 M + \alpha_2 J(M)) &= \lambda P, \\ b(P-Z) &= \lambda Z, \\ d(Z-M) &= \lambda M, \end{aligned} \tag{1.8.5}$$

whose essential spectrum is given by:

$$\begin{aligned} -D\xi^2\tilde{P} - \frac{1}{\alpha}\left(1-\frac{1}{\alpha}\right)\left(\alpha_1\tilde{M} + \alpha_2\tilde{M}\tilde{\phi}(\xi)\right) - \lambda\tilde{P} = 0, \\ \tilde{M} = \frac{bd}{(\lambda+b)(\lambda+d)}\tilde{P}. \end{aligned} \tag{1.8.6}$$

Thus, one obtains the following ξ-family of λ polynomials

$$q(\lambda,\xi) = \lambda^3 + a_2(\xi)\lambda^2 + a_1(\xi)\lambda + a_0(\xi) = 0, \tag{1.8.7}$$

where

$$\begin{aligned} a_2(\xi) &= b + d + D\xi^2 > 0, \\ a_1(\xi) &= bd + D\xi^2(b+d) > 0, \\ a_0(\xi) &= \frac{bd}{\alpha^2}\left[D\xi^2\alpha^2 + (\alpha-1)(\alpha_1 + \alpha_2\widetilde{\phi})\right]. \end{aligned}$$

Thus $\mathbf{E}_2$ is stable iff $a_0(\xi) > 0$ and

$$H_1(\xi) = a_2(\xi)a_1(\xi) - a_0(\xi) > 0,$$

that is:

$$H_1(\xi) = \frac{1}{\alpha^2}\left\{(d+b)D^2\xi^4\alpha^2 + (b+d)^2 D\xi^2\alpha^2 + bd\left[(b+d)\alpha^2 - (\alpha-1)(\alpha_1+\alpha_2\widetilde{\phi})\right]\right\} > 0. \tag{1.8.8}$$

Recall that a change of sign of H_1 in non-spatial systems is associated to the onset of a Hopf bifurcation, a change of sign in a spatiotemporal context give rise to a Hopf-Turing bifurcation [72] and finally the only change of sign of $a_0(\xi)$ would give rise to a "pure" Turing bifurcation [72, 158].
In this context, it is important to distinguish instabilities that genuinely involve the spatio–temporal model (1.8.4) from those that would have been also found in the corresponding non–spatial model (NSM). As regards the NSM, it is easy to observe that

$$a_0|_{D=0,\tilde{\phi}=1} = \frac{bd}{\alpha}(\alpha-1) > 0.$$

Thus, for Routh-Hurwitz criterion to be satisfied by the NSM, it must be:

$$H_1^{NSM} = H_1|_{D=0,\tilde{\phi}=1} = \frac{bd}{\alpha}\left[\alpha(b+d-1)+1\right] > 0.$$

Thus:
i) if $b+d > 1-1/\alpha$, then $H_1^{NSM} > 0$ and the equilirbium of the the NSM is LAS;
ii) if $b+d < 1-1/\alpha$, then $H_1^{NSM} < 0$ and the equilibrium of the NSM is unstable via Hopf bifurcation.
The above result on H_1^{NSM} actually implies that $H_1(\xi) > 0$. Indeed from (1.8.8), we have that $H_1(\xi)$ is composed by three addenda: $(d+b)D^2\xi^4 > 0$, $(b+d)^2 D\xi^2 > 0$ and

$$\begin{aligned} & \frac{bd}{\alpha^2}\left[(b+d)\alpha^2 - (\alpha-1)(\alpha_1+\alpha_2\widetilde{\phi})\right] \\ = & \frac{bd}{\alpha^2}\left[(b+d-1)\alpha^2 + \alpha - (\alpha-1)\alpha_2(-1+\widetilde{\phi})\right] \\ = & \frac{bd}{\alpha^2}(\alpha-1)\left[\frac{\alpha}{\alpha-1}\left(1+(b+d-1)\alpha\right) + \alpha_2(1-\widetilde{\phi})\right] > 0. \end{aligned}$$

So no Turing-Hopf bifurcation can be generated if the equilibrium of the NSM is LAS.
Thus, apparently the only route to instability at $\mathbf{E}_2$ is via changes of sign of $a_0(\xi)$. However it is easy matter to verify that the condition $a_0(\xi) > 0$ is nothing else that the LAS condition of the intermediate equilibrium $P_2 = 1/\alpha$ defined in (1.4.2) of the model (1.2.10) without memory.
Summarizing, it may state that the introduction of temporal non-locality via the AFK does not make $\mathbf{E}_2$ unstable unless:
i) $b+d \geq 1-1/\alpha$, i.e. the NSM is unstabilized at $\mathbf{E}_2$ by the memory effect;
ii) there exist ξ such that $a_0(\xi) < 0$, i.e. the original model without memory is unstable.
The above analysis, with simple changes, can also be repeated in the case of local and of global information.
In the Figure 1.6 we give an illustration of the stability character of the state of equilibrium $\mathbf{E}_2$ for the system (1.8.4), with $\phi(x) = \phi_4(x)$, choosing a small perturbation as initial data. In Figure 1.6- (a) we see that the solutions evolve in time to reach the stable equilibrium $\mathbf{E}_2$, while in Figure 1.6- (b) the stability is lost and we see the convergence to a periodic spatial structure. This depends on the diffusion coefficient D, the ratio $\rho = \alpha_2/\alpha_1$ and the parameter h. Even if the presence of GTW has not been proved analytically for the system (1.8.4), in Figure 1.7 we provide an example of possible GTW in the case of system (1.8.4). The kernel $\phi(x)$ is the function $\phi_4(x)$ and the initial data is decay exponentially function at infinity. We focus our attention on delay parameters b and d. If b and d are small enough, then spatial periodic structures appear, while increasing the value of b and d, this kind of structure disappear.

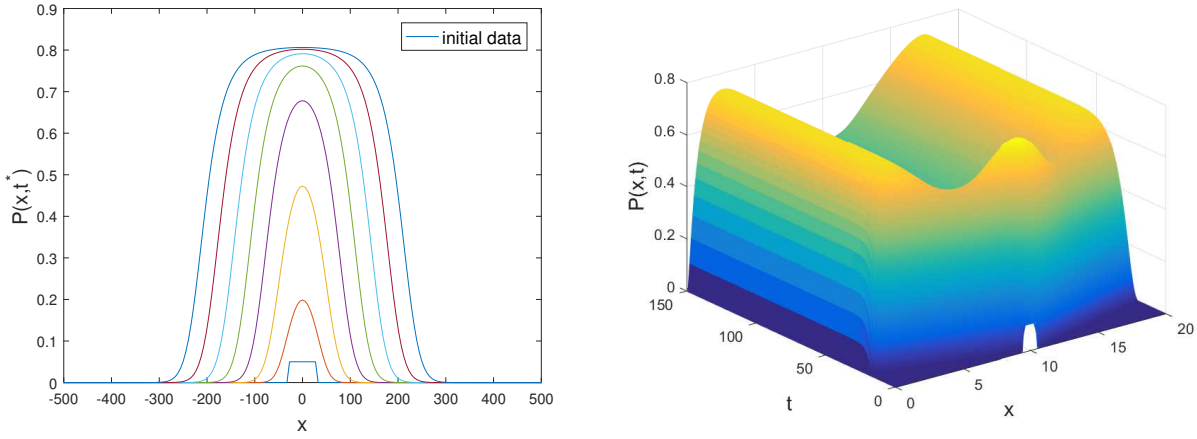

(a) (b)

Figure 1.6: Illustration of stability analysis of equilibrium $\mathbf{E}_2$ for system (1.8.4) with $\phi(x) = \phi_4(x)$. In (a), the parameters used are those listed in the Figure 1.3-(a) with $b = 1$, $d = 2$; in (b) we have $\alpha_1 = 0.7$, $\alpha_2 = 1.2$, $h = 7.7$, $D = 0.1$, $b = 3$ and $d = 5$.

1.8.2 Traveling Wave with Local Information

Now, wave solutions for equation (1.8.4) are described, setting the Dirac delta $\delta(x)$ as kernel, i.e. solutions of the following system

$$\begin{aligned} \partial_t P &= D\nabla^2 P + P(1-P)(1-\alpha M), \\ \partial_t Z &= b(P-Z), \\ \partial_t M &= d(Z-M). \end{aligned} \tag{1.8.9}$$

Let $\mathbf{E} = (P, Z, M)^T$ be the variable vector of system (1.8.9) such that

$$\lim_{x \to \pm\infty} \mathbf{E}(x) = \mathbf{E}_{\pm} \tag{1.8.10}$$

with $\mathbf{E}_-$ and $\mathbf{E}_+$ homgeneous in space equilibria of system (1.8.9). After substitution of the wave variable $z = x - ct$ in model (1.8.9), the following system of ordinary differential equations is obtained:

$$\begin{aligned} Dp'' + cp' + p(1-p)(1-\alpha m) &= 0, \\ c\omega' + b(p-\omega) &= 0, \\ cm' + d(\omega - m) &= 0, \end{aligned} \tag{1.8.11}$$

where $P(x-ct) = p(z)$, $Z(x-ct) = \omega(z)$ and $M(x-ct) = m(z)$. When $\alpha < 1$, recall that $\mathbf{E}_0$ is unstable and $\mathbf{E}_1$ is stable with respect to the system (1.8.4). Thus, the following result holds [162]:

Theorem 1.8.1 *If $0 < \alpha < 1$, there exists a travelling wave solution of velocity c $\forall$ $c \in [c^{(1)}, +\infty[$, connecting equilibrium $\mathbf{E}_1$ and equilibrium $\mathbf{E}_0$, i.e. a vector function $\mathbf{E}(x-ct)$, solution of system (1.8.11) on the real line $]-\infty, +\infty[$ and satisfying equation (1.8.10) with $\mathbf{E}_- = \mathbf{E}_1$ and $\mathbf{E}_+ = \mathbf{E}_0$.*

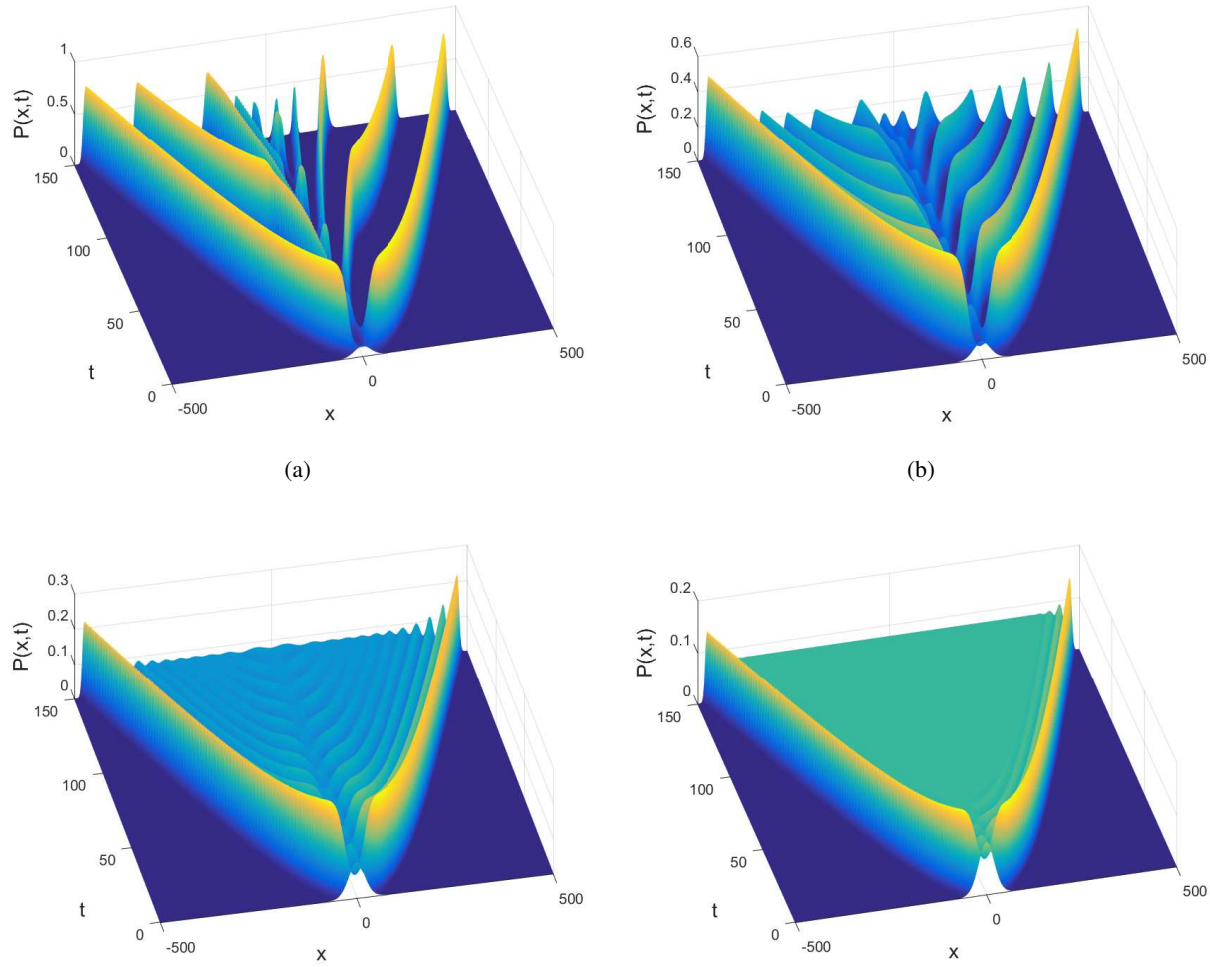

Figure 1.7: Propagation of waves for equation (1.8.4). Solution $P(x,t)$ as a function of two variables. Here the values of parameters are as in Figure 1.5 with $h = 7$. Moreover $b = 0.1$, $d = 0.2$ in (a), $b = 0.1$, $d = 0.78$ in (b), $b = 0.36$, $d = 0.78$ in (c) and $b = 0.8$, $d = 1$ in (d).

If $\alpha > 1$, then equilibrium $\mathbf{E}_1$ becomes unstable while equilibrium $\mathbf{E}_2$ is stable with respect to model (1.8.4). Therefore, it can affirmed that [162]:

Theorem 1.8.2 *If $\alpha > 1$, there exists a travelling wave solution of velocity $c\ \forall\ c \in [c^{(1)}, +\infty[$, connecting equilibrium $\mathbf{E}_2$ and equilibrium $\mathbf{E}_0$, i.e. a vector function $\mathbf{E}(x - ct)$, solution of system (1.8.11) on the real line $]-\infty, +\infty[$ and satisfying equation (1.8.10) with $\mathbf{E}_- = \mathbf{E}_2$ and $\mathbf{E}_+ = \mathbf{E}_0$; moreover, traveling wave solution between $\mathbf{E}_1$ to $\mathbf{E}_0$ cannot exist.*

In Figure 1.8, we show traveling wave solution for system (1.8.4) with minimal speed $c = c^{(1)} = 2\sqrt{D}$, connecting the equilibrium $\mathbf{E}_2$ at $-\infty$ and equilibrium $\mathbf{E}_0$ at $+\infty$.

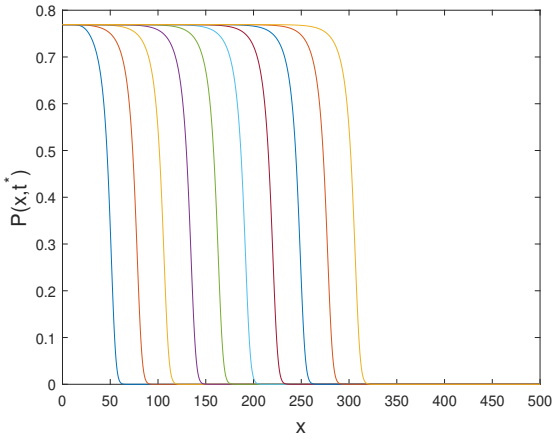

(a)

Figure 1.8: Travelling wave solution for system (1.8.4) with $\phi(x) = \delta(x)$: here the parameter used are those listed in Figure 1.4 with $b = 3$ and $d = 4$. Waves travel at minimal speed $c = 2\sqrt{D}$.

1.9 Vaccine awareness campaigns: Stability Analysis of Homogeneous Steady States

For the sake of simplicity, in this section a 1D spatial domain is considered.
With special focus on the case considered up to here, namely that of an infection which has been eliminated but requires to keep high degrees of herd immunity, an especially relevant task of a Public Health System (PHS) is that of investing to continuously sustain the vaccine uptake in the population. This is necessary in view of the low incentive to immunization for parents due to the low perceived risk, which is mirrored by the fact that $\vartheta(M_i) = \vartheta_0$.
The action of the PHS in enacting vaccine awareness campaigns was modelled in [65] by amending the basic imitation dynamics of strategies. Briefly, they assumed that the action by the PHS allows a steadily positive flux γA switching per time unit from the "non-vaccinator" to the "vaccinator" strategy.
Extending this idea to the present spatiotemporal setting [31, 33, 65], yields the model:

$$\begin{aligned} \partial_t P &= D\nabla^2 P + \vartheta(M_i)AP - \alpha(M_{se})AP + \gamma A, \\ \partial_t A &= D\nabla^2 A - \vartheta(M_i)AP + \alpha(M_{se})AP - \gamma A, \end{aligned} \tag{1.9.1}$$

where γ is a positive constant.
Keeping expressions (1.2.3) and (1.2.4), using $A = 1 - P$ and scaling as (1.2.9), from (1.9.1) we obtain:

$$\partial_t P = D\nabla^2 P + P(1-P)(1 - \alpha_1 P - \alpha_2 J(P)) + \gamma(1-P), \tag{1.9.2}$$

with $t > 0$, $x \in \Omega$ and Neumann condition (1.2.11).
A first effect of public action can immediately be seen: the NVE $P_0 = 0$ is no more an equilibrium point. Moreover, equation (1.9.2) has two spatially homogenous equilibria, namely the PVE $P_1 = 1$ and the equilibrium $P_\gamma \in (1/\alpha, 1)$ where P_γ is the solution of the quadratic:

$$\gamma = \alpha P^2 - P,$$

i.e.

$$P_\gamma = \frac{1+\sqrt{1+4\alpha\gamma}}{2\alpha}. \tag{1.9.3}$$

It is easy to verify that:
i) if $0 < \gamma < (\alpha - 1)$ then $P_\gamma \in (1/\alpha, 1)$; i.e., P_γ is epidemiologically meaningful;
ii) it is $d/d\gamma P_\gamma > 0$;
iii) it is $P_\gamma = P_2 = 1/\alpha$, if $\gamma = 0$. The previous results show that the new behavioral equilibrium P_γ, which replaces the "old" equilibrium P_2, allows a higher vaccine uptake than P_2 thanks to the univocal effect of public intervention.

1.9.1 Local Information

Under purely local information (i.e. $\phi(x) = \delta(x)$), equation (1.9.2) becomes:

$$\partial_t P = \nabla^2 P + P(1-P)(1-\alpha P) + \gamma(1-P). \tag{1.9.4}$$

Proceeding as in the case without vaccine awareness campaign, the following global stability results hold:

Theorem 1.9.1 *If $\alpha > 1$ and $\gamma \in (0, \alpha - 1)$ then P_γ is globally stable (and P_1 is unstable).*
If $\alpha > 1$ and $\gamma \geq \alpha - 1$ then P_1 is globally stable.
In the trivial case where $0 \leq \alpha \leq 1$ then P_1 is globally stable independently of $\gamma \geq 0$.

The previous results straightforwardly extend to the present spatially structured case the findings in [65], showing that the behavioral equilibrium P_γ is always GAS whenever it exists, while when it disappears the PVE inherits its global stability. As for possible heteroclinic connections between P_γ and P_1, introducing the traveling variable $z = x - ct$, the following negative result is established [162]:

Theorem 1.9.2 *There are no monotone decreasing travelling wave solutions for equation (1.9.4) connecting equilibrium P_1 at equilibrium P_γ with positive speed.*

1.9.2 Non–Local Information

The case of Ω unbounded

As noted above, assuming that $L/l \gg 1$, we have the following equation

$$\partial_t P = D\nabla^2 P + P(1-P)\left(1 - \alpha_1 P - \alpha_2 \int_{-\infty}^{\infty} \phi(x-y)P(y,t)dy\right) + \gamma(1-P), \tag{1.9.5}$$

with $x \in \Omega = \mathbb{R}$, $t > 0$ and Neumann condition (1.2.11).
The associated linearized equation at a generic homogeneous steady state P^* reads

$$\partial_t w = D\nabla^2 w + \left[(1-2P^*)(1-\alpha P^*) - \alpha_1 P^*(1-P^*) - \gamma\right] w - \alpha_2 P^*(1-P^*)\int_{-\infty}^{\infty} \phi(x-y)w(y,t)dy, \tag{1.9.6}$$

and the related eigenvalue problem has the form:

$$D\nabla^2 W + \left[(1-2P^*)(1-\alpha P^*) - \alpha_1 P^*(1-P^*) - \gamma\right] W - \alpha_2 P^*(1-P^*)\int_{-\infty}^{\infty} \phi(x-y)W(y)dy = \lambda W. \tag{1.9.7}$$

If $P^* = P_\gamma$, then the following eigenvalue is obtained:

$$\nu(\xi) = -D\xi^2 + (1-2P_\gamma)(1-\alpha P_\gamma) - \alpha_1 P_\gamma(1-P_\gamma) - \gamma - \alpha_2 P_\gamma(1-P_\gamma)\tilde{\phi}(\xi). \tag{1.9.8}$$

To determine the sign of the quantity

$$\chi_\gamma = (1-2P_\gamma)(1-\alpha P_\gamma) - \gamma,$$

it is useful to take into the account that

$$\alpha P_\gamma^2 = \gamma + P_\gamma,$$

yielding

$$\chi_\gamma = 1 - \alpha P_\gamma + \gamma,$$

i.e.

$$\chi_\gamma = \frac{1 + 2\gamma - \sqrt{1+4\alpha\gamma}}{2}.$$

It is easy to show that if $\gamma < \alpha - 1$ then $\chi < 0$. Thus, eigenvalues (1.9.8) become

$$\nu(\xi) = -D\xi^2 + \chi_\gamma - P_\gamma(1-P_\gamma)\left(\alpha_1 + \alpha_2\tilde{\phi}(\xi)\right). \tag{1.9.9}$$

Therefore, the following results are demonstrated :
i) since $\chi_\gamma < 0$, for both $\phi(x) = \phi_1(x) = C_g e^{-ax^2}$ and $\phi(x) = \phi_2(x) = C_e e^{-a|x|}$ it is

$$\nu(\xi) < 0,$$

so that P_γ is LAS;
ii) for $\phi(\xi) = \phi_3(x) = C_N(1 - (|x|/N)^2)Hev(N - |x|)$ and $\phi(\xi) = \phi_4(x) = (1/2h)Hev(h - |x|)$ the equilibrium P_γ can be unstable.
Moreover, if $P^* = P_1 = 1$, consider the eigenvalue problem (1.9.7), then we obtain

$$\nu(\xi) = -D\xi^2 + \alpha - 1 - \gamma.$$

If $\gamma > \alpha - 1$, then $\nu(\xi)$ is negative for any ξ and equilibrium P_1 is LAS.

The case of bounded Ω

Assuming that the set Ω is bounded, from (1.9.2) the following equation is obtained :

$$\partial_t P = D\nabla^2 P + P(1-P)\left(1 - \alpha_1 P - \alpha_2 \int_\Omega \phi(x-y)P(y,t)dy\right) + \gamma(1-P), \tag{1.9.10}$$

and Neumann conditions (1.2.11).
We will consider here $\Omega = [-L, L]$.
The eigenvalues problem associated at the linearization about a generic steady state P^* is given by

$$DW'' + \left[(1-2P^*)(1-\alpha P^*) - \alpha_1 P^*(1-P^*) - \gamma\right] W - \alpha_2 P^*(1-P^*) \int_{-L}^{L} \phi(x-y) W(y) dy = \lambda W. \tag{1.9.11}$$

Since for the equilibrium $P_1 = 1$ the nonlocal term disappears, the ensuing local stability analisys is straightforward and it is omitted. Thus only focus on the equilibrium P_γ.
Assuming that the kernel $\phi(x)$ satisfy conditions (1.5.21) and (1.2.7) i.e., function ϕ is periodic with period $2L$, even and normalized, if $P^* = P_\gamma$, solution of the following eigenvalue problem

$$DW'' + \left[\chi_\gamma - \alpha_1 P_\gamma(1-P_\gamma)\right] W - \alpha_2 P_\gamma(1-P_\gamma) \int_{-L}^{L} \phi(x-y) W(y) dy = \lambda W,$$

are searched in the form

$$w(x) = \cos\left(\xi_m x\right), \ \xi_m = \frac{m\pi}{L}, \ m = 0, 1, 2, ...$$

Then the boundary conditions are satisfied. Taking into account that the function ϕ is periodic and even, the m–th eigenvalue reads as follows:

$$\nu_m = -D\xi_m^2 + \left[\chi_\gamma - \alpha_1 P_2\left(1-P_2\right)\right] - \alpha_2 P_\gamma(1-P_\gamma)\phi_m, \tag{1.9.12}$$

where ϕ_m is defined in (1.5.23). Note that ν_m is negative for $m = 0$ and for m sufficiently large.
If ϕ_m is a positive function, then the corresponding eigenvalue ν_m is also positive. If the kernel ϕ has a bounded support, then, depending on the parameters, the corresponding eigenvalues can be negative and stability is lost.

1.9.3 Global information

In case of global information, the equation deduced from (1.9.5), is

$$\partial_t P = D\nabla^2 P + P(1-P)\left(1 - \alpha_1 P - \alpha_2 \frac{1}{\mu(\Omega)} \int_\Omega P(y,t) dy\right) + \gamma(1-P), \tag{1.9.13}$$

with $x \in \Omega = \mathbb{R}$, $t > 0$ and Neumann condition (1.2.11). It is trivial to show that P_γ is LAS. Indeed, setting $W(x) = \cos(\xi_m x)$ as eigenfunction of the problem:

$$DW'' + \left[\chi_\gamma - \alpha_1 P_\gamma(1-P_\gamma)\right] W - \alpha_2 P_\gamma(1-P_\gamma) \frac{1}{\mu(\Omega)} \int_\Omega W(y) dy = \lambda W,$$

we get the following eigenvalues:

$$\widetilde{\nu}_0 = \chi_\gamma - \alpha P_\gamma(1-P_\gamma) < 0,$$

$$\widetilde{\nu}_m = -D\xi_m^2 + \chi_\gamma - \alpha_1 P_\gamma(1-P_\gamma) < 0.$$

1.10 A preliminary simulation of the impact of Public Health System Action

Before investigating the effects of the awareness intervention by the PHS on the stability of the equilibria of (1.9.2) (and its dependence on the distinct hypotheses on the spatial information kernel), by means of a simulation, how the Public Health System intervention to favour vaccination can impact on the behaviour of the system is illustrated. Is assumed that subjects make their decisions by taking into the account their memory. In particular we choose the scenario depicted in the panel (a) of Figure 1.7: a GTW whose features are deeply influenced by the temporal non–locality. It is assumed that initially there is not public health intervention, which starts at about two third of the simulation interval and grows up to a maximal value γ_{Max}:

$$\gamma(t) = \frac{\gamma_{Max}}{50} Hev(t - 100). \tag{1.10.1}$$

Thus, we simulate the equation:

$$\begin{aligned} \partial_t P &= D\nabla^2 P + P(1-P)\left(1 - \alpha_1 \int_0^{+\infty} W(\tau)P(x,t-\tau)d\tau - \alpha_2 \int_\Omega \int_0^{+\infty} \phi(x-y)W(\tau)P(y,t-\tau)d\tau dy\right) \\ &+ \gamma(t)(1-P), \end{aligned} \tag{1.10.2}$$

where $W(\tau)$ is the delay function defined in (1.8.3) and $\gamma(t)$ the function defined in (1.10.1). Figures 1.9 and 1.10 (view from the top) show that initially the GTW pattern coexists with a rapidly increasing uniform pattern. This pattern relatively soon destroys the GTW and, any case, it immediately increases the minimum value attained by the GTW.

1.11 Comparison with the Theory of Diffusion of the Innovations

In this section we aim at highlighting similarities and key differences between our models (1.2.1) and (1.9.1) and the Theory of Innovation Diffusion (TID) by Mahajan and others [104, 129]. For the sake of the notation simplicity we mainly consider non-spatial models.

The TID models focus on the dynamics of the adoption of innovation. Defining $Y(t)$ as the fraction of adopters of the innovation at time t, and $U(t) = 1 - Y(t)$ the fraction of 'non–adopters' the basic family of models is the following:

$$Y' = g(t)(1 - Y), \tag{1.11.1}$$

where $g(t) > 0$, which was initially interpreted as an 'hazard of adoption' [16], has later been compared by Capasso and Zonno to the force of infection of epidemic models [39], with whom it has striking analogies. Thus, we will call it 'Force of Innovation Adoption' (FIA)

The positivity of the FIA $g(t)$ has an important consequence for our comparison: all specific models belonging to the family (1.11.1) are such that $Y(t) \to 1^-$, i.e. there is a unique equilibrium point, which can be termed 'all adopters'.

As a consequence, assuming $Y = P$, all possible analogies with our family of models is limited to the unrealistic cases where the 'all vaccinators' equilibrium is GAS. For example, the family of models (1.11.1) for $g(t) = \gamma$ corresponds to our model in the trivial case where there is no contagion of ideas.

The positivity of $g(t)$ and its interpretation as a 'force' of infection also stress the key difference between

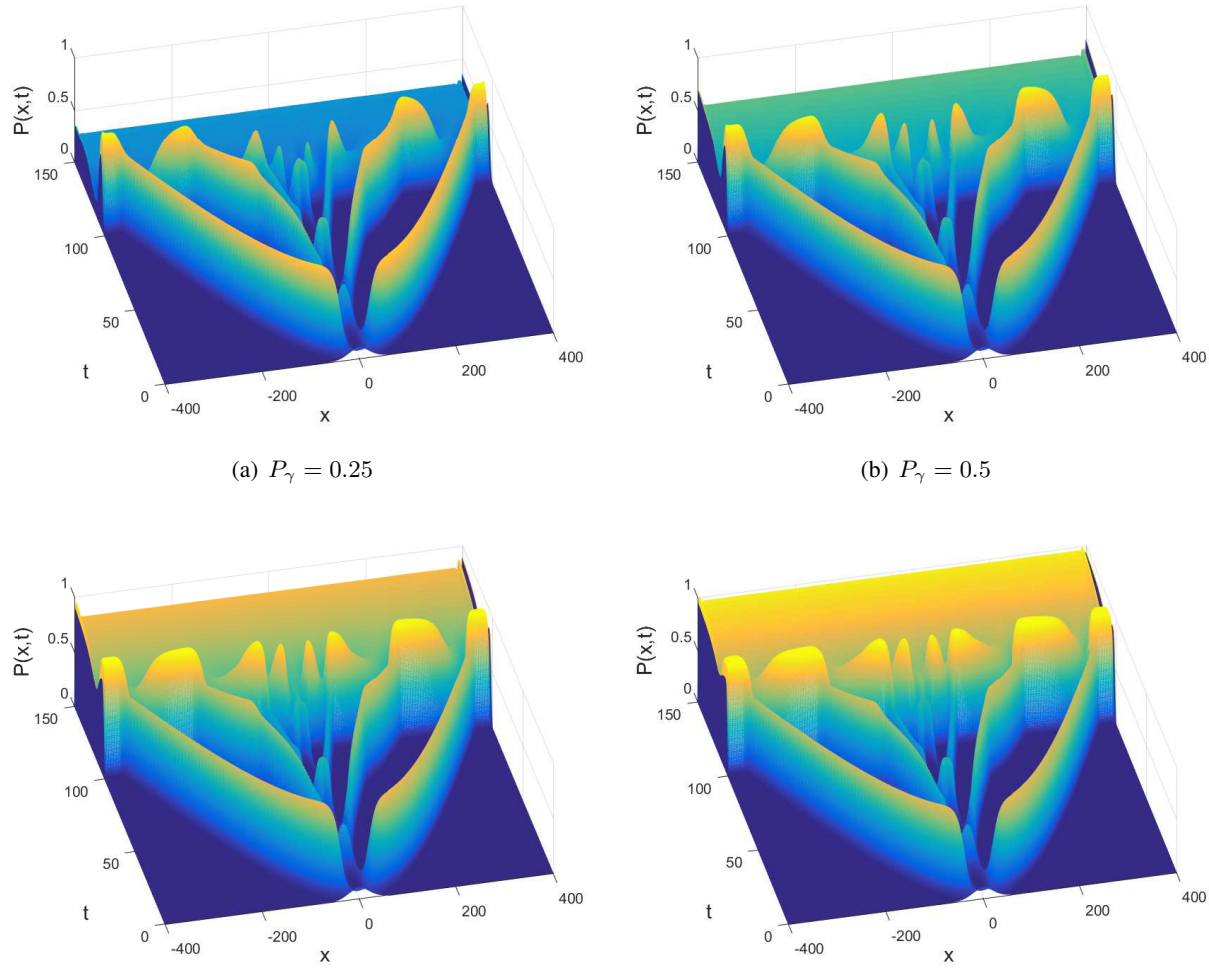

(a) $P_\gamma = 0.25$ (b) $P_\gamma = 0.5$

(c) $P_\gamma = 0.75$ (d) $P_\gamma = 0.9$

Figure 1.9: Solution $P(x,t)$ as a function of two variables for equation (1.8.3) . Here $\alpha_1 = 1.1$, $\alpha_2 = 13.1$, $D = 1$, $h = 7$, $b = 0.1$ and $d = 0.2$. Moreover $\gamma_{Max} = 0.6375$ in (a), $\gamma_{Max} = 3.05$ in (b), $\gamma_{Max} = 7.2375$ in (c) and $\gamma_{Max} = 10.602$ in (d).

the family of models we investigated here and the family of model (1.11.1): in the scenario we investigated there is a double contagion of ideas, i.e. a double flux: i) from A to P; ii) from P to A. On the contrary, the family (1.11.1) implies an uni–directional contagion of ideas. This is a direct consequence of the deeply different nature of the underlying 'social processes'.

However, it is of interest to investigate formal analogies between the two theories.

The specific instances of imitation game-like equations of TID [104, 129] are obtained phenomenologically by assuming that $g(t)$ is an analytical function of Y [104]:

$$g(t) = a_0 + a_1 Y(t) + \sum_{j=2}^{+\infty} a_j Y^j(t) \tag{1.11.2}$$

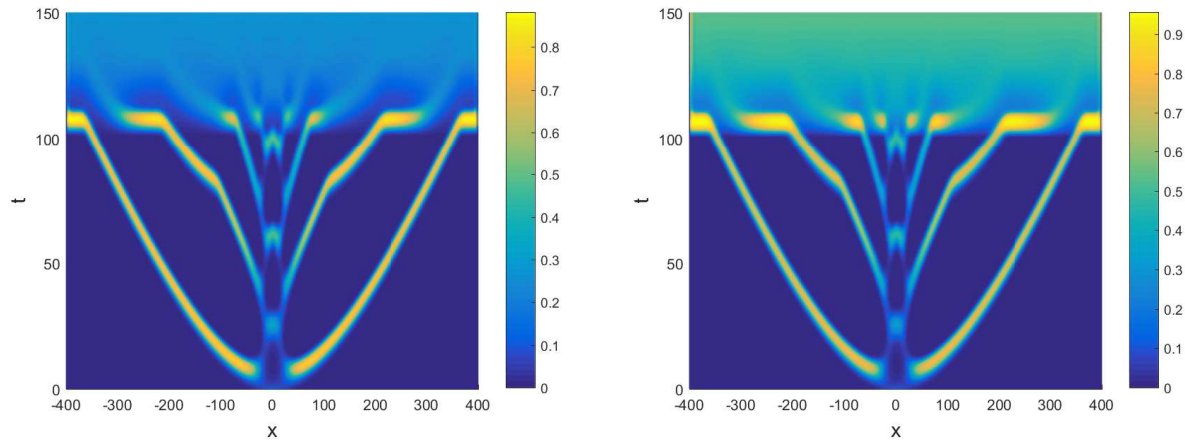

(a) $P_\gamma = 0.25$

(b) $P_\gamma = 0.5$

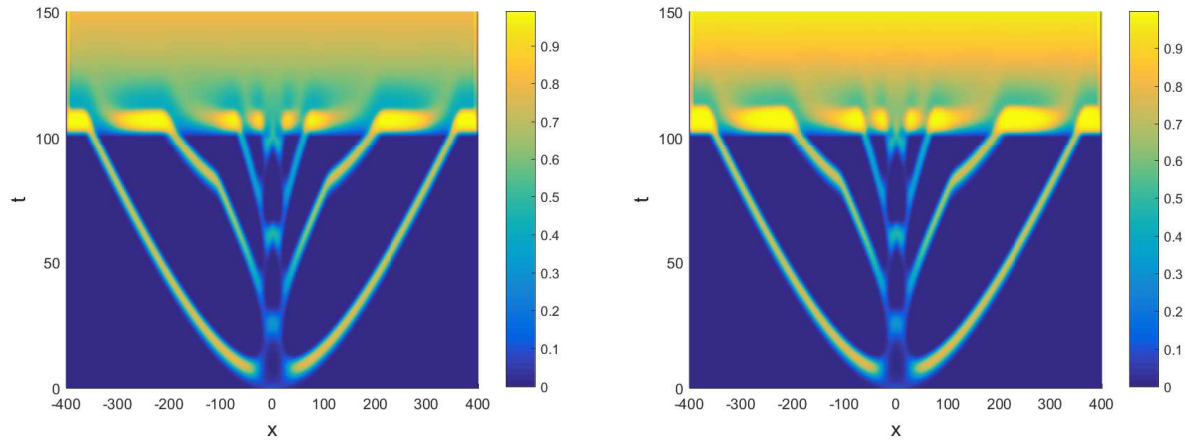

(c) $P_\gamma = 0.75$

(d) $P_\gamma = 0.9$

Figure 1.10: Top view of the images in Figure 1.9.

where $a_k \geq 0$ can also be function of time [36, 39]. For example, assuming that the non–linear terms are null, $g(t) = a_0 + a_1 Y(t)$, yields the most popular popular model of the TID: the Bass model [16, 104], which reads as follows:

$$Y' = a_1 Y(1 - Y) + a_0(1 - Y). \tag{1.11.3}$$

The non–negativity of the coefficients a_k would preclude formal analogies with our models. However, maintaining the constraint of positivity of the FIA $g(t) > 0$ but relaxing for $k \geq 2$ the hypothesis that $a_k \geq 0$ yields the following $g(t)$ that allows a formal analogy with *some* models of the family of models considered in this work:

$$g(t) = Y(t)\left(\theta_0 - \alpha(Y(t))\right) \tag{1.11.4}$$

with, however, the following sharp constraint ($\alpha(Y)$ is non–decreasing):

$$\theta_0 - \alpha(1) \geq 0$$

that again leads to the global stability of the 'all adopters' ('all vaccinators') model.
The important case of linear–affine $\alpha(y)$ can be expressed within the frame of the TDI family of models as follows:

$$g(t) = \gamma + (\theta_0 - \alpha_0)Y - \alpha_1 Y^2 \tag{1.11.5}$$

Note that this generalized framework is such that: i) can be framed with the epidemiological theory by Capasso where forces of infection can also be non–monotone [38], which can also be applied to diffusion of information [39]; ii) it remains a formal model of a uni-dimensional flow.
Namely, a FIA $g(t)$ of the type (1.11.4) can be read in terms of TID as an initially beneficial effect of the product qualities, possibly followed, for larger Y, by a partial mitigation of the 'enthusiasm' for the product due to the spread of information of its possible (real of presumed) defects. Thus, a reduced FIA is observed.
As far as the space is concerned, let us first consider the Fisher-Kolgomorov–like model (1.2.12), for which the equilibrium 'all vaccinators' is GAS. If we further assume $\alpha_0 = 0$ then we have a unidirectional flux from the group 'non-vaccinators' to the group 'vaccinators'. In such a case our model (1.2.12) is equivalent to the Mahajan spatiotemporal model of Innovation Diffusion [104].
More interestingly, in [36, 39] Capasso proposed, in the framework of an SIR-like diffusion of innovation model, a family of non-local models of the FIA. This family of models is non-locally depending on the adopters, again in the context of a uni-directional flux. In our case, instead, we have two fluxes and it is the force of infections from the adopters towards non–adopters that is non–local.

1.12 Discussion and concluding remarks

The role played by the spatial structure of information used by vaccination decision makers is a main topic of behavioral epidemiology. In this chapter, within a spatial framework based on classical diffusion, the effects of three different structures of information ((i) purely "local" information, "local" plus a "global", country-wide, average information, (iii) a mix of local and non-local information) on the dynamics of vaccine uptake in absence of the infection have been investigated, so that - given the background of low incentive to immunization - the dynamics of VAEs emerge as the key determinants of vaccination decisions and collective coverage. This possibly represents a main case of the current public health landscape in modern industrialized countries, where a number of vaccine preventable infectious disease were successfully eliminated "locally" (think e.g, to polio which was locally eliminated long ago in most Europe), but there is still the need to maintain a high-coverage immunization policy in the post-elimination period to prevent the risk of infection re-emergence and consequent failure of global scale targets, such as eradication.
The analyzes focused on the pattern and properties - namely stability, bifurcation, existence of travelling waves, effects of time memories, and the effects of awareness campaigns by the Public Health System - of the key space-homogeneous equilibrium solutions, that are termed the "behavioral equilibria".
The main results were as follows.
As regards the stability properties of the behavioural equilibrium, these show a nice interplay between the form of the spatial information kernel and the nature of the spatial domain (bounded vs unbounded). Under "purely local information" the BE is always LAS (and GAS) whenever it exists. Under "local and global" information the BE is always LAS whenever it exists. However, convergence is slower than in the case of

purely local information. Under "mixed" information results are more articulated. For unbounded domains stability will prevails independently of the shape of the spatial information kernel under large values of the diffusion coefficients. In particular kernels that are strictly decreasing in the distance from the local position are always stabilising independently of the spatial kernel. However, bounded-support kernels (e.g., strictly positive up to some threshold distance and zero thereafter) can yield instability at low levels of the diffusion coefficient when the strength of non-local information tend to prevail on local one.

Interestingly, the instability caused by the presence of non–local information can generate generalized traveling waves characterised by more or less pronounced oscillations as well as other not static spatial patterns. The onset of these travelling waves depends on the interplay between behavioral parameters and the structure of the spatial kernel. This means that the fraction of individuals favourable to vaccination can show oscillations. As regards the effects of the presence of time memories i.e., the possibility that agents also use past - and not only current - information about VAEs in forming their perceptions of risk, at least in the realistic case of the acquisition–fading kernel, no further specific instability can arise. This result contrasts with the fact, widely known in the dynamic system literature and first stressed in the behavioral epidemiology debate in [66], that the presence of past information typically has destabilising effects on equilibria that were at least locally stable in the absence of delays.

However, the presence of information memories can remarkably impact on the "shape" of the generalised travelling waves. In particular, for certain combination of the characteristic times of the memory kernel, it might happen that internally to the propagating front the oscillation are wild enough that, at each simulated time, there are large zones where the proportion favorable to vaccination approaches zero, thereby compromising the herd immunity of the population.

Remarkably, instabilities and emergence of generalised travelling waves are cleared out when vaccine awareness campaign are enacted by the public health system, in line with the intuitions supplied in [65].

This work obviously has a number of limitations.

A key limitation lies in the basic hypotheses that at the macroscale the agents' mobility can be approximated by classical diffusion i.e., by random movements around geographic space. This clearly represents a coarse approximation that makes it the present model essentially a benchmark for providing clear-cut baseline results, whose robustness will have to be grounded - in future work - against more robust hypotheses. In fact, real patterns of mobility of human individuals are complex [83] and can introduce remarkable implications for infection patterns, such as unexpected phase transitions [13]. A promising recent route towards the modeling of human mobility - still within the PDE setting - is the one currently known as superdiffusion [24, 144, 145, 146]. Superdiffusion allows flexible, and therefore potentially more realistic, representations of spatial mobility while, at the same time, it keeps a good deal of analytical tractability. This makes it superdiffusion as a natural candidate for future extensions of the present work. Remarkably indeed, Brockmann and Hufnagel [28] have modelled a double chemical reaction leading to an classical imitation game in case of superdiffusive mobility of molecules and to follow this approach in a follow-up work is planned.

A second limitation of the present work lies in the specific case-study, namely a vaccination scenario in the absence of the infection. As argued in the introduction, this case is a central one but pairwise importance is played by those alternative scenarios - still in relation to vaccine preventable infections - where the disease is continuously re-introduced, as is the case of measles, which has caused sizable epidemics all around Eu-

rope and the US in the last few years (ECDC2019,WHO2019). Further forthcoming work will therefore be devoted to the study of the spatio-temporal interplay between the vaccine opinion dynamics and infection spread.

Chapter 2

A MATHEMATICAL MODEL OF CHOLERA ENVIRONMENT-HOST-ENVIRONMENT TRANSMISSION DYNAMICS

Part of this chapter, concerning the exclusively non-spatial model, was presented at the International Conference MathCompEpi 2018, held in Erice, Trapani, from 28/8 to 05/09 2018 and has materialized in the following paper:

A. Lupica, A. B. Gumel and A. Palumbo. On the computation of reproduction numbers for the environment-host-environment cholera transmission dynamics,

that is currently submitted in *Journal of Biological Systems* (the paper was recommended for publication after minor revisions).

2.1 Introduction

Cholera, a bacterial disease that affects the intestinal track, is caused by the bacterium *Vibrio cholerae*. Infection with the disease, which can be effectively treated using antibiotics if caught early (typically within the first two days of onset of symptoms), can result in severe diarrhoea and (subsequently) dehydration, which, if untreated, can be fatal. Cholera continues to be a major public health problem in many parts of the world (most notably in the Indian sub-continent and some parts of Africa, Asia and Latin America) [5, 172, 173, 175] (Figure 2.1). Figures from the World Health Organization (WHO) [173] show that, each year, the disease accounts for between [1.3- 4] million cases and [21.000-143.000] fatalities globally. It is noteworthy that many cholera-endemic countries are now pledging to end cholera outbreaks by 2030 [172].

Although a secondary (but less important) human-to-human mode of cholera transmission exist [82,

139, 155], cholera is primarily transmitted to humans from the environment by ingesting food or water contaminated with the bacterium *V. cholerae* [52, 84]. The disease has a short incubation period (ranging from a few hours to five days [138]) and its common symptoms are diarrhoea (leading to severe dehydration), vomiting, loss of skin elasticity, thirst, and muscle cramps [138, 184]. Most cholera-infected people (at least 80%) do not become ill, although they may carry the *V. cholerae* bacterium for weeks and slowly excreting it into the water supply [15, 138, 173]. However, when illness does occur, about 80%-90% of episodes are of mild or moderate severity and are difficult to distinguish clinically from other types of acute diarrhoea [173].

Basic preventive measures, such as improvements in sanitation systems, effective and adequate drinking water and sewage treatment, and improved food and personal hygiene, are generally adopted in cholera-endemic areas to minimize human contact with *V. cholorae*-contaminated sources. In particular, the water, sanitation and hygiene (WASH) strategy is widely implemented in endemic areas [79]. The disease can be successfully treated, in most cases, using oral rehydration therapy [170, 177] (which is highly effective, safe, and simple to administer) and antibiotics [95, 136, 170, 177]. Owing to the common and widespread administration of antibiotics to treat cholera-infected humans, the emergence of antibiotic resistant strains of *V. cholerae* is very well documented in the literature [93, 95, 138]. Furthermore, a number of safe and effective anti-cholera vaccines have been developed for use in humans (see, for instance, Safi et al. [81, 138] and some of the references therein). People infected with *V. cholerae* are generally treated using fluid replacement therapy and antibiotics [138, 139]. Cholera-endemic regions around the world that do not adhere to the aforementioned preventive measures, and provide access to treatment to infected people, continue to experience cholera outbreaks [5, 172, 173, 175].

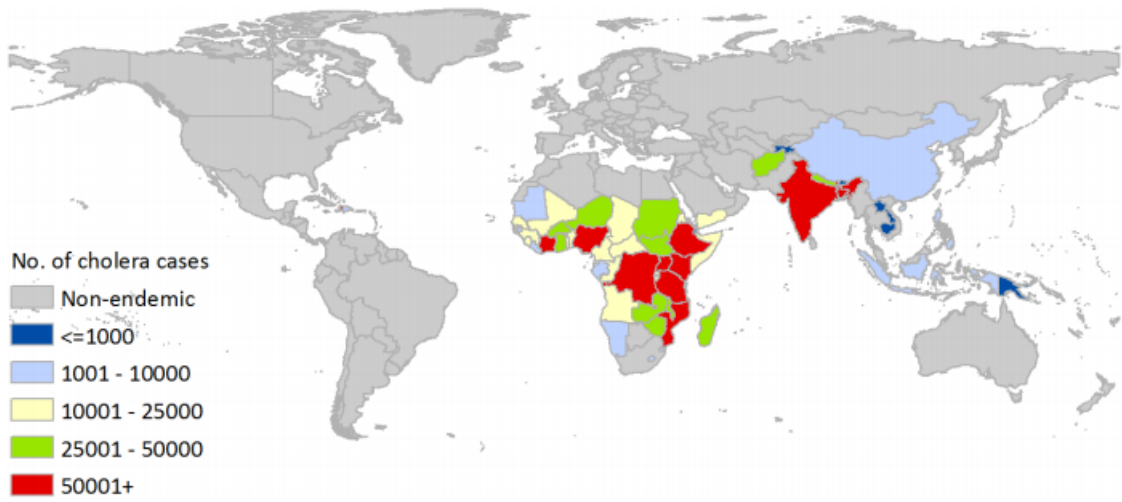

(a)

Figure 2.1: Global cholera map: geographical patterns of annual number of cholera cases in endemic countries. [5].

Mathematical models, typically of the form of deterministic system of nonlinear differential equations, have been used to gain insight into the transmission dynamics and control of cholera in endemic areas.

For instance, Capasso and Paveri-Fontana [37] developed the earliest model to describe the 1973 cholera epidemic in Bari, Italy [12]. Codeço [50] extended the two-dimensional model developed by Capasso and Paveri-Fortana to include the dynamics of the susceptible population. More recently, Pascual et al. [128] reviewed some quantitative facts about cholera and climate. In a short section, they proposed a model with four variables, i.e. the number of susceptible individuals, the number of infected individuals, the number of fomites (or bacterial abundance) and the water volume. Further, authors in [18, 19, 20, 21, 49, 111] explored the problem of the spread of cholera, considering two or more populations of bacteria living in two different but connected aquatic environments. Safi et al. [138] developed an 11-dimensional deterministic model for assessing the combined impact of dose-structured cholera vaccination and treatment on the dynamics of two cholera strains in a population.

The dynamics of the models developed for cholera transmission dynamics and control are generally governed by an epidemiological threshold, known as the *reproduction number* (and generally denoted by $\mathcal{R}_0$). Epidemiologically-speaking, the quantity $\mathcal{R}_0$ measures the average number of secondary infections generated by a typical infectious individual introduced into a completely susceptible population [7, 86]. In general, the disease dies out when $\mathcal{R}_0 < 1$ and persists in the population when $\mathcal{R}_0 > 1$. The *next generation operator method* (NGM), developed by Diekmann et al. [62, 61] and elaborated by van den Driessche and Watmough [161], is popularly-used in the mathematical biology community to compute this epidemiological quantity.

As noted by van den Driessche and Watmough [161], owing to the fact that cholera is an environment-host-environment epidemic, different expressions for $\mathcal{R}_0$ can be obtained, depending on the interpretation of the role of the environment. For example, Bani-Yaghoub et al. [14] highlighted the issue of calculating a valid expression for $\mathcal{R}_0$ for diseases transmitting through the contaminated environment. This problem, of computing the correct $\mathcal{R}_0$ for environmentally-transmitted diseases, can be overcome by using the notion of *type* reproduction numbers [85, 133], which provides a unique threshold value, regardless of the interpretations of the role of the environment.The concept of type reproduction number was further generalized by Shuai et al. [141, 142], useful when the control strategies act on a part of the population or on the interactions between the different populations.

The dynamics of cholera is greatly associated with environmental contamination (it is well-known that the bacterium is autochthonous to the aquatic environment [52]). In particular, *V. cholerae* inhabits seas, estuaries, brackish waters, rivers, and ponds of coastal areas of the tropical world [53, 119] (and surface water in proximity to cholera-infected individuals is frequently contaminated with the *V. cholerae* agent [147]). Further, the bacterium can survive long-term, perhaps for years, in such aquatic environments [52]. Hence, models for the transmission dynamics of the disease should incorporate the highly significant role such environmental factors play in the disease dynamics (vis a vis the production and long-term survival of *V. chlorea* in the aquatic habitat). Consequently, the aim of this study is to propose a new model for cholera transmission dynamics that take into account the role of environmental factors on the disease dynamics in addition to explicitly accounting for the impact of the hydrological fluctuations of the volume of available drinking water in a cholera-endemic setting. In particular, a cholera-endemic community with a local pond-river network as its source (reservoir) of available drinking water will be considered. The notion of the type reproduction number will be used to assess the population-level impact of various anti-cholera control

strategies.

Another challenge in current discussion is to take into account spatial heterogeneity, that usually is rarely considered, giving a broader understanding of the phenomenon. Indeed, in the discussion so far presented, it has been assumed that there is a unique community of people who interact and share the same resources. However, the spatial distribution of communities and how they interact is crucial to understanding the spatial spread of the epidemic in a disease-free region [18]. Furthermore, as reported in [19], [51], [99], *V. cholerae* is a natural member of the coastal aquatic microbial community and can survive outside the human host in the associated aquatic environment with chitinaceous zooplankton such as copepods, molluscs and also with aquatic vegetation. Therefore, the disease can spread from the coastal region, where it is indigenous, to the internal area through waterways and river networks. Similarly, the infection can spread from the inner regions with epidemic explosions in the surrounding areas. On the other hand, authors in [118], povide the basic reproduction numbers estimated for all 10 Zimbabwean provinces and the results were highly heterogeneous, which implies that the underlying transmission model varied widely across the country. Similarly, Tuite et al. [157] obtained very different reproduction numbers for the 10 administrative departments of Haiti during the outbreak of cholera. Different models take into account spatial spreading of cholera: for example, systems in [18, 19] consider a spatial network addressed by viewing the environmental matrix as an oriented graph (i.e., a directed graph having no symmetric pair of directed edges). Nodes represent human communities (cities, towns, and villages) in which the disease can be diffused and grow. The edges represent links between the communities, typically hydrological links. Edge direction is chosen accordingly to the flow direction. Authors in [165, 166] presented, under Fickian diffusion hypothesis, an epidemic model for cholera transmission dynamics. In the present dissertation, the ODE model will then be extended to the spatially heterogeneous case, using the simplest approximation, already presented by Noble [125] for epidemic propagation: the Fickian diffusion.

The chapter is organized as follows. The ODE model is formulated in Section 2.2. Its basic qualitative properties are also explored. Detailed computation of the basic reproduction numbers of the model, for all possible transmission scenarios, is reported in Section 2.3. The associated types reproduction numbers of the model are computed in Section 2.4. The developed model is used to assess the population-level of various anti-cholera control strategies are carried out in Section 2.5. A qualitative study of endemic equilibrium state is placed in Section 2.6. Section 2.7 presents the formulation of the PDE model: for this system a qualitative study of traveling waves solutions in Section 2.8 was provided a qualitative study of the estimate of the basic reproductive number related to the spatial model in the Section 2.9. The numerical simulations on the PDE model are placed in Section 2.10.

2.2 Formulation of Mathematical Model

The model to be designed in this study is built on two basic components, namely an epidemiology component for the disease dynamics in a human population and a hydrology component for the water balance (within the local pond-river system) . Cholera is endemic in many countries in Africa and Asia (mainly in India and Bangladesh), although a number of outbreaks have also occurred in Eastern Europe and Haiti. In most of the rural areas of these countries, drinking water supply source (and reserve) mostly comes from

ponds and small rivers that are often interconnected [131]. Thus, cholera dynamics in such settings is associated with the contamination of the two local water sources with *V. cholerae* (i.e., cholera *ecology*), the inflow and outflow of water to and from the two interconnected water sources (i.e., water balance or *hydrology*), and *V. cholerae* transmission between humans due to human contact with the contaminated water sources (i.e., cholera *epidemiology*). The model proposed for this setting captures the three main elements (of ecology, epidemiology and hydrology). In particular, the ecology-epidemiology-hydrology model to be designed in this study is that of the transmission dynamics of cholera in a cholera-endemic community whose main source of drinking water is a local network of a pond (typically defined as a small basin consisting of stagnant water) and a river (consisting of flowing water). Figure 2.2 depicts a schematic of a pond-river water network system for a typical cholera-endemic community.

The total human population at time t, denoted by $N(t)$, is split into mutually-exclusive compartments of susceptible ($S(t)$) and infected ($I(t)$) individuals, so that $N(t) = S(t) + I(t)$. Similarly, the total volume of water available to the community is split into the volume of water in the local pond (denoted by $V_p(t) > 0$) and the volume of water in the river ($V_r^* > 0$, assumed constant). Consequently, following [18, 19, 20, 21, 49, 111], the total *V. cholerae* bacteria population in the community at time t, is split into the total number of bacteria in the pond (denoted by $B_p(t)$) and the total concentration of *V. cholerae* bacteria in the river ($B_r(t)$). While it is assumed that the water volume in the river is constant, the water volume in the pond is assumed to vary with time (as this is affected by rainfall, evaporation and/or drainage [21, 49, 132]).

(a) (b)

Figure 2.2: A pond-river network in a typical cholera-endemic setting. Figure 2.2(a) was adapted from [154], while Figure 2.2(b) was adapted from [156].

The population of susceptible humans is increased by recruitment (due to birth or immigration) at a *per capita* rate Π and by the recover from cholera infection at a rate γ^*. This population is decreased following the acquisition of cholera infection from the cholera-contaminated pond at a rate $\beta_p^* \dfrac{B_p}{k_p^* V_p + B_p}$, where β_p^* is the rate of cholera infection from bacteria in pond and k_p^* is the minimum concentration of *V. cholerae* in the pond that guarantees 50% chance of *V. cholerae* transmission per contact [128]. Similarly, infection is acquired from the (contaminated) river reservoir at a rate $\beta_r^* \dfrac{B_r}{k_r + B_r}$, where β_r^* is the infection rate from bacteria in river to host and k_r is the saturation parameter that accounts for the minimum *V. cholerae* concentration in the river that guarantees 50% chance of cholera transmission. It is assumed that humans in all epidemiological compartments die naturally at a rate μ^*. Thus (where a dot represents differentiation

with respect to time t):

$$\dot{S} = \Pi + \gamma^* I - \left(\beta_p^* \frac{B_p}{k_p^* V_p + B_p} + \beta_r^* \frac{B_r}{k_r + B_r} \right) S - \mu^* S.$$

The population of infected individuals is generated by the acquisition of infection from the pond or the river. It is decreased by recovery (at the rate γ^*), natural death (at the rate μ^*) and cholera-induced mortality at a rate δ^*. Hence,

$$\dot{I} = \left(\beta_p^* \frac{B_p}{k_p^* V_p + B_p} + \beta_r^* \frac{B_r}{k_r + B_r} \right) S - (\gamma^* + \mu^* + \delta^*) I.$$

It follows from the above two equations that the rate of change of the total human is given by:

$$\dot{N} = \Pi - \mu^* N - \delta I.$$

It is worth noting that, in the above formulation, the Michales-Menten (Holling type-II) incidence function is used to model the cholera transmission rates above.

The bacterial population in the pond is increased by *V. cholerae* shedding by infected humans at a rate θ_p^* and by the natural reproduction of free-living *V. cholerae* bacteria in the pond at the logistic rate $r\left(1 - \frac{B_p}{k_{bp}}\right)$ (where r is the reproduction rate and $k_{bp} > B_p(t)$ for all t is the carrying-capacity of free-living *V. cholerae* in the pond (i.e., k_{bp} is the maximal capacity of free-living bacteria in the environment)). This formulation is motivated by the fact that warmer temperatures (near the surface of the water body) are known to favor the attachment, growth, and multiplication of *V. cholerae* [21] (this is accounted by assuming that, within the pond, the bacterial concentration $B_p(t)$ at time t increases according to a logistic per-biomass growth rate). The bacterial population in the pond is further increased by the influx of contaminated water from the river, at a rate $\lambda_r^* V_r^* B_r$ (where V_r^* is the constant volume of water in the river). This population is decreased by the outflow of water from the pond to the river, at a rate $\lambda_p^* B_p$, and by the natural death of the bacterium at a rate μ_B^*. Thus,

$$\dot{B}_p = \theta_p^* I + r B_p \left(1 - \frac{B_p}{k_{bp}}\right) + \lambda_r^* V_r^* B_r - \lambda_p^* B_p - \mu_B^* B_p.$$

Similarly, the bacterial population in the river is increased by shedding (at a rate θ_r^*/V_r^*) and by the influx of contaminated water from the pond, at the rate $\lambda_p^* B_p / V_r^*$. This population is decreased by the outflow of water from the river to the pond (at the rate λ_r^*) and by natural death (at the rate μ_B^*). Hence,

$$\dot{B}_r = \frac{\theta_r^*}{V_r^*} I + \lambda_p^* \frac{B_p}{V_r^*} - \lambda_r^* B_r - \mu_B^* B_r.$$

Thus, denoting with $B(t) = B_p(t) + V_r^* B_r(t)$ the total number of bacteria in the pond and the river, we obtain the following equation:

$$\dot{B} = (\theta_p^* + \theta_r^*) I + r B_p \left(1 - \frac{B_p}{k_{pb}}\right) - \mu_B^* B.$$

Finally, the total volume of water in the pond is increased by precipitation at a rate p and by the inflow of water from the river (at the rate λ_r^*). It is decreased by the outflow to the river (at the rate λ_p^*) and by drainage, at a rate d_r^*. This gives:

$$\dot{V}_p = p + \lambda_r^* V_r - \lambda_p^* V_p - d_r^* V_p.$$

It is assumed that there is always a minimum amount of water $V_p^{(min)} > 0$ in the pond, such that $0 < V_p^{(min)} \leq V_p(t)$ for all $t \geq 0$. This assumption guarantees water exchange between the pond and the river, in addition to sustaining *V. cholerae* transmission to the human host *via* contact with the contaminated water in the pond.

In summary, the ecology-epidemiology-hydrology model for the transmission dynamics of *V. cholerae* in a population is given by the following deterministic system of nonlinear differential equations (Figure 2.3 depicts a general transmission schematic of the model. The state variables and parameters of the model are described in Table 2.1):

$$\begin{aligned}
\dot{S} &= \Pi + \gamma^* I - \left(\beta_p^* \frac{B_p}{k_p^* V_p + B_p} + \beta_r^* \frac{B_r}{k_r + B_r}\right) S - \mu^* S, \\
\dot{I} &= \left(\beta_p^* \frac{B_p}{k_p^* V_p + B_p} + \beta_r^* \frac{B_r}{k_r + B_r}\right) S - (\gamma^* + \mu^* + \delta^*) I, \\
\dot{B}_p &= \theta_p^* I + \left[r\left(1 - \frac{B_p}{k_{bp}}\right) - \lambda_p^* - \mu_B^*\right] B_p + \lambda_r^* V_r^* B_r, \\
\dot{B}_r &= \frac{\theta_r^*}{V_r^*} I + \lambda_p^* \frac{B_p}{V_r^*} - \left(\mu_B^* + \lambda_r^*\right) B_r, \\
\dot{V}_p &= p + \lambda_r^* V_r - \left(\lambda_p^* + d_r^*\right) V_p.
\end{aligned} \tag{2.2.1}$$

The main assumptions in the formulation of the model (2.2.1) include:

1. Exponentially-distributed waiting times in each compartment of the model.
2. Recovery from cholera does not induce permanent (or partial) immunity against future *V. cholerae* infection.
3. The total volume of water in the pond ($V_p(t)$) equals or exceeds a certain minimum amount (denoted by $V_p^{(min)}$) for all time $t \geq 0$. This is the minimum amount needed to support water exchange between the pond and the river, and sustain *V. cholerae* transmission to humans from the contaminated pond. Further, the total volume of water in the river (V_r^*) is strictly positive for all time $t \geq 0$.
4. Nonlinear (Michales-Menten) incidence functions are used to account for saturation in the infection rates [21, 128].
5. No growth rate is assumed for the concentration of *V. cholerae* in the river ($B_r(t)$) [18, 19, 20, 21, 49, 111].

6. The two local water reservoirs (pond and river) are interconnected.

The model (2.2.1) is an extension of many of the models for cholera transmission dynamics, such as those in [18, 19, 20, 21, 49, 111, 50, 128, 132, 139], by, *inter alia*:

1. incorporating the dynamics of *V. cholerae* in an interconnected pond-river water network (i.e., we consider two different but interconnected aquatic environments for *V. cholerae* dynamics). A single water source was considered in [50, 128, 139];

2. including the inflow and outflow of water between two different aquatic environments (pond and river), not considered in ([50, 128, 139]);

3. using a nonlinear logistic function for the growth of bacteria in the pond (no bacterial growth rate is considered in [21, 49, 132, 139]; further, a linear bacterial growth function was considered in [50, 128]);

4. including an equation describing the dynamics of water volume in the pond, taking into account precipitation, drainage and water transfer to and from the river (this was not considered in [50, 128]);

5. including the possibility that humans can become infected and can spread bacteria both in the pond and in the river. Thus, we consider a dual *V. cholerae* transmission (from river and from pond) and shedding (into the river and the pond) rates. These dual transmission and shedding pathways were not taken into account in [18, 19, 20, 21, 49, 111, 50, 128, 132, 139].

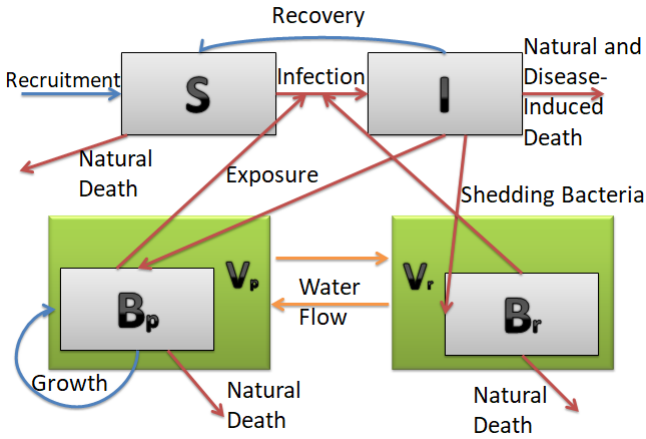

(a)

Figure 2.3: *V. cholerae* transmission scheme in an interconnected pond-river network

It is convenient to introduce the following change of variables and re-scaling on the model (2.2.1):

State Variable	Description
$S(t)$	Number of susceptible individuals at time t
$I(t)$	Number of infected individuals at time t
$B_p(t)$	*V. cholerae* number in the pond at time t
$B_r(t)$	*V. cholerae* concentration in the river at time t
$V_p(t)$	Volume of water in the pond at time t

Parameter	Description	Unit	Baseline Value	References
Π	Recruitment rate of humans (by birth or immigration)	day^{-1}	12.05	[14]
μ^*	Natural death rate of humans	day^{-1}	9×10^{-5}	[14]
γ^*	Recovery rate for human	day^{-1}	0.2	[14, 49, 132]
δ^*	Disease-induced death rate for humans	day^{-1}	4×10^{-4}	[49]
β_p^* (β_r^*)	Transmission rate in the pond (river)	day^{-1}	5 (5)	[49]
$k_p^*(k_r)$	Concentration of *V. cholerae* in the pond (river) that yields 50% chance of being infected with cholera	m^{-3}	$10^6(10^6)$	[139]
μ_B^*	Natural death rate for bacteria	day^{-1}	0.8	[14]
$\theta_p^*(\theta_r^*)$	Bacterial shedding rate in the pond (river)	day^{-1}	10^4 (10^4)	[49]
r	Reproductive rate of free-living bacteria	day^{-1}	0.3	[14, 89]
k_{bp}	Carrying-capacity of free-living bacteria in the pond	-	10^6	[89]
p	Precipitation (and river flow) rate into the pond	$m^3\text{day}^{-1}$	0.02	[132]
d_r^*	Drainage rate of the water in the pond	day^{-1}	0.02	[132]
$\lambda_p^*(\lambda_r^*)$	Rate of inflow of water from pond (river) to river (pond)	day^{-1}	0.5 (10)	Assumed
$V_p^{(min)}$	Minimum amount of water in the pond (constant) needed to support water exchange and transmission	m^3	-	-
V_r^*	Volume of water in the river (constant)	m^3	1.62×10^6	[49]

Table 2.1: Description of state variables and parameters of the model (2.2.1)

$$
\begin{array}{lllllll}
s=\frac{S}{H}, & i=\frac{I}{H}, & b_p=\frac{B_p}{k_{bp}}, & b_r=\frac{B_r}{k_r}, & v_p=\frac{V_p}{P}, & t=rt^*, & \\
\beta_p=\frac{\beta_p^*}{r}, & \beta_r=\frac{\beta_r^*}{r}, & \gamma=\frac{\gamma^*}{r}, & \delta=\frac{\delta^*}{r}, & \theta_p=\frac{\theta_p^*\Pi}{\mu^* r k_{bp}}, & \theta_r=\frac{\theta_r^*\Pi}{r\mu^* V_r^* k_r}, & \\
\lambda_r=\frac{\lambda_r^*}{r}, & \lambda_p=\frac{\lambda_p^*}{r}, & \mu=\frac{\mu^*}{r}, & \mu_B=\frac{\mu_B^*}{r}, & d_r=\frac{d_r^*}{r}, & k_p=\frac{k_p^* P}{k_{bp}}, & V_r=\frac{V_r^* k_r}{k_{bp}},
\end{array}
\tag{2.2.2}
$$

where $P=\frac{p+\lambda_r^* V_r^*}{d_r^*+\lambda_p^*}$ and $H=\frac{\Pi}{\mu^*}$. It should be noted that the growth rate of the bacterial population in the pond (r) is now re-scaled to 1 (i.e., $r=1$ in the normalized model (2.2.3)). It follows from the above re-scaling that the total human population, n, is now given by $n=s+i$. Using the change of variables and re-scaling (2.2.2) in the model (2.2.1) gives the following equivalent normalized system:

$$
\begin{cases}
\dot{s}=\mu(1-s)-\left(\beta_p\dfrac{b_p}{k_p v_p+b_p}+\beta_r\dfrac{b_r}{1+b_r}\right)s+\gamma i, \\
\dot{i}=\left(\beta_p\dfrac{b_p}{k_p v_p+b_p}+\beta_r\dfrac{b_r}{1+b_r}\right)s-(\gamma+\delta+\mu)i, \\
\dot{b}_p=\theta_p i+(1-b_p-\mu_B-\lambda_p)\,b_p+\lambda_r V_r b_r, \\
\dot{b}_r=\theta_r i+\lambda_p\frac{b_p}{V_r}-(\mu_B+\lambda_r)\,b_r, \\
\dot{v_p}=(d_r+\lambda_p)(1-v_p).
\end{cases}
\tag{2.2.3}
$$

The analysis in this study will be carried out on the normalized model (2.2.3). Since, like the original model (2.2.1), the model (2.2.3) monitors the temporal dynamics of human and bacterial populations, all its state variables and parameters are non-negative. In order to ensure substantial back-and-forth flow of water between the pond and the river, it is assumed, from now on, that $\lambda_p \geq 1$ (i.e., $\lambda_p^* \geq r$) and $\lambda_r \geq 1$ (i.e., $\lambda_r^* > r$).

2.2.1 Basic Properties of the Model

In this section, the basic qualitative properties of the normalized system (2.2.3) are explored. In particular, results for the existence, uniqueness, boundedness and non-negativity of its solutions are established. It is convenient to define the following sets:

$$
\begin{aligned}
\mathcal{D}_H &= \left\{(s,i)\in\mathbb{R}_+^2 : 0<s+i\leq 1\right\}, \\
\mathcal{D}_B &= \left\{(b_p,b_r)\in\mathbb{R}_+^2 : 0<b_p+V_r b_r\leq b^*\right\}, \\
\mathcal{D}_P &= \left\{v_p\in\mathbb{R}_+ : 0<v_p^{(min)}\leq v_p\leq 1\right\},
\end{aligned}
$$

where $b^*=\dfrac{\theta_p+\theta_r V_r+\frac{1}{4}}{\mu_B}>0$ and $v_p^{(min)}=\dfrac{V_p^{(min)}}{P}>0$.

Let $\mathcal{D}=\mathcal{D}_H\times\mathcal{D}_B\times\mathcal{D}_P$. We claim the following result:

Theorem 2.2.1 *The normalized model (2.2.3) with initial conditions in $\mathcal{D}$ has a unique solution that exists and remains in $\mathcal{D}$ for all time t. Furthermore, the positively-invariant region $\mathcal{D}$ attracts all solutions in $\mathbb{R}^2_+ \times \mathbb{R}^2_+ \times \mathbb{R}_+$.*

Proof. Since it is clear that, for all initial solutions of the normalized model (2.2.3) in the region $\mathcal{D}$, the functions in the right hand-sides of the system (2.2.3) are locally Lipschitz in $(s, i, b_p, b_r, v_p)^T$. Hence, it follows, by the Cauchy-Lipschitz theorem, that the normalized model (2.2.3) admits a unique local solution. Furthermore, adding the first two equations of the system (2.2.3) gives (noting that $n(t) = s(t) + i(t)$)

$$\frac{dn(t)}{dt} = \mu[1 - n(t)] - \delta i(t), \tag{2.2.4}$$

so that,

$$\mu - (\mu + \delta)n(t) \leq \frac{dn(t)}{dt} \leq \mu[1 - n(t)].$$

Hence, it follows, by standard comparison theorem [87], that

$$0 < \frac{\mu}{\mu + \delta} \leq n(t) \leq 1, \text{ for all } t > 0 \text{ if } n(0) < 1.$$

Furthermore, it follows from Equation (2.2.4) that $dn(t)/dt \leq 0$ whenever $n(t) \geq 1$. Hence, the subsystem of the model (2.2.3) containing the equations for the dynamics of the human populations ($s(t)$ and $i(t)$) is non-negative, bounded and invariant in $\mathcal{D}_H$.

Let $b(t) = b_p(t) + V_r b_r(t)$. It follows then that the total bacterial population in the aquatic environment (i.e., bacterial populations in the pond and the river) satisfy the following equation:

$$\frac{db(t)}{dt} = (\theta_p + \theta_r V_r) i(t) + b_p(t)[1 - b_p(t)] - \mu_B b(t). \tag{2.2.5}$$

Since $b_p(t)[1 - b_p(t)] \leq 1/4$ for all t, and noting that $i(t) \leq 1$ in $\mathcal{D}_H$, Equation (2.2.5) can be written as:

$$\frac{db(t)}{dt} \leq \left(\theta_p + \theta_r V_r + \frac{1}{4}\right) - \mu_B b(t). \tag{2.2.6}$$

It follows, by solving the inequality (2.2.6), that (where $b_0 = b(0)$):

$$\begin{aligned} b(t) &\leq \frac{1}{\mu_B}\left[\theta_p + \theta_r V_r + \frac{1}{4} + \left(b_0\mu_B - \theta_p - \theta_r V_r - \frac{1}{4}\right) e^{-\mu_B t}\right], \\ &= b^*\left[1 + \frac{1}{b^*} e^{-\mu_B t}\left(b_0 - b^*\right)\right]. \end{aligned} \tag{2.2.7}$$

By applying a standard comparison theorem [87], the inequality (2.2.7) can be re-written as:

$$0 < b(t) < b^* \text{ for all } t > 0 \text{ if } 0 < b_0 \leq b^*.$$

Further, it follows from (2.2.6) and (2.2.7) that $db(t)/dt \leq 0$ whenever $b(t) \geq b^*$. Hence, the total bacterial population in the aquatic environment, $b(t)$, is bounded, non-negative and positively-invariant in $\mathcal{D}_B$.

Finally, it is clear from the last equation of (2.2.3) that $dv_p/dt < 0$ whenever $v_p(t) > 1$. Further, integrating this equation gives:

$$v_p(t) = 1 + (v_{\mathrm{p}0} - 1)e^{-(d_r+\lambda_p)t},\ v_p(0) = v_{\mathrm{p}0},$$

from which it follows that

$$\lim_{t\to+\infty} v_p(t) = 1,\ 0 < v_p(t) \leq 1 \text{ if } 0 < v_{\mathrm{p}0} \leq 1,\ \text{and} \limsup_{t\to\infty} v_p(t) = 1.$$

Hence, the subsystem of the model (2.2.3) consisting of the equation for the dynamics of the water volume in the pond (v_p) is non-negative, bounded and invariant in $\mathcal{D}_P$.

In summary, it follows from the above analyses that the region $\mathcal{D}$ is positively-invariant for the normalized model (2.2.3), and all solutions of the normalized model are non-negative and bounded (since these results hold for the three constituent subregions, $\mathcal{D}_H$, $\mathcal{D}_B$ and $\mathcal{D}_P$). □

2.3 Reproduction Numbers for Various Transmission Pathways

The disease-free equilibrium of the normalized model (2.2.3) is given by $\mathbf{E}_0 = (s^*, i^*, b_p^*, b_r^*, v_p^*) = (1, 0, 0, 0, 1)$. Its local stability can be analysed using the next generation operator method (NGM) [61, 62, 161]. This method entails tracking the new infection terms as well as the linear transition terms in and out of infected compartments. In particular, the method involves computing two associated matrices, F (of the new infection terms) and V (of the linear transition terms), and the associated *basic reproduction number*, denoted by $\mathcal{R}_0$, is then given by $\mathcal{R}_0 = \rho(FV^{-1})$ [61, 62, 161], where ρ is the spectral radius (the dominant eigenvalue of the next generation matrix, $K = FV^{-1}$). The consequence of this approach is that the disease can be effectively controlled (or eliminated) if $\mathcal{R}_0 < 1$, and will persist in the community if $\mathcal{R}_0 > 1$. In other words, the dynamics of the disease transmission model is (often) completely determined by the reproduction number $\mathcal{R}_0$. Epidemiologically-speaking, the threshold quantity $\mathcal{R}_0$ represents the average number of new infections generated by a typical infected individual introduced into a completely susceptible population. In the context of the normalized model (2.2.3), the reproduction number will represent the average number of new cholera cases generated by a *V. cholerae* particle introduced the local pond-river network. It can also be a measure of the average number of *V. cholerae* particles shedded into the environment (i.e., into the pond-river network) by a typical cholera-infected human.

Thus, a control strategy (e.g., vaccinating a segment of the population) that can bring (and maintain) $\mathcal{R}_0$ to a value less than unity may lead to effective control or elimination of the disease. However, for a disease with multiple population types (e.g., cholera with *V. cholerae* residing in the human host as well as in the aquatic environment (i.e., in either the local pond or river)), anti-cholera control measures can be directed to, or focussed on one, population type. This leads to a different expression for the associated reproduction number ($\mathcal{R}_0$) corresponding to each population type targeted for anti-cholera control. For instance, in the models considered in [43, 118, 155], the expressions for the associated reproduction number ($\mathcal{R}_0$) is represented as a sum of two separate terms corresponding to the host-to-host and to the environment-to-host

transmission paths. This could suggest the independence of these pathways in the disease transmission cycle. Furthermore, the $\mathcal{R}_0$ for the model in [25] has a square root term that suggests a more complicated interaction between host-to-host and environment-to-host transmission pathways. It is clear from the above that, for a cholera model such as the one presented in the current study, the expression for the associated reproduction number obtained will be dependent on how the role of the environment is interpreted *vis a vis* cholera transmission dynamics (i.e., how the role of the environment is interpreted in transition between disease compartments and in transmission of secondary infectious hosts and free-living *V. cholerae* [14]). As noted by Bani-Yaghoub et al. [14], the interpretation of this role has been controversial in the literature. In particular, while numerous studies environment-host-pathogen interactions suggest that the pathogen-contaminated environment serves as a reservoir of infectious free-living pathogens for infection of various host populations (e.g., humans, other non-human animals and plants) [27, 55, 140], other studies show that the environment plays only a somewhat marginal role on the complex dynamics of infectious diseases [10, 58, 59, 108, 168] . Consequently ([14]), we hypothesize the following four scenarios where the environment acts as a (1) Transition, (2) Transition-Reservoir case I, (3) Transition-Reservoir case II and (4) Reservoir of *V. cholerae* in the environment-host-environment cholera transmission dynamics we consider in this study . In other words, the following four possible interpretations (i.e., transmission pathways) of the role the environment plays on cholera transmission dynamics will be considered for the normalized model (see also Table 2.2):

Scenario 1 (the environment acts as Transition): in this scenario, both the shedding of *V. cholerae* into the environment and the growth of *V. cholerae* within the environment are considered as transitions within the initial infectious state of the host population. Therefore, the the parameters of the model related to the shedding and growth rates of the bacteria are placed in the V matrix.

Scenario 2 (the environment acts as Transition-Reservoir case I): for this scenario, the growth of bacteria in the environment is regarded as vertical transmission of an infectious pathogen (*V. cholerae*) from the environment to the environment. Therefore, the parameter related to the growth rate of the bacteria in the environment (i.e., in the pond) is counted as new infection generated in the environment, and is, consequently, placed in the F matrix.

Scenario 3 (the environment acts as Transition-Reservoir case II): the environment has a double role under this scenario. In particular, while the shedding of bacteria by the host into the environment is counted as new *V. cholerae* infection, the growth of bacteria within the environment is considered as transitions within the initial infectious state of the host population (thus, the environment acts partially as reservoir and partially as transition). Consequently, the parameters related to the shedding rates are placed in the F matrix, while the parameter related to the bacteria growth in the environment (i.e., in the pond) is placed in the V matrix.

Scenario 4 (the environment acts as Reservoir): in this scenario, the environment is assumed to act as a reservoir. Hence, new infections are added into the environment both through bacteria growth (in the pond)

and bacterial shedding by infectious humans. Hence, the parameters related to both bacterial shedding and growth are placed in the F matrix.

	Cholera Transmission Rates β_p and β_r	Bacteria Shedding Rates θ_p and θ_r	Growth of Bacteria in the Pond $(r = 1)$
Scenario 1	✓		
Scenario 2	✓		✓
Scenario 3	✓	✓	
Scenario 4	✓	✓	✓

Table 2.2: Contributions of the various cholera transmission pathways (direct environment-host transmission and bacterial shedding) into the next generation matrix of new infection terms (F).

It is worth mentioning that Scenario 3 (where bacterial shedding rates are considered as new infections, while bacterial growth is counted as transition term) is not included in the scenarios considered in the cholera transmission model presented in [14].

It is convenient to define the following positive constants:

$$\begin{aligned} a_1 &= V_r\theta_r\lambda_r + \theta_p(\lambda_r + \mu_B), \quad & a_2 &= (\theta_p + V_r\theta_r)\lambda_p + V_r\theta_r\mu_B, \\ a_3 &= \gamma + \delta + \mu, & a_4 &= \lambda_r + \mu_B. \end{aligned} \tag{2.3.1}$$

The computation of the reproduction number of the normalized model (2.2.3), associated with each of the aforementioned scenarios, is given below.

2.3.1 Scenario 1 (the environment acts as Transition): pathogen shedding into, and growth within, the environment considered as transitions within the infected host population

For this setting, terms related to bacterial shedding and growth are included in the matrix V of transition terms. For this scenario, it can be shown that the associated matrices F and V are given, respectively, by

$$F_1 = \begin{pmatrix} 0 & \frac{\beta_p}{k_p} & \beta_r \\ 0 & 0 & 0 \\ 0 & 0 & 0 \end{pmatrix} \quad \text{and} \quad V_1 = \begin{pmatrix} a_3 & 0 & 0 \\ -\theta_p & \mu_B - 1 + \lambda_p & -\lambda_r V_r \\ -\theta_r & -\frac{\lambda_p}{V_r} & a_4 \end{pmatrix}, \tag{2.3.2}$$

so that,

$$
\begin{aligned}
K_1 &= F_1 V_1^{-1} \\
&= \begin{pmatrix}
\dfrac{V_r\beta_p a_1 + k_p\beta_r(a_2 - V_r\theta_r)}{a_3 V_r k_p[a_4(\mu_B - 1) + \mu_B\lambda_p]} & \dfrac{k_p\beta_r\lambda_p + V_r\beta_p a_4}{V_r k_p[a_4(\mu_B - 1) + \mu_B\lambda_p]} & \dfrac{V_r\beta_p\lambda_r + k_p\beta_r(\lambda_p + \mu_B - 1)}{k_p[a_4(\mu_B - 1) + \mu_B\lambda_p]} \\
0 & 0 & 0 \\
0 & 0 & 0
\end{pmatrix}.
\end{aligned} \tag{2.3.3}
$$

It follows that the spectral radius of NGM (K_1)is given by the quantity:

$$
\mathcal{R}_0^{(1)} = \rho(K_1) = \frac{V_r\beta_p a_1 + k_p\beta_r\left[(\theta_p + V_r\theta_r)\lambda_p + V_r\theta_r(\mu_B - 1)\right]}{k_p V_r a_3[a_4(\mu_B - 1) + \mu_B\lambda_p]}, \tag{2.3.4}
$$

that represents the average number of secondary infections through environment-to-host transmission caused by one infectious individual in its infectious lifetime, regulated respect to the bacteria growth or decay rates in the environment. It is worth noting from (2.3.4) that the condition $\mu_B > 1$ must be imposed to ensure that $\mathcal{R}_0^{(1)} > 0$. Hence, it is assumed, from now on, that $\mu_B - 1 \geq 0$. It should be mentioned that Bani et al. [14] assumed the strict inequality $\mu_B > 1$ (however, for our normalized model (2.2.3), it is possible to extend the strict inequality assumption in [14] to also include the case where $\mu_B = 1$ (there is no singularity in the normalized model when μ_B is set to 1; this is due to the interconnected nature of the pond-river network we considered in this study).

In the context of the normalized model (2.2.3), the assumption $\mu_B > 1$ means that the natural death rate of bacteria (μ_B) equals the growth rate of bacteria in the pond (1; recalling that, for the normalized model (2.2.3), the growth rate r is re-scaled to 1). The ecological implication of this assumption is that the bacterial population in the pond ($b_p(t)$) is unable to maintain itself in the environment in the absence of human shedding (represented by θ_p). We note that this also applies to the bacterial population in the river (in fact, in the case of bacterial population in the river ($b_r(t)$), this assumption means that the $\mu_B > 0$, since, for the normalized model, the bacterial growth rate in the river is 0). Therefore, considering the entire bacterial population in the pond and in the river, the above assumption implies that the bacteria is unable to survive in the absence of infection from the host (i.e., the bacteria cannot maintain itself in the environment). It is important to underline that, with this assumption, all the entries of the NGM K_1 are non-negative and the well-posedness of $\mathcal{R}_0^{(1)}$ is ensured.

It should be mentioned that the eigenvalues of the matrix of linearization of the entire ODE system (2.2.3) around the disease-free equilibrium $\mathbf{E}_0$ (denoted by λ_i; $i = 1, \cdots, 5$) satisfy the quintic polynomial:

$$
(\lambda + \mu)(\lambda + d_r + \lambda_p)(\lambda^3 + b_2\lambda^2 + b_1\lambda + b_0) = 0, \tag{2.3.5}
$$

where,

$$
\begin{aligned}
b_2 &= a_3 + a_4 + \lambda_p + \mu_B - 1, \qquad b_0 = a_3[a_4(\mu_B - 1) + \mu_B\lambda_p]\left(1 - \mathcal{R}_0^{(1)}\right), \\
b_1 &= (a_3 + a_4)(\mu_B - 1) + a_3(a_4 + \lambda_p) + \mu_B\lambda_p - \beta_r\theta_r - \frac{\beta_p\theta_p}{k_p}.
\end{aligned} \tag{2.3.6}
$$

It follows from the first two terms of (2.3.5) that the eigenvalues $\lambda_1 = -\mu < 0$ and $\lambda_2 = -(d_r + \lambda_p) < 0$. Further, it follows from (2.3.6) that the coefficients b_2 and b_0 of the cubic in (2.3.5) are automatically positive for $\mu_B - 1 \geq 0$ and $\mathcal{R}_0^{(1)} < 1$. It can also be shown, with algebraic manipulations, that the coefficient $b_1 > 0$ whenever $\mathcal{R}_0^{(1)} < 1$ (noting the assumption $\lambda_p > 1$). Moreover, the associated Routh-Hurwitz condition $b_2 b_1 - b_0 > 0$ holds if and only if $\mathcal{R}_0^{(1)} < 1$ (see Appendix A1). Hence, the roots of the cubic in (2.3.5) have negative real part whenever $\mathcal{R}_0^{(1)} < 1$. Thus, the disease-free equilibrium ($\mathbf{E}_0$) of the normalized model (2.2.3) is locally-asymptotically stable whenever $\mathcal{R}_0^{(1)} < 1$. In other words, the application of the method of standard linearization (around the disease-free equilibrium of the normalized model) corresponds to Scenario 1 of this study. It is noteworthy that the matrix F_1 (and also K_1) is rank 1 (corresponding to the associated single transmission pathway).

2.3.2 Scenario 2 (the environment acts as Transition-Reservoir case I): growth of bacteria regarded as vertical transmission of *V. cholerae* in the environment

Here, the bacterial growth term is considered as a new infection of the environment. That is, the bacteria growth rate is placed in the F matrix. For this setting,

$$F_2 = \begin{pmatrix} 0 & \frac{\beta_p}{k_p} & \beta_r \\ 0 & 1 & 0 \\ 0 & 0 & 0 \end{pmatrix} \quad \text{and} \quad V_2 = \begin{pmatrix} a_3 & 0 & 0 \\ -\theta_p & \mu_B + \lambda_p & -\lambda_r V_r \\ -\theta_r & -\frac{\lambda_p}{V_r} & a_4 \end{pmatrix}. \tag{2.3.7}$$

Thus,

$$K_2 = F_2 V_2^{-1} = \begin{pmatrix} \frac{V_r\beta_p(V_r\theta_r\lambda_r a_4\theta_p)+k_p\beta_r(\theta_p\lambda_p+V_r\theta_r(\lambda_p+\mu_B))}{k_p V_r\mu_B a_3(a_4+\lambda_p)} & \frac{V_r\beta_p a_4+k_p\beta_r\lambda_p}{k_p V_r\mu_B(a_4+\lambda_p)} & \frac{V_r\beta_p\lambda_r+k_p\beta_r(\lambda_p+\mu_B)}{k_p\mu_B(a_4+\lambda_p)} \\ \frac{V_r\theta_r\lambda_r+\theta_p a_4}{a_3\mu_B(a_4+\lambda_p)} & \frac{a_4}{\mu_B(a_4+\lambda_p)} & \frac{V_r\lambda_r}{\mu_B(a_4+\lambda_p)} \\ 0 & 0 & 0 \end{pmatrix}. \tag{2.3.8}$$

Therefore,

$$\mathcal{R}_0^{(2)} = \rho(K_2) = \frac{g_1 + \sqrt{g_1^2 + 4g_2}}{2}, \tag{2.3.9}$$

where,

$$g_1 = \frac{V_r\beta_p a_1 + k_p\beta_r a_2 + V_r k_p a_3 a_4}{k_p V_r \mu_B a_3(a_4 + \lambda_p)}, \quad g_2 = \frac{\beta_r\theta_r}{\mu_B a_3(a_4 + \lambda_p)}. \tag{2.3.10}$$

The expression for $\mathcal{R}_0^{(2)}$, given by (2.3.9), suggests a more complicated interaction of the environment-to-host and host-to-host pathways (in comparison to $\mathcal{R}_0^{(1)}$ for Scenario 1). Further, it is worth noting that the matrix F_2 (and also K_2) is rank 2 (corresponding to the two transmission pathways associated with Scenario 2).

2.3.3 Scenario 3 (the environment acts as Transition-Reservoir case II): shedding of bacteria considered as new infections but bacterial growth is a transition term

In this scenario, bacterial shedding rates are placed in the F matrix, while the bacterial growth rate is placed in the V matrix. Here,

$$F_3 = \begin{pmatrix} 0 & \frac{\beta_p}{k_p} & \beta_r \\ \theta_p & 0 & 0 \\ \theta_r & 0 & 0 \end{pmatrix} \quad \text{and} \quad V_3 = \begin{pmatrix} a_3 & 0 & 0 \\ 0 & \mu_B - 1 + \lambda_p & -\lambda_r V_r \\ 0 & -\frac{\lambda_p}{V_r} & a_4 \end{pmatrix}, \tag{2.3.11}$$

so that,

$$K_3 = F_3 V_3^{-1} = \begin{pmatrix} 0 & \frac{V_r\beta_p a_4 + k_p\beta_r\lambda_p}{k_p V_r[a_4(\mu_B - 1) + \lambda_p\mu_B]} & \frac{V_r\beta_p\lambda_r + k_p\beta_r(\lambda_p+\mu_B-1)}{k_p[a_4(\mu_B-1)+\lambda_p\mu_B]} \\ \frac{\theta_p}{a_3} & 0 & 0 \\ \frac{\theta_r}{a_3} & 0 & 0 \end{pmatrix}, \tag{2.3.12}$$

and,

$$\mathcal{R}_0^{(3)} = \rho(K_3) = \sqrt{\frac{V_r\beta_p a_1 + k_p\beta_r\left[(\theta_p + V_r\theta_r)\lambda_p + V_r\theta_r(\mu_B - 1)\right]}{k_p V_r a_3[a_4(\mu_B - 1) + \mu_B\lambda_p]}}. \tag{2.3.13}$$

It should be noted that the quantity $\mathcal{R}_0^{(3)} > 0$ (whenever $\mu_B - 1 \geq 0$). Furthermore, it is clear that $\mathcal{R}_0^{(1)} = \left(\mathcal{R}_0^{(3)}\right)^2$. For this scenario, the associated matrix of new infections (F_3) is rank 2 (corresponding to the two associated transmission pathways; the matrix K_3 is also rank 2).

2.3.4 Scenario 4 (the environment acts as Reservoir): the environment is assumed to act as a reservoir

In this case, both bacterial growth and shedding are considered as new infections of the environment. Hence, both the shedding and growth rates are placed in the F matrix. For this scenario,

$$F_4 = \begin{pmatrix} 0 & \frac{\beta_p}{k_p} & \beta_r \\ \theta_p & 1 & 0 \\ \theta_r & 0 & 0 \end{pmatrix} \quad \text{and} \quad V_4 = \begin{pmatrix} a_3 & 0 & 0 \\ 0 & \mu_B + \lambda_p & -\lambda_r V_r \\ 0 & -\frac{\lambda_p}{V_r} & a_4 \end{pmatrix}, \tag{2.3.14}$$

so that,

$$K_4 = F_4 V_4^{-1} = \begin{pmatrix} 0 & \frac{V_r\beta_p a_4 + k_p\beta_r\lambda_p}{k_p V_r \mu_B(a_4+\lambda_p)} & \frac{V_r\beta_p\lambda_r + k_p\beta_r(\lambda_p+\mu_B)}{k_p\mu_B(a_4+\lambda_p)} \\ \frac{\theta_p}{a_3} & \frac{a_4}{\mu_B(a_4+\lambda_p)} & \frac{V_r\lambda_r}{\mu_B(a_4+\lambda_p)} \\ \frac{\theta_r}{a_3} & 0 & 0 \end{pmatrix}. \tag{2.3.15}$$

Hence, it follows that $\mathcal{R}_0^{(4)} = \rho(K_4)$ is the spectral radius of the following associated characteristic polynomial (of K_4):

$$p(\lambda) = \lambda^3 + d_2\lambda^2 + d_1\lambda + d_0, \tag{2.3.16}$$

where,

$$\begin{aligned} d_2 &= -\frac{a_4}{\mu_B(a_4+\lambda_p)}, \quad d_1 = -\frac{V_r\beta_p(V_r\theta_r\lambda_r + \theta_p a_4) + k_p\beta_r[\theta_p\lambda_p + V_r\theta_r(\lambda_p+\mu_B)]}{k_p a_3 V_r\mu_B(a_4+\lambda_p)}, \\ d_0 &= \frac{\beta_r\theta_r}{a_3\mu_B(a_4+\lambda_p)}. \end{aligned} \tag{2.3.17}$$

The discriminant of the cubic (2.3.16) is given by [159]:

$$\Delta_p = d_2^2 d_1^2 + 18 d_1 d_2 d_0 - 4d_1^3 - 4d_0 d_2^3 - 27 d_0^2,$$

and it can be shown, after some algebraic manipulations, that $\Delta_p > 0$ (see Appendix A). Thus, all three roots of the cubic (2.3.16) are real. Moreover, since the coefficients $d_2 < 0$, $d_1 < 0$ and $d_0 > 0$, it follows, by the Descartes's Rule of Signs ([98]), that $p(\lambda)$ has two positive and one negative real roots. Therefore, its largest root (i.e., $\mathcal{R}_0^{(4)}$) is real and positive, and is given by (obtained from solving the cubic (2.3.16) [159]):

$$\mathcal{R}_0^{(4)} = \sqrt[3]{-\frac{q_1}{2} + \sqrt{\frac{q_1^2}{4} + \frac{q_2^3}{27}}} + \sqrt[3]{-\frac{q_1}{2} - \sqrt{\frac{q_1^2}{4} + \frac{q_2^3}{27}}}, \tag{2.3.18}$$

where,

$$\begin{aligned} q_1 &= -\frac{m_1 + m_2}{27 k_p V_r \mu_B^3 a_3 (a_4+\lambda_p)^3}, \\ q_2 &= -\frac{3V_r\beta_p\mu_B(a_4+\lambda_p)a_1 + k_p(V_r a_3 a_4^2 + 3\beta_r\mu_B(a_4+\lambda_p)a_2)}{3k_p V_r\mu_B^2 a_3(a_4+\lambda_p)^2}, \end{aligned} \tag{2.3.19}$$

with,

$$\begin{aligned} m_1 &= 9V_r\beta_p\mu_B a_4(a_4+\lambda_p)a_1, \\ m_2 &= k_p(2V_r a_3 a_4^3 + 9\beta_r\mu_B(a_4+\lambda_p)(\theta_p\lambda_p a_4 + V_r\theta_r(\lambda_r(\lambda_p - 2\mu_B) - 2\mu_B(\lambda_p+\mu_B)))). \end{aligned}$$

The matrix F_4 (and also K_4) is rank 3 (corresponding to the associated three transmission pathways).

In summary, the analyses in this section reveal that, by considering multiple transmission pathways, multiple reproduction numbers were obtained for the normalized model (2.2.3). The fact that these reproduction numbers are not unique may lead to the possible underestimation or overestimation of the control efforts needed to effectively control or eliminate the disease. To address this problem (of lack of uniqueness of the reproduction threshold associated with disease transmission dynamics), Roberts and Heesterbeek [133] and Heesterbeek and Roberts [85] introduced the notion of *type reproduction number*, denoted by $\mathcal{T}$. This allows for the determination of a single threshold quantity that is valid for each of the four scenarios described above (and listed in Table 2.2).

The four basic reproduction numbers ($\mathcal{R}_0^{(i)}; i = 1, \cdots, 4$) computed above are compared as follows. In particular, a plot of each of the reproduction as a function of bacterial shedding rate in the river (θ_r) and as a function of cholera transmission rate in the river (β_r) are depicted in Figure 2.4 (left and right panels, respectively). This figure shows that, with the assumption $\mu_B - 1 \geq 0$, all four basic reproduction numbers agree on the threshold value 1(i.e., unity). That is,

$$\mathcal{R}_0^{(1)} = 1 \Leftrightarrow \mathcal{R}_0^{(2)} = 1 \Leftrightarrow \mathcal{R}_0^{(3)} = 1 \Leftrightarrow \mathcal{R}_0^{(4)} = 1.$$

Further, for a fixed set of parameter values, numerical simulations (Figure 2.4) suggest that the four reproduction numbers are all greater, equal or less than unity. It was further observed that when any of the basic reproduction numbers exceeds unity, the following ordering always holds:

$$\mathcal{R}_0^{(1)} > \mathcal{R}_0^{(2)} > \mathcal{R}_0^{(3)} > \mathcal{R}_0^{(4)} > 1.$$

The order is reversed if any of the basic reproduction numbers is less than unity (that is, $\mathcal{R}_0^{(1)} < \mathcal{R}_0^{(2)} < \mathcal{R}_0^{(3)} < \mathcal{R}_0^{(4)} < 1$).

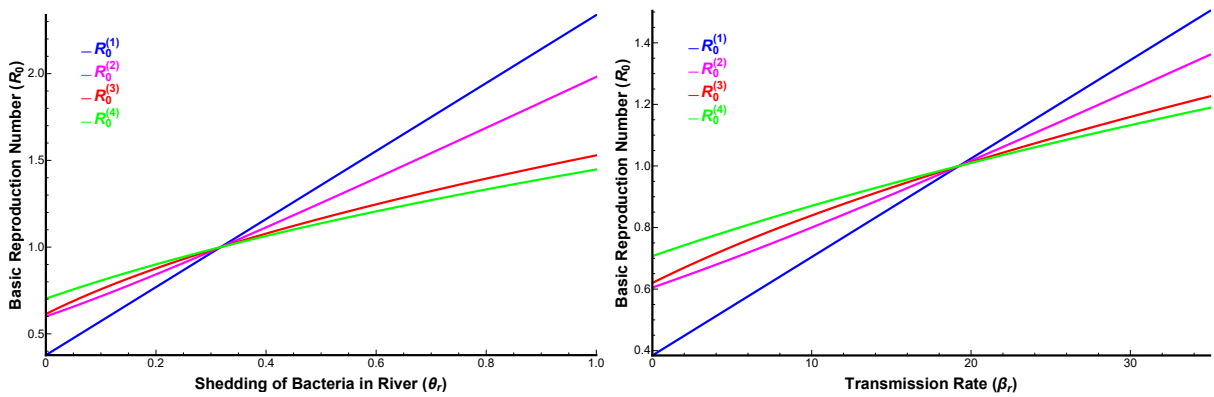

(a) (b)

Figure 2.4: The plots represent the behaviours of the different expression of $\mathcal{R}_0$ derived: $\mathcal{R}_0^{(1)}$ is the blue line, $\mathcal{R}_0^{(2)}$ magenta line, $\mathcal{R}_0^{(3)}$ the red line and $\mathcal{R}_0^{(4)}$ the green line. The parameter values used are listed in Table 2.1 with $\theta_p^* = 10^3$. $\mathcal{R}_0$ is a function of the parameter θ_r in graph (a) and of β_r in graph (b).

2.4 Type Reproduction Number

First of all, it should be noted that the entry k_{ij} of the NGM K is defined as the expected number of new cases that a infected individual of type j causes among the susceptible individuals of type i, in a fully susceptible population. To prevent or mitigate an outbreak of a disease, preventive intervention measures (such as vaccination, quarantine, isolation, public health education etc.) are generally implemented, depending on the type of the disease and availability of control resources. If these interventions are implemented to all the sub-populations involved in the disease transmission cycle, regardless of their infection status, then the quantity $\mathcal{R}_0$ also provides a measure of the minimum coverage level of the adopted control measures needed to eliminate the disease [7, 61]. Otherwise, if a control strategy is aimed only at particular population type, such as the use of chemical insecticides to control bacterial population in the aquatic environment or vaccinating the human hosts, the so-called type reproduction number (denoted by $\mathcal{T}_s$, where s is the population type) takes on the role of $\mathcal{R}_0$ (hence, it also has a direct relationship with the minimum coverage level of the control strategy or strategies implemented) [85, 133]. In other words, the threshold quantity $\mathcal{R}_0$ (or, in this case, equivalently, $\mathcal{T}_s$) provides a measure of the effort (or coverage level) required to achieve population-wide elimination of the disease when the adopted control interventions are aimed at a particular type of population.

In the context of the normalized model (2.2.3), let humans represent population of type 1. Further, let the bacterial population in the pond and in the river represent bacterial populations of type 2 and 3, respectively. Let k be the number of disease transmission scenarios considered (i.e., $k = 1, \cdots, 4$, as discussed in Section 2.3) . It then follows that, in most cases, a strategy that reduces the susceptibility to infection of humans (type 1), for example, influences all the entries of the NGM that represents potentially infectious contacts between the bacterium and a susceptible of type 1 (i.e., a susceptible human). Mathematically-speaking, this strategy affects the entries of the first row of the NGM (K). Similarly, a strategy aimed at reducing the infectiousness of infected humans (type 1) affects the entries of the first column of the NGM K [14, 85]. It is worth recalling the following definition.

Definition 2.4.1 *[85, 133] The type reproduction number ($\mathcal{T}_s$) associated with the population type s is defined by*

$$\mathcal{T}_s^{(j)} = \boldsymbol{e}_s^T K_j [I - (I - P_s)K_j]^{-1} \boldsymbol{e}_s, \ j = 1, \cdots, k \tag{2.4.1}$$

where K_j is a given NGM of order n related to Scenario j, I is the $n \times n$ identity matrix, $\boldsymbol{e}_s$ is an n-dimensional column vector with all entries zero except that the s entry is equal to 1, and P_s is a projection matrix with the (s, s) entry equal to 1 and all other entries equal to zero.

Using the notation in [14], let $K_i = F_i V_i^{-1}$ $(i = 1, ..., k)$ be the NGMs obtained from different epidemiological scenarios. Further, assume (without loss of generality) that [14]

$$V_j = V_i + U_m \text{ and } F_j = F_i + U_m, \ \{i, j\} \in \{1, ..., k\}, \text{ with } i \neq j, \tag{2.4.2}$$

where U_m is a matrix with m non-zero rows (say, rows $l_1, ..., l_m$, which correspond to the m disease compartments above) and $n - m$ zero rows. Furthermore, V_i and F_i are transition and transmission matrices corresponding to Scenario i, respectively, while V_j and F_j are the transition and transmission matrices corresponding to Scenario j, respectively (with $i \neq j$). It is convenient to recall the following result (proved in [14]):

Theorem 2.4.1 *[14] Let $\mathcal{T}_s^i$ and $\mathcal{T}_s^j$ be the type reproduction numbers associated with population type s defined by (2.4.1) and, respectively, derived from the NGMs K_i and K_j, with $\{i, j\} \in \{1, ..., k\}$, with $i \neq j$. If $s \neq l_w$, with $w = 1, ..., m$ and both $\mathcal{T}_s^i$ and $\mathcal{T}_s^j$ are well defined, then $\mathcal{T}_s^i = \mathcal{T}_s^j$.*

Theorem 2.4.1 will be used to determine whether or not the type reproduction number computed for each of the three populations types will be unique for all four scenarios discussed in Section 2.3 (by showing whether or not the hypotheses of the above theorem are satisfied for each case).

The normalized model (2.2.3) has $n = 3$ disease compartments (i.e., $i(t)$, $b_p(t)$ and $b_r(t)$) and, the value of the parameter m (for the interactions within and between the disease compartments $b_p(t)$ and $b_r(t)$) depends on the scenarios being compared. For example, if we consider Scenarios 1 and 2, only the role of the compartment $b_p(t)$ is interpreted differently (since, in Scenario 1, the bacteria growth parameter ($r = 1$) is placed in the V_1 matrix, while in Scenario 2 it is placed in the F_2 matrix). Hence, in this case, $m = 1$. If we, instead, compare Scenario 1 with Scenario 3 or Scenario 4, then $m = 2$ (since, in this case, both $b_p(t)$ and $b_r(t)$ are epidemiologically interpreted differently; for example, in Scenario 1 the parameters for the shedding rate of bacteria, represented by θ_p and θ_r, are placed in the V_1 matrix, while in Scenario 3 they are placed in the F_3 matrix).

2.4.1 Targeting population of type 1 (humans)

In Section 2.3, we showed four different scenarios, leading to different NGM (K_i, with $i = 1, 2, 3, 4$). For the normalized model (2.2.3), the total number of *V. cholerae* transmission scenario considered is four (i.e., $k = 4$). Here, consider population of type $s = 1$ (that is, we consider the compartment $i(t)$). Therefore, in order to apply Definition (2.4.1) for the computation of the associated type reproduction numbers ($\mathcal{T}_1^{(j)}; j = 1, \cdots, 4$), the associated vector $\mathbf{e}_1$ and projection matrix P_1 are introduced as follows:

$$\mathbf{e}_1 = \begin{pmatrix} 1 \\ 0 \\ 0 \end{pmatrix}, \quad P_1 = \begin{pmatrix} 1 & 0 & 0 \\ 0 & 0 & 0 \\ 0 & 0 & 0 \end{pmatrix}. \tag{2.4.3}$$

Considering Scenario 1 (i.e., $j = 1$) and substituting $j = 1$ (and using K_1, $\mathbf{e}_1$ and P_1) into (2.4.1), one gives the the following associated type reproduction number related to (targeting) the infected human population $i(t)$ (i.e., $s = 1$):

$$\begin{aligned} \mathcal{T}_1^{(1)} &= \mathbf{e}_1^T K_1 [I - (I - P_1)K_1]^{-1} \mathbf{e}_1, \\ &= \frac{V_r \beta_p a_1 + k_p \beta_r \left[(\theta_p + V_r \theta_r)\lambda_p + V_r \theta_r (\mu_B - 1)\right]}{k_p V_r a_3 [a_4(\mu_B - 1) + \mu_B \lambda_p]}, \end{aligned} \tag{2.4.4}$$

where K_1 is the NGM of Scenario 1 given in (2.3.3). Now it is proved that the same expression for $\mathcal{T}_1^{(1)}$ is obtained in the other three transmission scenarios. First of all, it can be shown that Assumption (2.4.2) holds for the normalized model (2.2.3). Indeed, if $i = 1$ and $j = 2$ (i.e., if we compare Scenario 1 and Scenario 2), then it follows from (2.4.2) that (note that $m = 1$ in this case):

$$V_2 = V_1 + U_1, \text{ and } F_2 = F_1 + U_1,$$

where,

$$U_1 = \begin{pmatrix} 0 & 0 & 0 \\ 0 & 1 & 0 \\ 0 & 0 & 0 \end{pmatrix}.$$

In this case, we have $l_1 = 2$ (the second row of U_m (or, equivalently, U_1) corresponds to the compartment b_p, that is interpreted differently).

Moreover, if $i = 1$ and $j = 3$ (i.e., if Scenario 1 and Scenario 3 are compared), Equation (2.4.2) gives (note that $m = 2$ in this case):

$$V_3 = V_1 + U_2, \text{ and } F_3 = F_1 + U_2,$$

where,

$$U_2 = \begin{pmatrix} 0 & 0 & 0 \\ \theta_p & 0 & 0 \\ \theta_r & 0 & 0 \end{pmatrix}.$$

In this case, we have $l_1 = 2$ and $l_2 = 3$ (the second and third rows of U_m (i.e., U_2 in this case) correspond to the compartments b_p and b_r, that are interpreted differently). Finally, if $i = 1$ and $j = 4$ (i.e., we comparing Scenario 1 and Scenario 4), it then follows from (2.4.2) that (noting that $m = 2$ in this case):

$$V_4 = V_1 + U_2, \text{ and } F_4 = F_1 + U_2,$$

where,

$$U_2 = \begin{pmatrix} 0 & 0 & 0 \\ \theta_p & 1 & 0 \\ \theta_r & 0 & 0 \end{pmatrix}.$$

In this case, $l_1 = 2$ and $l_2 = 3$ (the second and third rows of U_m correspond to the compartments b_p and b_r, that are interpreted differently). It should be mentioned that these can, of course, also be achieved by comparing all other scenario permutations (i.e., comparing Scenario 2 with Scenario 3, or Scenario 2 with Scenario 4 or Scenario 3 with Scenario 4).

Second, let $\mathcal{T}_1^i$ $(i = 1, 2, 3, 4)$ be the type reproduction numbers associated with population type $s = 1$ defined by (2.4.1) and, respectively, derived from the NGMs K_i $(i = 1, 2, 3, 4)$. It has just been pointed out that there can be at most two compartments that are interpreted differently in the scenarios considered, which are $b_p(t)$ (which corresponds to $s = 2$) and $b_r(t)$ (which corresponds to $s = 3$). So the compartment that is targeted here, $i(t)$ (which corresponds to $s = 1$), is interpreted the same way in all scenarios. It is easy to see that the hypotheses of the Theorem 2.4.1 are verified. Since in this case with humans as the population

type considered (i.e., $s = 1$), and for all the aforementioned scenarios we compared $s = 1$ always differs from l_1 and l_2 (with $l_1 = 2$ and $l_2 = 3$), it follows from Theorem 2.4.1 that the associated type reproduction number ($\mathcal{T}_1$) is unique. Indeed, $s = 1$ is different from l_w ($w = 1, 2$), when Scenario 1 is compared with the other three scenarios. Hence, regardless of how the associated human-bacteria interactions are interpreted, the type reproduction number related to the infected human host population ($i(t)$) is unique. That is, the following result holds (by Theorem 2.4.1 [14]):

$$\mathcal{T}_1 = \mathcal{T}_1^{(j)} = \mathcal{R}_0^{(1)} = \left(\mathcal{R}_0^{(3)}\right)^2, \quad \text{for} \quad j = 1, \cdots, 4. \tag{2.4.5}$$

Noting that $\mu_B - 1 \geq 0$, it follows from the expression of $\mathcal{R}_0^{(1)}$ given in Section 2.3 that $\mathcal{T}_1^j$ is well defined for $j = 1, \cdots, 4$ (corresponding, respectively, to Scenarios 1, 2, 3 and 4 in Section 2.3). The result below follows from Theorem 2 of [161].

Theorem 2.4.2 *The disease-free equilibrium point, $\boldsymbol{E}_0$ of the normalized model (2.2.3), is locally-asymptotically stable if $\mathcal{T}_1 < 1$ (or, equivalently, $\mathcal{R}_0^{(1)} < 1$), and unstable if $\mathcal{T}_1 > 1$ (or, equivalently, $\mathcal{R}_0^{(1)} > 1$), where $\mathcal{T}_1$ is the associated type reproduction number defined in (2.4.5).*

The epidemiological implication of Theorem 2.4.2 is that a small influx of infected individuals (i.e., in the basin of attraction of the disease-free equilibrium $\mathbf{E}_0$) will not cause a major outbreak in the community. In other words, cholera can be eliminated from the community if the initial number of individuals is not large enough. To ensure that disease elimination is not dependent on the initial number of infected individuals, a global asymptotic stability result must be established for the disease-free equilibrium $\mathbf{E}_0$. This is done below for a special case where the volume of water in the pond is maximum (i.e., $v_p(t) = 1$).

Theorem 2.4.3 *Consider the special case of the normalized model (2.2.3) with $v_p(t) = 1$ for all t. The disease-free equilibrium, $\boldsymbol{E}_0$, of the model is globally-asymptotically stable in $\mathcal{D}$ if $\mathcal{T}_1 < 1$ (or, equivalently, if $\mathcal{R}_0^{(1)} = \left(\mathcal{R}_0^{(3)}\right)^2 < 1$), and unstable if $\mathcal{T}_1 > 1$ (or, equivalently, if $\mathcal{R}_0^{(1)} = \left(\mathcal{R}_0^{(3)}\right)^2 > 1$).*

The proof of Theorem 2.4.3, based on using a Lyapunov function theory and LaSalle's Invariance Principle [96], is given in Appendix C. It is worth mentioning that the results of Theorems 2.4.2 and 2.4.3 also hold (but only with respect to the reproduction number, $\mathcal{R}_0^{(j)}$; $j = 1, \cdots, 4$) when the other population types (i.e., $s = 2$ or $s = 3$) are targeted (Bani et al. [14] also showed that the disease-free equilibrium of their cholera model is globally-asymptotically stable whenever any of the constituent reproduction number of the model is less than unity).

The epidemiological implication of Theorem 2.4.3 is that bringing (and maintaining) the Type reproduction number ($\mathcal{T}_1$ or, equivalently, $\mathcal{R}_0^{(1)}$ or $\mathcal{R}_0^{(3)}$) to a value less than unity is necessary and sufficient for the elimination of cholera from the population. Further, following Bani et al. [14], this result can be expressed in terms of the *herd immunity threshold*. In particular, a control strategy that targets the population type 1 (i.e., bacteria in the human host) can lead to the effective control or elimination of the disease if the control is administered to at least the proportion

$$p_1^{(j)} = 1 - \frac{1}{\mathcal{R}_0^{(1)}} = 1 - \frac{1}{\mathcal{T}_1} \ (\text{with } j = 1, 2, 3, 4),$$

of the human host population. Using a simple model for the 2006 cholera epidemic in Angola (which accounts for direct and indirect cholera transmission with a single *V. cholerae* compartment), Eisenberg et al. [71] estimate $\mathcal{R}_0$ in the range $\mathcal{R}_0 \in [1.32, 5.9]$. Thus, based on this data (and estimates), our study shows that, for the best-case scenario (with $\mathcal{R}_0 = 1.32$), the control need to be implemented to at least 24.2% of the human host population. For the worst-case scenario (with $\mathcal{R}_0 = 5.9$), the control need to be administered to at least 83% of the human host population. It should be emphasized that, for the purpose of disease control, the herd immunity threshold can also be computed in terms of the basic reproduction number, and without targeting any specific disease or environmental compartments, using the relation [91] (where the subscript representing the population type considered is now omitted):

$$p^{(i)} = 1 - \frac{1}{\mathcal{R}_0^{(i)}},\ i = 1, \cdots, 4.$$

The drawback associated with using $\mathcal{R}_0^{(i)}$ to compute the herd immunity threshold is the fact that there will now be a different threshold for each individual scenario (due to this reason, we exclusively use the type reproduction number to compute the herd immunity threshold for each targeted population type).

It is worth emphasizing that the above theoretical results hold only when $\mu_B \geq 1$. Otherwise (i.e., if $\mu_B < 1$), the environment becomes a reservoir of the pathogen and control measures acting on the host human population will not be sufficient to eradicate the infection. Moreover, if $\mu_B < 1$, then additional conditions need to be imposed on the model parameters to ensure the positivity of the associated threshold quantities, $\mathcal{R}_0^{(i)}$ (with $i = 1, 2, 3, 4$). Similar conditions need to be imposed on $\mathcal{T}_1$ as well. The results of Theorems 2.4.2 and 2.4.3 are numerically illustrated by simulating the normalized model (2.2.3) using parameter values such that $\mathcal{R}_0^{(i)} < 1$ ($i = 1, \cdots, 4$) (equivalently, $\mathcal{T}_1 < 1$). The results obtained, depicted in Figure 2.5, show convergence of initial conditions to the DFE $\mathbf{E}_0$ in all the four transmission scenarios considered.

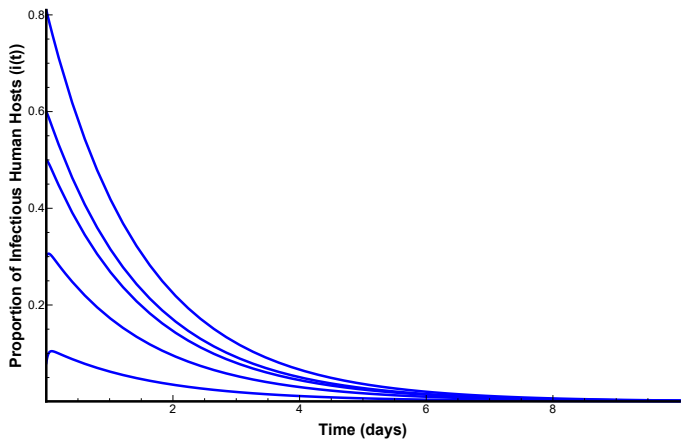

(a)

Figure 2.5: Numerical simulations of the normalized model (2.2.3) showing convergence to 0 of multiple initial conditions. Parameter values used are as given in Table 2.1 with $\beta_p^* = \beta_r^* = 2$ and $\theta_p^* = \theta_r^* = 10^3$ (so that, $\mathcal{R}_0^{(1)} = \mathcal{T}_1 = 0.37$, $\mathcal{R}_0^{(2)} = 0.57$, $\mathcal{R}_0^{(3)} = 0.61$ and $\mathcal{R}_0^{(4)} = 0.68$).

2.4.2 Targeting population of type 2 (bacteria in the pond)

Suppose, now, that an anti-cholera control measure (e.g., the use of chemical insecticides) is implemented only on population of type 2 (i.e., bacteria in the pond). In this case, it follows from Definition (2.4.1) that the vector $\mathbf{e}_2$ and projection matrix P_2 are given, respectively, by:

$$\mathbf{e}_2 = \begin{pmatrix} 0 \\ 1 \\ 0 \end{pmatrix} \text{ and } \quad P_2 = \begin{pmatrix} 0 & 0 & 0 \\ 0 & 1 & 0 \\ 0 & 0 & 0 \end{pmatrix}. \tag{2.4.6}$$

Substituting $j = 1$ (and using the NGM K_1, $\mathbf{e}_2$ and P_2) into (2.4.1) gives the following type reproduction number for Scenario 1 (for $s = 2$):

$$\mathcal{T}_2^{(1)} = \mathbf{e}_2^T K_1[I - (I - P_2)K_1]^{-1}\mathbf{e}_2 = 0. \tag{2.4.7}$$

Indeed, in Scenario 1, the growth rate of bacteria in the pond ($r = 1$) and the shedding rates (θ_p and θ_r) are placed in the matrix V, as transitions within the populations. In fact, in Scenario 1, only the human host (and not any of the other two population types) contribute to the matrix F of new infection terms. Thus, targeting the type 2 population (i.e., the pond) has no effect in hindering the generation of new infected individuals (i.e., targeting $b_p(t)$ does not contribute to the matrix F of new infections).

For Scenario 2, setting $j = 2$ (and using the NGM K_2, $\mathbf{e}_2$ and P_2) into (2.4.1) gives the following type reproduction number for Scenario 2 (for $s = 2$):

$$\begin{aligned} \mathcal{T}_2^{(2)} &= \mathbf{e}_2^T K_2[I - (I - P_2)K_2]^{-1}\mathbf{e}_2, \\ &= \frac{k_p V_r(\beta_r\theta_r - a_3a_4)}{V_r\beta_p a_1 + k_p\beta_r a_2 - V_r\mu_B k_p a_3(a_4 + \lambda_p)}, \end{aligned} \tag{2.4.8}$$

provided $\mathcal{T}_2^{(2)} > 0$. Similarly, setting $j = 3$ (and using the NGM K_3, $\mathbf{e}_2$ and P_2) into (2.4.1) gives the following type reproduction number for Scenario 3 (for $s = 2$):

$$\begin{aligned} \mathcal{T}_2^{(3)} &= \mathbf{e}_2^T K_3[I - (I - P_2)K_3]^{-1}\mathbf{e}_2, \\ &= \frac{\theta_p[V_r\beta_p a_4 + k_p\beta_r\lambda_p]}{-V_r[\beta_p V_r\lambda_r\theta_r + k_p\beta_r\theta_r(\lambda_p + \mu_B - 1) - k_p a_3(a_4(\mu_B - 1) + \lambda_p\mu_B)]}, \end{aligned} \tag{2.4.9}$$

provided $\mathcal{T}_2^{(3)} > 0$. Finally, setting $j = 4$ (and using the NGM K_4, $\mathbf{e}_2$ and P_2)) into (2.4.1) gives the following type reproduction number for Scenario 4 (for $s = 2$):

$$\begin{aligned} \mathcal{T}_2^{(4)} &= \mathbf{e}_2^T K_4[I - (I - P_2)K_4]^{-1}\mathbf{e}_2, \\ &= \frac{-V_r\beta_p\theta_p a_4 - k_p\beta_r\lambda_p\theta_p + k_p V_r(\beta_r\theta_r - a_3a_4)}{V_r[\beta_p V_r\lambda_r\theta_r + k_p\beta_r\theta_r(\lambda_p + \mu_B) - k_p\mu_B a_3(a_4 + \lambda_p)]}, \end{aligned} \tag{2.4.10}$$

provided $\mathcal{T}_2^{(4)} > 0$. Since the interactions between the compartment $b_p(t)$ and the other compartments of the normalized model are interpreted in different ways in each of the four scenarios, none of the type reproduction numbers ($\mathcal{T}_2^{(j)}$; $j = 1, 2, 3, 4$)) correspond to any of the reproduction numbers $\mathcal{R}_0^{(j)}$ ($j = 1, 2, 3, 4$). Hence, Theorems 2.4.2 and 2.4.3 do not automatically hold for Type Reproduction Number $\mathcal{T}_2^{(j)}$ ($j = 1, 2, 3, 4$) corresponding to type 2 population. So in this case, the problem of underestimation or overestimation of the efforts necessary to eliminate the epidemic is not overcome, since in each Scenario, one must act on a different number of cholera particles $b_p(t)$. It is worth noting that, for this population type, the associated type reproduction numbers are not unique. That is, each scenario considered has a type reproduction number that differs from that of the other three scenarios. It should further be stated that, for this population type (i.e., $s = 2$), the minimum threshold coverage needed for *V. cholerae* elimination in the pond is given by $p_2^{(i)} = 1 - \dfrac{1}{\mathcal{T}_2^{(j)}}$ ($j = 1, \cdots, 4$) [14, 91].

2.4.3 Targeting population of type 3 (bacteria in the river)

Suppose, now, that a control measure is applied only to population of type 3 (i.e., bacteria in the river). For this case, it follows from Definition (2.4.1) that the associated vector ($\mathbf{e}_3$) and projection matrix (P_3) are given, respectively, by:

$$\mathbf{e}_3 = \begin{pmatrix} 0 \\ 0 \\ 1 \end{pmatrix} \text{ and } \quad P_3 = \begin{pmatrix} 0 & 0 & 0 \\ 0 & 0 & 0 \\ 0 & 0 & 1 \end{pmatrix}. \tag{2.4.11}$$

Setting $j = 1$, and using $\mathbf{e}_3$, P_3 and the NGM K_1 in Equation (2.4.1) gives:

$$\mathcal{T}_3^{(1)} = \mathbf{e}_3^T K_1 [I - (I - P_3)K_1]^{-1} \mathbf{e}_3 = 0. \tag{2.4.12}$$

It has already been observed in Section 2.4.1 that comparing Scenario 1 to the Scenario 2, the assumption (2.4.2) is satisfied. Moreover, it is easy to see that the hypotheses of the Theorem 2.4.1 are verified considering the population of type 3 and Scenarios 1 and 2. Since in this case with bacteria in river as the type considered (i.e., $s = 3$), and for all the aforementioned scenarios we compared $s = 3$ always differs from l_1 (with $l_1 = 2$), it follows from Theorem 2.4.1 that the associated type reproduction number is unique. That is,

$$\mathcal{T}_3^{(1)} = \mathcal{T}_3^{(2)} = 0. \tag{2.4.13}$$

Indeed, in Scenarios 1 and 2, no new infected bacterial particles are generated in the b_r population. Setting $j = 3$ in Definition (2.4.1) (together with $\mathbf{e}_3$, P_3 and the NGM K_3) gives:

$$\begin{aligned} \mathcal{T}_3^{(3)} &= \mathbf{e}_3^T K_3 [I - (I - P_3)K_3]^{-1} \mathbf{e}_3, \\ &= \frac{V_r \theta_r [\beta_p V_r \lambda_r + k_p \beta_r (\lambda_p + \mu_B - 1)]}{-V_r \beta_p \theta_p a_4 - k_p \beta_r \theta_p \lambda_p + k_p V_r a_3 [a_4(\mu_B - 1) + \mu_B \lambda_p]}, \end{aligned} \tag{2.4.14}$$

provided $\mathcal{T}_3^{(3)} > 0$.

Comparing Scenarios 3 and 4, it is evident, first of all, that Assumption (2.4.2) holds. In particular (note that $m = 1$ in this case):

$$V_4 = V_3 + U_1, \text{ and } F_4 = F_3 + U_1,$$

where,

$$U_1 = \begin{pmatrix} 0 & 0 & 0 \\ 0 & 1 & 0 \\ 0 & 0 & 0 \end{pmatrix}.$$

In this case, we have $l_1 = 2$ (the second row of U_m (or, equivalently, U_1) corresponds to the compartment b_p, that is interpreted differently). Moreover, it is easy to see that the hypotheses of the Theorem 2.4.1 are verified considering the population type 3 and Scenarios 3 and 4. Since in this case with bacteria in river as the type considered (i.e., $s = 3$), and for all the aforementioned scenarios we compared $s = 3$ always differs from l_1 (with $l_1 = 2$), it follows from Theorem 2.4.1 that the associated type reproduction number is unique. That is,

$$\mathcal{T}_3^{(3)} = \mathcal{T}_3^{(4)}. \tag{2.4.15}$$

Further, none of $\mathcal{T}_3^{(j)}$ (with $j = 1, 2, 3, 4$) coincide with $\mathcal{R}_0^{(j)}$, (with $j = 1, 2, 3, 4$). In other words, the type reproduction numbers $\mathcal{T}_3^{(j)}$ ($j = 1, 2, 3, 4$) cannot be used to establish the local or global asymptotic stability of the disease-free equilibrium, $\mathbf{E}_0$. Furthermore, in this case, if the bacterial population in the river ($b_r(t)$) is reduced by a fraction that exceeds $p_3^{(j)} = 1 - \frac{1}{\mathcal{T}_3^{(j)}}$, with $j = 1, \cdots, 4$, [14] (this can be achieved by implementing strategies that minimize bacterial shedding into the river, for instance, by vaccinating susceptible humans and/or treating cholera-infected humans), the cholera epidemic will die out.

2.5 Assessment of Control Strategies

In this section, the normalized model (2.2.3) will be simulated to assess the population-level impact of various anti-cholera control measures. Unless otherwise stated, the numerical simulations will be carried out using the baseline parameter values given in Table 2.1. Further, the simulations are for the case where the human population is targeted for control (i.e., we are simulating the normalized model for $s = 1$). The values of the various reproduction numbers of the model ($\mathcal{R}_0^{(1)}; i = 1, \cdots, 4$) and herd immunity threshold ($p_s^{(i)}$, with $i = 1, \cdots, 4$ and $s = 1, 2, 3$) are first computed. The results obtained, tabulated in Table 2.3, show that, for each of the four scenarios, the reproduction number exceeds unity (lying in the range $\mathcal{R}_0^{(i)} \in [2.7, 9.2]$). Hence, in this case (with no anti-cholera intervention implemented in the community), the disease will remain endemic.

Furthermore, this table shows that the amount of effort needed to reduce $\mathcal{T}_1$ to a value less than unity increases with increasing values of $\mathcal{R}_0^{(i)}$. It is also seen that $\mathcal{T}_1^{(i)} = \mathcal{T}_1$, $i = 1, \cdots, 4$ (in line with Equation (2.4.5)). Moreover, $\mathcal{T}_s^{(1)} = 0$ for $s = 2, 3$, and $\mathcal{T}_3^{(2)} = 0$. This can be explained as follows: In Scenario 1, the bacterial populations in the aquatic environment (b_p and b_r, corresponding to $s = 2$ and $s = 3$,

respectively) do not contribute to the generation of new cholera infections (i.e., they do not contribute to the F matrix). Further, in Scenario 2, the population type 3 (i.e., bacteria in the river) does not contribute to the F matrix. Consequently, $p_s^{(1)} = -\infty$ and $p_3^{(2)} = -\infty$. The consequence of this result is that applying an anti-cholera control measure on the population of types $s = 2$ and $s = 3$ in Scenario 1, or on population of type $s = 3$ in Scenario 2, will not lead to the elimination of the disease (this result is consistent with that reported in [14]).

Note also that, if the population of type $s = 2, 3$ is targeted, then none of the associated type reproduction numbers ($\mathcal{T}_s^{(i)}$, $s = 2, 3$, $i = 1, \cdots, 4$) behaves like $\mathcal{R}_0^{(i)}$, $i = 1, \cdots, 4$. In particular, while $\mathcal{T}_s^{(i)} < 1$ for $s = 2$ and $s = 3$, the reproduction numbers $\mathcal{R}_0^{(i)} > 1$ ($i = 1, \cdots, 4$). Hence, when targeting populations of type 2 or 3, the use of type reproduction number (in all four scenarios) does not provide any useful information on the state (endemic or not) of the disease. Further, it does not represent a good estimate of the herd immunity effort needed to eliminate the disease.

Finally, note that, since $\mathcal{R}_0^{(1)} > \mathcal{R}_0^{(2)} > \mathcal{R}_0^{(3)} > \mathcal{R}_0^{(4)}$, it follows that, using $\mathcal{R}_0^{(1)} = \mathcal{T}_1$ as a threshold parameter to eliminate the infection, a greater effort is needed in Scenario 1, in comparison to the effort needed in Scenarios 2, 3 and 4. It is worth mentioning that the above simulations results are sensitive to the values of the bacterial shedding rates into the water environment (θ_p and θ_r). It should be recalled from Table 2.3 that these parameters are fixed at a baseline value of $\theta_p^* = \theta_r^* = 10^4$ per day. This baseline value is justified as follows. As noted by Feachem et al. [73], it is known that in asymptomatic cases of infection with *V. cholerae*, an individual excrete from 10^2 to 10^5 bacteria per gram of feces, while in symptomatic cases this value can rise to as high as $10^6 - 10^9$ per milliliter of rice-water stool. Further, data from [49] show that a patient with severe cholera infection can produce between 500 to 1000 mL of stool per day (corresponding to 10^{12} *V. cholerae* particles a day, of which a very high fraction (given the reported challenging hygienic conditions prevalent in the area) reaches the water reserve daily).

2.5.1 Assessment of Single Control Interventions

In this section, the population-level impact of the singular implementation of two anti-cholera interventions, namely a basic control measure and treatment of humans infected with cholera, will be assessed. This is described below.

Basic anti-Cholera control measures (WASH-only strategy)

Basic anti-cholera control entail the use of measures aimed at preventing or mitigating cholera outbreak in the community. These measures typically include the implementation of the water, sanitation and hygiene (WASH) strategy [79]. The essential elements of the WASH strategy include the chlorination of water sources, household water treatment and the promotion of personal hygienic precautions, use of chemical insecticides, etc. Hence, in the context of the normalized model, the implementation of basic control measures will be associated with strategies that decrease the transmission rates (β_p and β_r) and increase the *V. cholerae* decay (natural death) rate (μ_B). This is obtained by making the following replacements in the model:

	Basic Reproductive Number $\mathcal{R}_0$	Target infective host $i(t)$ $(s=1)$	Target bacteria in the pond $b_p(t)$ $(s=2)$	Target bacteria in the river $b_r(t)$ $(s=3)$
Scenario 1	$\mathcal{R}_0^{(1)} = 9.17$ $p^{(1)} = 0.89$	$(\mathcal{T}_1^{(1)} = 9.17)$ $p_1^{(1)} = 0.89$	$(\mathcal{T}_2^{(1)} = 0)$ $p_2^{(1)} = -\infty$	$(\mathcal{T}_3^{(1)} = 0)$ $p_3^{(1)} = -\infty$
Scenario 2	$\mathcal{R}_0^{(2)} = 6.83$ $p^{(2)} = 0.853551$	$(\mathcal{T}_1^{(2)} = 9.17)$ $p_1^{(2)} = 0.89$	$(\mathcal{T}_2^{(2)} = 0.06)$ $p_2^{(2)} < 0$	$(\mathcal{T}_3^{(2)} = 0)$ $p_3^{(2)} = -\infty$
Scenario 3	$\mathcal{R}_0^{(3)} = 3.03$ $p^{(3)} = 0.67$	$(\mathcal{T}_1^{(3)} = 9.17)$ $p_1^{(3)} = 0.89$	$(\mathcal{T}_2^{(3)} = 0.86)$ $p_2^{(3)} < 0$	$(\mathcal{T}_3^{(3)} < 0)$ $p_3^{(3)} > 1$
Scenario 4	$\mathcal{R}_0^{(4)} = 2.7$ $p^{(4)} = 0.63$	$(\mathcal{T}_1^{(4)} = 9.17)$ $p_1^{(4)} = 0.89$	$(\mathcal{T}_2^{(4)} < 0)$ $p_2^{(4)} > 1$	$(\mathcal{T}_3^{(4)} < 0)$ $p_3^{(4)} > 1$

Table 2.3: Basic reproduction numbers ($\mathcal{R}_0^{(i)}; i = 1, \cdots, 4$), type reproduction numbers ($\mathcal{T}_s^{(i)}; i = 1, \cdots, 4; s = 1, 2, 3$) and herd immunity thresholds ($p_s^{(i)}; i = 1, \cdots, 4;\ s = 1, 2, 3$) for the normalized model (2.2.3). Parameter values used are as given by the baseline values in Table 2.1.

$$\begin{aligned} \beta_p &\to \beta_p\left(1-\varepsilon_B c_B\right), \\ \beta_r &\to \beta_r\left(1-\varepsilon_B c_B\right), \\ \mu_B &\to \mu_B\left(1+\varepsilon_B c_B\right), \end{aligned} \tag{2.5.1}$$

where $0 \leq \varepsilon_B \leq 1$ and $0 \leq c_B \leq 1$ represent, respectively, the efficacy and coverage of the WASH-only control strategy. Although a clear consensus on the realistic estimate of the efficacy and/or coverage of the basic control measures in cholera-endemic areas seems to be lacking, a number of studies have provided some clues as to what these estimates should be. For instance, in a modeling study on assessing the impact of WASH and oral cholera vaccine on the 2008 cholera epidemic in Haiti, Fung et al. [79] reported that (in 2008) only 63% of the Haitian population had access to improved water and only 17% had access to improved sanitation. Furthermore, after the 2010 earthquake in Haiti, the Haitian Directorate for Potable Water and Sanitation reported that 26% of the rural population received improved water, while only 10% had improved sanitation (in particular, the coverage for improved water and sanitation in the urban Port-au-Prince metropolitan area was 35% and 20%, respectively). Fung et al. [79] introduced non-linear relationships between coverage and effectiveness of the aforementioned interventions. Based on all these, it seems reasonable to assume that the WASH coverage lies in the range 30% and 50%, while its efficacy can be anywhere between 10% and 60%.

Replacing β_p, β_r and μ_B in the normalized model (2.2.3) with the expressions in (2.5.1), it follows that the associated basic type reproduction number (defined in (2.4.5)) now becomes (with $i = 1, \cdots, 4$):

$$\begin{aligned} \mathcal{T}_{1B} &= \mathcal{T}_{1B}^{(i)} = \mathcal{R}_{0B}{}^{(1)} \\ &= \frac{V_r\beta_p(1-\varepsilon_B c_B)a_{1B} + k_p\beta_r(1-\varepsilon_B c_B)\left[(\theta_p + V_r\theta_r)\lambda_p + V_r\theta_r(\mu_B(1+\varepsilon_B c_B)-1)\right]}{k_p V_r a_3[(\lambda_r + \mu_B(1+\varepsilon_B c_B))(\mu_B(1+\varepsilon_B c_B)-1) + \mu_B(1+\varepsilon_B c_B)\lambda_p]}, \end{aligned} \tag{2.5.2}$$

where,

$$a_{1B} = V_r\theta_r\lambda_r + \theta_p(\lambda_r + \mu_B(1+\varepsilon_B c_B)).$$

Thus, the associated threshold herd immunity threshold becomes: $p_{1B}^{(i)} = 1 - \dfrac{1}{\mathcal{T}_{1B}}$ $(i = 1, \cdots, 4)$, with $\mathcal{T}_{1B}$ defined in (2.5.2).

For simulation purposes, the following effectiveness levels of the basic control measures (based on reducing β_p and β_r and increasing μ_B, in comparison to the baseline values of the respective non-normalazed parameters tabulated in Table 2.1) are considered:

1. **Low effectiveness level of WASH-only strategy**: involves reducing the baseline values of b_p and b_r by 10% (i.e., $\beta_p = \beta_r = 15$, $\beta_p^* = \beta_r^* = 4.5$), and increasing the baseline value of μ_B by 10% (i.e., $\mu_B = 2,93$, $\mu_B^* = 0.88$).

2. **Moderate effectiveness level of WASH-only strategy**: involves reducing the baseline values of b_p and b_r by 25% (i.e., $\beta_p = \beta_r = 12.5$, $\beta_p^* = \beta_r^* = 3.75$) and increasing the baseline value of μ_B by 25% (i.e., $\mu_B = 3.33$, $\mu_B^* = 1$).

3. **High effectiveness level of WASH-only**: involves reducing the baseline values of b_p and b_r by 50% (i.e., $\beta_p = \beta_r = 8.33$, $\beta_p^* = \beta_r^* = 2.5$) and increasing the baseline value of μ_B by 50% (i.e., $\mu_B = 4$, $\mu_B^* = 1.2$).

Figure 2.6 depicts the contour plots of $\mathcal{R}_{0B}{}^{(1)} = \mathcal{T}_{1B}$ (defined in (2.5.2)), as a function of efficacy (ε_B) and coverage (c_B) of the basic anti-cholera control measures for the low, moderate and high effectiveness levels. It follows from this figure ((a)) that even with the highest possible estimated efficacy and coverage of the basic control measure (i.e., $\varepsilon_B = 0.6$ and $c_B = 0.5$), none of the effectiveness levels of this basic control strategy can lead to the elimination of the disease (albeit each will greatly decrease the disease burden). The reason is that, with efficacy at 60% and coverage at 50%, none of the effectiveness levels can bring the associated reproduction number to a value less than unity regardless of the level of coverage. If, however, the efficacy of the basic control measure can be dramatically increased to 90%, then both the moderate and high effectiveness levels of this strategy can lead to such elimination if the coverage level is high enough (at least 80%) (Figures (b) and (c)). If the efficacy and coverage can further be increased to 100% each (the study in Fung et al. [79] showed that 100% coverage is possible, over a 20-year period, in urban areas of Haiti), then low effectiveness level can also achieve such elimination (Figure (a)).

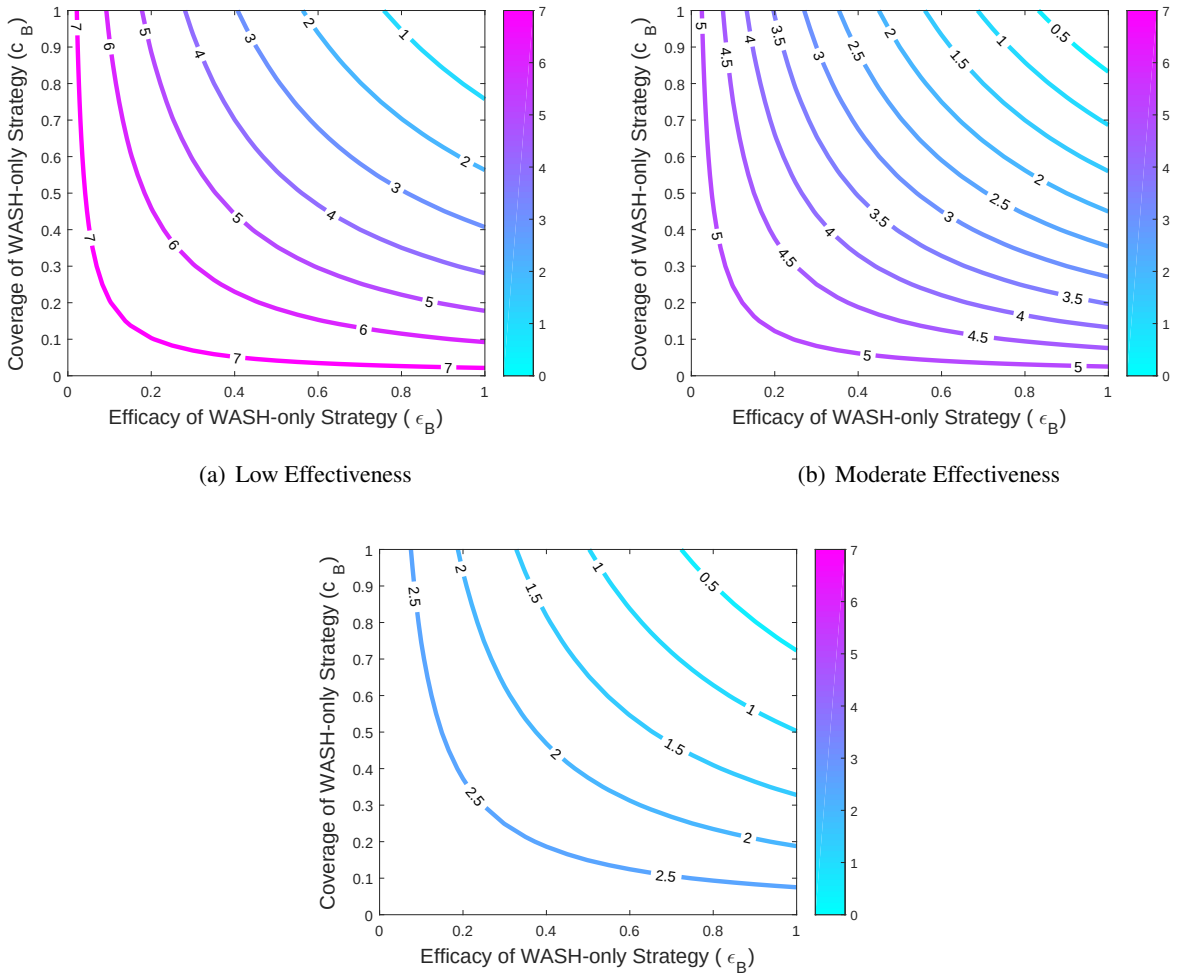

(a) Low Effectiveness

(b) Moderate Effectiveness

(c) High Effectiveness

Figure 2.6: Simulations of the model (2.2.3) with low (a), moderate (b) and high (c) effectiveness level of the WASH-only strategy. Contour plot of $\mathcal{R}_{0B}{}^{(1)}$ as a function of efficacy ε_B and coverage c_B. Parameter values used are as given in Table 2.1, with a reduction (increase) of the value of parameters β_p^* and β_r^* (μ_B^*) by: (a) 10%, (b) 25% (b) and (c) 50%, in comparison to their baseline values given in Table 2.1.

Treatment-only strategy

In this section, a treatment-only strategy, targeting infected humans, is considered. Cholera can be successfully treated, in most cases, using oral rehydration therapy [170, 177]. Although recovery from cholera infection is feasible without taking antibiotics (if sufficient hydration is maintained) [170, 177], the WHO recommends the use of antibiotic treatments (for one to three days), aimed at reducing the severity of the disease symptoms [170, 177]. In particular, in patients with severe dehydration [170, 177], *Doxycycline* is typically used as a first line drug (although some strains of *V. cholerae* have shown resistance to it [136]). Other antibiotics that have been proven to be effective againts *V. cholerae* infection include *cotrimoxazole, erythromycin, tetracycline, chloramphenicol*, and *furazolidone* [170, 177]. Furthermore, *Fluoroquinolones*, such as *ciprofloxacin*, may be used (but the ability of *V. cholerae* to resist the effects of this substance has

also been reported in [95]). The use of antibiotics also reduces the need for fluid replacement therapy. It is known that zinc supplementation reduces the duration and severity of diarrhea in Bangladeshi children with cholera when given in combination with antibiotics and rehydration therapy as needed (in particular, it reduced the duration of the disease (i.e., duration of cholera-related diarrheal illness) by eight hours, in addition to reducing the amount of diarrhea stool by 10% [170, 177]).

The use of treatment against *V. cholerae* infection in the community affects the parameters related to the shedding of bacteria by humans and the recovery of those who contracted the disease. In particular, the use of treatment decreases the shedding rate parameters (θ_p and θ_r), while increasing the recovery parameter (γ). Consequently, the treatment-only strategy is incorporated into the normalized model by replacing the three associated parameters as follows:

$$\begin{aligned} \theta_p &\to \theta_p(1-\varepsilon_T c_T), \\ \theta_r &\to \theta_r(1-\varepsilon_T c_T), \\ \gamma &\to \gamma(1+\varepsilon_T c_T), \end{aligned} \tag{2.5.3}$$

where ε_T and c_T are, respectively, the efficacy and coverage of the treatment-only strategy. Using data for cholera epidemics in Bangladesh from 1985-1991, Siddique et al. [143] estimated that only 20% of cholera-infected people were treated in government health facilities (with 80% of the infected population treated at home). Furthermore, only about 23% of the cholera-infected people were actually treated by qualified physicians (with 68% of the infected individuals treated by unqualified rural practitioners and 9% had no access to any health care providers). Sack et al. [137] reported that rehydration treatment (which is inexpensive and simple to implement) is approximately 100% successful (or effective).

Replacing θ_p, θ_r and γ in the normalized model (2.2.3) with the expressions in (2.5.3), it follows that the associated basic type reproduction number (defined in (2.4.5)) now becomes (with $i = 1, \cdots, 4$):

$$\begin{aligned} \mathcal{T}_{1T} &= \mathcal{T}_{1T}^{(i)} = {\mathcal{R}_{0T}}^{(1)} \\ &= \frac{V_r\beta_p a_{1T} + k_p\beta_r\left[(\theta_p(1-\varepsilon_T c_T) + V_r\theta_r(1-\varepsilon_T c_T))\lambda_p + V_r\theta_r(1-\varepsilon_T c_T)(\mu_B-1)\right]}{k_p V_r a_{3T}[a_4(\mu_B-1)+\mu_B\lambda_p]}, \end{aligned} \tag{2.5.4}$$

where,

$$a_{1T} = V_r\lambda_r\theta_r(1-\varepsilon_T c_T) + \theta_p(1-\varepsilon_T c_T)(\lambda_r+\mu_B),$$

$$a_{3T} = \gamma(1+\varepsilon_T c_T) + \delta + \mu.$$

Thus, the associated herd immunity threshold becomes: $p_{1T}^{(i)} = 1 - \dfrac{1}{\mathcal{T}_{1T}}$ $(i = 1, \cdots, 4)$, with $\mathcal{T}_{1T}$ defined in (2.5.4).

As before, we consider the following effectiveness levels of the treatment-only strategy (based on reducing θ_p and θ_r and increasing γ, in comparison to the baseline values of the respective non-normalized parameters tabulated in Table 2.1):

1. **Low effectiveness level of treatment-only strategy**: involves reducing the baseline values of θ_p and θ_r by 10% (i.e., $\theta_p = \theta_r = 3 \times 10^4$, $\theta_p^* = \theta_r^* = 9 \times 10^3$), and increasing the baseline value of γ by 10% (i.e., $\gamma = 0.73$, $\gamma^* = 0.22$).

2. **Moderate effectiveness level of treatment-only strategy**: involves reducing the baseline values of θ_p and θ_r by 25% (i.e., $\theta_p = \theta_r = 2.5 \times 10^4$, $\theta_p^* = \theta_r^* = 7.5 \times 10^3$) and increasing the baseline value of γ by 25% (i.e., $\gamma = 0.83$, $\gamma^* = 0.25$).

3. **High effectiveness level of treatment-only strategy**: involves reducing the baseline values of θ and θ_r by 50% (i.e., $\theta_p = \theta_r = 1.6666 \times 10^4$, $\theta_p^* = \theta_r^* = 5 \times 10^3$) and increasing the baseline value of γ by 50% (i.e., $\gamma = 1$, $\gamma^* = 0.3$).

Figure 2.7 depicts the contour plots of $\mathcal{R}_{0T}{}^{(1)} = \mathcal{T}_{1T}$ (defined in (2.5.4)), as a function of efficacy (ε_T) and coverage (c_T) of the treatment-only strategy for the low, moderate and high effectiveness levels of the treatment-only strategy. It follows from Figure 2.7 that, with the 23% anti-cholera treatment coverage, cholera elimination is not feasible no matter the efficacy level of the treatment used (this is because the associated reproduction number remains above unity when $c_T = 0.23$ and $\varepsilon_T = 1$). However, if the coverage can be significantly increased to at least 80%, this figure shows that even the low effectiveness level of this strategy can lead to the elimination of the disease (requiring a treatment efficacy of at least 100%). Furthermore, such elimination can be achieved if the coverage is lowered to 70% using the moderate effectiveness level of the treatment strategy (here, a minimum treatment efficacy of 100% would be needed). Finally, for 50% treatment coverage, the high effectiveness level of the treatment-only strategy can lead to disease elimination if its efficacy is at least 100%. In summary, these simulations suggest that a highly-effective treatment-only strategy (with efficacy of at least 100%) can lead to the elimination of cholera if a modest coverage level (of at least 50% can be attained and maintained).

2.5.2 Assessment of Combined WASH-Treatment Strategy

In this section, the population-level impact of a hybrid strategy that combines both the WASH-only and the treatment-only strategy will be assessed. The essential elements of the combined strategy include a reduction in both the transmission and shedding rates, in addition to an increase in both the natural bacterial death rate and the recovery rate for humans. For this strategy, the associated parameters β_p, β_r, θ_p, θ_r, μ_B and γ are replaced by the following relations:

$$\begin{aligned}
\beta_p &\to \beta_p(1-\varepsilon_{BT}c_{BT}), \quad \theta_p \to \theta_p(1-\varepsilon_{BT}c_{BT}),\\
\beta_r &\to \beta_r(1-\varepsilon_{BT}c_{BT}), \quad \theta_r \to \theta_r(1-\varepsilon_{BT}c_{BT}),\\
\mu_B &\to \mu_B(1+\varepsilon_{BT}c_{BT}), \quad \gamma \to \gamma(1+\varepsilon_{BT}c_{BT}),
\end{aligned} \tag{2.5.5}$$

where ε_{BT} and c_{BT} are efficacy and coverage of combined WASH-treatment strategy.

Replacing β_p, β_r, θ_p, θ_r μ_B and γ in the normalized model (2.2.3) with the expressions in (2.5.5), it follows that the associated basic type reproduction number (defined in (2.4.5)) now becomes (with $i =$

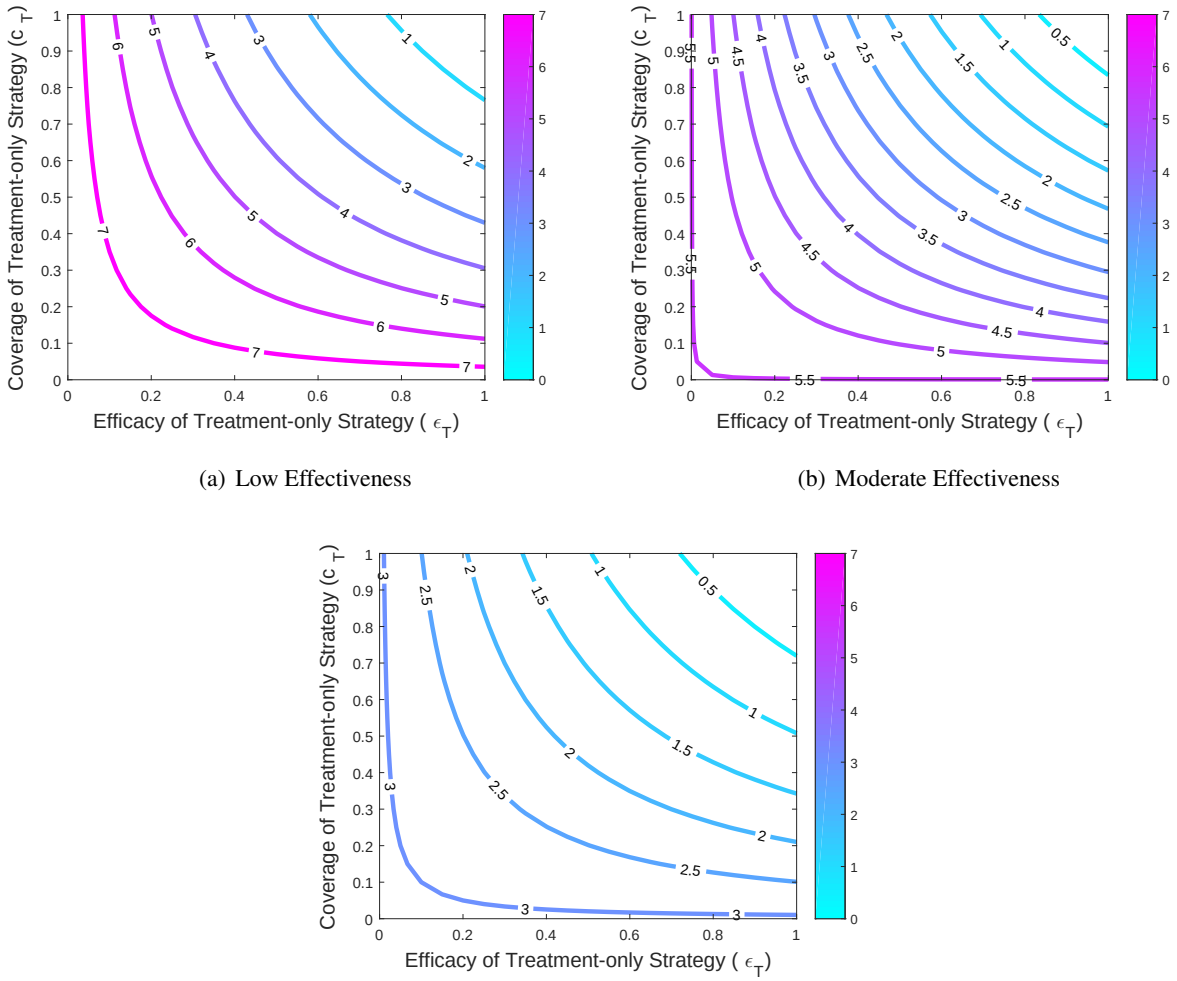

(a) Low Effectiveness

(b) Moderate Effectiveness

(c) High Effectiveness

Figure 2.7: Simulations of the model (2.2.3) with low (a), moderate (b) and high (c) effectiveness level of the treatment-only strategy. Contour plot of ${\mathcal{R}_{0T}}^{(1)}$ as a function of efficacy ε_T and coverage c_T. Parameter values used are as given in Table 2.1, with a reduction (increase) of the value of parameters θ_p^* and θ_r^* (γ^*) by: (a) 10%, (b) 25% and (c) 50%, in comparison to their baseline value given in Table 2.1.

$1, \cdots, 4$):

$$\mathcal{T}_{1BT} = \mathcal{T}_{1BT}^{(i)} = {\mathcal{R}_{0BT}}^{(1)} \tag{2.5.6}$$

$$= \frac{V_r\beta_p(1-\varepsilon_{BT}c_{BT})a_{1BT} + k_p\beta_r(1-\varepsilon_{BT}c_{BT})a_7}{k_pV_ra_{3BT}[a_4(\mu_B(1+\varepsilon_{BT}c_{BT})-1)+\mu_B(1+\varepsilon_{BT}c_{BT})\lambda_p]},$$

where,

$$a_{1BT} = V_r\lambda_r\theta_r(1-\varepsilon_{BT}c_{BT}) + \theta_p(1-\varepsilon_{BT}c_{BT})(\lambda_r+\mu_B(1+\varepsilon_{BT}c_{BT})),$$

$$a_{3BT} = \gamma(1+\varepsilon_Tc_T)+\delta+\mu,\ a_4 = \lambda_r+\mu_B(1+\varepsilon_{BT}c_{BT}),$$

$$a_7 = (\theta_p(1-\varepsilon_{BT}c_{BT}) + V_r\theta_r(1-\varepsilon_{BT}c_{BT}))\lambda_p + V_r\theta_r(1-\varepsilon_{BT}c_{BT})(\mu_B(1+\varepsilon_{BT}c_{BT})-1).$$

Thus, the corresponding threshold herd immunity becomes $p_{1BT}^{(i)} = 1 - \frac{1}{\mathcal{T}_{1BT}}$, with $\mathcal{T}_{1BT}$ defined in (2.5.6). We estimate the coverage and efficacy of this strategy by taking, for example, the mean of the coverages and efficacies of the WASH-only and treatment-only strategies. That is, $\varepsilon_{BT} = (\varepsilon_B + \varepsilon_T)/2 = (0.6+1)/2 = 0.8$ and $c_{BT} = (c_B + c_T)/2 = (0.5 + 0.23)/2 = 0.365$.

We consider the following effectiveness levels of the combined strategy

1. **Low effectiveness level of combined WASH-treatment strategy**: involves reducing the baseline values of β_p, β_r, θ_p and $\theta_r$by 10% (i.e., $\beta_p = \beta_r = 15$, $\beta_p^* = \beta_r^* = 4.5$, $\theta_p = \theta_r = 3 \times 10^4$, $\theta_p^* = \theta_r^* = 9 \times 10^3$), and increasing the baseline value of μ_B and γ by 10% (i.e., $\mu_B = 2.93$, $\mu_B^* = 0.88$, $\gamma = 0.73$, $\gamma^* = 0.22$).

2. **Moderate effectiveness level of combined WASH-treatment strategy**: involves reducing the baseline values of β_p, β_r, θ_p and θ_r by 25% (i.e. $\beta_p = \beta_r = 12.5$, $\beta_p^* = \beta_r^* = 3.75$, $\theta_p = \theta_r = 2.5 \times 10^4$, $\theta_p^* = \theta_r^* = 7.5 \times 10^3$) and increasing the baseline value of μ_B and γ by 25% (i.e., $\mu_B = 3.33$, $\mu_B^* = 1$ and $\gamma = 0.83$, $\gamma^* = 0.25$).

3. **High effectiveness level of combined WASH-treatment strategy**: involves reducing the baseline values of β_p, β_r, θ_p and θ_r by 50% (i.e.,$\beta_p = \beta_r = 8.33$, $\beta_p^* = \beta_r^* = 2.5$, $\theta_p = \theta_r = 1.6666 \times 10^4$, $\theta_p^* = \theta_r^* = 5 \times 10^3$) and increasing the baseline value of μ_B and γ by 50% (i.e.,$\mu_B = 4$, $\mu_B^* = 1.2$ and $\gamma = 1$, $\gamma^* = 0.3$).

Figure 2.8 depicts the contour plots of $\mathcal{R}_{0BT}{}^{(1)} = \mathcal{T}_{1BT}$ (defined in (2.5.6)), as a function of efficacy (ε_{BT}) and coverage (c_{BT}) of the treatment strategy for the low, moderate and high effectiveness levels. This figure shows that the high effectiveness level of this (combined) strategy will lead to cholera elimination even for sufficiently small coverage and efficacy (Figure 2.8(c)). For the aforementioned 80% efficacy and 36.5% coverage assumed for this strategy, it is shown that neither the low or moderate effectiveness level of this intervention can lead to disease elimination. However, if the coverage is increased to 50%, even the low effectiveness level of this intervention can lead to cholera elimination (Figure 2.8(a)). The moderate effectiveness level at 80% efficacy can lead to elimination with even a 40% coverage (Figure 2.8(b))). Thus, it can be concluded that the combined strategy offers the best prospect for cholera elimination in the community (since it requires the lowest minimum coverage needed to achieve such elimination). In summary, this study ranks the three interventions (in order of their effectiveness, *vis a vis* their ability to lead to cholera elimination) as follows:

Combined Strategy > Treatment-only Strategy > WASH-only Strategy

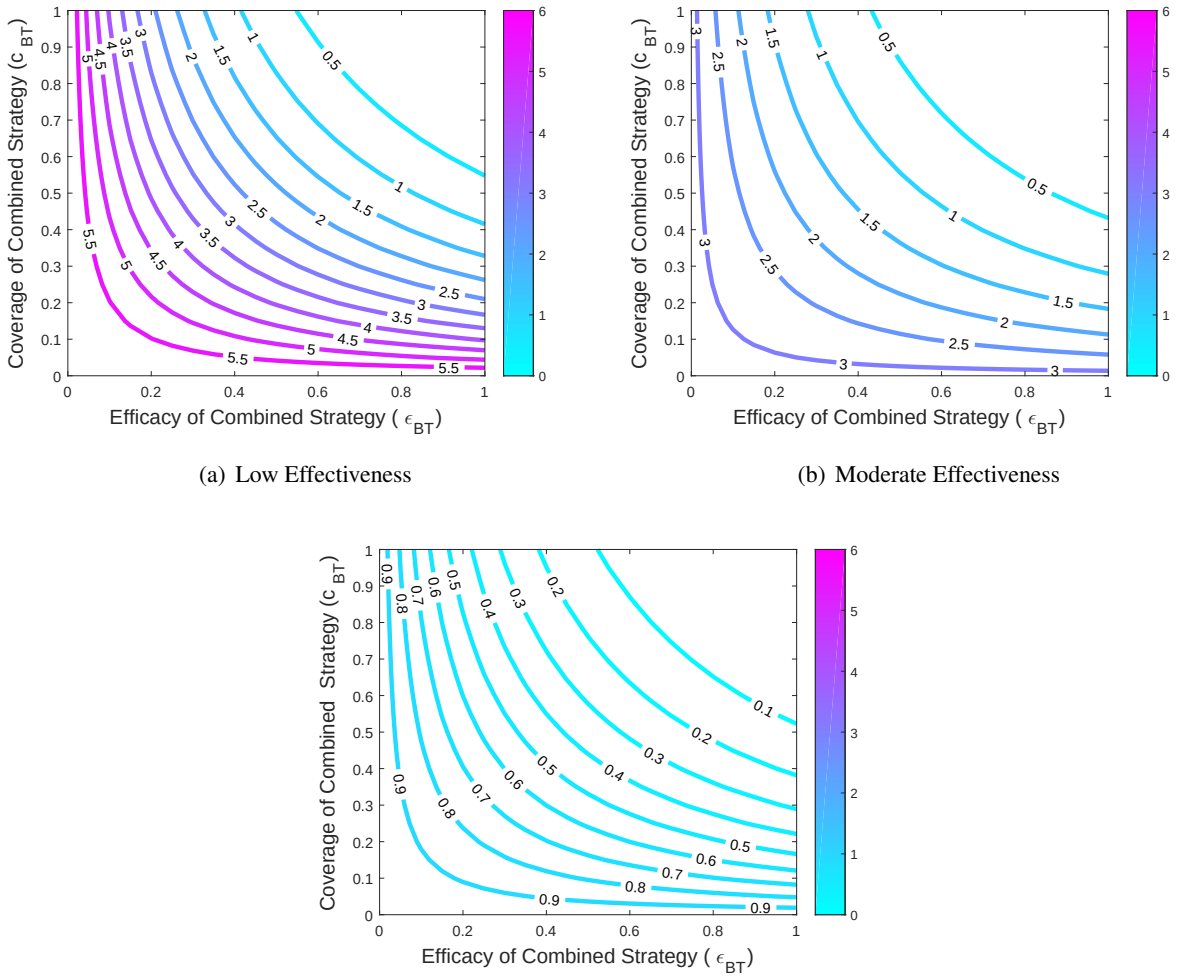

(a) Low Effectiveness

(b) Moderate Effectiveness

(c) High Effectiveness

Figure 2.8: Simulations of the model (2.2.3) with low (a), moderate (b) and high (c) effectiveness level of the hybrid strategy. Contour plot of $\mathcal{R}_0^{(1)}$ as a function of efficacy ε_{BT} and coverage c_{BT}. Parameter values used are as given in Table 2.1, with a reduction (increase) of the value of parameters β_p^*, β_r^*, θ_p^* and θ_r^* (γ^* and μ_B^*) by: (a) 10%, (b) 25% and (c) 50%, in comparison to their baseline values given in Table 2.1.

2.6 Existence of Endemic Equilibrium

Let us denote by $\mathcal{R}_0$ any one of the expressions defined in (2.3.4), (2.3.9), (2.3.13) or (2.3.18).
In this section we study the dynamic of system (2.2.3) as the threshold $\mathcal{R}_0$ changes. The endemic equilibrium

point is a steady state solution where cholera persists in the population and satisfy the following system:

$$\begin{cases} \mu(1-s) - \left(\beta_p \frac{b_p}{k_p v_p + b_p} + \beta_r \frac{b_r}{1+b_r}\right) s + \gamma i = 0, \\ \left(\beta_p \frac{b_p}{k_p v_p + b_p} + \beta_r \frac{b_r}{1+b_r}\right) s - a_3 i = 0, \\ \theta_p i + (1 - b_p - \mu_B - \lambda_p) b_p + \lambda_r V_r b_r = 0, \\ \theta_r i - a_4 b_r + \lambda_p \frac{b_r}{V_r} = 0, \\ (e + \lambda_p)(1 - v_p) = 0. \end{cases} \tag{2.6.1}$$

Solving in terms of b_p, we obtain

$$\begin{aligned} s^* &= \frac{(k_p+b_p)(V_r\theta_r b_p^2+(a_2-V_r\theta_r)b_p+V_r a_1)(\gamma a_4 b_p^2+\gamma(a_4(\mu_B-1)+\mu_B\lambda_p)b_p+\mu a_1)}{a_1[V_r\theta_r(\beta_p+\beta_r+\mu)b_p^3+a_5 b_p^2+(V_r(\beta_p+\mu)a_1+k_p(\beta_r+\mu)(a_2-V_r\theta_r))b_p+kV_r\mu a_1]}, \\ i^* &= \frac{b_p(a_4 b_p+a_4(\mu_B-1)+\mu_B\lambda_p)}{a_1}, \\ b_r^* &= \frac{b_p(V_r\theta_r b_p+a_2-V_r\theta_r)}{V_r a_1}, \\ v_p^* &= 1, \end{aligned} \tag{2.6.2}$$

where

$$a_5 = V_r\theta_r(\beta_p+\beta_r+\mu)(\mu_B-1) + \lambda_p(\beta_p+\beta_r+\mu)(\theta_p+V_r\theta_r) + V_r\theta_r k_p(\beta_p+\mu), \tag{2.6.3}$$

while b_p is the positive solution of the following equation of fourth degree

$$f(b_p) = a b_p^4 + b b_p^3 + c b_p^2 + d b_p + e = 0, \tag{2.6.4}$$

in which the expressions of the coefficients are reported in appendix D. The study of the solutions of (2.6.4) implies the following result.

Theorem 2.6.1 *Consider (2.6.4), with the coefficients a, b, c and d reported in Appendix D. The model (2.2.3) has:*

1. *no endemic equilibrium whenever $\mathcal{R}_0 \leq 1$,*
2. *a unique endemic equilibrium point when $\mathcal{R}_0 > 1$.*

Proof. A brief outline of the demonstration is provided.
Following [90], the study of the solutions of the quartic (2.6.4) implies introduction of the following quantities [90]:

$$\begin{aligned} F &= \frac{3b^4 - 16ab^2c + 16a^2c^2 + 16a^2bd - 64a^3e}{a^4}, & H &= \frac{8ac - 3b^2}{a^2}, \\ J &= \frac{72ace - 2c^3 + 9bcd - 27ad^2 - 27b^2e}{a^3}, & P &= \frac{c^2 - 3bd + 12ea}{a^2}, \\ \Delta_t &= \frac{b^2c^2 + 18abcd - 4ac^3 - 4b^3d - 27a^2d^2}{a^4}, & \Delta_q &= 4P^3 - J^2. \end{aligned} \tag{2.6.5}$$

First of all, we observe that there are no parameter value for which the following system of inequalities

$$\begin{cases} H \geq 0, \\ \Delta_q > 0, \end{cases} \tag{2.6.6}$$

is satisfied. This implies that the quartic (2.6.4) admits always at least two real solutions [90].
It should be noted that the coefficients a and b are always negative.
If $\mathcal{R}_0 < 1$, then $e < 0$; moreover, many numerical tests suggest that coefficients c and d are both negative in this case. Therefore, when $\mathcal{R}_0 < 1$, it can be stated that the quartic (2.6.4):
i) does not admit positive roots, if they are all real,
ii) does not admit two positive real roots and two complex roots with positive real part, if they are two real and two complex.
Therefore, when $\mathcal{R}_0 < 1$, there is no endemic equilibria.
If $\mathcal{R}_0 = 1$, then $e = 0$. In this case, (2.6.4) reduces to

$$b_p f(b_p) = b_p(ab_p^3 + bb_p^2 + cb_p + d) = 0. \tag{2.6.7}$$

If its discriminant Δ_t (see [159]) defined in (2.6.5) is non-negative, then cubic $f(b_p)$ admits all real solutions; instead, if $\Delta_t < 0$, the cubic admits two complex and one real solutions. Also in this case, the simulations suggest that the coefficients c and d are both negative. Therefore, is can be summarized that:
i) the cubic $f(b_p)$ does not admit positive solutions, if they are all real ($\Delta_t > 0$),
ii) the cubic $f(b_p)$ does not admit one real positive solution and two complex solutions with positive real parte, if they are two complex and one real ($\Delta_t < 0$).
Thus, even if $\mathcal{R}_0 = 1$, there is no endemic equilibrium.
If $\mathcal{R}_0 > 1$, then $e > 0$. In this case the sign of the coefficients c and d changes according to the values of the parameters. First of all, note that in the case $\mathcal{R}_0 > 1$, there are no parameter values for which there are four real solutions, of which three positive and one negative, i.e. the system

$$\begin{cases} F > 0,\ H < 0,\ \Delta_q \geq 0 \\ c > 0,\ d < 0,\ e > 0 \end{cases} \tag{2.6.8}$$

is never satisfied. Moreover, the simulations suggest that all other the possibilities are:
i) if all the roots of the quartic (2.6.4) are real, then they are one positive and three negative roots,
ii) if the roots of the quartic (2.6.4) are two real and two complex, then thay are one with positive real part and three with negative real part.
The results are summaized in Table 2.4.
Thus, when $\mathcal{R}_0 \leq 1$, then there is no endemic equilibrium, while if $\mathcal{R}_0 > 1$, system (2.2.3) admits only one endemic equilibrium. □
Let us denote by $\mathbf{E}_2$ the unique endemic equilibrium (EE) existing when $\mathcal{R}_0 > 1$.
Many numerical simulations suggest that the characteristic polynomial obtained with the linearization method around the equilibrium point $\mathbf{E}_2$ admits solutions all with negative real part. This fact can be seen from the figure 2.9, in which the numerical solution related to the infective people I obtained for parameters value such that $R > 1$ and with different initial data is shown . The figure suggests the local stability of the endemic equilibrium point.

$\mathcal{R}_0$ value	Coefficients sign	Existence Conditions	Number of Real Solutions
$\mathcal{R}_0 < 1$	$c, d, e < 0$	$\Delta_q < 0$ (two real solutions)	$\Rightarrow$ 2 negative
		$F > 0,\ H < 0,\ \Delta_q \geq 0$ (all real solutions)	$\Rightarrow$ 4 negative
$\mathcal{R}_0 = 1$	$c, d < 0,\ e = 0$	$\Delta_t < 0$ (one real solutions)	$\Rightarrow$ 1 negative
		$\Delta_t \geq 0$ (all real solutions)	$\Rightarrow$ 3 negative
$\mathcal{R}_0 > 1$	$c, d < 0$ $c > 0,\ d < 0$ $c, d > 0$	$\Delta_q < 0$ (two real solutions)	$\Rightarrow$ 1 positive, 1 negative
	$c < 0,\ d > 0$ $c, d < 0$ $c, d > 0$ $c < 0,\ d > 0$	$F > 0,\ H < 0,\ \Delta_q \geq 0$ (all real solutions)	$\Rightarrow$ 1 positive, 3 negative

Table 2.4: All possibilities (regarding number of positive solutions) arising from the quartic equation (2.6.4).

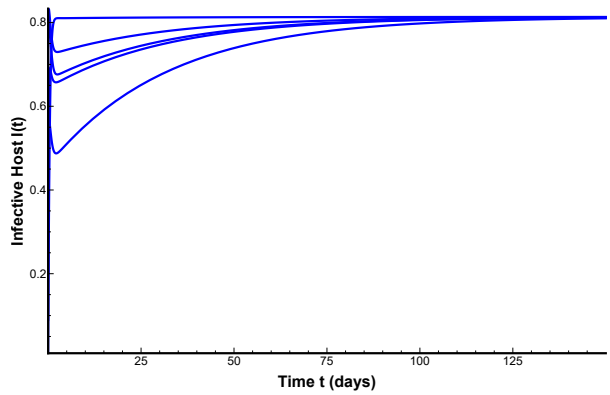

(a)

Figure 2.9: Numerical simulations of the normalized model (2.2.3) showing convergence to endemic equilibrium of multiple initial conditions. Parameter values used are as given in Table 2.1 with $\beta_p^* = \beta_r^* = 30$ and $\theta_p^* = \theta_r^* = 5 \times 10^4$ (so that, $\mathcal{R}_0^{(1)} = \mathcal{T}_1 = 19.0126$, $\mathcal{R}_0^{(2)} = 15.2869$, $\mathcal{R}_0^{(3)} = 4.36035$ and $\mathcal{R}_0^{(4)} = 3.9832$).

2.7 Spatial Dynamics of Cholera

As already explained in the Introduction, the model for the transmission of cholera so far is extended to the spatially heterogeneous case. Assuming that the simple Fickian diffusion approximation is valid, let D_S^* and D_I^* be the diffusion coefficients related to the population of susceptible and infected people, respectively. It is assumed that $D_S^* > D_I^*$, as the disease could limit the mobility of individuals. Also the diffusion coefficients linked to the population of the bacteria in the pond and in the water network, respectively, are $D_{\mathrm{B}_p}^*$ and $D_{\mathrm{B}_r}^*$. Furthermore, it is taken into account that the vibrios can be transported through the drift of the water flow both in the pond and in the river network. Therefore, the transport parameters ν_p and ν_r are introduced for pond and river, respectively. They should not be thought of as physical parameters that reflect only the hydrological transport, but rather they are conceptual parameters aimed at modelling all physical, chemical and biological processes involved in the vibrios spreading. The model (2.2.1) can be extended to

the spatial case by setting the following set of five partial differential equations:

$$\begin{aligned}
\partial_{\mathrm{t}_*} S &= D_S^* \nabla^2 S + \Pi - \beta_p^* \frac{B_p}{k_p^* V_p + B_p} S - \beta_r^* \frac{B_r}{k_r + B_r} S - \mu^* S + \gamma^* I, \\
\partial_{\mathrm{t}_*} I &= D_I^* \nabla^2 I + \beta_p^* \frac{B_p}{k_p^* V_p + B_p} S + \beta_r^* \frac{B_r}{k_r + B_r} S - (\mu^* + \gamma^* + \delta^*) I, \\
\partial_{\mathrm{t}_*} B_p &= D_{\mathrm{B}_p}^* \nabla^2 B_p - \nu_p^* \partial_{\mathrm{x}_*} B_p + \theta_p^* I + r B_p (1 - \frac{B_p}{k_{pb}}) - \mu_B^* B_p + \lambda_r^* V_r^* B_r - \lambda_p^* B_p, \\
\partial_{\mathrm{t}_*} B_r &= D_{\mathrm{B}_r}^* \nabla^2 B_r - \nu_r^* \partial_{\mathrm{x}_*} B_r + \frac{\theta_r^*}{V_r^*} I - \mu_B^* B_r - \lambda_r^* B_r + \lambda_p^* \frac{B_p}{V_r^*}, \\
\partial_{\mathrm{t}_*} V_p &= p - d_r^* V_p + \lambda_r^* V_r^* - \lambda_p^* V_p.
\end{aligned} \tag{2.7.1}$$

Here $x \in \Omega^* = [0, L]$ bounded domain of $\mathbb{R}$, $t > 0$ and $\nabla^2 = \partial^2_{\mathrm{x}_*}$ is the Laplacian operator in 1D. System (2.7.1) is subject to following Neumann conditions

$$\partial_{\mathrm{x}_*} S = \partial_{\mathrm{x}_*} I = \partial_{\mathrm{x}_*} B_p = \partial_{\mathrm{x}_*} B_r = 0, \ x_* = 0, L. \tag{2.7.2}$$

The new parameters and variables that appear in model (2.7.1) are described in Table 2.5. To mathematically

State Variable	**Description**
$S(x,t)$	Number of susceptible individuals at time t and at location x
$I(x,t)$	Number of infected individuals at time t and at location x
$B_p(x,t)$	*V. cholerae* number in the pond at time t and at location x
$B_r(x,t)$	*V. cholerae* concentration in the river at time t and at location x
$V_p(t)$	Volume of water in the pond at time t

Parameter	**Description**	**Unit**	**Baseline Value**	**References**
$D_S^*, D_I^*, D_{\mathrm{B}_p}^*, D_{\mathrm{B}_r}^*$	Diffusion Coefficients of susceptibles and infectives humans, bacteria in pond and river, respectively	$m^2\mathrm{day}^{-1}$	$D_S^* = D_I^* = 10$, $D_{\mathrm{B}_p}^* = D_{\mathrm{B}_r}^* = 10$	Assumed
ν_p^*, ν_r^*	Advection Coefficients of bacteria in pond and river,respectively	$m\mathrm{day}^{-1}$	$\nu_p^* = 1, \nu_r^* = 2$	Assumed

Table 2.5: Description of state variables and new parameters of the model (2.7.1)

simplify the analysis, the model is reformulated in terms of normalized variables (2.2.2) plus the following statments

$$\begin{aligned}
&x = \tfrac{x^*}{L}, \qquad D_S = \tfrac{D_S^*}{L^2 r}, \quad D_I = \tfrac{D_I^*}{L^2 r}, \quad D_{\mathrm{B}_p} = \tfrac{D_{\mathrm{B}p}^*}{L^2 r}, \\
&D_{\mathrm{B}_r} = \tfrac{D_{\mathrm{B}r}^*}{L^2 r}, \quad \nu_r = \tfrac{\nu_r^*}{Lr}, \qquad \nu_p = \tfrac{\nu_p^*}{Lr}.
\end{aligned} \tag{2.7.3}$$

The re-scaled model therefore reads as :

$$\begin{cases}
\partial_t s = D_S \nabla^2 s + \mu(1-s) - \left(\beta_p \frac{b_p}{k_p v_p + b_p} + \beta_r \frac{b_r}{1+b_r}\right) s + \gamma i, \\
\partial_t i = D_I \nabla^2 i + \left(\beta_p \frac{b_p}{k_p v_p + b_p} + \beta_r \frac{b_r}{1+b_r}\right) s - (\gamma + \delta + \mu) i, \\
\partial_t b_p = D_{\mathrm{B}_p} \nabla^2 b_p - \nu_p \partial_x b_p + \theta_p i + (1 - b_p - \mu_B - \lambda_p) b_p + \lambda_r V_r b_r, \\
\partial_t b_r = D_{\mathrm{B}_r} \nabla^2 b_r - \nu_r \partial_x b_r + \theta_r i - \mu_B b_r - \lambda_r b_r + \lambda_p \frac{b_p}{V_r}, \\
\partial_t v_p = (d_r + \lambda_p)(1 - v_p),
\end{cases} \tag{2.7.4}$$

with $x \in \Omega = [0,1]$, $t > 0$ and Neumann boundary conditions

$$\partial_x s = \partial_x i = \partial_x b_p = \partial_x b_r = 0, \ x = 0, 1. \tag{2.7.5}$$

2.8 Traveling Wave Solutions

Now, the conditions for the propagation of the epidemics in the population are investigated. To this aim, the reaction-diffusion phenomena are considered and system (2.7.4) is taken into account. For the theoretical study the space domain will be the entire real line $]-\infty, +\infty[$ and for the numerical simulations it will be the segment $[0, L]$.

Such a phenomenon is not rigorously proved in the present dissertation but will be confirmed by many numerical simulations.

Traveling wave solutions will be searched for in the following form:

$$\mathbf{W}(x - ct) = \begin{pmatrix} s(x,t) \\ i(x,t) \\ b_p(x,t) \\ b_r(x,t) \\ v_p(x,t) \end{pmatrix}, \tag{2.8.1}$$

with c the positive speed of the wave and

$$\lim_{x \to \pm\infty} \mathbf{W}(x) = \mathbf{W}_{\pm}, \tag{2.8.2}$$

where $\mathbf{W}_{\pm}$ are two homogeneous in space equilibria of system (2.7.4).

In this section, for mathematical tractability, it is assumed that $D_I = D_{\mathrm{B}_r} = 0$. Substituting Eq. (2.8.1) into (2.7.4), the following system of ordinary differential equations is obtained:

$$\begin{aligned}
D_S s'' + cs' + \mu(1-s) - \left(\beta_p \frac{b_p}{k_p v_p + b_p} + \beta_r \frac{b_r}{1+b_r}\right) s + \gamma i &= 0, \\
ci' + \left(\beta_p \frac{b_p}{k_p v_p + b_p} + \beta_r \frac{b_r}{1+b_r}\right) s - a_3 i &= 0, \\
D_{\mathrm{B}_p} b_p'' + (c - \nu_p) b_p' + \theta_p i + b_p(1 - b_p - \mu_B - \lambda_p) + \lambda_r V_r b_r &= 0, \\
(c - \nu_r) b_r' + \theta_r i - a_4 b_r + \lambda_p \frac{b_p}{V_r} &= 0, \\
cv_p' + (d_r + \lambda_p)(1 - v_p) &= 0.
\end{aligned} \tag{2.8.3}$$

In the previous discussion, the existence of the spatially homogeneous equilibrium point DFE that always exists and is globally stable if $\mathcal{R}_0 < 1$ and unstable if $\mathcal{R}_0 > 1$ is highlighted . Moreover, in last case ($\mathcal{R}_0 > 1$), there exists an endemic equilibrium point EE which is locally stable. Therefore, it is assumed in this section that $\mathcal{R}_0 > 1$.

Therefore, in this context, equilibrium $\mathbf{E}_0$ admits a stable (incoming) manifold and $\mathbf{E}_1$ an unstable (departing) manifold, with respect to the system (2.8.3). Thus, a trajectory linking the two equilibria, starting from

$\mathbf{E}_1$ and reaching $\mathbf{E}_0$, may exist [162].
Given the biological meaning of our variables, the trajectories cannot oscillate around the state $\mathbf{E}_0$. This is equivalent to requiring that the solutions of the characteristic polynomial relative to the linearization of the system (2.8.3) around the state $\mathbf{E}_0$ cannot be complex roots. By imposing this with algebraic method, we estimate the minimal speed for which exist monotone waves [162].
Consider Jacibian matrix evaluated at the equilibrium $\mathbf{E}_0$: the corresponding eigenvalues are roots of the following c-family of ξ polynomials

$$p(\xi, c) = (-d_r - \lambda_p - c\xi)(-\mu + c\xi + D_S\xi^2)(\xi^4 + b_3\xi^3 + b_2\xi^2 + b_1\xi + a_0), \tag{2.8.4}$$

where

$$\begin{aligned}
b_3 &= \frac{1}{cD_{\mathrm{B}_p}(c-\nu_r)}\left[c^3 - c^2(\nu_r+\nu_p) - c(a_3D_{\mathrm{B}_p} + a_4D_{\mathrm{B}_p} - \nu_r\nu_p) + a_3D_{\mathrm{B}_p}\nu_r\right], \\
b_2 &= \frac{1}{cD_{\mathrm{B}_p}(c-\nu_r)}\{a_3a_4D_{\mathrm{B}_p} - a_3\nu_r\nu_p - D_{\mathrm{B}_p}\beta_r\theta_r + c[\nu_r(-1+a_3+\lambda_p+\mu_B) + (a_3+a_4)\nu_p] \\
&- c^2(-1+a_3+a_4+\lambda_p+\mu_B)\}, \\
b_1 &= \frac{1}{cD_{\mathrm{B}_p}k_p(c-\nu_r)}\{-ck_p\beta_r\theta_r + k_p\nu_p\beta_r\theta_r - c\beta_p\theta_p + \nu_r\beta_p\theta_p - ck_p\lambda_r\lambda_p + a_4ck_p(-1+\lambda_p \\
&+ \mu_B) + a_3k_p[-a_4\nu_p - \nu_r(-1+\lambda_p+\mu_B) + c(-1+a_4+\lambda_p+\mu_B)]\}, \\
b_1 &= \frac{1}{cD_{\mathrm{B}_p}(c-\nu_r)k_pV_r}\left(\left(\mathcal{R}_0^{ODE}\right)^2 - 1\right).
\end{aligned} \tag{2.8.5}$$

All solutions of (2.8.4) must be real. Three solutions of (2.8.4) are always real, i.e.

$$\xi_1 = \frac{d_r+\lambda_p}{c} > 0, \quad \xi_2 = -\frac{c+\sqrt{c^2+4D_S\mu}}{2D_S} < 0, \quad \xi_3 = \frac{c-\sqrt{c^2+4D_S\mu}}{2D_S} > 0. \tag{2.8.6}$$

Then, it must be requested that the roots of the quartic in equation (2.8.4) must be reals. Following [90], we write the following quantities (note that they are the quantities (2.6.5) written for the polynomial (2.8.4)):

$$\begin{aligned}
&H(c) = 8b_2 - 3b_3^2, && F(c) = 16b_2^2 + 3b_3^4 - 16b_2b_3^2 - 64b_0 + 16b_3b_1, \\
&P(c) = b_2^2 + 12b_0 - 3b_1b_3, && J(c) = 72b_2b_0 + 9b_1b_2b_3 - 2b_2^3 - 27b_1^2 - 27b_0b_3^2, \\
&\Delta_q(c) = 4P^3 - J^2.
\end{aligned} \tag{2.8.7}$$

The solutions of equation (2.8.4) are real iff [90]

$$H(c) < 0, \quad F(c) > 0, \quad \Delta_q(c) \geq 0. \tag{2.8.8}$$

The leading coefficients of the functions $H(c)$, and $F(c)$ are given by:

$$lc(H(c)) = -3 < 0, \quad lc(F(c)) = k_pV_r > 0. \tag{2.8.9}$$

Thus, it can be easily deduced that $\lim_{c\to\infty} H(c) = -\infty$ and $\lim_{c\to\infty} F(c) = \infty$. Moreover, depending on the model parameters, the leading coefficient of the quantity $\Delta_q(c)$ can be positive or negative. If $lc(\Delta_q(c))$ is negative, monotone waves cannot exist. Therefore, to ensure the existence of non-oscillating waves, it is

necessary to choose an appropriate set of model parameters such that $lc(\Delta_q(c)) > 0$. In this way, you will have $\lim_{c \longrightarrow \infty} \Delta_q(c) = \infty$. Therefore, it can be defined:

$$\begin{aligned} c_1 &= \max_j \left\{ c_j \in \mathbb{R}^+ \ : \ H = 0 \right\}, \\ c_2 &= \max_j \left\{ c_j \in \mathbb{R}^+ \ : \ F = 0 \right\}, \\ c_3 &= \max_j \left\{ c_j \in \mathbb{R}^+ \ : \ \Delta_q = 0 \right\}. \end{aligned} \tag{2.8.10}$$

Finally, the solutions of the quartic in equation (2.8.4) are always real iff

$$c \geq c_{min} = \max\{c_1, c_2, c_3\}. \tag{2.8.11}$$

Thus a possible range of speeds due to linearization at the stationary point is given. Note that *Volpert et al* [162], concerning monotone parabolic systems without advection, proved that in monostable case (one of the two equilibria is stable and the other unstable), monotone waves exist, for a half-interval or a half-axis of speeds.

In this case, in correspondence with values of the speed c greater then the minimal value c_{min}, may exist a vector valued funcion $\mathbf{W}(x - ct)$ solution of system (2.8.3), satisfying boundary conditions (2.8.2) with $\mathbf{W}_- = \mathbf{E}_1$ and $\mathbf{W}_+ = \mathbf{E}_0$

In Fig. 2.10, we show the numerical solution of model (2.7.4) choosing as initial condition a vector function with a bounded support, linking the two equilibria. Fig 2.10 shows that the initial data evolves in time as an advancing wave front and the shape of each trace is unchanged during the propagation. These waves move at minimal speed given by $c_{min} = 0.888548$. We can deduce that cholera model (2.7.4) approches traveling waves solutions and the infection can propagates downstream, for example from inland to cost areas.

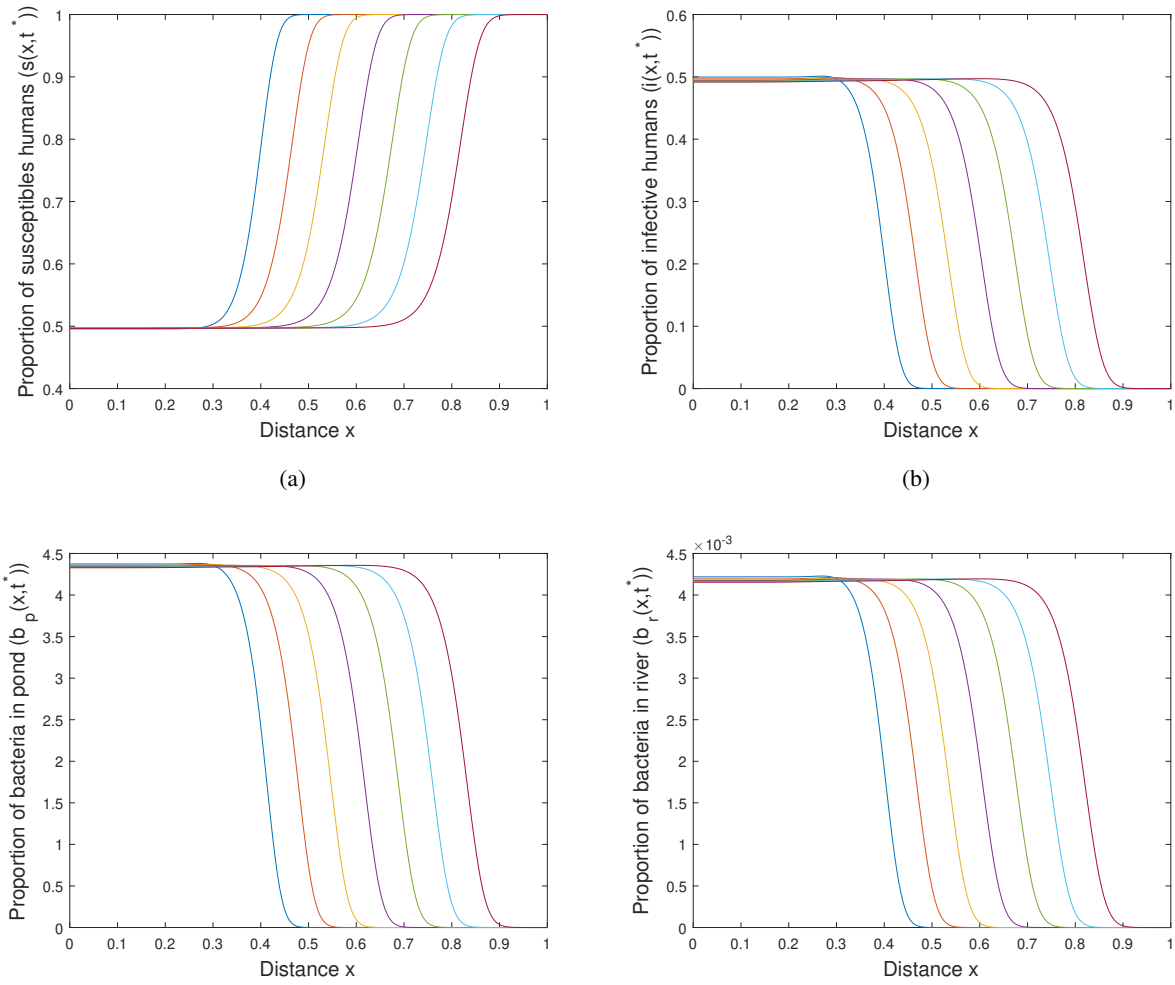

(a) (b)

(c) (d)

Figure 2.10: Numerical solutions of system (2.7.4) for $s(x,t)$ (a), $i(x,t)$ (b), $b_p(x,t)$ (c) and $b_r(x,t)$ (c) with bounded support functions as initial data. Parameters used are listed in Table 2.1 with $\mu^* = 9\times10^{-3}$, $L = 100$, $\beta_p^* = \beta_r^* = 30$, $\lambda_r^* = 0.5$ and $D_S = D_{\mathrm{B}_p} = 1$, $D_I = D_{\mathrm{B}_r} = 0$.

2.9 Basic Reproductive Number associated to PDE model

The aim of this section is to extend the Basic Reproductive Number to the spatially non–homogeneous case, following the idea exposed by the authors in [164]. This will provide a threshold for the eradication of the infection even in the spatial case.

First of all, for mathematical tractability, we consider the special case of the model where exchange of water between the two basins does not occur (i.e., $\lambda_p = \lambda_r = 0$). Based on these assumptions, the PDE

model (2.7.4) reduces to:

$$\begin{aligned}
\partial_t s &= D_S\nabla^2 s + \mu(1-s) - \left(\beta_p \frac{b_p}{k_p v_p + b_p} + \beta_r \frac{b_r}{1+b_r}\right) s + \gamma i,\\
\partial_t i &= D_I\nabla^2 i + \left(\beta_p \frac{b_p}{k_p v_p + b_p} + \beta_r \frac{b_r}{1+b_r}\right) s - a_3 i,\\
\partial_t b_p &= D_{\mathrm{B}_p}\nabla^2 b_p - \nu_p \partial_x b_p + \theta_p i + b_p\left(1 - b_p - \mu_B\right),\\
\partial_t b_r &= D_{\mathrm{B}_r}\nabla^2 b_r - \nu_r \partial_x b_r + \theta_r i - \mu_B b_r,\\
\partial_t v_p &= d_r(1 - v_p),
\end{aligned} \tag{2.9.1}$$

with $t > 0$, $x \in \Omega = [0,1]$ and Neumann condition (2.7.5) at the boundary $\partial\Omega$.

In the section 2.3, the possible behaviors of the bacis reproductive number related to the corresponding ODE model (2.2.3), deriving from different interpretations of the role of the environment in the transmission dynamics were explored (see expressions (2.3.4), (2.3.9), (2.3.13) and (2.3.18)). It has been proved that all agree on the same threshold value and retain their order of magnitude with respect to unity. Thus, without loss of generality, Scenario 3, studied in subsection **??**, is chosen for the extension to the spatial case: the growth of bacteria in the pond ($r = 1$) is placed in the V matrix, while the shedding rates (θ_p and θ_r) constitute a new infection. Thus, the transmission and transition matrices F and V of the NGM approach [62, 61] in Scenario 3 for the reduced model (2.9.1) are given by:

$$F = \begin{pmatrix} 0 & \frac{\beta_p}{k_p} & \beta_r \\ \theta_p & 0 & 0 \\ \theta_r & 0 & 0 \end{pmatrix}, \quad V = \begin{pmatrix} a_3 & 0 & 0 \\ 0 & \mu_B - 1 & 0 \\ 0 & 0 & \mu_B \end{pmatrix}. \tag{2.9.2}$$

Thus, it can be computed that, the basic reproduction number for the equivalent ODE model of system (2.9.1) in Scanario 3 is given by:

$$\mathcal{R}_0^{ODE} = \sqrt{\frac{\beta_p\theta_p\mu_B + k_p\beta_r\theta_r(\mu_B - 1)}{k_p a_3 \mu_B(\mu_B - 1)}}. \tag{2.9.3}$$

It is worth to mentioning that the number $\mathcal{R}_0^{(3)}$, given in (2.3.13), reduces to $\mathcal{R}_0^{ODE}$ above when $\lambda_p = \lambda_r = 0$.

It should be stressed that, in the case we are dealing with, since there is no water flow between the pond and the river, condition $\mu_B = 1$ constitutes a singularity for system (2.9.1) and for $\mathcal{R}_0^{ODE}$ defined in (2.9.3). To ensure positivity and well-position of (2.9.1) and (2.9.3), it is necessary to impose $\mu_B > 1$.

Following the idea in [164], it is assumed that the state variables are near the disease-free steady state $\mathbf{E}_0$. Let $\phi(x) = (i(x,0), b_p(x,0), b_r(x,0)) = (\phi_1(x), \phi_2(x), \phi_3(x))$ be the distribution of initial infection. Consider the reaction-advection diffusion model, consisting of only the equations relating to the disease and

environmental compartments

$$\begin{aligned}
\partial_t i &= D_I \nabla^2 i + \left(\beta_p \frac{b_p}{k_p v_p + b_p} + \beta_r \frac{b_r}{1 + b_r} \right) s - a_3 i, \\
\partial_t b_p &= D_{\mathrm{B}_p} \nabla^2 b_p - \nu_p \partial_x b_p + \theta_p i + (1 - b_p - \mu_B)\, b_p, \\
\partial_t b_r &= D_{\mathrm{B}_r} \nabla^2 b_r - \nu_r \partial_x b_r + \theta_r i - \mu_B b_r.
\end{aligned} \tag{2.9.4}$$

Wang and Zhao [164], extended the NGM method [62, 61], defining the basic reproductive number for reaction-diffusion systems as follows

$$\mathcal{R}_0^{PDE} = \rho(\mathcal{L}), \tag{2.9.5}$$

where

$$\mathcal{L} = -F\mathcal{B}^{-1}. \tag{2.9.6}$$

Matrix F is the transmission matrix of the NGM approch, while $\mathcal{B}$ is an extension to the spatial case of the transition matrix V of the NGM approach, which in this case reads as [164],[165]

$$\mathcal{B} = \nabla(D \cdot \nabla) - v\nabla - V, \tag{2.9.7}$$

with D the diagonal matrix with diffusion coeffients and v the diagonal matrix of advection coefficients. For the reduced cholera model (2.9.1), one gets $D = Diag[D_I, D_{\mathrm{B}_p}, D_{\mathrm{B}_r}]$, $\nu = Diag[0, \nu_p, \nu_r]$ and the matrix $\mathcal{B}$ takes the form:

$$\mathcal{B} = \begin{pmatrix} D_I \nabla^2 - a_3 & 0 & 0 \\ 0 & D_{\mathrm{B}_p} \nabla^2 - \nu_p \partial_x - (\mu_B - 1) & 0 \\ 0 & 0 & D_{\mathrm{B}_r} \nabla^2 - \nu_r \partial_x - \mu_B \end{pmatrix}. \tag{2.9.8}$$

Note that, if $D \to 0$ and $\nu \to 0$, then $\mathcal{B} \to -V$ and $\mathcal{L} \to FV^{-1}$, where FV^{-1} is the NGM related to the non-spatial model corresponding to (2.9.1).

From now on, suppose $D \neq 0$.

Following [166], [165], let us proceed to calculate $\mathcal{B}^{-1}$ by solving $\mathcal{B}(\phi_1, \phi_2, \phi_3)^T = (y_1, y_2, y_3)^T$ subject to homogeneous Neumann boundary conditions. Let us first consider the equation

$$\mathcal{B}[\phi_1] := D_I \nabla^2 \phi_1(x) - a_3 \phi_1(x) = y_1(x), \tag{2.9.9}$$

with $\phi_1'(0) = \phi_1'(1) = 0$. This problem can be conveniently solved by using the Laplace transform. Denote the Laplace transforms of $\phi_1(x)$ and $y_1(x)$ by $\Phi_1(s)$ and $Y_1(s)$, respectively. Then,

$$\Phi_1(s) = \frac{Y_1(s)}{D_I s^2 - a_3} + \frac{s D_I \phi_1(0)}{D_I s^2 - a_3}, \tag{2.9.10}$$

where the first boundary condition of ϕ_1 is applied. The inverse Laplace transform then yields

$$\phi_1(x) = \frac{1}{D_I a_3} \int_0^x \sinh\left[\sqrt{\frac{a_3}{D_I}} (x - \tau) \right] y_1(\tau) d\tau + \phi_1(0) \cosh\left[\sqrt{\frac{a_3}{D_I}} x \right]. \tag{2.9.11}$$

Now differentiating ϕ_1 and using the second boundary condition, one obtains

$$\begin{aligned}\phi_1(x) &= \mathcal{B}^{-1}[y_1] = \frac{1}{\sqrt{D_I a_3}}\int_0^x \sinh\left[\sqrt{\frac{a_3}{D_I}}(x-\tau)\right] y_1(\tau)d\tau \\ &- \frac{\cosh\left[\sqrt{\frac{a_3}{D_I}}x\right]}{\sqrt{D_I a_3}\sinh\left[\sqrt{\frac{a_3}{D_I}}\right]}\int_0^1 \cosh\left[\sqrt{\frac{a_3}{D_I}}(1-\tau)\right] y_1(\tau)d\tau. \end{aligned} \tag{2.9.12}$$

In this expression, the second part represents the homogeneous solution, whereas the first part represents a particular solution to the original non-homogeneous equation, as reported in [166]. In a similar way, the boundary value problem

$$\mathcal{B}[\phi_2] := D_{\mathrm{B}_p}\nabla^2\phi_2(x) - \nu_p\partial_x\phi_2(x) - (\mu_B - 1)\phi_2(x) = y_2(x), \tag{2.9.13}$$

with $\phi_2^{'}(0) = \phi_2^{'}(1) = 0$, can be solved. Denote the Laplace transforms of $\phi_2(x)$ and $y_2(x)$ by $\Phi_2(s)$ and $Y_2(s)$, respectively. Then

$$\Phi_2(s) = \frac{Y_2}{D_{\mathrm{B}_p}s^2 - \nu_p s - (\mu_B - 1)} + \frac{\phi_2(0)(D_{\mathrm{B}_p}s - \nu_p)}{D_{\mathrm{B}_p}s^2 - \nu_p s - (\mu_B - 1)}, \tag{2.9.14}$$

where the first boundary condition of ϕ_2 is applied. It is convenient to define the following positive constant $\varepsilon = \frac{\sqrt{\nu_p^2 + 4D_{\mathrm{B}_p}(\mu_B - 1)}}{2D_{\mathrm{B}_p}}$. The inverse Laplace transform then yields

$$\begin{aligned}\phi_2(x) &= \frac{1}{D_{\mathrm{B}_p}\varepsilon}\int_0^x e^{\frac{\nu_p}{2D_{\mathrm{B}_p}}(x-\tau)}\sinh\left[\varepsilon(x-\tau)\right] y_2(\tau)d\tau + \frac{\phi_2(0)e^{\frac{\nu_p}{2D_{\mathrm{B}_p}}x}}{2}(\cosh\left[\varepsilon x\right] \\ &- \frac{\nu_p}{2D_{\mathrm{B}_p}\varepsilon}\sinh\left[\varepsilon x\right]). \end{aligned} \tag{2.9.15}$$

Now differentiating ϕ_2 and using the second boundary condition, one gets

$$\begin{aligned}\phi_2(x) &= \mathcal{B}_2^{-1}[y_2] = \frac{1}{D_{\mathrm{B}_p}\varepsilon}\int_0^x e^{\frac{\nu_p}{2D_{\mathrm{B}_p}}(x-\tau)}\sinh\left[\varepsilon(x-\tau)\right] y_2(\tau)d\tau - \frac{e^{-\frac{\nu_p}{2D_{\mathrm{B}_p}}(1-x)}}{(\mu_B-1)\sinh\left[\varepsilon\right]}(\cosh\left[\varepsilon x\right] \\ &- \frac{\nu_p}{2D_{\mathrm{B}_p}\varepsilon}\sinh\left[\varepsilon x\right])\int_0^1 e^{\frac{\nu_p}{2D_{\mathrm{B}_p}}(1-\tau)}\left\{\frac{\nu_p}{2D_{\mathrm{B}_p}}\sinh\left[\varepsilon(1-\tau)\right] + \varepsilon\cosh\left[\varepsilon(1-\tau)\right]\right\} y_2(\tau)d\tau. \end{aligned} \tag{2.9.16}$$

Finally, solving the equation

$$\mathcal{B}[\phi_3] := D_{\mathrm{B}_r}\nabla^2\phi_3(x) - \nu_r\partial_x\phi_3(x) - \mu_B\phi_3(x) = y_3(x), \tag{2.9.17}$$

with the boundary conditions $\phi_3^{'}(0) = \phi_3^{'}(1) = 0$, one finds that

$$\begin{aligned}\phi_3(x) &= \mathcal{B}_3^{-1}[y_3] = \frac{1}{D_{\mathrm{B}_r}\omega}\int_0^x e^{\frac{\nu_r}{2D_{\mathrm{B}_r}}(x-\tau)}\sinh\left[\omega(x-\tau)\right] y_3(\tau)d\tau - \frac{e^{-\frac{\nu_r}{2D_{\mathrm{B}_r}}(1-x)}}{\mu_B\sinh\left[\omega\right]}(\cosh\left[\omega x\right] \\ &- \frac{\nu_r}{2D_{\mathrm{B}_r}\omega}\sinh\left[\omega x\right])\int_0^1 e^{\frac{\nu_r}{2D_{\mathrm{B}_r}}(1-\tau)}\left\{\frac{\nu_r}{2D_{\mathrm{B}_r}}\sinh\left[\omega(1-\tau)\right] + \omega\cosh\left[\omega(1-\tau)\right]\right\} y_3(\tau)d\tau, \end{aligned} \tag{2.9.18}$$

where $\omega = \frac{\sqrt{\nu_r^2 + 4\mu_B D_{\mathrm{B}_r}}}{2D_{\mathrm{B}_r}} > 0$. For consistence in notations, below ϕ_1 and y_1 in Equation (2.9.12) are exchanged, as well as ϕ_2 and y_2 in Equation (2.9.16) and ϕ_3 and y_3 in Equation (2.9.18). Now, the eigenvalue problem which must be resolved turns out

$$-F\mathcal{B}^{-1}\phi = \lambda\phi. \tag{2.9.19}$$

The following three equations are obtained:

$$
\begin{aligned}
k_{i1} \quad & \int_0^x \sinh\left[\sqrt{\frac{a_3}{D_I}}(x-\tau)\right]\phi_1(\tau)d\tau + \\
k_{i2} \quad & \cosh\left[\sqrt{\frac{a_3}{D_I}}x\right]\int_0^1 \cosh\left[\sqrt{\frac{a_3}{D_I}}(1-\tau)\right]\phi_1(\tau)d\tau + \\
k_{i3} \quad & \int_0^x e^{\frac{\nu_p}{2D_{\mathrm{B}_p}}(x-\tau)}\sinh\left[\varepsilon(x-\tau)\right]\phi_2(\tau)d\tau + \\
k_{i4} \quad & e^{-\frac{\nu_p}{2D_{\mathrm{B}_p}}(1-x)}\left(\cosh\left[\varepsilon x\right]-\frac{\nu_p}{2D_{\mathrm{B}_p}\varepsilon}\sinh\left[\varepsilon x\right]\right)\int_0^1 e^{\frac{\nu_p}{2D_{\mathrm{B}_p}}(1-\tau)}\{\frac{\nu_p}{2D_{\mathrm{B}_p}}\sinh\left[\varepsilon(1-\tau)\right]+ \\
& \varepsilon\cosh\left[\varepsilon(1-\tau)\right]\}\phi_2(\tau)d\tau + \\
k_{i5} \quad & \int_0^x e^{\frac{\nu_r}{2D_{\mathrm{B}_r}}(x-\tau)}\sinh\left[\omega(x-\tau)\right]\phi_3(\tau)d\tau + \\
k_{i6} \quad & e^{-\frac{\nu_r}{2D_{\mathrm{B}_r}}(1-x)}\left(\cosh\left[\omega x\right]-\frac{\nu_r}{2D_{\mathrm{B}_r}\omega}\sinh\left[\omega x\right]\right)\int_0^1 e^{\frac{\nu_r}{2D_{\mathrm{B}_r}}(1-\tau)}\{\frac{\nu_r}{2D_{\mathrm{B}_r}}\sinh\left[\omega(1-\tau)\right]+ \\
& \omega\cosh\left[\omega(1-\tau)\right]\}\phi_3(\tau)d\tau = \lambda\phi_i \quad i=1,2,3
\end{aligned}
\tag{2.9.20}
$$

where

$$
\begin{aligned}
k_{13} &= -\frac{\beta_p}{k_p D_{\mathrm{B}_p}\varepsilon}, & k_{14} &= \frac{\beta_p}{k_p(\mu_B-1)\sinh\left[\varepsilon\right]}, \\
k_{15} &= -\frac{\beta_r}{D_{\mathrm{B}_r}\omega}, & k_{16} &= \frac{\beta_r}{\mu_B\sinh\left[\omega\right]}, \\
k_{21} &= -\frac{\theta_p}{\sqrt{D_I a_3}}, & k_{22} &= \frac{\theta_p}{\sqrt{D_I a_3}\sinh\left[\sqrt{\frac{a_3}{D_I}}\right]}, \\
k_{31} &= -\frac{\theta_r}{\sqrt{D_I a_3}}, & k_{32} &= \frac{\theta_r}{\sqrt{D_I a_3}\sinh\left[\sqrt{\frac{a_3}{D_I}}\right]},
\end{aligned}
\tag{2.9.21}
$$

$$
k_{11}=k_{12}=k_{23}=k_{24}=k_{25}=0, \quad k_{26}=k_{33}=k_{34}=k_{35}=k_{36}=0.
$$

2.9.1 Numerical Treatment of Eigenvalue Problem (2.9.20)

Analysis of the eigenvalue problem associated with the integral equations (2.9.20) appears difficult. Instead, following the ideas in [166], some insights into the eigenvalue problem ((2.9.20) can be studied by looking at its discrete form. Let us partition the interval $[0,1]$ uniformly with the nodes $x_i = i\Delta x,\ (0 \le i \le M)$, where $M\Delta x = 1$. Evaluating Equation (2.9.20) at x_i for $i = 1, 2, ..., M$, and simply approximating each integral by using the right endpoint of each subinterval (see [166]), the following matrix equation is obtained

$$
AZ = \lambda Z \tag{2.9.22}
$$

with $Z = [\phi_1(x_1), \phi_1(x_2), ..., \phi_1(x_M), \phi_2(x_1), \phi_2(x_2), ..., \phi_2(x_M), \phi_3(x_1), \phi_3(x_2), ..., \phi_3(x_M)]^T$. The problem is now reduced to analysing the spectral radius, $\rho(A)$, of the coefficient matrix A; in particular

$$\lim_{\Delta x \to 0} \rho(A) = \rho(L) = \mathcal{R}_0^{PDE}.$$

The coefficient matrix A in can be written as

$$A = A_1 + A_2 + A_3 + A_4 + A_5 + A_6, \tag{2.9.23}$$

where each matrix A_i $(1 \leq i \leq 4)$, of dimension $3M \times 3M$, results from the discretization of the i-th integral in equations (2.9.20). Specifically, A_1 can be represented by a block form

$$A_1 = \Delta x \begin{pmatrix} 0_M & 0_M & 0_M \\ k_{21}\tilde{A}_1 & 0_M & 0_M \\ k_{31}\tilde{A}_1 & 0_M & 0_M \end{pmatrix}, \tag{2.9.24}$$

where 0_M denotes the zero square matrix of dimension $M \times M$, and $\tilde{A}_1 = (a_{i,j}^{(1)})$ is an $M \times M$ lower-triangular matrix given by

$$a_{i,j}^{(1)} = \begin{cases} \sinh\left[\sqrt{\frac{a_3}{D_I}}(x_i - x_j)\right], & \text{if } i \geq j, \\ 0, & \text{otherwise.} \end{cases} \tag{2.9.25}$$

Similarly,

$$A_3 = \Delta x \begin{pmatrix} 0_M & k_{13}\tilde{A}_3 & 0_M \\ 0_M & 0_M & 0_M \\ 0_M & 0_M & 0_M \end{pmatrix}, \tag{2.9.26}$$

where $\tilde{A}_3 = (a_{i,j}^{(3)})$ is also an $M \times M$ lower-triangular matrix:

$$a_{i,j}^{(3)} = \begin{cases} e^{\frac{\nu_p}{2D_{\mathrm{B}p}}(x_i - x_j)} \sinh\left[\varepsilon(x_i - x_j)\right], & \text{if } i \geq j, \\ 0, & \text{otherwise.} \end{cases} \tag{2.9.27}$$

In a similar way,

$$A_5 = \Delta x \begin{pmatrix} 0_M & 0_M & k_{13}\tilde{A}_5 \\ 0_M & 0_M & 0_M \\ 0_M & 0_M & 0_M \end{pmatrix}, \tag{2.9.28}$$

where $\tilde{A}_5 = (a_{i,j}^{(5)})$ is also an $M \times M$ lower-triangular matrix:

$$a_{i,j}^{(5)} = \begin{cases} e^{\frac{\nu_r}{2D_{\mathrm{B}r}}(x_i - x_j)} \sinh\left[\omega(x_i - x_j)\right], & \text{if } i \geq j, \\ 0, & \text{otherwise.} \end{cases} \tag{2.9.29}$$

The matrix A_2 takes the form

$$A_2 = \Delta x \begin{pmatrix} 0_M & 0_M & 0_M \\ k_{22}\tilde{A}_2 & 0_M & 0_M \\ k_{32}\tilde{A}_2 & 0_M & 0_M \end{pmatrix}, \tag{2.9.30}$$

with the $M \times M$ block $\tilde{A}_2 = (a_{i,j}^{(2)})$ for which

$$a_{i,j}^{(2)} = \cosh\left[\sqrt{\tfrac{a_3}{D_I}}x_i\right]\cosh\left[\sqrt{\tfrac{a_3}{D_I}}(1-x_j)\right], \quad \text{if} \quad 1 \leq i,j \leq M. \tag{2.9.31}$$

Then, the matrix A_4 takes the form

$$A_4 = \Delta x \begin{pmatrix} 0_M & k_{14}\tilde{A}_4 & 0_M \\ 0_M & 0_M & 0_M \\ 0_M & 0_M & 0_M \end{pmatrix}, \tag{2.9.32}$$

with the $M \times M$ block $\tilde{A}_4 = (a_{i,j}^{(4)})$ for which

$$\begin{aligned} a_{i,j}^{(4)} &= e^{-\frac{\nu_p}{2D_{\mathrm{B}_p}}(1-x_i)}\left\{\cosh[\varepsilon x_i] - \frac{\nu_p}{2D_{\mathrm{B}_p}\varepsilon}\sinh[\varepsilon x_i]\right\}e^{\frac{\nu_p}{2D_{\mathrm{B}_p}}(1-x_j)}\{\frac{\nu_p}{2D_{\mathrm{B}_p}}\sinh[\varepsilon(1-x_j)] \\ &+ \varepsilon\cosh[\varepsilon(1-x_j)]\}, \quad \text{if} \quad 1 \leq i,j \leq M. \end{aligned} \tag{2.9.33}$$

Finally, The matrix A_6 takes the form

$$A_6 = \Delta x \begin{pmatrix} 0_M & 0_M & k_{16}\tilde{A}_6 \\ 0_M & 0_M & 0_M \\ 0_M & 0_M & 0_M \end{pmatrix}, \tag{2.9.34}$$

with the $M \times M$ block $\tilde{A}_6 = (a_{i,j}^{(6)})$ for which

$$\begin{aligned} a_{i,j}^{(6)} &= e^{-\frac{\nu_r}{2D_{\mathrm{B}_r}}(1-x_i)}\left\{\cosh[\omega x_i] - \frac{\nu_r}{2D_{\mathrm{B}_r}\omega}\sinh[\omega x_i]\right\}e^{\frac{\nu_r}{2D_{\mathrm{B}_r}}(1-x_j)}\{\frac{\nu_r}{2D_{\mathrm{B}_r}}\sinh[\omega(1-x_j)] \\ &+ \omega\cosh[\omega(1-x_j)]\}, \quad \text{if} \quad 1 \leq i,j \leq M. \end{aligned} \tag{2.9.35}$$

There is no general relationship between $\rho(A)$ and $\rho(A_i)$, $(1 \leq i \leq 6)$. Nevertheless, if we assume $\frac{a_3}{D_I} \ll 1$, $\frac{\nu_p^2}{4D_{\mathrm{B}_p}^2} + \frac{\mu_B - 1}{D_{\mathrm{B}_p}} \ll 1$ and $\frac{\nu_r^2}{4D_{\mathrm{B}_r}^2} + \frac{\mu_B}{D_{\mathrm{B}_r}} \ll 1$, then each entry of $\tilde{A}_1$, $\tilde{A}_3$ and $\tilde{A}_5$ is very small; it is bounded between 0 and $\sinh\left[\sqrt{\frac{a_3}{D_I}}\right]$ if in $\tilde{A}_1$, between 0 and $\sinh\left[\sqrt{\frac{\nu_p^2}{4D_{\mathrm{B}_p}^2} + \frac{\mu_B - 1}{D_{\mathrm{B}_p}}}\right]$ if in $\tilde{A}_3$ and between 0 and $\sinh\left[\sqrt{\frac{\nu_r^2}{4D_{\mathrm{B}_r}^2} + \frac{\mu_B}{D_{\mathrm{B}_r}}}\right]$ if in $\tilde{A}_5$. Thus, A_1, A_3 and A_5 can be treated as small perturbation to A_2, A_4 and A_6 in this case, and

$$\rho(A) \approx \rho(A_2 + A_4 + A_6). \tag{2.9.36}$$

2.9.2 Main Results on $\mathcal{R}_0^{PDE}$

The quantity $\mathcal{R}_0^{PDE}$ represents a threshold value for the eradication of the disease for the spatially non-homogeneous model (2.9.1). Indeed, consider the spatially homogeneous equivalents of the equations $(2.9.1)_1$ and $(2.9.1)_5$: let M be the matrix consisting of the derivatives of the right hand-side of these equations with respect to the variables S and V_p, evaluated at DFE $\mathbf{E}_0$, i.e.:

$$M = \begin{pmatrix} -\mu & 0 \\ 0 & -(d_r + \lambda_p) \end{pmatrix}. \tag{2.9.37}$$

Since the off-diagonal entries are non-negative, M is cooperative. In addition, the opposite of the transition matrix $-V$ related to the model (2.9.1) and evaluated at the DFE $\mathbf{E}_0$ defined in (2.9.2), is also cooperative. Let $\mathcal{A}$ a closed linear operator and $\sigma(\mathcal{A})$ its spectrum. Let us denote its spectral bound with

$$s(\mathcal{A}) = \sup\{\mathrm{Re}(\lambda) \mid \lambda \in \sigma(\mathcal{A})\}. \tag{2.9.38}$$

Thus, consider the following statements, introduced by Wang and Zhao [164] for reaction-diffusion systems (without advection):

$$\lambda^0(M) \equiv s(\nabla(D\nabla) + M) < 0, \quad \lambda^0(-V) \equiv s(\nabla(D\nabla) - V) = s(\mathcal{B}) < 0. \tag{2.9.39}$$

The following result, proved for reaction-diffusion model by Wang and Zhao [164], is an extension to the spatial case of theorem for local stability of the DFE proved in [161]:

Theorem 2.9.1 *[164] Assume that (2.9.39) holds. Then*

- $\mathcal{R}_0^{PDE} - 1$ *has the same sign as* $\lambda^* \equiv s(\mathcal{B} + F)$.
- *If* $\mathcal{R}_0^{PDE} < 1$*, then DFE* $\boldsymbol{E}_0$ *is asymptotically stable for system (2.9.1) if* $\nu_p = \nu_r = 0$.

Thus, when assumptions (2.9.39) hold, $\mathcal{R}_0^{PDE}$ is a threshold quantity for model (2.9.1) without advection. A natural extension for systems with advection of requests (2.9.39) seems to be

$$\lambda^0(M) \equiv s(\nabla(D\nabla) - \nu\nabla + M) < 0, \quad \lambda^0(-V) \equiv s(\nabla(D\nabla) - \nu\nabla - V) = s(\mathcal{B}) < 0. \tag{2.9.40}$$

Assuming that (2.9.40) are valid, the theorem 2.9.1 can apply to systems with advection, like the model (2.9.1). Therefore, $\mathcal{R}_0^{PDE}$, greatest solutions of the eigenvalue problem (2.9.20), turns out to be a good threshold for the eradication of the infection, as confirmed by many simulations (see next section).
To conclude this section, a result that compares the two reproduction numbers $\mathcal{R}_0^{ODE}$ (given in (2.9.3)) and $\mathcal{R}_0^{PDE}$ (greatest solutions of the eigenvalue problem (2.9.20)) is provided.

Theorem 2.9.2 *If* $a_3 \ll D_I$, $\nu_p + \mu_B - 1 \ll D_{\mathrm{B}_p}$ *and* $\nu_r + \mu_B \ll D_{\mathrm{B}_r}$, *then*

$$\mathcal{R}_0^{PDE} \doteq \mathcal{R}_0^{ODE} \tag{2.9.41}$$

The proof is given in Appendix E.
The result in Theorem 2.9.2 indicates that when diffusion in the human and bacterial populations is large enough, and convection is insigniticant, the spatial heterogeneity (reflected by the PDE model) tends to be smoothed out so that the disease threshold is reduced to that for the homogeneous environments (represented by the ODE model).
A similar result is obtained in [165], with a single bacteria population.

2.10 Numerical Simulation associated to PDE Model

In this section, again we have $\lambda_p = \lambda_r = 0$ and $\mathcal{R}_0^{ODE}$ like in formula (2.9.3). Analytical results are now verified by means of numerical simulation. In particular, the threshold dynamics based on our ODE and PDE cholera models are compared. The main interest is to study the influence of the shedding of bacteria θ_p and the transmission parameter β_p of bacteria population in pond on $\mathcal{R}_0^{PDE}$. Fig. 2.11 shows the difference in the basic reproduction numbers of the PDE model (2.7.4) and the ODE model (2.2.3) with $\lambda_p = \lambda_r = 0$. We observe, from Figure 2.11(a), that $\left|\mathcal{R}_0^{ODE} - \mathcal{R}_0^{PDE}\right|$ is nearly invisible when the diffusion coefficients of the hosts and bacteria in pond and river (D_I, D_{B_p} and D_{B_p}, respectively) are getting large with respect to the advection coefficient v_p and v_r. This result confirms that $\mathcal{R}_0^{PDE} \to \mathcal{R}_0^{ODE}$ when $\dfrac{v_p}{D_{\mathrm{B}_p}}$ and $\dfrac{v_r}{D_{\mathrm{B}_r}}$ are getting small . When $\dfrac{v_p}{D_{\mathrm{B}_p}}$ and $\dfrac{v_r}{D_{\mathrm{B}_r}}$ are getting large, Figure 2.11(b) illustrates that the difference $\left|\mathcal{R}_0^{ODE} - \mathcal{R}_0^{PDE}\right|$ is quite large. This result is consistent with Theorem 2.9.2 and extends what has been shown in [165, 166].

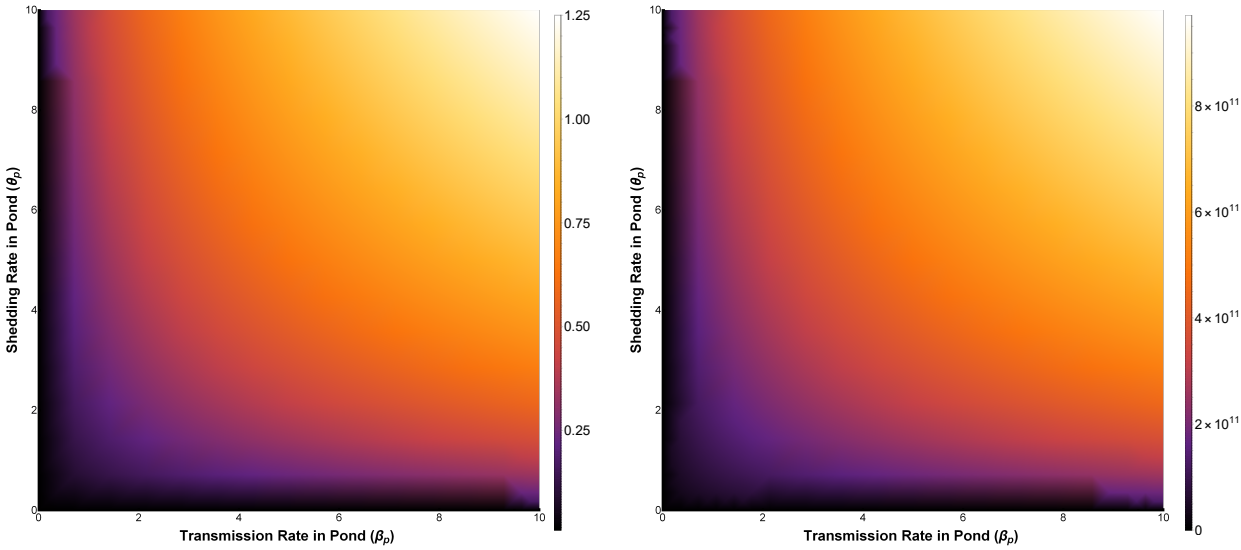

(a) $D_{\mathrm{B}_p} \gg v_p, D_{\mathrm{B}_r} \gg v_r$ (c) $D_{\mathrm{B}_p} \ll v_p, D_{\mathrm{B}_r} \ll v_r$

Figure 2.11: The difference in the basic reproduction number between the PDE model (2.7.4) and the ODE model (2.2.3) (with $\lambda_p = \lambda_r = 0$) $\left|\mathcal{R}_0^{PDE} - \mathcal{R}_0^{ODE}\right|$. The thresholds $\mathcal{R}_0^{ODE}$ and $\mathcal{R}_0^{PDE}$ are function of β_p and θ_p. The value of parameters used in this simulation are those listed in Table 2.1 and Table 2.5 with $\beta_r^* = 10^3$ and $L = 10$. In plot (a) $D_S^* = D_I^* = 10^2$, $D_{\mathrm{B}_p}^* = D_{\mathrm{B}_r}^* = 10^3$, while in graph (b) $D_S^* = 10^{-2}$, $D_I^* = 10^{-3}$ and $D_{\mathrm{B}_p}^* = D_{\mathrm{B}_r}^* = 10^{-1}$.

Figures 2.12 illustrates the number of infectious individuals based on the PDE model (2.7.4) with uniform initial distribution, as a function of space and time when the associated $\mathcal{R}_0^{PDE}$ is lower or higher than the unity. Other initial conditions with various distribution types have been tested, and they all lead to similar patterns in terms of the extinction (when $\mathcal{R}_0^{PDE} < 1$) and endemic state (when $\mathcal{R}_0^{PDE} > 1$) of cholera infection. They verify that $\mathcal{R}_0^{PDE}$ is a disease threshold.

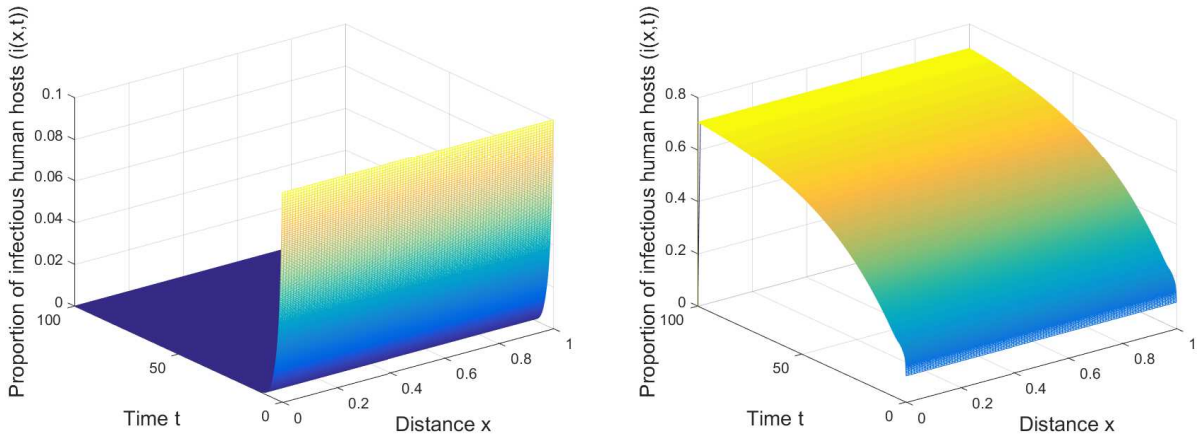

(a) $\mathcal{R}_0^{PDE} < 1$ (b) $\mathcal{R}_0^{PDE} > 1$

Figure 2.12: Number of infected human hosts associated with the PDE model (2.7.4) vs. space and time, when $\mathcal{R}_0^{PDE} = 0.767926 < 1$ (a) and $\mathcal{R}_0^{PDE} = 23.9854 > 1$ (b). The parameter value are those listen in Table 2.1 and Table 2.5 $\lambda_r^* = \lambda_p^* = 0$ and $L = 100$. Moreover $\beta_p^* = \beta_r^* = \theta_p^* = \theta_r^* = 0.01$ and $\mu^* = 9 \times 10^{-4}$ in panel (a) and $\beta_p^* = \beta_r^* = \theta_p^* = \theta_r^* = 1$ and $\mu^* = 9 \times 10^{-3}$ in panel (b).

2.11 Conclusions and Future Scope

Cholera, a water-borne disease characterized by severe diarrhea, remains a major public health burden in many parts of the world. In particular, the disease, caused by *Vibrio cholerae*, is endemic in parts of Asia, Africa, and Latin America. Owing to the enormous public health burden associated with cholera disease, there is now a concerted global effort to effectively control and/or eliminate the disease in endemic areas. In particular, the Global Task Force on Cholera Control (GTFCC) has launched a laudable collaborative initiative in 2017 with the dual aim of reducing cholera mortality by 90% in the existing 47 countries affected by cholera and, subsequently, ending cholera as a threat to public health by 2030 [174]. The essential elements of the laudable GTFCC initiative include intensifying anti-cholera control efforts (in particular improved WASH strategy, safe drinking water, quick access to treatment, intravenous fluids and antibiotic for severe cholera cases), enhancing preparedness of health case systems and building strong capacity to effectively and rapidly contain cholera outbreaks [174]. The aforementioned global effort to eliminate cholera necessitate the design and use of novel mathematical modeling framework for gaining insight into cholera transmission dynamics and control, aimed at finding effective strategies for achieving cholera elimination (*vis a vis* the 2030 elimination goal).

In this chapter, a novel ecology-epidemiology-hydrology model for the environment-host-environment transmission dynamics and control of *V. cholerae* bacteria in a human host population having an interconnected pond-river water network is proposed. The model, which takes the form of a deterministic system of nonlinear differential equations, accounted for the back-and-forth flow of water within the pond-river network. Further, the model stratified the total bacterial population in the community based on where the bacteria reside. That is, the total bacterial population is split into sub-population for bacteria in the pond and in the river. Other notable features of the novel model include the use of a nonlinear logistic growth

rate for bacteria in the pond (and no such growth is considered for *V. cholerae* dynamics in the river) and accounting for the temporal evolution of the volume of water in the pond (to account for the impact of environmental factors, such as drainage, precipitation, evaporation etc., on *V. cholerae* concentration in the pond). Humans acquire *V. cholerae* infection by coming in contact with contaminated water in either the pond or river, and infected humans shed *V. cholerae* to the two water sources (thereby completing the environment-host-environment cholera transmission cycle).

The developed model was rigorously analysed to gain insight into its dynamical features. In particular, results for the non-negativity, invariance and boundedness of the model were derived (thereby establishing the well-posedness of the developed model). The asymptotic stability of the disease-free equilibrium of the model was shown to be governed by whether or not a certain epidemiological threshold, known as the basic reproduction number (denoted by $\mathcal{R}_0$), is less than unity. Explicit expressions for $\mathcal{R}_0$ of the developed model were derived under four different anti-cholera control scenarios. The four control scenarios were formulated based on using four different interpretations of the role of the environment in the transmission cycle.

For the special case of the model where the bacterial growth is less than the bacterial death, it was shown that all the four expressions of $\mathcal{R}_0$ are well-posed. Further, the four constituent reproduction numbers exhibit the same threshold property with respect to the value unity (i.e., if one is less(equal)(greater) than unity, then the remaining three are all less(equal)(greater) than unity). In this context, each control scenario is associated with its own (different) threshold quantity that governs its effectiveness *vis a vis* disease elimination or persistence (i.e., each constituent reproduction number is associated with the amount of effort, in terms of the associated *herd immunity* threshold, needed for the elimination of the disease). In order to overcome the problem of having to deal with different estimates of the effort needed to eliminate the disease corresponding to each of the aforementioned four scenarios considered, the associated *type reproduction number* [14, 85, 133, 141, 142] of the model was computed for each of the three populations type considered in the study (i.e., humans, pond and river). For the case where control efforts exclusively target the human host population, it was shown that the associated type reproduction number (denoted by $\mathcal{T}_1$) was precisely the same for each of the four control scenarios. The uniqueness of the target reproduction when the human hosts are targeted (which plays a critical role in disease control) was, however, not maintained when the other two population types (bacteria in pond and river) are targeted. It should be recalled from the computations in Section 2.3 that the entries of the first row of the matrix F, of new infection terms, remain the same regardless of which of the four transmission scenarios is considered. Thus, mathematically-speaking (in line with Theorem 2.4.1), targeting population type corresponding to the first row of the matrix F (i.e., the human host) guarantees the uniqueness of the associated type reproduction number ($\mathcal{T}_1$). Biologically-speaking, the type reproduction number is unique if it corresponds to a population type that always assumes the same epidemiological role in every scenario. In fact, targeting the bacterial population (in the pond and/or in the river), the corresponding type reproduction number is not unique. This is owing to the fact that the two population types for the bacterial populations (i.e., the pond and the river) assume different epidemiological roles depending on the transmission scenario considered.

Using Lypapunov function theory and LaSalle's Invariance Principle, it was shown that, for each of the four control scenarios considered, the disease-free equilibrium of the model is globally-asymptotically stable, for a special case where the volume of water in the pond is maximized, whenever the associated repro-

duction number of the model ($\mathcal{R}_0$; or, equivalently, $\mathcal{T}_1$) is less than unity. The epidemiological implication of this result is that cholera elimination can be achieved if the anti-cholera control strategies adopted can bring (and maintain) $\mathcal{R}_0$ (or $\mathcal{T}_1$) to a value less than unity. Mathematically-speaking, this result means that bringing (and maintaining) $\mathcal{R}_0$ (or $\mathcal{T}_1$) to a value less than unity is necessary and sufficient for the elimination of the disease. This result enabled the determination of the herd immunity threshold (i.e., the minimum proportion of the population that should be targeted for the control) needed for disease elimination.

The developed model was used to assess various effectiveness levels of singular and combined anti-cholera control strategies. In particular, three strategies, namely WASH-only, treatment-only and combined WASH-treatment strategies were considered. Further, for each of these strategies, three effectiveness levels (low, moderate and high) were considered in the numerical simulations of the developed model. Extensive numerical simulations of the model, using reasonably-realistic set of parameters obtained from the literature, showed that, with its current estimated efficacy (of 60%) and coverage (of 50%) [79], the WASH-only strategy (i.e., a strategy that focus on improved water, sanitation and hygiene) is unable to lead to the elimination of cholera in the community, regardless of the effectiveness level (since none of its three effectiveness levels can bring $\mathcal{R}_0$ to a value less than unity). However, our simulations show that such elimination can be achieved, using either the moderate or high effectiveness level of this singular strategy, if the coverage can be increased to 80% and efficacy of implementation greatly increased to 90%. This may not be realistic targets in resource-challenged communities.

For the treatment-only strategy (i.e., a strategy based on using oral rehydration therapy and the administration of antibiotics), it was also shown that, with the current estimate of efficacy and coverage at 100% and 23%, respectively [79, 136, 143], none of the effectiveness levels of this singular strategy can to cholera elimination. Such elimination will, however, be achieved, using even the low effectiveness level, if the coverage can be increased to 80%. In fact, while the implementation of the moderate effectiveness level of this strategy can lead to such elimination with reduced coverage of 70%, the high effectiveness level of this treatment-only strategy can lead to disease elimination even with 50% coverage. Thus, our simulations suggest that treatment-based interventions may be more effective than WASH-based interventions. It is probably plausible to surmise that treatment-based interventions may be more realistic (i.e., achieve the required efficacy and coverage) than WASH-based interventions, particularly in resource-challenged rural areas.

Simulations of the model for the combined (hybrid) WASH-treatment strategy showed that, with the estimated efficacy of 80% and coverage of 36.5% [136, 143], while the low and moderate effectiveness levels of this hybrid strategy failed to eliminate the disease, the high effectiveness level of this strategy can eliminate the disease. If the coverage is increased to 50%, even the low effectiveness level of this intervention can lead to cholera elimination (in fact, the moderate effectiveness level can achieve such elimination even with a 40% coverage). Hence, it can be concluded, based on our extensive numerical simulations, that the anti-cholera control strategies considered in this study can be ranked in the following order of population-level effectiveness:

| Combined Strategy > Treatment-only Strategy > WASH-only Strategy |.

The model was then extended to the spatial case using the Fickian approximation, considering the diffusion both in the human population and in the bacterial population; furthermore, the fact that the vibrios are transported by water is taken into account. For the new PDE model, monotone traveling wave solutions have been studied, providing an estimate of the minimal speed at which this wave front can travel. These trajectories connect the EE and the DFE: this suggests that, under appropriate conditions, the epidemic could invade the territory, for example from inland areas (where the disease is present) to coastal regions (where it is not present) and vice versa. Moreover, in order to provide a good threshold for the eradication of the disease even in the heterogeneous spatial case, an estimate of the basic reproductive number in the spatial case was provided, following the idea presented in [164]. The conditions for which the basic reproductive numbers relating to the spatial and non-spatial case coincide have been found. Numerical simulations were conducted to confirm the results obtained.
We intend to integrate this model with elements regarding vaccination. In fact, in addition to the anti-cholera strategies shown in the previous sections, the published literature highlights how administering the vaccine is the most effective method for the eradication of this infection. The new proposal will consist of the model analyzed in this chapter, but including the component of the vaccine in the host population, thus obtaining new results for a better understanding of this epidemic.

Chapter 3

A MATHEMATICAL MODEL OF VERTICALLY TRANSMITTED VECTOR DISEASES

Part of this chapter, concerning the exclusively non-spatial model,was presented at the International Convention MM.SE.OR 2017, held in Giardini-Naxos, Messina, from 18 to 21/09 2017 and has materialized in the following publication:

A. Lupica and A. Palumbo. A mathematical model of vertically transmitted vector diseases. *Atti della Accademia Peloritana dei Pericolanti-Classe di Scienze Fisiche, Matematiche e Naturali*, 96(S3):11, 2018.

3.1 Introduction

Vector-borne diseases are infectious diseases caused by pathogens which are transmitted by insects, bacteria and protozoa (called vectors), infected by biological agents (anthropoids). Malaria, dengue, yellow fever, St Louis Encephalitis and West Nile Fever (WNF) are examples of such vector-borne diseases whose vectors are mosquitoes. Some of the main facts listed by WHO are [178]:

- vector-borne diseases account for more than 17% of all infectious diseases, causing more than 700000 deaths annually,
- More than 3.9 billion people in over 128 countries are at risk of contracting dengue, with 96 million cases estimated per year,
- malaria causes more than 400000 deaths every year globally, most of them children under 5 years of age,
- other diseases such as Chagas disease, leishmaniasis and schistosomiasis affect hundreds of millions of people worldwide.

Mosquitoes are the best known disease vector. Others include ticks, flies, sandflies, fleas, triatomine bugs and some freshwater aquatic snails. As reported in [176], their ability to carry and spread disease to humans causes millions of deaths every year. In 2015 malaria alone caused 438000 deaths. The worldwide incidence of dengue has risen 30-fold in the past 30 years, and more countries are reporting their first outbreaks of the disease. Zika, dengue, chikungunya, and yellow fever are all transmitted to humans by the Aedes aegypti mosquito. More than half of the world's population live in areas where this mosquito species is present. The figure 3.1 shows the probability of occurrence of dengue in 2015, reported by Messina et al [114]. These

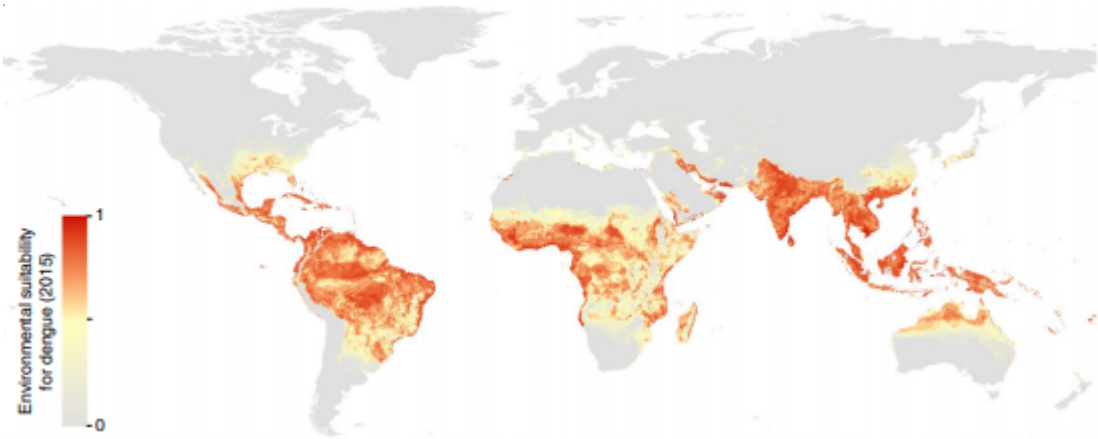

(a)

Figure 3.1: Maps displaying global probability data of occurrence of dengue in 2015 [114].

infectious diseases can be transmitted to two types of host populations: reservoir (which in this discussion will be the birds) and accidental (humans and horses in this discussion).

In these diseases, the primary cycle (endemic) of the virus is characterized by mosquito-bird-mosquito transmission: adult mosquitoes become infected by biting viremic birds (reservoir) [6]. Once the virus is ingested, it spreads within the mosquito organism and is subsequently transmitted to the host vertebrate.

The secondary epidemic cycle manifests itself when accidental hosts, such as humans or horses, enter the transmission cycle and are affected by the infection [6]. The virus is not transmitted from person to person or from horse to horse via mosquito bites due to the low level of virus concentration in the blood.

In addition to the horizontal transmission cycle (vector-host-vector), some species of mosquitoes transmit the pathogen to their offspring (vertical transmission). Indeed, even in the absence of infected hosts, the disease is transmitted by the adult mosquitoes to eggs that survive the dry season and evolve as adult and infectious mosquitoes (see for example [4, 22, 45]). Vertical transmission is observed, for example, in dengue virus transmitting mosquitoes such as Aedes aegypti, Aedes albopitus, the Culex species and other mosquito-borne flavivirus.

In recent years, various epidemic models have been proposed to describe and control the spread of infectious diseases such as malaria, dengue and WNF ([9]-[22] and related references). Models differ in the description of the interaction between vectors and host populations. Furthermore some authors incorporate the vertical transmission ([4, 22, 45]), others analyse the interaction of different species of birds with vectors ([106]), while others examine the effect of seasonality on disease transmission ([56]). These models describe

the interaction between birds and mosquitoes and only a few studies have explored the transmission of WNF between birds, mosquitoes and humans, see for example [26, 44].

In many mathematical models, the aquatic stage of the vector population consisting of eggs, larvae and pupae is not included in the transmission of the virus (see for example [44, 106, 107]).

First in work [171], the classical SIR model for malaria transmission is extended to a model describing WNF cross-infection between birds and mosquitoes, including the larval stage of vector population.

In order to incorporate the vertical transmission of the virus, in the model that is presented here, the aquatic stage with its epidemiological classes is inserted. The exposed class for the adult stage, accidental hosts, the exposed class in host populations, together with vertical transmission in vector populations are also included. In this way, horizontal and vertical transmission of vector-borne diseases are investigated. The model extends the Chen et al. proposal in [44].

Of course, it is easy to understand that, since mosquitoes are responsible for transmitting most of these diseases, their movement plays a decisive role in spreading the epidemic and in creating reservoirs of viruses [152]. Note that, only adult stage of mosquitoes can spread the vitus, while aquatic stage is immobile in the marshes or stagnant environments. Moreover, experts recognize urbanization as one of the most important drivers of global change, and predict that rapid increases in urban populations throughout the world will have major implications for human health in general and vector-borne diseases specifically [30]. There are reasons to believe that the spatial movement of humans may be important for the epidemiology of vector-borne diseases. This is one of the factors contributing to the re-emergence of malaria is human migration, as reported in [54] (and references therein). Empirical studies supporting the idea that travel outside urban areas is an important factor in maintaining malaria in urban areas where transmission is low [63, 127, 135]. For example Adams and Kapan [3] study a mathematical model to investigate the impact of human movement and the viscosity of mosquitoes on the dynamics and persistence of the disease transmitted by vectors at the level of city. Maidana et al [105] study a mathematical model considering only the movement of adult mosquitoes, assuming hosts not subject to movement.

Thus, in this chapter, spatial models are used to examine how the movements of birds and mosquitoes in heterogeneous environments affect the transmission of vector-borne diseases, using the simplest appsoximation of fickian propagation.

This chapter is organized as follows. In Section 3.2 a new mathematical model for vector-borne epidemics is derived, taking into account the interaction between birds and mosquitoes, mosquitoes and humans, as well as the transmission from adult mosquitoes and eggs. In Section 3.3 a linear stability analysis around the steady states is investigated both analytically and numerically together with the possible existence of a backward bifurcation. The extension of the model to the spatial case is placed in the section 3.4. Section 3.5 contains some results regarding the Basic Reproductive Number related to the spatial case. Finally, some concluding remarks are made in Section 3.6.

3.2 Mathematical Model

The populations involved in transmission are the vector population (mosquitoes) divided into aquatic (eggs, larvae, pupae) and adult stages. The reservoir host population are birds while humans constitute the dilution

host population. It is also assumed that only adult mosquitoes are able to spread the disease.

Due to the short duration of the aquatic phase [60], there is no incubation period and no healing from the disease, so exposed and removed classes for the aquatic stage are not considered. For the same reason, the removed class for the adult stage is also not examined. While, for host populations, all the epidemiological classes of the SEIR model (susceptibles, exposed, infectives and removed) are taken into account.

Let $N_A(t) = S_A(t) + I_A(t)$ and $N_M(t) = S_M(t) + E_M(t) + I_M(t)$ be the total number of mosquitoes in the aquatic stage and adult stage, $N_B(t) = S_B(t) + E_B(t) + I_B(t) + R_B(t)$ and $N_H(t) = S_H(t) + E_H(t) + I_H(t) + R_H(t)$ the total number of birds and humans, respectively.

The host populations (birds and humans) have constant recruitment rates, γ_B and γ_H, and they decrease by natural and disease-induced death rates, d_B, d_H, δ_B and δ_H, respectively. The vector population increases through logistic growth, with r the intrinsic oviposition rate and γ the intrinsic maturation rate from aquatic stage to adult stage. The carrying capacity in the aquatic stage, k_A, is defined as the available amount of breeding sites [105], while the carrying capacity in the adult stage, k_M, takes into account the fact that the mosquitoes cannot survive at high altitudes or temperatures [105]. Therefore, the per-capita oviposition rate is given by $r\left(1 - \frac{N_A}{k_A}\right)$ and the per-capita growth rate in the adult stage is $\gamma\left(1 - \frac{N_M}{k_M}\right)$.

The vector populations (aquatic and adult stages) decrease by natural death rates, d_A and d_M, by the predation rate, m_A, and by chemical control rates, μ_A and μ_M, respectively. The infectious mosquitoes can transmit the virus to host populations and, via vertical transmission, to their eggs, but they can only be infected by viremic birds.

It is assumed that the mosquito biting rate to host populations is constant and the validity of the "frequency dependent law" for the infection force is accepted [92]. The cross-infection between birds or humans and mosquitoes is modeled as $a_B\beta_{MB}\frac{I_M}{N_B}S_B$ or $a_H\beta_{MH}\frac{I_M}{N_H}S_H$, where a_B and a_H describe per capita biting rate of mosquitoes on birds and humans, respectively. The probabilities of transmission from mosquitoes to birds and humans are denoted by β_{MB} and β_{MH}, respectively. Similarly, the infection of mosquitoes through biting infectious birds is described by $a_B\beta_{BM}\frac{I_B}{N_B}S_M$, where β_{BM} is the probability of transmission from birds to mosquitoes.

To incorporate the vertical transmission, it is assumed that a fraction of newborns q, with $0 < q < 1$, is already infectious at birth [9]. For this reason, the rate of newborns in the S_A class is $r\left(1 - \frac{N_A}{k_A}\right)(S_M + E_M + (1-q)I_M)$, while the rate of newborns in I_A class is $r\left(1 - \frac{N_A}{k_A}\right)qI_M$. Instead, the rate of newborns in the S_M class is $\gamma\left(1 - \frac{N_M}{k_M}\right)S_A$ and similarly the rate of newborns in I_M class is given by $\gamma\left(1 - \frac{N_M}{k_M}\right)I_A$. Adult mosquitoes, birds and humans shift from the exposed class to the infectious class with rates τ_M, τ_B and τ_H, respectively. Furthermore, infectious birds and infectious humans migrate into the corresponding removed class with rates ω_B and ω_H, respectively.

Under these assumptions, the model is described by the following system of thirteen ordinary differential equations

$$
\begin{cases}
\dot{S}_A = r\left(1-\frac{N_A}{k_A}\right)\left[S_M+E_M+(1-q)I_M\right]-\alpha_A S_A,\\
\dot{I}_A = r\left(1-\frac{N_A}{k_A}\right)qI_M-\alpha_A I_A,\\
\dot{S}_M = \gamma\left(1-\frac{N_M}{k_M}\right)S_A-a_B\beta_{BM}\frac{I_B}{N_B}S_M-\alpha_M S_M,\\
\dot{E}_M = a_B\beta_{BM}\frac{I_B}{N_B}S_M-\nu_M E_M,\\
\dot{I}_M = \gamma\left(1-\frac{N_M}{k_M}\right)I_A+\tau_M E_M-\alpha_M I_M,\\
\dot{S}_B = \gamma_B-a_B\beta_{MB}\frac{I_M}{N_B}S_B-d_B S_B,\\
\dot{E}_B = a_B\beta_{MB}\frac{I_M}{N_B}S_B-\alpha_B E_B,\\
\dot{I}_B = \tau_B E_B-\nu_B I_B,\\
\dot{R}_B = \omega_B I_B-d_B R_B,\\
\dot{S}_H = \gamma_H-a_H\beta_{MH}\frac{I_M}{N_H}S_H-d_H S_H,\\
\dot{E}_H = a_H\beta_{MH}\frac{I_M}{N_H}S_H-\alpha_H E_H,\\
\dot{I}_H = \tau_H E_H-\nu_H I_H,\\
\dot{R}_H = \omega_H I_H-d_H R_H,
\end{cases}
\tag{3.2.1}
$$

where, for the sake of simplicity, in (3.2.1) it is:

$$
\begin{aligned}
&\alpha_A=\gamma+d_A+m_A+\mu_A, \quad \alpha_M=d_M+\mu_M, \quad \nu_M=d_M+\mu_M+\tau_M,\\
&\nu_B=d_B+\delta_B+\omega_B, \qquad \alpha_B=d_B+\tau_B, \qquad \nu_H=d_H+\delta_H+\omega_H, \qquad \alpha_H=d_H+\tau_H.
\end{aligned}
\tag{3.2.2}
$$

The model (3.2.1) is an extension of many of the models for vector-borne transmission dynamics, indeed:

- we incorporate the aquatic phase of mosquitoes together with its epidemiological classes (susceptible and infectious), vartical transmission in vector population, the class of exposed for both adult mosquitoes and both host populations, disease-induced mortality in host populations. These features are not considered in [105];

- we include the aquatic phase of the mosquito population (together with the associated epidemiological classes), vertical transmission in vector population and a non-constant growth (source of logistic type) both for the aquatic state and for the adult state of mosquitoes compared to the work presented in [44]

- we include vertical transmission in vector population with a different functional form with respect to [45], in addition to the dilution host population.

Adding the appropriate equations in (3.2.1), it is possible to see that the growth of the whole populations of aquatic mosquitoes, adult mosquitoes, birds and humans satisfy the following equations

$$\begin{cases} \dot{N}_A = r\left(1-\frac{N_A}{k_A}\right)N_M - \alpha_A N_A, \\ \dot{N}_M = \gamma\left(1-\frac{N_M}{k_M}\right)N_A - \alpha_M N_M, \\ \dot{N}_B = \gamma_B - d_B N_B - \delta_B I_B, \\ \dot{N}_H = \gamma_H - d_H N_H - \delta_H I_H. \end{cases} \tag{3.2.3}$$

Thus, all total populations may vary in time. In particular, in the absence of disease, the population size N_B and N_H converge to the equilibrium value $\frac{\gamma_B}{d_B}$ and $\frac{\gamma_H}{d_H}$, respectively. Furthermore, from $(3.2.3)_{3,4}$, it follows that $\limsup_{t\to\infty} N_B(t) \leq \frac{\gamma_B}{d_B}$ and $\limsup_{t\to\infty} N_H(t) \leq \frac{\gamma_H}{d_H}$.

Since the first nine equations are independent of the other four, the following two vectors can be defined:

$$\mathbf{X}_1(t) = (S_A(t), I_A(t), S_M(t), E_M(t), I_M(t), S_B(t), E_B(t), I_B(t), R_B(t))^T, \tag{3.2.4}$$

$$\mathbf{X}_2(t) = (S_H(t), E_H(t), I_H(t), R_H(t))^T, \tag{3.2.5}$$

so system (3.2.1) can be recast in the following compact form:

$$\begin{cases} \dot{\mathbf{X}}_1 = \mathbf{F}_1(\mathbf{X}_1), \\ \dot{\mathbf{X}}_2 = \mathbf{F}_2(\mathbf{X}_1, \mathbf{X}_2), \end{cases} \tag{3.2.6}$$

where $\mathbf{F}_1$ and $\mathbf{F}_2$ can be easily deduced from system (3.2.1).

Now, denoting with $\mathbb{R}^n_+$ the positive orthant in $\mathbb{R}^n$ and with $\partial\mathbb{R}^n_+$ its boundary, the model $(3.2.6)_1$ is epidemiologically well-posed in the domain

$$\begin{aligned} \mathcal{D}_1 \;=\; & \{(S_A, I_A, S_M, E_M, I_M, S_B, E_B, I_B, R_B) \in \mathbb{R}^9_+ : S_A + I_A < k_A,\ S_M + E_M + I_M < k_M, \\ & \frac{\gamma_B}{d_B+\delta_B} \leq S_B + E_B + I_B + R_B \leq \frac{\gamma_B}{d_B}\}, \end{aligned} \tag{3.2.7}$$

while system $(3.2.6)_2$ is epidemiologically well-posed in the domain

$$\mathcal{D}_2 = \left\{(S_H, E_H, I_H, R_H) \in \mathbb{R}^4_+ : \frac{\gamma_H}{d_H+\delta_H} \leq S_H + E_H + I_H + R_H \leq \frac{\gamma_H}{d_H}\right\}; \tag{3.2.8}$$

so the whole system (3.2.1) is biologically well-defined in $\mathcal{D} = \mathcal{D}_1 \times \mathcal{D}_2$.

3.3 Mathematical Analysis

In this section, we determine the equilibria permitted by the model and study local stability.

3.3.1 Existence, unicity and boundedness of solutions

Theorem 3.3.1 *For any initial condition which lies in $\mathcal{D}$, system (3.2.1) has a unique solution that exists and remains in D, $\forall\ t \geq 0$. Furthermore, the compact $\mathcal{D}$ is a positively invariant set, which attracts all positive orbits in $\mathbb{R}^{13}_+$.*

Proof. For all initial conditions belonging to $\mathcal{D}$, the function $\mathbf{F} = (\mathbf{F}_1, \mathbf{F}_2)^T$ is locally lipschitzian in $\mathbf{X}(t) = (\mathbf{X}_1(t), \mathbf{X}_2(t))^T$, then the Cauchy-Lipschitz theorem ensures that system (3.2.1) admits a unique local solution.

Furthermore, from $(3.2.3)_{3,4}$, it is

$$\gamma_B - (d_B + \delta_B)N_B \leq \dot{N}_B \leq \gamma_B - d_B N_B, \quad \gamma_H - (d_H + \delta_H)N_H \leq \dot{N}_H \leq \gamma_H - d_H N_H,$$

by applying the standard comparison theorem [87], it follows

$$\frac{\gamma_B}{d_B + \delta_B} \leq N_B(t) \leq \frac{\gamma_B}{d_B}, \quad \frac{\gamma_H}{d_H + \delta_H} \leq N_H(t) \leq \frac{\gamma_H}{d_H},$$

$\forall\ t > 0$ and if initially $N_B(0) \leq \frac{\gamma_B}{d_B}$ and $N_H(0) \leq \frac{\gamma_H}{d_H}$. By standard arguments (see [1, 2, 117]), it follows that the total population in acquatic phase is bounded by k_A (from equation $(3.2.3)_1$) and the total population in adult phase is bounded by k_M (from equation $(3.4.6)_2$).
Then, $\mathcal{D}$ is positively invariant and all solutions of (3.2.1) are non-negative and bounded. □

3.3.2 Disease Free Equilibrium. Basic Reproduction Number

Theorem 3.3.2 *Between all possible equilibria, model $(3.2.6)_1$ admits the two equilibrium points with no disease in the population on $\mathcal{D}_1 \cap \partial\mathbb{R}^9_+$*

$$\boldsymbol{E}_0 = \left(0, 0, 0, 0, 0, \frac{\gamma_B}{d_B}, 0, 0, 0\right)^T, \ \boldsymbol{E}_1 = \left(A_0, 0, M_0, 0, 0, \frac{\gamma_B}{d_B}, 0, 0, 0\right)^T, \tag{3.3.1}$$

which are the trivial and non-trivial one, where

$$A_0 = \frac{M_0 k_M \alpha_M}{\gamma(k_M - M_0)}, \quad M_0 = \frac{k_A k_M (r\gamma - \alpha_M \alpha_A)}{r(\gamma k_A + k_M \alpha_M)}. \tag{3.3.2}$$

The equilibrium $\mathbf{E}_1$ exists if the condition $r\gamma > \alpha_A \alpha_M$ holds.

Theorem 3.3.3 *The whole model (3.2.1) admits the following trivial and non trivial disease free equilibrium points*

$$\boldsymbol{P}_0 = \left(0, 0, 0, 0, 0, \frac{\gamma_B}{d_B}, 0, 0, 0, \frac{\gamma_H}{d_H}, 0, 0, 0\right)^T, \ \boldsymbol{P}_1 = \left(A_0, 0, M_0, 0, 0, \frac{\gamma_B}{d_B}, 0, 0, 0, \frac{\gamma_H}{d_H}, 0, 0, 0\right)^T, \tag{3.3.3}$$

on $\mathcal{D} \cap \partial\mathbb{R}^{13}_+$.

It follows directly by substituting the equilibria (3.3.1) of $(3.2.6)_1$ into $(3.2.6)_2$.

In the following, the more biologically realistic equilibrium $\mathbf{P}_1$ is considered. Its character is related to the basic reproduction number $\mathcal{R}_0$, which is defined as the average number of new cases of an infection caused by an infected individual, in a population consisting of susceptibles only and where the disease is vertically transmitted.

Following [61, 62, 161], and linearizing system (3.2.1) around $\mathbf{P}_1$, it is possible to compute the transmission matrix F, describing the production of new infections, and the transition matrix V, representing changes in state (including removal by death or the acquisition of immunity). The spectral radius ρ of the matrix $K_L = FV^{-1}$ is the basic reproduction number

$$\mathcal{R}_0 = \frac{1}{2}\left(q + \sqrt{q^2 + \frac{4M_0 a_B^2 d_B \beta_{BM}\beta_{MB}\tau_B\tau_M}{\gamma_B \alpha_M \alpha_B \nu_M \nu_B}}\right) = \frac{1}{2}\left(\mathcal{R}_{vt} + \sqrt{\mathcal{R}_{vt}^2 + 4\mathcal{R}_{ht}}\right), \tag{3.3.4}$$

where

$$\mathcal{R}_{vt} = q, \quad \mathcal{R}_{ht} = \mathcal{R}_H\mathcal{R}_V = \frac{a_B^2 d_B \beta_{BM}\tau_B}{\alpha_B \nu_B}\frac{M_0\beta_{MB}\tau_M}{\alpha_M\nu_M}. \tag{3.3.5}$$

$\mathcal{R}_0$ consists of two contributions: the first is due to vertical transmission, whereas the second is caused by horizontal transmission. In particular, R_{ht} is the product of the number of new infections in the host population and the number of new infections in the vector population. $\mathcal{R}_0$ contains only terms related to the populations that spread and transmit the disease and not terms related to the human population that, in this model, constitutes the accidental host population.

The following local stability result about $\mathbf{P}_1$ holds [161]:

Theorem 3.3.4 *The disease-free equilibrium point, $\mathbf{P}_1$ of the model (3.2.1), is locally asymptotically stable if $\mathcal{R}_0 < 1$ and unstable if $\mathcal{R}_0 > 1$, where $\mathcal{R}_0$ is defined by (3.3.4).*

Theorem 3.3.4 shows that in the case $\mathcal{R}_0 < 1$ the disease could be eliminated for a small initial value.

3.3.3 Endemic Equilibrium States. Bifurcation Analysis

Existence of endemic equilibria

In this part, the dynamic of system (3.2.1) is studied, as the threshold $\mathcal{R}_0$ changes. Let us start calculating the endemic equilibrium points, which are solutions of the algebraic system

$$\begin{cases} \mathbf{F}_1(\mathbf{X}_1) = 0, \\ \mathbf{F}_2(\mathbf{X}_1, \mathbf{X}_2) = 0. \end{cases} \tag{3.3.6}$$

Firstly, from $(3.3.6)_1$ we deduce

$$I_A = \frac{q a_B d_B A_0 \beta_{BM}\tau_M I_B}{(1-q)\alpha_M\nu_M(\gamma_B - \delta_B I_B) + I_B a_B d_B \beta_{BM}((1-q)\alpha_M + \tau_M)},$$

$$E_M = \frac{(1-q) a_B d_B M_0 \alpha_M \beta_{BM} I_B}{(1-q)\alpha_M\nu_M(\gamma_B - \delta_B I_B) + I_B a_B d_B \beta_{BM}((1-q)\alpha_M + \tau_M)},$$

$$I_M = \frac{a_B d_B M_0 \beta_{BM} \tau_M I_B}{(1-q)\alpha_M \nu_M (\gamma_B - \delta_B I_B) + I_B a_B d_B \beta_{BM}((1-q)\alpha_M + \tau_M)}, \tag{3.3.7}$$

$$S_A = A_0 - I_A,\ S_M = M_0 - E_M - I_M,\ S_B = \frac{\tau_B \gamma_B - \alpha_B \nu_B I_B}{\tau_B d_B},\ E_B = \frac{\nu_B}{\tau_B} I_B,\ R_B = \frac{\omega_B}{d_B} I_B,$$

while I_B is the positive solution of the following equation

$$f(I_B) = a_b I_B^2 + b_b I_B + c_b = 0, \tag{3.3.8}$$

where

$$\begin{aligned} a_b &= \alpha_B \delta_B \nu_B [a_B \beta_{BM} d_B((1-q)\alpha_M + \tau_M) - (1-q)\alpha_M \nu_M \delta_B], && (3.3.9)\\ b_b &= 2(1-q)\alpha_B \alpha_M \gamma_B \delta_B \nu_B \nu_M - a_B d_B \alpha_B \beta_{BM} \gamma_B \nu_B ((1-q)\alpha_M + \tau_M) \\ &- a_B^2 d_B \beta_{BM} \beta_{MB} \tau_M \alpha_B \nu_B M_0, && (3.3.10)\\ c_b &= -\gamma_B \alpha_M \alpha_B \nu_M \nu_B \gamma_B (1-q)(1-\mathcal{R}_0). \end{aligned}$$

Existence of endemic equilibrium requires that the roots of (3.3.8) are real and positive. Moreover, since S_B must be positive, we also have to impose the further condition $I_B < I_B^{**} = \frac{\tau_B \gamma_B}{\alpha_B \nu_B}$.

Let us denote with Δ_b the discriminant of (3.3.8). Solving $\Delta_b = 0$ in terms of $\mathcal{R}_0$ we obtain the critical value

$$\mathcal{R}_0^c = 1 + \frac{b_b^2}{4r(1-q)a_b \alpha_B \nu_B \gamma_B^2 \alpha_M \nu_M (\gamma k_A + k_M \alpha_M)}, \tag{3.3.11}$$

so the following relations are verified:

$$\Delta_b < 0 \ \Leftrightarrow\ \mathcal{R}_0 < \mathcal{R}_0^c, \quad \Delta_b = 0 \ \Leftrightarrow\ \mathcal{R}_0 = \mathcal{R}_0^c, \quad \Delta_b > 0 \ \Leftrightarrow\ \mathcal{R}_0 > \mathcal{R}_0^c. \tag{3.3.12}$$

The study of the solutions of (3.3.8) implies the following result.

Theorem 3.3.5 *1. Let $a_b = 0$. Equation (3.3.8) is a linear equation with a unique solution $I_B = -\frac{c_b}{b_b}$. Then the system (3.2.6)$_1$ has a unique endemic equilibrium when $\mathcal{R}_0 > 1$ and $b_b < 0$ and has no endemic equilibrium when $\mathcal{R}_0 \leq 1$.*

2. *Let $a_b \neq 0$.*
   a) System (3.2.6$_1$) has a unique endemic equilibrium whenever $\mathcal{R}_0 > 1$
   b) System (3.2.6$_1$) has a unique endemic equilibrium whenever $\mathcal{R}_0 = 1$, $a_b < 0$ and $b_B > 0$
   c) System (3.2.6$_1$) has two endemic equilibria $\boldsymbol{E}_i$ when $\mathcal{R}_0^c < \mathcal{R}_0 < 1$, $a_b < 0$ and $b_b > 0$
   d) System (3.2.6$_1$) has a unique endemic equilibrium of multiplicity 2 when $\mathcal{R}_0 = \mathcal{R}_0^c$, $a_b < 0$ and $b_b > 0$
   e) System (3.2.6$_1$) has no endemic equilibria whenever $\mathcal{R}_0 < \mathcal{R}_0^c$ or whenever $\mathcal{R}_0 \leq 1$ and $a_b > 0$

Proof.. Evaluating $f(I_B)$ at $I_B = I_B^{**}$ we have $f(I_B^{**}) < 0$.

1. Let $a_b = 0$. This case happens when the disease-induced death rate $\delta_B = 0$ or $a_B \beta_{BM} d_B((1-q)\alpha_M + \tau_M) - (1-q)\alpha_M \nu_M \delta_B = 0$. Equation (3.3.8) has one positive solution $I_B = -\frac{c_b}{b_b}$ if $b_b < 0$. If $\mathcal{R}_0 < 1$, then $f(0) < 0$. In this case there are no positive real solutions in the interval $[0, I_B^{**}]$. For $\mathcal{R}_0 = 1$, from (3.3.7) we find the non-trivial DFE $\mathbf{E}_1$.

2. Let $a_b \neq 0$.

   If $\mathcal{R}_0 > 1$ than $f(0) > 0$. In this case there is always a unique positive real solution in the interval $[0, I_B^{**}]$. This solution is $I_B = \frac{-b_b+\sqrt{\Delta_b}}{2a_b}$ if $a_b > 0$ and $I_B = \frac{-b_b-\sqrt{\Delta_b}}{2a_b}$ if $a_b < 0$. If $\mathcal{R}_0 = 1$ there is a positive solution $I_B = -\frac{b_b}{a_b}$ if and only if $a_b < 0$ and $b_b > 0$ (otherwise there are no positive solutions in the interval $[0, I_B^{**}]$). If $\mathcal{R}_0 < 1$ then $f(0) < 0$. When $a_b > 0$ equation (3.3.8) has no positive solutions in the interval $[0, I_B^{**}]$. When $a_b < 0$, $b_b > 0$ and $\Delta_b > 0$ there are two positive real solutions $I_B^1 = \frac{-b_b-\sqrt{\Delta_b}}{2a_b}$ and $I_B^2 = \frac{-b_b+\sqrt{\Delta_b}}{2a_b}$ of equation (3.3.8). These solutions coalesce if $\Delta_b = 0$.

□

To each endemic equilibrium state for the system $(3.2.6)_1$, solution of the equation $(3.3.6)_1$, there is a corresponding equilibrium state for system $(3.2.6)_2$. Known I_M^i from Theorem 3.3.5 and solving equation $(3.3.6)_2$ in terms of I_H, we obtain the following relations

$$S_H = \frac{\tau_H\gamma_H - \alpha_H\nu_H I_H}{\tau_H d_H},\ E_H = \frac{\nu_H}{\tau_H} I_H,\ R_H = \frac{\omega_H}{d_H} I_H, \tag{3.3.13}$$

in which the endemic value I_H is the positive solution of

$$g(I_H) = a_h I_H^2 + b_h I_H + c_h = 0, \tag{3.3.14}$$

where

$$\begin{aligned} a_h &= \alpha_H\delta_H\nu_H, \\ b_h &= -(\alpha_H\gamma_H\nu_H + I_M^i a_H\beta_{MH}\alpha_H\nu_H), \\ c_h &= a_H\beta_{MH}\tau_H\gamma_H I_M^i. \end{aligned} \tag{3.3.15}$$

Put $\Delta_h = b_h^2 - 4a_hc_h > 0$ which ensures that the solutions of the equation (3.3.14) are real. Since $S_H > 0$, then $I_H < I_H^{**} = \frac{\tau_H\gamma_H}{\alpha_H\nu_H}$. Because of $a_h > 0$ and $c_h > 0$, equation (3.3.14) has a unique positive solution $I_H = \frac{-b_h-\sqrt{\Delta_h}}{2a_h}$ in the interval $[0, I_H^{**}]$.

Now,denoting as $\mathbf{P}^* = (S_A^*, I_A^*, S_M^*, E_M^*, I_M^*, S_B^*, E_B^*, I_B^*, R_B^*, S_H^*, E_H^*, I_H^*, R_H^*)$ a generic endemic equilibrium point of system (3.2.1), Jacobian matrix evaluated at $\mathbf{P}^*$ is given by

$$J(\mathbf{P}_*) = \begin{pmatrix} A_{11} & 0 \\ A_{21} & A_{22} \end{pmatrix}, \tag{3.3.16}$$

where A_{11} and A_{22} are the Jacobian matrices of the two partial systems in (3.2.6) evaluated at $\mathbf{E}^* = (S_A^*, I_A^*, S_M^*, E_M^*, I_M^*, S_B^*, E_B^*, I_B^*, R_B^*)$ and $\mathbf{U}^* = (S_H^*, E_H^*, I_H^*, R_H^*)$ respectively, while A_{21} is a matrix that takes into account the interactions between the two partial systems.

Applying the Routh-Hurwith criterion to the matrix

$$A_{22} = \begin{pmatrix} -d_H - \frac{a_H\beta_{MH}I_M^*(E_H^*+I_H^*+R_H^*)}{(N_H^*)^2} & \frac{a_H\beta_{MH}I_M^*S_H^*}{(N_H^*)^2} & \frac{a_H\beta_{MH}I_M^*S_H^*}{(N_H^*)^2} & \frac{a_H\beta_{MH}I_M^*S_H^*}{(N_H^*)^2} \\ \frac{a_H\beta_{MH}I_M^*(E_H^*+I_H^*+R_H^*)}{(N_H^*)^2} & -\alpha_H - \frac{a_H\beta_{MH}I_M^*S_H^*}{(N_H^*)^2} & -\frac{a_H\beta_{MH}I_M^*S_H^*}{(N_H^*)^2} & -\frac{a_H\beta_{MH}I_M^*S_H^*}{(N_H^*)^2} \\ 0 & \tau_H & -\nu_H & 0 \\ 0 & 0 & \omega_H & -d_H \end{pmatrix}, \tag{3.3.17}$$

it is easy to prove that all eigenvalues of A_{22} have negative real parts. Following this, the stability of the equilibrium $\mathbf{P}^*$ depends only on the eigenvalues of the matrix A_{11}. This means that the system $(3.2.6)_1$, which describes the primary transmission of disease between birds and mosquitoes, adult mosquitoes and the aquatic stage, determines the stability of any arbitrary equilibrium point of the whole system (3.2.1). To conclude this Section, it is good to mention that the stability of the endemic equilibria is determined by the eigenvalues of the matrix A_{11}. However, since it is difficult to determine their signs analytically, in Section 3.3.4 the possible dynamical behaviors for the whole system (3.2.1) is examined by means of numerical simulations.

Backward Bifurcation Analysis

In this section we use analytical and numerical techniques to assess the directions of bifurcations. Theorem 3.3.5 shows the possibility of backward bifurcation in model (3.2.1) when $\mathcal{R}_0^c < \mathcal{R}_0 < 1$, $a_b < 0$ and $b_b > 0$. Backward bifurcation is a phenomenon where two endemic equilibria, one stable and the other unstable co-exist along with the disease-free equilibrium for $\mathcal{R}_0 < 1$. The existence of a backward bifurcation indicates that reduction of the epidemiology threshold, $\mathcal{R}_0$, below unity is simply not a sufficient condition for disease control. In this section it is established that once the epidemiology threshold $\mathcal{R}_0$ is reduced below a critical value R_0^c, under some conditions, the disease could be eliminated for any initial size.

To do so, the transmission probability from mosquitoes to birds β_{MB}^* is choosen as the bifurcation parameter, obtained by solving for β_{MB} from $\mathcal{R}_0 = 1$:

$$\beta_{MB}^* = \frac{(1-q)\gamma_B\alpha_B\alpha_M\nu_B\nu_M}{a_B^2 d_B M_0 \beta_{BM}\tau_B\tau_M}. \tag{3.3.18}$$

Let $\mathbf{J}^*$ be the Jacobian matrix of the system $(3.2.6)_1$ evaluated at the DFE $\mathbf{E}_1$ and at the bifurcation value β_{MB}^*. It has a simple eigenvalue with zero real part and the other eigenvalues with negative real parts, so it can be used the "center manifold theory" [61] to analyze the dynamics of the model (3.2.1) near the criticality $\beta_{MB} = \beta_{MB}^*$ and apply a theorem proved by Castillo-Chavez and Song in [41] that states the conditions for the existence of backward bifurcation.

Let $\mathbf{v} \equiv (v_i)$ and $\mathbf{w} \equiv (w_i)$ be the left and right eigenvectors corresponding to the zero eigenvalue of the Jacobian matrix $\mathbf{J}^*$, respectively,

$$\begin{aligned}
&v_1 = 0, && v_2 = \tfrac{I_M\gamma\alpha_M(rk_M+\alpha_Ak_A)}{r\alpha_A(\gamma k_A+\alpha_Mk_M)}, && v_3 = 0,\\
&v_4 = \tfrac{\tau_M I_M}{\nu_M}, && v_5 = I_M, && v_6 = 0,\\
&v_7 = \tfrac{a_Bd_B\beta_{BM}\tau_B\tau_M M_0}{\alpha_B\gamma_B\nu_B\nu_M}, && v_8 = \tfrac{a_Bd_B\beta_{BM}\tau_M M_0}{\gamma_B\nu_B\nu_M}, && v_9 = 0,\\
&w_1 = -I_A, && w_2 = I_A, && w_3 = -\tfrac{\gamma(rk_M+\alpha_Ak_A)([(1-q)\alpha_M+\tau_M]I_A}{qr\tau_M(\gamma k_A+\alpha_Mk_M)},\\
&w_4 = \tfrac{\alpha_M\gamma(rk_M+\alpha_Ak_A)I_A}{qr\tau_M(\gamma k_A+\alpha_Mk_M)}, && w_5 = \tfrac{\gamma(rk_M+\alpha_Ak_A)I_A}{qr(\gamma k_A+\alpha_Mk_M)}, && w_6 = -\tfrac{\alpha_B\alpha_M\gamma_B\nu_B\nu_M(1-q)I_A}{qa_Bd_B^2A_0\beta_{BM}\tau_B\tau_M},\\
&w_7 = \tfrac{\alpha_B\gamma_B\nu_B\nu_M(1-q)I_A}{qa_Bd_BA_0\beta_{BM}\tau_B\tau_M}, && w_8 = \tfrac{\alpha_B\gamma_B\nu_M(1-q)I_A}{qa_Bd_BA_0\beta_{BM}\tau_M}, && w_9 = \tfrac{\alpha_B\gamma_B\nu_M(1-q)\omega_BI_A}{qa_Bd_B^2A_0\beta_{BM}\tau_M}.
\end{aligned}$$

Let $f_k(\mathbf{X}_1, \phi)$ be the k-th component of vector $\mathbf{F}_1$, x_k the k-th component of vector state $\mathbf{X}_1$ and $\phi = \beta_{MB} - \beta^*_{MB}$. The model (3.2.1) exhibits a backward bifurcation at $\mathcal{R}_0 = 1$ ($\phi = 0$) if the following coefficients [41]

$$\begin{aligned} a_1 &= \sum_{k,i,j=1}^{9} v_k w_i w_j \frac{\partial^2 f_k}{\partial x_i \partial x_j}(\mathbf{E}_1, 0) = B_1 - B_2, \\ a_2 &= \sum_{k,i=1}^{9} v_k w_i \frac{\partial^2 f_k}{\partial x_i \partial \phi}(\mathbf{E}_1, 0) = v_7 w_5 a_B, \end{aligned} \tag{3.3.19}$$

are positive, where

$$\begin{aligned} B_1 &= -2v_2 w_1 w_5 \frac{qr}{k_A} - 2v_5 w_2 w_3 \frac{\gamma}{k_M} > 0, \\ B_2 &= 2v_2 w_2 w_5 \frac{qr}{k_A} - 2v_4 w_3 w_8 \frac{a_B \beta_{BM} d_B}{\gamma_B} + 2v_4 w_8 \frac{a_B \beta_{BM} d_B^2 M_0}{\gamma_B^2}(w_6 + w_7 + w_8 + w_9) \\ &+ 2v_5 w_2 \frac{\gamma}{k_M}(w_4 + w_5) + 2v_7 w_5 \frac{a_B \beta^*_{MB} d_B}{\gamma_B}(w_7 + w_8 + w_9) > 0. \end{aligned} \tag{3.3.20}$$

The coefficient a_2 is always positive, but for the other coefficient the further condition

$$B_1 > B_2, \tag{3.3.21}$$

must be imposed. Thus, the following result is established.

Theorem 3.3.6 *Model (3.2.1) exhibits a backward bifurcation at $\mathcal{R}_0 = 1$ ($\beta_{MB} = \beta^*_{MB}$) whenever the inequality (3.3.21) holds. If the reversed inequality holds, then the bifurcation at $\mathcal{R}_0 = 1$ is forward.*

Thus the backward bifurcation scenario involve the existence of a subcritical transcritical bifurcation at $\mathcal{R}_0 = \mathcal{R}_0^c < 1$. The qualitative bifurcation diagrams describing two types of bifurcation at $\mathcal{R}_0 = 1$ are depicted in Fig.3.2.

3.3.4 Numerical Simulations

In the subsequent discussion observations are made on the nature of the stability of each fixed point through numerical simulation. These simulations are made for both primary and secondary transmission cycle.

The case $\mathcal{R}_0 < 1$: system (3.2.1) has a disease-free equilibrium $\mathbf{P}_1$. Three numerical simulations corresponding to different initial data sets are shown, with $\mathcal{R}_0 = 0.854753$.

Fig. 3.3 illustrates that each solution is close to the DFE. The occurrence of the backward bifurcation can be also seen in Fig. 3.4, where $\mathcal{R}_0$ is less than the transcritical bifurcation threshold $\mathcal{R}_0 = 1$, but the solution of the system $(3.2.6)_1$ can approach either the endemic equilibrium point or the DFE point, depending on initial condition values.

The case $\mathcal{R}_0 > 1$: system (3.2.1) has a endemic point when $\mathcal{R}_0 > 1$ which can be shown by simulation. The endemic value is obtained using the parameter values listed in Fig.3.2-(b) with $a_B = 3.9$. So an endemic equilibrium point $\mathbf{P}^* = (S_A^*, I_A^*, S_M^*, E_M^*, I_M^*, S_B^*, E_B^*, I_B^*, R_B^*, S_H^*, E_H^*, I_H^*, R_H^*)$ is founded, with $\mathcal{R}_0 = 6.31514$. Alle the eigenvalues of the Jacobian matrix of model (3.2.1), evaluated in $\mathbf{P}^*$, have a negative real part, so the local linear stability of the endemic equilibrium point is verified. The following figures show the behavior of each population in the existing state of the disease.

We see that,after an initial oscillating trend, each solution riches its endemic value.

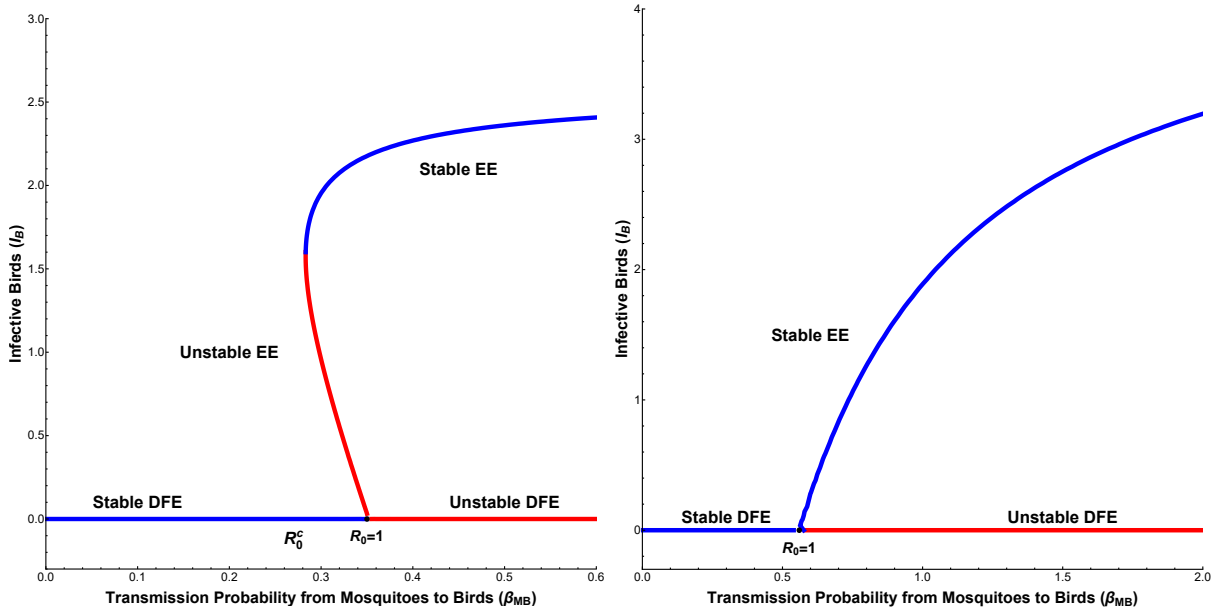

(a) (b)

Figure 3.2: Bifurcation diagram showing the equilibrium value of the Infective Birds as the Reproduction Number is varied. (a) Backward bifurcation. Suitable set of parameters value for the exhibition of backward bifurcation d_A=0.056, k_A=1000, $r = 0.5$, q=0.2, μ_A=0, m_A=0, d_M=0.0286, $k_M = 500$, γ=0.2, $\tau_M = 0.143$, μ_M=0, d_B=0.003, γ_B=3.1, β_{BM}=0.9, δ_B=0.9, τ_B=0.6, ω_B=0.3, a_B=0.5. Two endemic equilibrium points coexist for value of $\mathcal{R}_0 \in (0.908433, 1)$. (b) Forward bifurcation corresponding to the parameters value d_A=0.056, k_A=100, $r = 0.1$, q=0.1, μ_A=0, m_A=0, d_M=0.0286, k_M=25, γ=0.2, $\tau_M = 0.143$, μ_M=0, d_B=0.02, γ_B=2.1, β_{BM}=0.4, δ_B=0.1, τ_B=0.2, ω_B=0.3, a_B=0.5, $d_H = 9 \times 10^{-4}$, $\gamma_H = 5 \times 10^{-2}$, β_{MH}=0.5, δ_H=0.001, τ_H=0.25, ω_H=0.143, a_H=0.143.

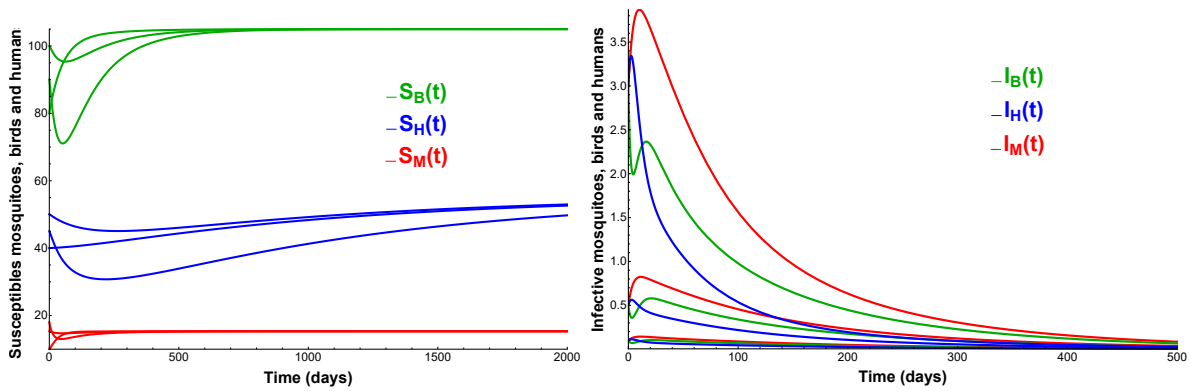

(a) (b)

Figure 3.3: Evolution over time of the susceptible (a) and infective (b) classes of mosquito (magenta line), bird (orange line) and human (blue line) populations, corresponding to different initial condition values and parameter values listed in Fig.3.2-(b) with $\beta_{MB} = 0.7$. (a)-(b) show that system (3.2.1) has only one disease-free equilibrium $\mathbf{P}_1 = (5, 65771, 0, 15, 3257, 0, 0, 105, 0, 0, 0, 55.5556, 0, 0, 0)$ and it is locally asymptotically stable

3.4 Spatial Dynamics

In this section, the vector-borne model (3.2.1) is extended to a PDE system, in order to investigate the spatial dynamics of disease.

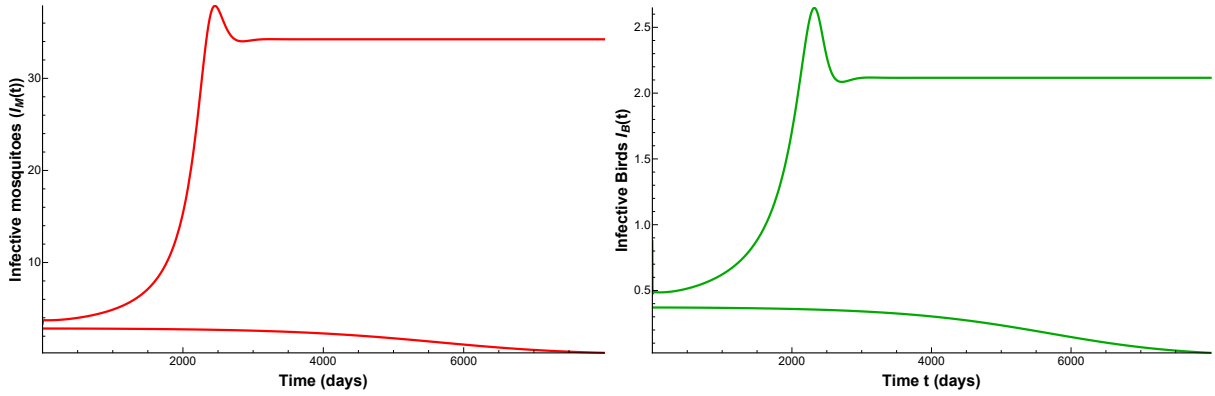

(a) (b)

Figure 3.4: Solutions regarding model $(3.2.6)_1$ of the number of infectious adult mosquitoes, I_M, and the number of infectious birds, I_B, for parameter values given in the bifurcation diagram (Fig.3.2-(a)), with $\beta_{MB} = 0.33$, so $\mathcal{R}_0 = 0.971781 < 1$, for two different sets of initial conditions. (a)-(b) show that system $(3.2.6)_1$ has the bistable equilibria: the DFE $\mathbf{E}_1$ and an endemic equilibrium , and the other endemic equilibrium is unstable.

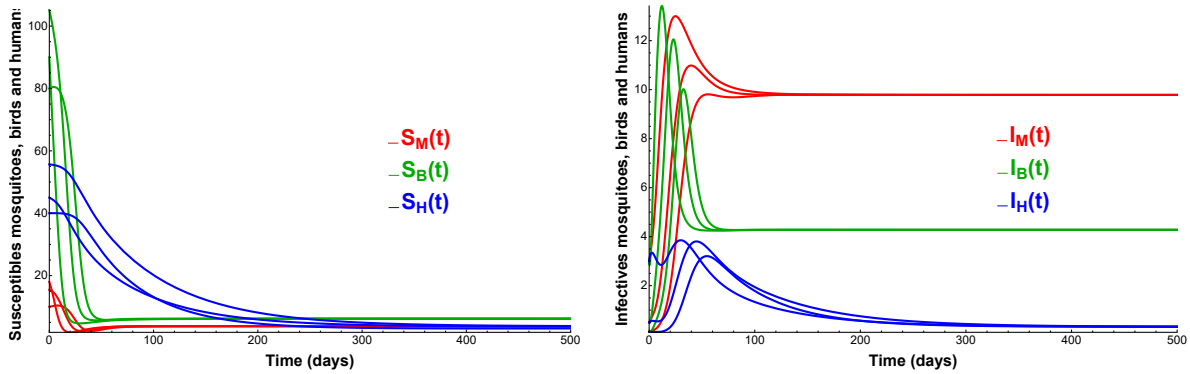

(a) (b)

Figure 3.5: Evolution over time of susceptible (a) and infective (b) classes of mosquito (magenta line), bird (orange line) and human (blue line) populations, corresponding to different initial data. We use the parameter values of Fig.3.2-(b) with $a_B = 3.9$ and $\beta_{MB} = 0.7$. (a)-(b) show that system (3.2.1) has a DFE $\mathbf{P}_1$, which is unstable, and an endemic equilibrium $\mathbf{P}^*$, which is LAS.

It is assumed that the number difference of adult stage and birds at different location causes diffusion, characterized by the diffusion coefficient D_M^* and D_B^*, respectively. Meanwhile, it is supposed that the adult mosquitoes can be transported by wind with speed v_M^*.

For mathematical tractability, some semplification are made with respect to the model (3.2.1). It is always stressed that the human population is a dilution host population and does not contribute to transmission dynamics. For this reason, from now on, only the population of birds is considered as a host population. Furthermore, it is supposed that both the incubation period and the recovery period from the disease are negligible: therefore, the population of birds and the adult stage are divided into susceptible and infectious compartments. Therefore, let us denote with $S_j(x,t)$, $j = A, M, B$, the number of susceptibles individuals of mosquitoes in aquatic stage, mosquitoes in adult stage and birds, respectively, at location x and time t;

in addition, denote with $I_j(x,t)$, $j = A, M, B$, the number of infective individuals of mosquitoes in aquatic stage, mosquitoes in adult stage and birds, respectively, at location x and time t; thus, $N_j(x,t) = S_j(x,t) + I_j(x,t)$, $j = A, M, B$, is the number of total population of mosquitoes in aquatic stage, mosquitoes in adult stage and birds, respectively, at location x and time t.

Under these assumptions and using (3.2.2), the model is described by the following system of six partial differential equations

$$\begin{cases} \partial_t S_A = r\left(1 - \frac{N_A}{k_A}\right)[S_M + (1-q)I_M] - \alpha_A S_A, \\ \partial_t I_A = r\left(1 - \frac{N_A}{k_A}\right) q I_M - \alpha_A I_A, \\ \partial_t S_M = D_M^* \nabla^2 S_M - v_M^* \partial_{\mathrm{x}_*} S_M + \gamma\left(1 - \frac{N_M}{k_M}\right) S_A - a_B \beta_{BM} \frac{I_B}{N_B} S_M - \alpha_M S_M, \\ \partial_t I_M = D_M^* \nabla^2 I_M - v_M^* \partial_{\mathrm{x}_*} I_M + \gamma\left(1 - \frac{N_M}{k_M}\right) I_A + a_B \beta_{BM} \frac{I_B}{N_B} S_M - \alpha_M I_M, \\ \partial_t S_B = D_B^* \nabla^2 S_B + \gamma_B - a_B \beta_{MB} \frac{I_M}{N_B} S_B - d_B S_B + \omega_B I_B, \\ \partial_t I_B = D_B^* \nabla^2 I_B + a_B \beta_{MB} \frac{I_M}{N_B} S_B - \nu_B I_B, \end{cases} \tag{3.4.1}$$

where $x \in \Omega^* = [0, L]$, $t > 0$ and $\nabla^2 = \partial^2_{\mathrm{x}_*}$ the Laplacian operator in 1D. System (3.4.1) is subject to the following Neumann condition on the boundary

$$\partial_{\mathrm{x}_*} S_A = \partial_{\mathrm{x}_*} I_A = \partial_{\mathrm{x}_*} S_M = \partial_{\mathrm{x}_*} I_M = \partial_{\mathrm{x}_*} S_B = \partial_{\mathrm{x}_*} I_B = 0, \text{ at } \mathrm{x}_* = 0, L. \tag{3.4.2}$$

For mathematical tractability, the spatial variable is re-scaled, by introducing $x = x_* L^{-1}$. Thus, setting

$$D_M = \frac{D_M^*}{L^2}, \; D_B = \frac{D_B^*}{L^2}, v_M = \frac{v_M^*}{L}, \tag{3.4.3}$$

model (3.4.1) reads as

$$\begin{cases} \partial_t S_A = r\left(1 - \frac{N_A}{k_A}\right)[S_M + (1-q)I_M] - \alpha_A S_A, \\ \partial_t I_A = r\left(1 - \frac{N_A}{k_A}\right) q I_M - \alpha_A I_A \\ \partial_t S_M = D_M \nabla^2 S_M - v_M \partial_x S_M + \gamma\left(1 - \frac{N_M}{k_M}\right) S_A - a_B \beta_{BM} \frac{I_B}{N_B} S_M - \alpha_M S_M, \\ \partial_t I_M = D_M \nabla^2 I_M - v_M \partial_x I_M + \gamma\left(1 - \frac{N_M}{k_M}\right) I_A + a_B \beta_{BM} \frac{I_B}{N_B} S_M - \alpha_M I_M, \\ \partial_t S_B = D_B \nabla^2 S_B + \gamma_B - a_B \beta_{MB} \frac{I_M}{N_B} S_B - d_B S_B + \omega_B I_B, \\ \partial_t I_B = D_B \nabla^2 I_B + a_B \beta_{MB} \frac{I_M}{N_B} S_B - \nu_B I_B, \end{cases} \tag{3.4.4}$$

with $t > 0$, $x \in \Omega = [0, 1]$ and Neumann condition

$$\partial_x S_A = \partial_x I_A = \partial_x S_M = \partial_x I_M = \partial_x S_B = \partial_x I_B = 0, \text{ at } x = 0, 1. \tag{3.4.5}$$

Adding the appropriate equations in (3.4.4) it is possible to see that the growth of the whole populations of aquatic mosquitoes, adult mosquitoes and birds satisfy the following equations

$$\begin{cases} \partial_t N_A = r\left(1-\frac{N_A}{k_A}\right)N_M - \alpha_A N_A, \\ \partial_t N_M = D_M\nabla^2 N_M - v_M\partial_x N_M + \gamma\left(1-\frac{N_M}{k_M}\right)N_A - \alpha_M N_M, \\ \partial_t N_B = D_B\nabla^2 N_B + \gamma_B - d_B N_B - \delta_B I_B. \end{cases} \tag{3.4.6}$$

Thus, the total aquatic stage of mosquitoes may vary in time and the adult stage of mosquitoes and birds populations may vary in space and time.

Note that, model (3.4.4) admits two omogeneous in space equilibrium points with no disease in the population, that are $\mathbf{U}_0 = \left(0,0,0,0,\frac{\gamma_B}{d_B},0\right)^T$ and $\mathbf{U}_1 = \left(A_0,0,M_0,0,\frac{\gamma_B}{d_B},0\right)^T$, which are the trivial and non-trivial one, and where A_0 and M_0 are already defined in (3.3.2). The equilibrium $\mathbf{U}_1$ exists if the condition $r\gamma > \alpha_A\alpha_M$ holds.

Consider the more biologically realistic equilibrium $\mathbf{U}_1$: the following result about its local stability related to the associated ODE model of (3.4.4), holds [161]:

Theorem 3.4.1 *The spatially homogeneous disease-free equilibrium point, $\mathbf{U}_1$ of the model (3.4.4), is locally asymptotically stable for the equivalent ODE system, if $\mathcal{R}_0 < 1$ and unstable if $\mathcal{R}_0 > 1$, where $\mathcal{R}_0$ is the threshold value*

$$\mathcal{R}_0 = \mathcal{R}_0^{ODE} = \frac{1}{2}\left(q + \sqrt{q^2 + \frac{4M_0a_B^2d_B\beta_{MB}\beta_{BM}}{\gamma_B\alpha_M\nu_B}}\right). \tag{3.4.7}$$

3.5 Basic Reproductive Number

In this section, the Basic Reproductive Number given in (3.4.7) for the equivalent ODE model of system (3.4.4) is compared with the Basic Reproductive Number, named $\mathcal{R}_0^{PDE}$, related to the spatial non-homogeneous model (3.4.4).

In order to define $\mathcal{R}_0^{PDE}$, as already explained in Section 2.9 of the Chapter 2, following [164],it is assumed that the state variables are near the non trivial DFE $\mathbf{U}_1$. Let us introduce the distribution of initial infection described by $\phi(x)^T = (I_A(x,0), I_M(x,0), I_B(x,0)) = (\phi_1(x),\phi_2(x),\phi_3(x))$. Consider the the reaction-advection-diffusion system consisting only of equations related to the infected compartments

$$\begin{aligned} \partial_t I_A &= r\left(1-\frac{N_A}{k_A}\right)qI_M - \alpha_A I_A, \\ \partial_t I_M &= D_M\nabla^2 I_M - v_M\partial_x I_M + \gamma\left(1-\frac{N_M}{k_M}\right)I_A + a_B\beta_{BM}\frac{I_B}{N_B}S_M - \alpha_M I_M, \\ \partial_t I_B &= D_B\nabla^2 I_B + a_B\beta_{MB}\frac{I_M}{N_B}S_B - \nu_B I_B. \end{aligned} \tag{3.5.1}$$

The epidemiological threshold $\mathcal{R}_0^{PDE}$ is giben by [164]

$$\mathcal{R}_0^{PDE} = \rho(\mathcal{L}), \quad \mathcal{L} = -F\mathcal{B}^{-1}, \tag{3.5.2}$$

where F is the transmission matrix of the NGM approach [61], [62] and $\mathcal{B} = \nabla(D \cdot \nabla) - v\nabla - V$ with D the diagonal matrix of diffusion coefficients and v the diagonal matrix of advection coefficients. For the system (3.4.4), matrix F takes the form

$$F = \begin{pmatrix} 0 & qr\left(1 - \frac{A_0}{k_A}\right) & 0 \\ 0 & 0 & \frac{a_B \beta_{BM} d_B M_0}{\gamma_B} \\ 0 & a_B \beta_{MB} & 0 \end{pmatrix}, \tag{3.5.3}$$

while, matrix $\mathcal{B}$ reads as

$$\mathcal{B} = \begin{pmatrix} -\alpha_A & 0 & 0 \\ \gamma\left(1 - \frac{M_0}{k_M}\right) & D_M \frac{\partial^2}{\partial x^2} - v_M \frac{\partial}{\partial x} - \alpha_M & 0 \\ 0 & 0 & D_B \frac{\partial^2}{\partial x^2} - \nu_B \end{pmatrix}, \tag{3.5.4}$$

where $D = Diag[0, D_M, D_B]$ and $v = Diag[0, v_M, 0]$ have been used for its computation.

Let us proceed to calculate $\mathcal{B}^{-1}$ by solving $\mathcal{B}(\phi_1, \phi_2, \phi_3)^T = (y_1, y_2, y_3)^T$ subject to homogeneous Neumann boundary conditions, following [166, 165]. Let us first consider the equation

$$\mathcal{B}[\phi_1] := -\alpha_A \phi_1(x) = y_1(x). \tag{3.5.5}$$

It can be easely obtained that

$$\phi_1(x) = -\frac{y_1(x)}{\alpha_A}. \tag{3.5.6}$$

Let us consider the second equation

$$\mathcal{B}[\phi_2] := \gamma\left(1 - \frac{M_0}{k_M}\right)\phi_1(x) + D_M \frac{\partial^2 \phi_2}{\partial x^2} - v_M \frac{\partial \phi_2}{\partial x} - \alpha_M \phi_2 = y_2, \tag{3.5.7}$$

with $\phi_2'(0) = \phi_2'(1) = 0$. Plugging (3.5.6) in (3.5.7), this problem can be conveniently solved by using the Laplace transform. Denote the Laplace transforms of $\phi_2(x)$, $y_1(x)$ and $y_2(x)$ by $\Phi_2(s)$, $Y_1(s)$ and $Y_2(s)$, respectively. One obtains

$$\Phi_2(s) = \frac{Y_2(s)}{D_M s^2 - v_M s - \alpha_M} + \frac{\phi_2(0)(D_M s - v_M)}{D_M s^2 - v_M s - \alpha_M} + \frac{\gamma}{\alpha_A}\left(1 - \frac{M_0}{k_M}\right)\frac{Y_1(s)}{D_M s^2 - v_M s - \alpha_M}, \tag{3.5.8}$$

where the first boundary condition of ϕ_2 is applied. It is conveniente to define $\lambda = \frac{\sqrt{v_M^2 + 4 D_M \alpha_M}}{2 D_M} > 0$. The inverse Laplace transform then yields

$$\begin{aligned} \phi_2(x) &= \frac{1}{D_M \lambda}\int_0^x e^{\frac{v_M}{2D_M}(x-\tau)} \sinh\left[\lambda(x-\tau)\right]\left[\frac{\gamma}{\alpha_A}\left(1 - \frac{M_0}{k_M}\right) y_1(\tau) + y_2(\tau)\right] d\tau \\ &+ \phi_2(0) e^{\frac{v_M x}{2D_M}}\left(\cosh\left[\lambda x\right] - \frac{v_M}{2 D_M \lambda}\sinh\left[\lambda x\right]\right). \end{aligned} \tag{3.5.9}$$

Now differentiating ϕ_2 and using the second boundary condition, one gets

$$\begin{aligned}\phi_2(x) &= \frac{1}{D_M\lambda}\int_0^x e^{\frac{v_M}{2D_M}(x-\tau)}\sinh\left[\lambda(x-\tau)\right]\left[\frac{\gamma}{\alpha_A}\left(1-\frac{M_0}{k_M}\right)y_1(\tau)+y_2(\tau)\right]d\tau \\ &- \frac{e^{-\frac{v_M}{2D_M}(1-x)}}{\alpha_M\sinh[\lambda]}\left(\cosh[\lambda x]-\frac{v_M}{2D_M\lambda}\sinh[\lambda x]\right)\int_0^1 e^{\frac{v_M}{2D_M}(1-\tau)} \\ &\left\{\frac{v_M}{2D_M}\sinh[\lambda(1-\tau)]+\lambda\cosh[\lambda(1-\tau)]\right\}\left[\frac{\gamma}{\alpha_A}\left(1-\frac{M_0}{k_M}\right)y_1(\tau)+y_2(\tau)\right]d\tau.\end{aligned}$$

In this expression, the second part represents the homogeneous solution, whereas the first part represents a particular solution to the original non-homogeneous equation [166]. In a similar way, it can be solved the boundary value problem

$$\mathcal{B}[\phi_3] := D_B\frac{\partial^2\phi_3}{\partial x^2}-\nu_B\phi_3, \tag{3.5.10}$$

with $\phi_3'(0)=\phi_3'(1)=0$, obtaining

$$\phi_3(x)=\frac{1}{\sqrt{D_B\nu_B}}\int_0^x\sinh\left[\sqrt{\frac{\nu_B}{D_B}}(x-\tau)\right]y_3(\tau)d\tau-\frac{\cosh\left[\sqrt{\frac{\nu_B}{D_B}}x\right]}{\sqrt{D_B\nu_B}\sinh\left[\sqrt{\frac{\nu_B}{D_B}}\right]}\int_0^1\cosh\left[\sqrt{\frac{\nu_B}{D_B}}(1-\tau)\right]y_3(\tau)d\tau. \tag{3.5.11}$$

For consistence in notations, below ot is switched ϕ_i with y_i for $i=1,2,3..$ Now, the eigenvalue problem

$$-F\mathcal{B}^{-1}\phi=\lambda\phi, \tag{3.5.12}$$

should be solved, i.e.

$$\begin{aligned}
k_{i1}\quad & \int_0^x e^{\frac{v_M}{2D_M}(x-\tau)}\sinh\left[\lambda(x-\tau)\right]y_1(\tau)d\tau+ \\
k_{i2}\quad & \int_0^x e^{\frac{v_M}{2D_M}(x-\tau)}\sinh\left[\lambda(x-\tau)\right]y_2(\tau)d\tau+ \\
k_{i3}\quad & e^{-\frac{v_M}{2D_M}(1-x)}\left(\cosh[\lambda x]-\frac{v_M}{2D_M\lambda}\sinh[\lambda x]\right)\int_0^1 e^{\frac{v_M}{2D_M}(1-\tau)}\left\{\frac{v_M}{2D_M}\sinh\left[\lambda(1-\tau)\right]+\lambda\cosh[\lambda(1-\tau)]\right\}y_1(\tau)d\tau+ \\
k_{i4}\quad & e^{-\frac{v_M}{2D_M}(1-x)}\left(\cosh[\lambda x]-\frac{v_M}{2D_M\lambda}\sinh[\lambda x]\right)\int_0^1 e^{\frac{v_M}{2D_M}(1-\tau)}\left\{\frac{v_M}{2D_M}\sinh\left[\lambda(1-\tau)\right]+\lambda\cosh[\lambda(1-\tau)]\right\}y_2(\tau)d\tau+ \\
k_{i5}\quad & \int_0^x\sinh\left[\sqrt{\frac{\nu}{D_B}}(x-\tau)\right]y_3(\tau)d\tau \\
k_{i6}\quad & \cosh\left[\sqrt{\frac{\nu_B}{D_B}}x\right]\int_0^1\cosh\left[\sqrt{\frac{\nu_B}{D_B}}(1-\tau)\right]y_3(\tau)d\tau=\lambda\phi_i \qquad i=1,2,3,
\end{aligned} \tag{3.5.13}$$

with

$$\begin{aligned}
&k_{11}=-qr\left(1-\tfrac{A_0}{k_A}\right)\left(1-\tfrac{M_0}{k_M}\right)\tfrac{\gamma}{\alpha_A D_M\lambda}, && k_{12}=-qr\left(1-\tfrac{A_0}{k_A}\right)\tfrac{1}{D_M\lambda}, \\
&k_{13}=qr\left(1-\tfrac{A_0}{k_A}\right)\left(1-\tfrac{M_0}{k_M}\right)\tfrac{\gamma}{\alpha_M\alpha_A\sinh[\lambda]}, && k_{14}=qr\left(1-\tfrac{A_0}{k_A}\right)\tfrac{1}{\alpha_M\sinh[\lambda]}, \\
&k_{25}=-\tfrac{a_B\beta_{BM}d_BM_0}{\gamma_B\sqrt{D_B\nu_B}}, && k_{26}=\tfrac{a_B\beta_{BM}d_BM_0}{\gamma_B\sqrt{D_B\nu_B}\sinh\left[\sqrt{\frac{\nu_B}{D_B}}\right]}, \\
&k_{31}=-a_B\beta_{MB}\left(1-\tfrac{M_0}{k_M}\right)\tfrac{\gamma}{\alpha_A D_M\lambda}, && k_{32}=-a_B\beta_{MB}\tfrac{1}{D_M\lambda}, \\
&k_{33}=a_B\beta_{MB}\left(1-\tfrac{M_0}{k_M}\right)\tfrac{\gamma}{\alpha_M\alpha_A\sinh[\lambda]}, && k_{34}=a_B\beta_{MB}\tfrac{1}{\alpha_M\sinh[\lambda]}, \\
&k_{15}=k_{16}=k_{35}=k_{36}=0, && k_{21}=k_{22}=k_{23}=k_{24}=0.
\end{aligned} \tag{3.5.14}$$

3.5.1 Numerical Treatment of Eigenvalue Problem (3.5.13)

Please refer to the description of the method in the section 2.9.1 of the chapter 2.
The problem is reduced to analysing the spectral radius, $\rho(A)$, of the coefficient matrix A, i.e.

$$\lim_{\Delta x \to 0} \rho(A) = \rho(L) = \mathcal{R}_0^{PDE}.$$

where A satisfies the matrix equation,

$$AZ = \lambda Z, \tag{3.5.15}$$

with $Z = [\phi_1(x_1), \phi_1(x_2), ..., \phi_1(x_M), \phi_2(x_1), \phi_2(x_2), ..., \phi_2(x_M), \phi_3(x_1), \phi_3(x_2), ..., \phi_3(x_M)]^T$. The coefficient matrix A in can be written as

$$A = A_1 + A_2 + A_3 + A_4 + A_5 + A_6, \tag{3.5.16}$$

where each matrix A_i $(1 \leq i \leq 6)$, of dimension $3M \times 3M$, results from the discretization of the i-th integral in equations (3.5.13). Specifically, A_1 can be represented by a block form

$$A_1 = \Delta x \begin{pmatrix} k_{11}\tilde{A}_1 & 0_M & 0_M \\ 0_M & 0_M & 0_M \\ k_{31}\tilde{A}_1 & 0_M & 0_M \end{pmatrix}, \tag{3.5.17}$$

where 0_M denotes the zero square matrix of dimension $M \times M$, and $\tilde{A}_1 = (a_{i,j}^{(1)})$ is an $M \times M$ lower-triangular matrix given by

$$a_{i,j}^{(1)} = \begin{cases} e^{\frac{v_M}{2D_M}(x_i - x_j)} \sinh\left[\lambda(x_i - x_j)\right], & \text{if } i \geq j, \\ 0, & \text{otherwise.} \end{cases} \tag{3.5.18}$$

Similarly

$$A_2 = \Delta x \begin{pmatrix} 0_M & k_{12}\tilde{A}_2 & 0_M \\ 0_M & 0_M & 0_M \\ 0_M & k_{32}\tilde{A}_2 & 0_M \end{pmatrix}, \tag{3.5.19}$$

where $\tilde{A}_2 = (a_{i,j}^{(1)})$, as defined in (3.5.18). The matrix A_3 takes the form

$$A_3 = \Delta x \begin{pmatrix} k_{13}\tilde{A}_3 & 0_M & 0_M \\ 0_M & 0_M & 0_M \\ k_{33}\tilde{A}_3 & 0_M & 0_M \end{pmatrix}, \tag{3.5.20}$$

with the $M \times M$ block $\tilde{A}_3 = (a_{i,j}^{(3)})$ for which

$$\begin{aligned} a_{i,j}^{(3)} &= e^{-\frac{v_M}{2D_M}(1-x_i)} \left(\cosh\left[\lambda x_i\right] - \frac{v_M}{2D_M \lambda} \sinh\left[\lambda x_i\right] \right) e^{\frac{v_M}{2D_M}(1-x_j)} \left(\frac{v_M}{2D_M} \sinh\left[\lambda(1-x_j)\right] \right. \\ &+ \left. \lambda \cosh\left[\lambda(1-x_j)\right] \right) \quad \text{if} \quad 1 \leq i, j \leq M. \end{aligned} \tag{3.5.21}$$

Similarly, the matrix A_4 takes the form:

$$A_4 = \Delta x \begin{pmatrix} 0_M & k_{14}\tilde{A}_4 & 0_M \\ 0_M & 0_M & 0_M \\ 0_M & k_{34}\tilde{A}_4 & 0_M \end{pmatrix}, \tag{3.5.22}$$

in which the $M \times M$ block $\tilde{A}_4 = (a_{i,j}^{(3)})$, as in (3.5.21). Then,

$$A_5 = \Delta x \begin{pmatrix} 0_M & 0_M & 0_M \\ 0_M & 0_M & k_{25}\tilde{A}_5 \\ 0_M & 0_M & 0_M \end{pmatrix}, \tag{3.5.23}$$

where $\tilde{A}_5 = (a_{i,j}^{(5)})$ is lower-triangular matrix given by:

$$a_{i,j}^{(5)} = \begin{cases} \sinh\left[\sqrt{\frac{\nu_B}{D_B}}(x_i - x_j)\right] & \text{if } i \geq j, \\ 0 & \text{otherwise.} \end{cases} \tag{3.5.24}$$

Finally

$$A_6 = \Delta x \begin{pmatrix} 0_M & 0_M & 0_M \\ 0_M & 0_M & k_{26}\tilde{A}_6 \\ 0_M & 0_M & 0_M \end{pmatrix}, \tag{3.5.25}$$

where the $M \times M$ block $\tilde{A}_6 = (a_{i,j}^{(6)})$ is defined as:

$$a_{i,j}^{(6)} = \cosh\left[\sqrt{\frac{\nu_B}{D_B}}x_i\right]\cosh\left[\sqrt{\frac{\nu_B}{D_B}}(1 - x_j)\right], \quad \text{if} \quad 1 \leq i, j \leq M. \tag{3.5.26}$$

There is no general relationship between $\rho(A)$ and $\rho(A_i)$, $(1 \leq i \leq 6)$. Nevertheless, if we assume $\frac{\nu_B}{D_B} \ll 1$ and $v_M^2 + 4D_M\alpha_M \ll 1$, then each entry of $\tilde{A}_1$, $\tilde{A}_2$ and $\tilde{A}_3$ is very small; it is bounded between 0 and $\sinh\left[\sqrt{\frac{\nu_B}{D_B}}\right]$ if in $\tilde{A}_3$ and between 0 and $\sinh\left[\sqrt{v_M^2 + 4D_M\alpha_M}\right]$ if in $\tilde{A}_1$ or in $\tilde{A}_2$. Thus, A_1, A_2 and A_3 can be treated as small perturbation to A_4, A_5 and A_6 in this case, and

$$\rho(A) \approx \rho(A_4 + A_5 + A_6). \tag{3.5.27}$$

3.5.2 Main Results on $\mathcal{R}_0^{PDE}$

The quantity $\mathcal{R}_0^{PDE}$ represents a threshold value for the eradication of the disease for the spatially non-homogeneous model (3.4.4). Indeed, consider the spatially homogeneous equivalents of the equations $(3.4.4)_1$, $(3.4.4)_3$ and $(3.4.4)_5$: let M be the matrix consisting of the derivatives of the right hand-side of these equations with respect to the variables S_A, S_M and S_B, evaluated at DFE $\mathbf{U}_1$, i.e.:

$$M = \begin{pmatrix} -\frac{M_0 r}{k_A} - \alpha_A & r\left(1 - \frac{A_0}{k_A}\right) & 0 \\ \gamma\left(1 - \frac{M_0}{k_M}\right) & -\left(\frac{A_0\gamma}{k_M} + \alpha_M\right) & 0 \\ 0 & 0 & \omega_B - d_B \end{pmatrix}. \tag{3.5.28}$$

Since the off-diagonal entries are non-negative, M is cooperative. Consider, in addition, the opposite of the transition matrix $-V$ of the NGM approach [62, 61] related to the model (3.4.4) and evaluated at the DFE $\mathbf{U}_1$, given by

$$-V = \begin{pmatrix} -\alpha_A & 0 & 0 \\ \gamma\left(1 - \frac{M_0}{k_M}\right) & -\alpha_M & 0 \\ 0 & 0 & \nu_B \end{pmatrix}. \tag{3.5.29}$$

This matrix is also cooperative. Thus consider the following statements:

$$\lambda^0(M) \equiv s\left(\nabla(D\nabla) - v\nabla + M\right) < 0, \quad \lambda^0(-V) \equiv s\left(\nabla(D\nabla) - v\nabla - V\right) = s(\mathcal{B}) < 0, \tag{3.5.30}$$

where s is the spectral abscissa defined in (2.9.38). These assumptions extend to the case in which the advection is present, as in the model (3.4.4), those made by Wang and Zhao [164] for the validity of the subsequent theorem for reaction-diffusion systems. The following result holds [164]:

Theorem 3.5.1 *Assume that* (3.5.30) *holds with* $v = 0$. *Then*

- $\mathcal{R}_0^{PDE} - 1$ *has the same sign as* $\lambda^* \equiv s(\mathcal{B} + F)$.
- *If* $\mathcal{R}_0^{PDE} < 1$, *then DFE* $\mathbf{U}_1$ *is asymptotically stable for system* (3.4.4).

Thus, $\mathcal{R}_0^{PDE}$ is an epidemioloical threshold for model (3.4.4) withut advection. Many nymerical simulations suggest that this result hold even if $v \neq 0$ with assumptions (3.5.30).
Figures 3.6 illustrates the number of infectious birds based on the PDE model (3.4.4) with uniform initial distribution, as a function of space and time when the associated $\mathcal{R}_0^{PDE}$ is lower or higher than the unity. Other initial conditions with various distribution types have been tested, and they all lead to similar patterns in terms of the extinction (when $\mathcal{R}_0^{PDE} < 1$) and endemic state (when $\mathcal{R}_0^{PDE} > 1$) of vector-borne infection. They verify that $\mathcal{R}_0^{PDE}$ is a disease threshold.
The following result applies regarding the comparison between $\mathcal{R}_0^{ODE}$ and $\mathcal{R}_0^{PDE}$:

Theorem 3.5.2 *If* $\nu_B \ll D_B$ *and* $v_M^2 + 4D_M\alpha_M \ll 1$, *then*

$$\mathcal{R}_0^{PDE} \doteq \mathcal{R}_0^{ODE}. \tag{3.5.31}$$

The proof is given in Appendix F.
A similar result has been obtained for the cholera epidemic in [165], but this is the only result of this type existing for vector diseases.
The threshold dynamics based on $\mathcal{R}_0^{ODE}$ and R^{PDE} are now compared. The influence of the transmission probabilities β_{BM} and β_{MB} on $\mathcal{R}_0^{PDE}$ is studied. Fig. 3.7 shows the difference in the basic reproduction number of the PDE model (3.4.4) and the reproduction number of the equivalent ODE model defined in (3.4.7). Is is easy to observe, from Figure 3.7(a), that $\mathcal{R}_0^{PDE} \to \mathcal{R}_0^{ODE}$ when $\frac{v_M}{D_M}$ is getting small . When $\frac{v_M}{D_M}$ is getting large, Figure 3.7(b) illustrates that the difference $\left|\mathcal{R}_0^{ODE} - \mathcal{R}_0^{PDE}\right|$ increases and becomes very large. This result is consistent with Theorem 2.9.2 and extends what has been shown in [165, 166].

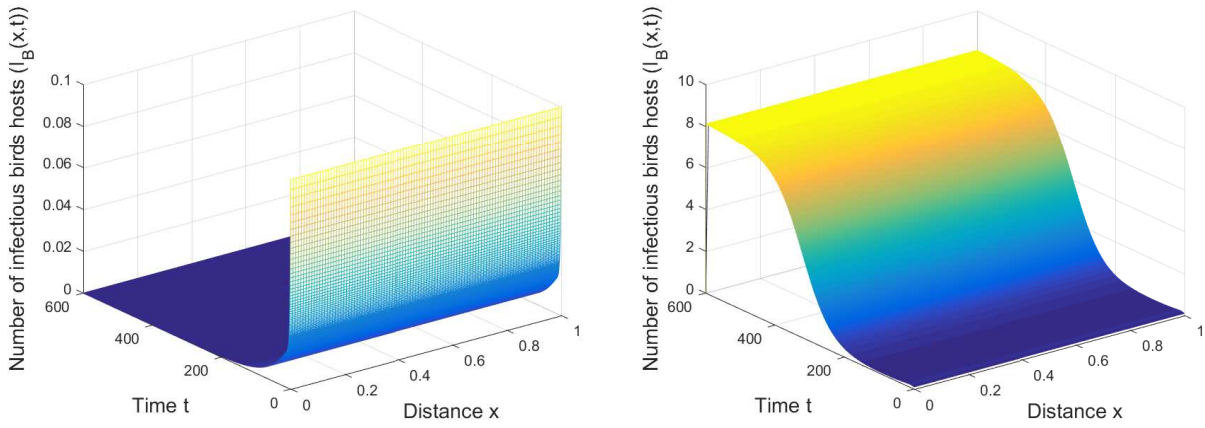

(a) $\mathcal{R}_0^{PDE} < 1$ (b) $\mathcal{R}_0^{PDE} > 1$

Figure 3.6: Number of infected birds associated with the PDE model (2.7.4) vs. space and time, when $\mathcal{R}_0^{PDE} = 0.165336 < 1$ (a) and $\mathcal{R}_0^{PDE} = 1.10991 > 1$ (b). The parameter value are those listen Fig. 3.2(b) with $\beta_{BM} = \beta_{MB} = 0.1$, $v_M^* = 0.5$, $D_M^* = D_B^* = 1$ and $L = 100$. Moreover $a_B = 0.5$ in panel (a) and $a_B = 3.9$ in panel (b).

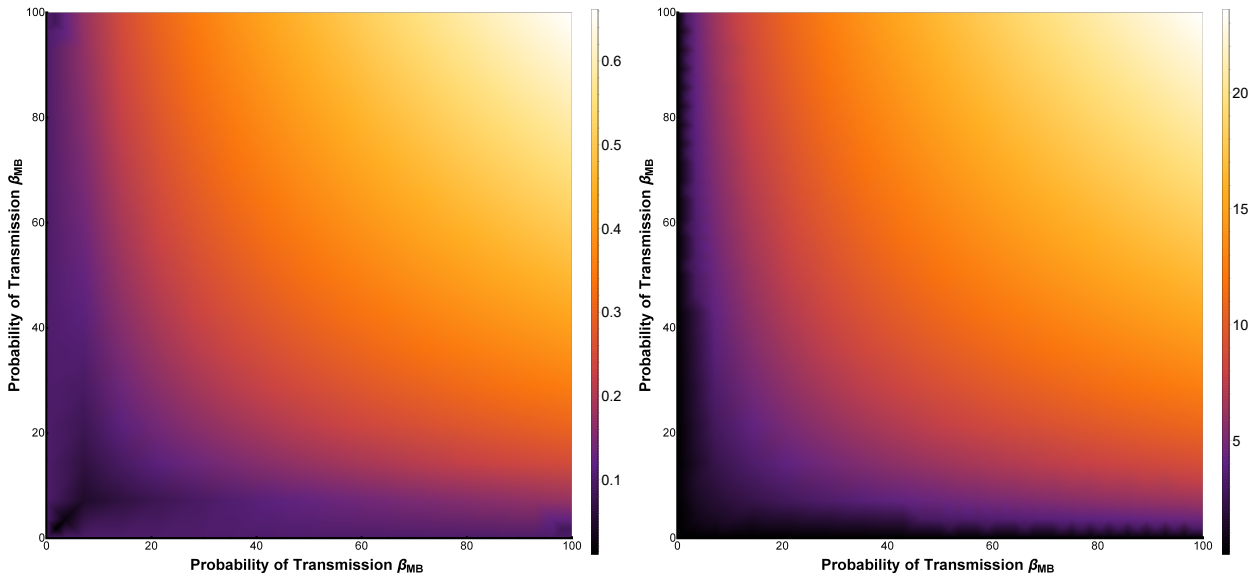

(a) $D_M \gg v_M$ (c) $D_M \ll v_M$

Figure 3.7: The difference in the basic reproduction number associated with PDE model (3.4.4) and the reproduction number related to the equivalent ODE model given in (3.4.7)$\left|\mathcal{R}_0^{PDE} - \mathcal{R}_0^{ODE}\right|$. The thresholds $\mathcal{R}_0^{ODE}$ and $\mathcal{R}_0^{PDE}$ are function of transmission probabilities β_{MB} and β_{BM}. The value of parameters used in this simulation are those listed in Fig.3.2(b) with $L = 10$, $v_M^* = 0.5$. Moreover $D_M^* = D_B^* = 100$ in (a) panel and $D_M^* = D_B^* = 0.1$ in (b) panel.

3.6 Conclusions

Most of the models in the published literature deal with the interaction between birds and mosquitoes. Humans are considered dead-end hosts (as has been pointed out several times in this discussion) because

infected humans do not further spread the virus in any species. Therefore it is reasonable to include only the transmission of the virus between birds and mosquitoes in order to understand the transmission dynamics of vector diseases. However, from the point of view of both public health and epidemiology, it is necessary to include the human component in the models: in fact, these epidemics have caused significant deaths throughout the world, in the absence of a specific treatment or vaccine; further research is therefore needed to understand the epidemiology and pathology of vector-borne diseases. Furthermore, most of the experimental data concerning these epidemics focus on the human cases reported by the Department of Public Health, which have almost never been simulated in the literature. In addition, the entire life cycle of the mosquitoes was considered, thus including their aquatic phase. This state has been divided into a class that is susceptible and infectious, in order to incorporate vertical transmission into the vector population. In fact, vertical transmission is observed in the dengue virus transmitted by mosquitoes of the species Aedes aegypti, Aedes albopitus and Culex. Similarly, the survival of Rift Valley fever that causes the virus in infected Aedes aegypti eggs is probably a key factor in the epidemic cycle following extreme weather and weather events. (Although Rift Valley fever is transmitted by two species of mosquito, Culex and Aedes aegypti, only the Aedes aegypti species transmit the pathogen to their offspring). Furthermore, vertical transmissions of West Nile virus in Culex and Aedes aegypti mosquito species and yellow fever in Aedes aegypti are known. For these purposes, an autonomous differential equation system for infectious diseases dynamics, which incorporates vertical transmission, logistic growth for vector population, reservoirs and dilution host is considered. An explicit formula for the basic reproductive number $\mathcal{R}_0$ is derived, the local stability of DFE and the existence of an endemic equilibrium state are investigated. A detailed analysis of the model, based on the use of center manifold theory, shows the presence of the phenomenon of backward bifurcation, where two stable equilibria co-exist, when the associated basic reproduction number is less than unity. Three parameter ranges are compiled: one representing the case $\mathcal{R}_0 < 1$, one representing the case $\mathcal{R}_0 > 1$ and finally a suitable set of parameters for to exhibit backward bifurcation. The presence of vertical transmission makes the model more realistic, as it takes into account that some eggs may already be infected at birth. The introduction of carrying capacity in the vector population places a limit on the number of existing mosquitoes: a lesser spread of the virus is evident and a reduction in the time necessary to reach equilibrium, with respect to the results present in published literature. After some semplifications (that is, neglecting the human guests and the exposed and removed classes), the model was then extended to the spatial case including the spread of mosquitoes in adult phase and of the hosts, and transport of adult mosquitoes due to the wind, using the Fickian approximation. An estimate of the basic reproductive number relative to the spatial case was provided, obtaining the conditions for which it coincides with that corresponding to the spatially homogeneous case. The simulations suggest that $\mathcal{R}_0^{PDE}$ constitutes a threshold for the eradication of the infection also in the spatial case, under opportune hypotheses.

Chapter 4

THE COEXISTENCE OF FAST AND SLOW DISSIPATIVE PROCESSES IN THE LIFE CYCLE OF AEDES AEGYPTI MOSQUITOES

This chapter has materialized in the following paper:

A. Lupica and A. Palumbo. The coexistence of fast and slow dissipative processes in the life cycle of Aedes Aegypti mosquitoes,

currently submitted in *International Journal of Biomathematics*.

4.1 Introduction

Vector-borne diseases are viral and are carried by vectors, such as mosquitoes. Aedes aegypti is one of the most dangerous mosquito species as a vector of dengue, chikungunya, yellow fever, "Zika disease" and other diseases [169]. It is native to Africa, but has been passively transported in maritime traffic in all tropical and subtropical regions, while it cannot survive the winter temperatures of temperate zones. It is a strongly anthropophilic species able to develop in water containers present in urban areas [169]. Figure 4.1 shows vector potential abundance during the decade 2000-2009 by seaseon, reported by Liu-Helmersson et al. [100]. The A. aegypti mosquito lives mainly in human houses and bites at any time of the day, which makes it a very efficient vector [151]. For oviposition, female A. aegypti mosquitoes need clear and undisturbed water to make their larvae proliferate, available mainly in unattended containers, natural as orchids or artificial as old tires, flower pots, empty bottles. Thus, man-made environmental conditions are the main reasons for A. aegypti infestation and, in view of this, the (presumably) most effective strategy to control its proliferation should be a permanent civic vigilance attitude towards farmers unattended [151]. Infected in-

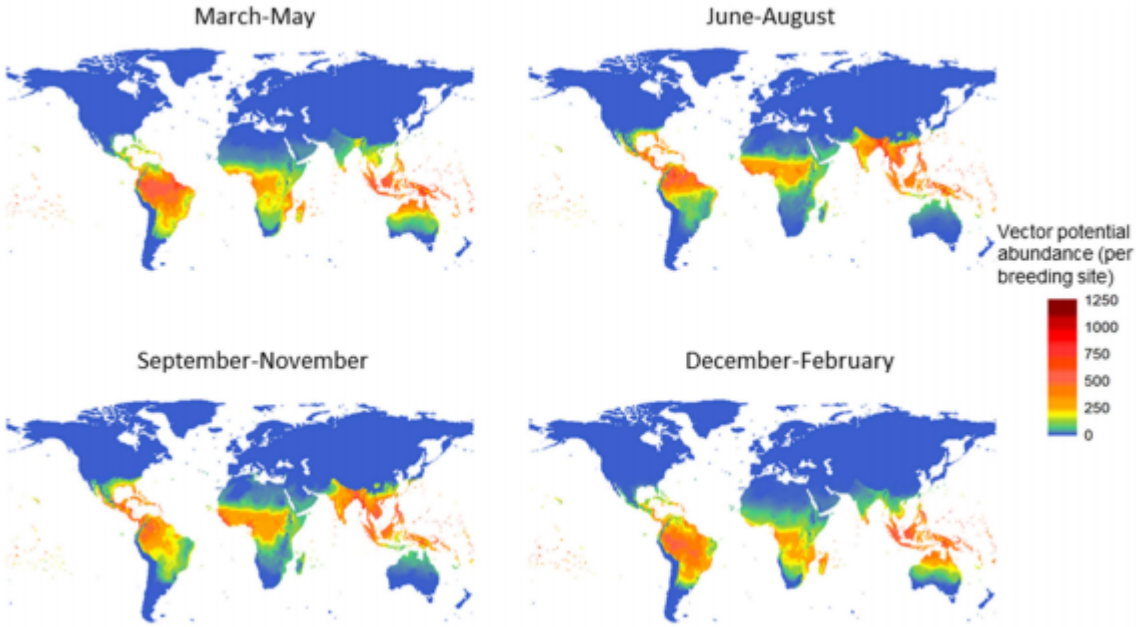

(a)

Figure 4.1: | Potential for global distribution and abundance of female Aedes aegypti over the decade 2000-2009, by season [100].

dividuals, human or mosquito, can very quickly start an epidemic in human populations if placed in a region previously infested with A. aegypti [151]. In the absence of a vector disease vaccine, any viable strategy to control their epidemiological dynamics must focus efforts on containing the population of A. aegypti, especially when an infection is detected. An effective and practical measures for controlling the population of A. aegypti is the classic chemical attack against the mosquito or against its larval form, that is carried out by using strong organophosphorus, insecticides and pyrethroids (Fenitrothion, Malathion, Cypermethrin) [151]. For example, The Centers for Disease Control and Prevention traveler's page on preventing dengue fever suggests using mosquito repellents that contain DEET (N, N-diethylmetatoluamide, 20% to 30%) [169]. Insect repellants containing DEET (particularly concentrated products) or p-menthane-3,8-diol (from lemon eucalyptus) were effective in repelling A. aegypti mosquitoes, while others were less effective or ineffective in a scientific study [134]. The Centers for Disease Control and Prevention article on "Protection against Mosquitoes, Ticks, & Other Arthropods" notes that "Studies suggest that concentrations of DEET above approximately 50% do not offer a marked increase in protection time against mosquitoes; DEET efficacy tends to plateau at a concentration of approximately 50%" [124]. However, in order to obtain adequate results with this strategy, it is necessary to apply and maintain a medium-high level of these toxic and costly chemicals over the entire infested region, mostly occupied also by human houses [153, 180]. These conditions make chemical control very difficult from a practical point of view and also dangerous from the point of view of public health [151]. The second type of strategy emphasizes prevention. Mosquito control is currently the best method for disease prevention. This primarily includes source reduction, pesticide spraying for larval control and "fogging" for adult control, or the use of mosquito traps like the lethal ovitrap. [169]. Vector

disease can become endemic in a region infested with a population of A. aegypti. Therefore, to develop public prevention policies and strategies for the control of this disease it is essential to establish a solid and treatable knowledge of the behavior and dynamics of the population of A. aegypti in order to find adequate parameters for treatment through practical interventions. Mathematical models can provide this knowledge, since they are necessarily simplified descriptions of reality and, if reasonably faithful, automatically produce the desired control parameters. A. aegypti mosquitoes are constantly looking for human blood or places for oviposition: this continuous movement is the main reason for the dispersion of the local population and the slow progress of a mosquito infestation. On the other hand, the wind currents can also cause a movement of advancing large masses of mosquitoes and consequently cause a rapid progression of the infestation. [151]. In addition to this, since A. aegypti is found mainly in urban regions, its movement is also largely influenced by human activities. For example, the effect of human transport networks on the propagation of dengue has been modeled by Takahashi [150]. Mathematical models already exist in the literature describing these phenomena, such as [74, 121, 151, 179, 181], that take into account the spatial dispersion of mosquitoes in the territory; in particular in [151] focuses his attention also on an urban scale of space, where a (local) diffusion process two to autonomous and random search movements of winged A. aegypti are coupled to a constant advection which may be interpreted as the result of wind transportation. The main defect of these models is that they were deduced by assuming that the diffusive flux of adult mosquitoes obeys Fick's constitutive equation, according to the principles of Classical Thermodynamics (CT) [29]. This leads to parabolic reaction-diffusion (PRD) equations characterized by instantaneous diffusive effects. On the other hand, many application in biological population dynamics require an appropriate approximation for finite propagation speed. In order to avoid the unphysical feature of infinite propagation speed in diffusion, hyperbolic reaction-diffusion (HRD) equations are successfully applied to many problems of biophysical interest [70, 77, 112, 113, 148, 149]. In this paper the main assumption for the model we will derive is the simultaneous coexistence of the Fick-type fast processes and Cattaneo-type slow processes in the mechanism of dispersion of adult mosquitoes, which are independent processes. A similar assumption was made in [183] for heat conduction processes and in [34] for mass transport in polymers. Consequently, it is assumed that the diffusive flux of adult mosquitoes is the sum of two contributions, one that satisfies Fick's law and the other that satisfies a Cattaneo evolution equation. This hypothesis is completely legitimate, since it was obtained as the main result in [47, 48]. In fact, in the study of thermodiffusion phenomena in fluid mixtures, Ciancio and Palumbo deduce the decomposition of dissipative fluxes (the heat conduction vector and the mass diffusion flux) into two contributions: a first contribution governed by the Fourier-type law and Fick-type law, respectively, and a second contribution that satisfies the Maxwell-Cattaneo-Vernotte equation, in the framework of Classical Irreversible Thermodynamics (CIT) with Internal Variables.

A generalized model will be deduced, that reproduces the parabolic model present in the published literature [151] and admits, as limiting case, a hyperbolic reaction-diffusion model, describing non Fickian behavior. The paper is organized as follows: the model is proposed in section 4.2, while the analysis of the corresponding ODE system is given in section 4.3. Traveling waves are investigated in section 4.4 while sections 4.5 and 4.6 are dedicated to the classical parabolic and hyperbolic limit cases, respectively. Numerical simulations are placed in section 4.7 and concluding remarks in section 4.8.

4.2 Mathematical model

In order to investigate biological invasions as a preventive method for the spread of infectious diseases, the model investigated by Takahashi *et al* [151] is extended in this section. Let us denote with $\widetilde{A}(x,t)$ the density of the mosquitoes in aquatic stage (consisting in eggs, larvae and pupae) and $\widetilde{M}(x,t)$ the density of the mosquitoes in adult stage. The population increases through logistic growth, with $\widetilde{r}$ the intrinsic oviposition rate and $\widetilde{\gamma}$ is the intrinsic maturation rate from aquatic stage to adult stage. Because of the presence of logistic growth, there is a carrying capacity both in aquatic and adult stage. The carrying capacity in aquatic stage $\widetilde{k}_A$ is defined as the available amount of breeding sites [105], while the carrying capacity in the adult stage $\widetilde{k}_M$ takes into account the fact that the mosquitoes cannot survive at high altitudes or temperatures [105]. So the per-capita oviposition rate is given by $\widetilde{r}(1-\frac{\widetilde{A}}{\widetilde{k}_A})$ and the per-capita growth rate in the adult stage is $\widetilde{\gamma}(1-\frac{\widetilde{M}}{\widetilde{k}_M})$. The aquatic and adult stages of mosquitoes population decrease by natural death rate $\widetilde{\nu}$ and $\widetilde{\mu}$, respectively. It is assumed that only the adult stage of mosquitoes can move and can be transported by the wind. Let $\widetilde{v}$ be the velocity of wind. Under these hypotheses, the basic equations are

$$\begin{aligned} \partial_{\widetilde{t}}\widetilde{A} &= \widetilde{r}\left(1-\frac{\widetilde{A}}{\widetilde{k}_A}\right)\widetilde{M}-(\widetilde{\nu}+\widetilde{\gamma})\widetilde{A}, \\ \partial_{\widetilde{t}}\widetilde{M}+\widetilde{v}\partial_{\widetilde{x}}M+\partial_{\widetilde{x}}\widetilde{J}_{\widetilde{M}} &= \widetilde{\gamma}\left(1-\frac{\widetilde{M}}{\widetilde{k}_M}\right)\widetilde{A}-\widetilde{\mu}\widetilde{M}, \end{aligned} \tag{4.2.1}$$

where $\widetilde{t}>0$, $\widetilde{x}\in\widetilde{\Omega}=[-\tilde{L},\tilde{L}]$ ($\tilde{L}>0$) bounded set of $\mathbb{R}$. $\widetilde{J}_{\widetilde{M}}$ is the diffusive flux related to the adult stage. Making the hypotheses that Fick-type fast processes that have infinite speed of propagation and Cattaneo-type slow processes that have finite speed of propagation independently coexist simultaneously in the diffusion process of adult mosquitoes, it is assumed that the diffusive flux of adult stage is given by

$$\widetilde{J}_{\widetilde{M}}=\widetilde{J}^{(0)}+\widetilde{J}^{(1)}, \tag{4.2.2}$$

where the first contribution $\widetilde{J}^{(0)}$ is governed by Fick's law [29], and the second one $\widetilde{J}^{(1)}$ obeys Cattaneo equation, in which a relaxation time is present [42].
As in the parabolic models, $\widetilde{J}^{(0)}$ obeys at the most common constitutive equation for the flux (the Fick's law, describing fast processes)

$$\widetilde{D}_0\partial_{\widetilde{x}}\widetilde{M}=-\widetilde{J}^{(0)},\quad \widetilde{D}_0>0, \tag{4.2.3}$$

where $\widetilde{D}_0$ is the constant diffusion coefficient related to the fickian propagation. Moreover as in hyperbolic model, the diffusive flux $\widetilde{J}^{(1)}$ satisfies the transport equation (describing slow processes)

$$\widetilde{\tau}\partial_{\widetilde{t}}\widetilde{J}^{(1)}+\widetilde{D}_1\partial_{\widetilde{x}}\widetilde{M}=-\widetilde{J}^{(1)},\quad \widetilde{D}_1>0, \tag{4.2.4}$$

where $\widetilde{\tau}$ is the constant relaxation time and $\widetilde{D}_1$ the constant diffusion coefficient related to the non-fickian propagation. This equation was derived in different contexts related to the heat conduction, i.e. in the theory of stochastic processes, phenomenologically, in the Extended Thermodynamics (ET) and Extended Irreversible Thermodynamics (EIT) framework [77, 97, 120]. Equation of type (4.2.4) is a generalization

of the classical Fourier/Fick law, which is valid under the assumption of local thermodynamic equilibrium, i.e. for $\tau = 0$. Its physical meaning is that the heat/mass transport in local non-equilibrium systems has inertial properties with a relaxation time τ. The assumption (4.2.2) expresses the fast and slow processes coexistence.
Now, let $\widetilde{D} = \widetilde{D}_0 + \widetilde{D}_1$ be the total diffusivity. Let us introduce the following adimensional parameter:

$$F_D = \frac{\widetilde{D}_0}{\widetilde{D}}. \tag{4.2.5}$$

By its definition, it is clear that F_D lies between 0 and 1 (i.e. $F_D \in [0, 1]$). Equations (4.2.3) and (4.2.4) can be re-written in terms of the parameter F_D, i.e.:

$$\widetilde{D} F_D \partial_{\widetilde{x}} \widetilde{M} = -\widetilde{J}^{(0)}, \quad \widetilde{\tau}\partial_{\widetilde{t}} \widetilde{J}^{(1)} + \widetilde{D}(1 - F_D)\partial_{\widetilde{x}} \widetilde{M} = -\widetilde{J}^{(1)}. \tag{4.2.6}$$

Remarks.
The assumptions (4.2.2) and (4.2.6) were made by Camera-Roda and Sarti in [34] in order to overcome the limitations of Fickian behavior and Cattaneo equation in the non-Fickian mechanisms of mass transfert observed in polymeric materials. They are also compatible with the second principle of Thermodynamics. In fact, Zhou et al [183], in their model for heat conduction in an elastic media , introduced a parameter, that they call *macroscale heat conduction model number* F_T, analogous to (4.2.5) and related both to the fast heat conduction (obedient to Fourier's law), and to the slow heat conduction (obedient to Cattaneo's equation). They prove that the second principle of Thermodynamics is satisfied if and only if $F_T \in [0, 1]$.
The coexistence of independent diffusion flows also exists in other works, as a consequence of the second principle of Thermodynamics. For example, Ciancio and Palumbo [47, 48], in the context of the Classical Irreversible Thermodynamics Theory with internal variables, in models describing thermodiffusion in a viscous fluid mixtures, find as a result that the dissipative fluxes are the sum of two flows, one fast and the other slow. A similar result was also obtained in [46], where the dynamics of a generic population of individuals is described by the introduction of an internal scalar variable. □

So, by virtue of (4.2.2) and (4.2.6), the evolution equations (4.2.1) became

$$\begin{aligned}
\partial_{\widetilde{t}} A &= \widetilde{r}\left(1 - \frac{\widetilde{A}}{\widetilde{k}_A}\right)\widetilde{M} - (\widetilde{\nu} + \widetilde{\gamma})\widetilde{A}, \\
\partial_{\widetilde{t}} \widetilde{M} + \widetilde{v}\partial_{\widetilde{x}} \widetilde{M} + \partial_{\widetilde{x}} \widetilde{J} &= \widetilde{D} F_D \nabla^2 \widetilde{M} + \widetilde{\gamma}\left(1 - \frac{\widetilde{M}}{\widetilde{k}_M}\right)\widetilde{A} - \widetilde{\mu}\widetilde{M}, \\
\widetilde{\tau}\partial_{\widetilde{t}} \widetilde{J} + \widetilde{D}(1 - F_D)\partial_{\widetilde{x}} \widetilde{M} &= -\widetilde{J},
\end{aligned} \tag{4.2.7}$$

where $\widetilde{t} > 0$, $\widetilde{x} \in \widetilde{\Omega} = [-\widetilde{L}, \widetilde{L}]$, $(\widetilde{L} > 0)$ bounded set of $\mathbb{R}$ and $\nabla^2 = \partial^2_{\widetilde{x}}$ the Laplacian operator in 1D. Moreover, for sake of simplicity, $\widetilde{J}^{(1)}$ has been replaced with $\widetilde{J}$. Parameters and variables of model (4.2.7) are described in Table 4.1.
The following scaled variables

$$t = \widetilde{r}\widetilde{t}, \quad x = \widetilde{x}\sqrt{\frac{\widetilde{r}}{\widetilde{D}}}, \quad M = \frac{\widetilde{M}}{\widetilde{k}_M}, \quad A = \frac{\widetilde{A}}{\widetilde{k}_A}, \quad J = \frac{\widetilde{J}}{\widetilde{k}_M\sqrt{\widetilde{r}\widetilde{D}}}, \tag{4.2.8}$$

State Variable	Description	Unit
$\widetilde{A}(\widetilde{x},\widetilde{t})$	Density of the mosquitoes in aquatic stage at time $\widetilde{t}$ and position $\widetilde{x}$	m^{-2}
$\widetilde{M}(\widetilde{x},\widetilde{t})$	Density of mosquitoes in adult stage at time $\widetilde{t}$ and position $\widetilde{x}$	m^{-2}
$\widetilde{J}(\widetilde{x},\widetilde{t})$	Diffusive flux of adult mosquitoes at time $\widetilde{t}$ and position $\widetilde{x}$	$\mathrm{m}^{-1}\mathrm{day}^{-1}$

Parameter	Description	Unit
$\widetilde{r}$	Intrinsic oviposition rate	day^{-1}
$\widetilde{k}_A$	Carrying capacity of aquatic stage	m^{-2}
$\widetilde{\nu}$	Natural death rate of aquatic stage	day^{-1}
$\widetilde{\gamma}$	Intrinsic maturation rate	day^{-1}
$\widetilde{k}_M$	Carrying capacity of adult stage	m^{-2}
$\widetilde{\mu}$	Natural death rate of adult stage	day^{-1}
$\widetilde{v}$	Wind velocity	mday^{-1}
$\widetilde{D}_0$, $\widetilde{D}_1$	Diffusion coefficients	$\mathrm{m}^2\mathrm{day}^{-1}$
$\widetilde{\tau}$	Relaxation time	day^{-1}

Table 4.1: Description of state variables and parameters of model (4.2.7).

and the dimensionless parameters

$$k=\frac{\widetilde{k}_M}{\widetilde{k}_A},\ \nu=\frac{\widetilde{\nu}}{\widetilde{r}},\ \mu=\frac{\widetilde{\mu}}{\widetilde{r}},\ \gamma=\frac{\widetilde{\gamma}}{\widetilde{r}},\ \tau=\widetilde{r}\widetilde{\tau},\ v=\frac{\widetilde{v}}{\sqrt{\widetilde{r}\widetilde{D}}},\ L=\widetilde{L}\sqrt{\frac{\widetilde{r}}{\widetilde{D}}}, \tag{4.2.9}$$

are introduced. In terms of scaled variables and dimensionless parameters, model (4.2.7) becomes:

$$\begin{aligned}\partial_t A &= k\,(1-A)\,M-(\nu+\gamma)A,\\ \partial_t M+v\partial_x M+\partial_x J &= F_D\nabla^2 M+\frac{\gamma}{k}\,(1-M)\,A-\mu M,\\ \tau\partial_t J+(1-F_D)\partial_x M &= -J,\end{aligned} \tag{4.2.10}$$

with $t>0$, $x\in\Omega=[-L,L]$ and Neumann condition on $M(x,t)$ at the boundary $\partial\Omega$, i.e.

$$\partial_x M=0,\ \text{at } x=-L,L. \tag{4.2.11}$$

From now on, we will refer to this system as a "combined model".

Remarks

- Suppose that $F_D=0$: system (4.2.10) becomes:

$$\begin{aligned}\partial_t A &= k\,(1-A)\,M-(\nu+\gamma)A,\\ \partial_t M+v\partial_x M+\partial_x J &= \frac{\gamma}{k}\,(1-M)\,A-\mu M,\\ \tau\partial_t J+\partial_x M &= -J,\end{aligned}$$

  which is an hyperbolic-reaction-diffusion (HRD) model. This system will be analyzed in Section 4.6 and its hyperbolic structure will allow to avoid the paradox of instantaneous propagation typical of parabolic models.

- Suppose $F_D \in (0,1)$: the combined representation of the Fick and Cattaneo model (4.2.10) is obtained.
- Suppose $F_D = 1$ (and $\tau = 0$). Thus model (4.2.10) can be rewritten as:

$$\begin{aligned} \partial_t A &= k\,(1-A)\,M - (\nu+\gamma)A, \\ \partial_t M + v\partial_x M &= \nabla^2 M + \frac{\gamma}{k}\,(1-M)\,A - \mu M. \end{aligned}$$

This is the parabolic system of equations analyzed in [151] (Takahashi et al).

□

4.3 Analysis of Spatially Homogeneous Dynamics

Let us analyse the spatially homogeneous dynamics described by the following system

$$\begin{aligned} \dot{A} &= k\,(1-A)\,M - (\nu+\gamma)A, \\ \dot{M} &= \frac{\gamma}{k}\,(1-M)\,A - \mu M, \\ \tau\dot{J} &= -J. \end{aligned} \tag{4.3.1}$$

where the over-dot denotes the time derivative.
The last equation is independent of the others and its integration provides

$$J(t) = J_0 e^{-\frac{1}{\tau}t},\ J_0 = J(0), \tag{4.3.2}$$

from which, it is easy to deduce that $J(t) \longrightarrow 0$ as $t \longrightarrow \infty$.
In what follows, the following threshold parameter [151] will be used

$$\mathcal{Q}_0 = \frac{\gamma}{\mu(\nu+\gamma)}, \tag{4.3.3}$$

which clearly arises when equlibria are computed.
In terms of dimensional parameters, the ecological quantity is expressed by

$$\widetilde{\mathcal{Q}}_0 = \frac{\widetilde{\gamma}}{\widetilde{\nu}+\widetilde{\gamma}}\frac{\widetilde{r}}{\widetilde{\mu}},$$

which gives the average number of female mosquitoes produced by one fertile mosquitoto survive the entire aquatic phase and emerge a female mosquito, while the second term $\frac{\widetilde{r}}{\widetilde{\mu}}$ is the average number of viable eggs laid by the emerging female mosquito during its entire lifespan.
It is easy to prove the following result:

Propostion 1 *System* (4.3.1) *always admits the Mosquitoes-Free Equilibrium*

$$\boldsymbol{E}_0 = (0,0,0). \tag{4.3.4}$$

Moreover:
i) if $\mathcal{Q}_0 \leq 1$*, then system* (4.3.1) *has no other equilibria;*
ii) if $\mathcal{Q}_0 > 1$*, then there is a unique endemic equilibrium given by*

$$\boldsymbol{E}_1 = (A_1, M_1, 0) = \left(1 - \frac{1}{\mathcal{Q}_0}\right)\left(\frac{k}{k+\nu+\gamma}, \frac{\gamma}{\gamma + k\mu}, 0\right). \tag{4.3.5}$$

Note that if the average number of female mosquitoes produced by one mosquito is higher than the unit ($\mathcal{Q}_0 > 1$), then the mosquito persist in the colonized region. Moreover, when $\mu > 1$, then $\mathcal{Q}_0$ is always less than 1, for each value of γ and ν. So, if $\mu > 1$, then $\mathcal{Q}_0 < 1$ and there can be no mosquito infestation (as will be seen later). To avoid this case, it is assumed that $0 < \mu < 1$. In this way, $\mathcal{Q}_0$ depends on the value assumed by the parameters $\gamma > 0$, $\nu > 0$, $0 < \mu < 1$.

4.3.1 Stability of Equilibria

The local stability of equilibrium states (4.3.4) and (4.3.5) is given by the analysis of Jacoabian matrix of system (4.3.1) evaluated at the generic steady state $\mathbf{E}^* = (A^*, M^*, 0)$, that is:

$$J(\mathbf{E}^*) = \begin{pmatrix} -\left(\frac{\gamma}{\mu\mathcal{Q}_0} + kM^*\right) & k(1-A^*) & 0 \\ \frac{\gamma}{k}(1-M^*) & -\left(\frac{\gamma}{k}A^* + \mu\right) & 0 \\ 0 & 0 & -1 \end{pmatrix}. \tag{4.3.6}$$

The characteristic polynomial of matrix (4.3.6) is given by:

$$p(\lambda) = -(1+\lambda)\left[\lambda^2 + \left(\mu + \frac{\gamma}{\mu\mathcal{Q}_0} + kM^* + \frac{\gamma}{k}A^*\right)\lambda + \left(kM^* + \frac{\gamma}{\mu\mathcal{Q}_0}\right)\left(\mu + \frac{\gamma}{k}A^*\right) - \gamma(1-A^*)(1-M^*)\right]. \tag{4.3.7}$$

The polinomyal $p(\lambda)$ has always the negative root $\lambda_1 = -1$.

Propostion 2 *The Mosquitoes-Free Equilibrium* $\boldsymbol{E}_0 = (0,0,0)$ *is Locally Asintotically Stable (LAS) iff* $\mathcal{Q}_0 \leq 1$ *and unstable if* $\mathcal{Q}_0 > 1$.

Proof. The polynomial (4.3.7), evaluated at $\mathbf{E}^* = \mathbf{E}_0$, admits the following other real roots

$$\lambda_{2,3} = \frac{1}{2}\left[-\left(\mu + \frac{\gamma}{\mu\mathcal{Q}_0}\right) \pm \sqrt{\left(\mu + \frac{\gamma}{\mu\mathcal{Q}_0}\right)^2 + 4\gamma\left(1 - \frac{1}{\mathcal{Q}_0}\right)}\right], \tag{4.3.8}$$

which are negative if $\mathcal{Q}_0 < 1$. Thus, in this case equilibrium $\mathbf{E}_0$ is LAS for system (4.3.1).
If $\mathcal{Q}_0 > 1$, then polynomial (4.3.7) evaluated at $\mathbf{E}^* = \mathbf{E}_0$ admits one positive root, thus equilirium $\mathbf{E}_0$ is not LAS.
If $\mathcal{Q}_0 = 1$, then $\lambda_2 = 0$ and $\lambda_3 = -\left(\mu + \frac{\gamma}{\mu}\right) < 0$. Thus, $\mathbf{E}_0$ is LAS. □

Propostion 3 *The Mosquitoes-Free Equilibrium* $\boldsymbol{E}_0 = (0,0,0)$ *is Globally Asintotically Stable (GAS) iff* $\mathcal{Q}_0 \leq 1$.

Proof. To prove that the Mosquitoes-Free Equilibrium $\mathbf{E}_0$ is GAS, the following Lyapunov function is defined:

$$\mathcal{V} : \mathbb{R}^3_+ \to \mathbb{R} \ : \ \mathcal{V}(A, M, J) = \frac{\gamma}{\nu + \gamma} A + + kM + J, \tag{4.3.9}$$

which verify the following conditions:
i) $\mathcal{V}(0, 0, 0) = 0$;
ii) $\mathcal{V}(A, M, J) > 0 \, \forall \, (A, M, J) \in \mathbb{R}^3_+$,
and admits the following orbital derivative:

$$\dot{\mathcal{V}}(A, M, J) = -\mu \left[\mathcal{Q}_0 \left(k + \nu + \gamma \right) A + k(1 - \mathcal{Q}_0) \right] M - \frac{J}{\tau}.$$

It is easy to observe that $\dot{\mathcal{V}} < 0$ if $\mathcal{Q}_0 < 1$, while for $\mathcal{Q}_0 = 1$, one obtains $\dot{\mathcal{V}} = 0$ if $J = 0$ and $J = A = 0$. Then the maximal invariant set of system (4.3.1) contained in $\dot{\mathcal{V}} = 0$ is the trivial equilibrium point $\mathbf{E}_0$. Then, the LaSalle-Lyapunov theorem [96] establishes that $\mathbf{E}_0$ is GAS for $\mathcal{Q}_0 \leq 1$. □
Consequently, once the mosquitoes colony is destroyed, even the introduction of a great amount of mosquitoes does not allow the re-colonization.

Propostion 4 *The Endemic Equilibrium* $\boldsymbol{E}_1 = (A_1, M_1, 0)$ *is LAS.*

Proof. The polynomial (4.3.7) evaluated at $\mathbf{E}^* = \mathbf{E}_1$ (defined in (4.3.5)) becomes:

$$p(\lambda) = - \left(1 + \lambda \right) \left(\lambda^2 + \alpha_1 \lambda + \alpha_0 \right), \tag{4.3.10}$$

where

$$\begin{aligned} \alpha_1 &= \gamma + \nu + \mu + \gamma \left(1 - \frac{1}{\mathcal{Q}_0} \right) \frac{k(k + \mu + \nu + \gamma) + \gamma}{(\gamma + k\mu)(k + \nu + \gamma)}, \\ \alpha_0 &= \gamma \left(1 - \frac{1}{\mathcal{Q}_0} \right). \end{aligned}$$

Since $\mathcal{Q}_0 > 1$, then $\alpha_1 > 0$ and $\alpha_0 > 0$. Thanks to Routh-Hurwitz criterion for second-degree polynomials, we can state that $\mathbf{E}_1$ is LAS. □
In conclusion, when $\mathcal{Q}_0 > 1$, then the trivial equilibrium $\mathbf{E}_0$ is unstable and and the non trivial equilibrium $\mathbf{E}_1$ is LAS; the infestation by mosquitoes becomes the stable situation. This situation is showed in Figure 4.2.
Stability result is in agreement also with numerical solutions of system (4.2.10) shown in Fig. 4.3. Both for aquatic and adult stage, the initial condition is taken as bounded support functions and zero Neumann condition were used at boundary for adult mosquitoes and flux. The solutions evolve in time approaching to the stable equilibrium $\mathbf{E}_1$. In particular three wind situations are considered.

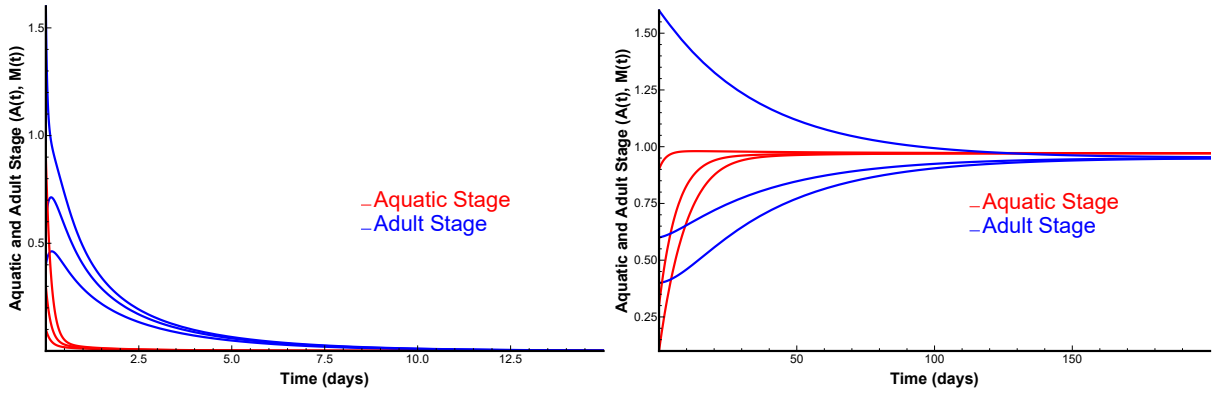

(a) (b)

Figure 4.2: Numerical solutions of system (4.3.1) for $A(t)$ (red line) and $M(t)$ (blue line) with parameters listedin Table 4.1. In left panel $\mathcal{Q}_0 < 1$; in right panel $\mathcal{Q}_0 > 1$.

4.4 Traveling Waves in The Combined Model

Now, in order to study mosquito infestation process in an environment that lacks it, possible heteroclinic connections between $\mathbf{E}_0$ and $\mathbf{E}_1$ are searched.
Traveling wave solutions will be searched for in the following form:

$$z = x - ct, \quad a(z) = A(x,t), \quad m(z) = M(x,t), \quad j(z) = J(x,t), \tag{4.4.1}$$

where c is the positive constant invasion velocity and $a(z)$, $m(z)$ and $j(z)$ are the wave profiles. Substituting Eq. (4.4.1) into (4.2.10), the following system of ordinary differential equations is obtained:

$$\begin{aligned} ca' + k(1-a)m - (\nu+\gamma)a &= 0, \\ F_D m'' + (c-v)m' - j' + \tfrac{\gamma}{k}(1-m)a - \mu m &= 0, \\ \tau c j' + (1-F_D)m' - j &= 0, \end{aligned} \tag{4.4.2}$$

with the boundary conditions:

$$\begin{aligned} a(-\infty) &= A_1, \quad a(+\infty) = 0, \\ m(-\infty) &= M_1, \quad m(+\infty) = 0, \\ j(-\infty) &= 0, \quad j(+\infty) = 0. \end{aligned} \tag{4.4.3}$$

In (4.4.2) the prime denotes derivative with respect to the z variable.
The boundary value problem (4.4.2) and (4.4.3) is defined in the interval $(-\infty, +\infty)$ and so its solutions can be interpreted geometrically as heteroclinic trajectories of the dynamical system (4.4.2) in the three-dimensional phase space (a, m, j) linking two different singular points. Let us suppose that the biological parameter $\mathcal{Q}_0 > 1$, for the existence of both equilibrium states. Of course, as can be deduced from the previous section, in this case equilibrium $\mathbf{E}_0$ is stable and equilibrium $\mathbf{E}_1$ is unstable with respect to the model (4.4.2): thus, $\mathbf{E}_0$ admits a stable (incoming) manifold and $\mathbf{E}_1$ an unstable (departing) manifold. Therefore, a traveling wave solution starting from $\mathbf{E}_1$ and reaching $\mathbf{E}_0$ may exist. It is known that, for

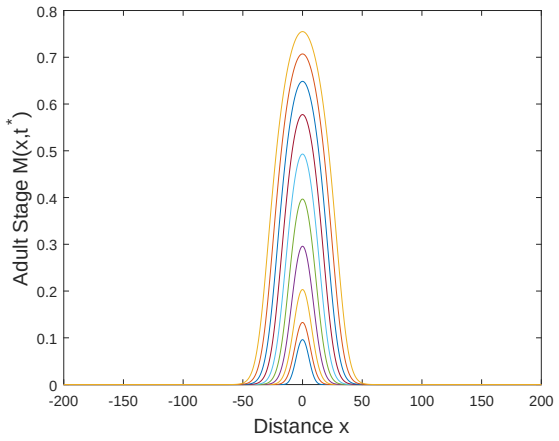

(a) $\widetilde{v} = 0$

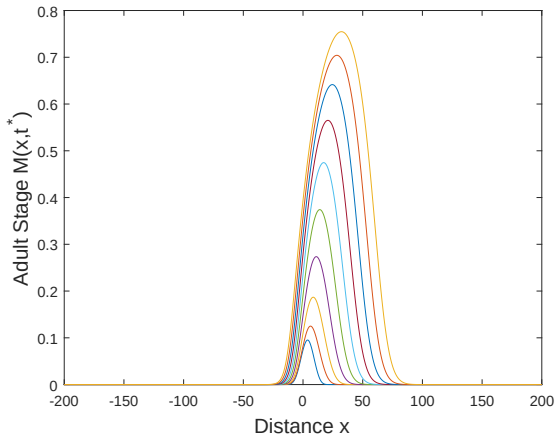

(b) $\widetilde{v} = 4$

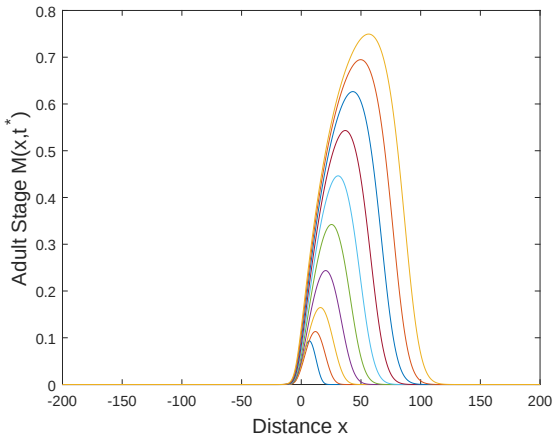

(c) $\widetilde{v} = 7$

Figure 4.3: Numerical solutions of system (4.2.10) $M(x,t)$. Parameters value used are listed in Table 4.1 with $\widetilde{\tau} = 0.04$ and $L = 200$. Moreover $\widetilde{v} = 0$ (a), $\widetilde{v} = 4$ (b) and $\widetilde{v} = 7$ (c).

classical parabolic system (as described in [162]), in the monostable case (one stable equilibrium and the other unstable), monotone waves exist for a right interval of velocity values. Now, the minimal speed for which such waves exist for our model is estimated.

At the origin $\mathbf{E}_0$ the characteristic polynomial of the appropriate Jacobian matrix is given by:

$$p_C(\xi, c) = \xi^4 + a_{3C}\xi^3 + a_{2C}\xi^2 + a_{1C}\xi + a_{0C}, \tag{4.4.4}$$

where

$$\begin{aligned} a_{3C} &= \frac{\tau c(c-v) - \tau F_D(\gamma+\nu) - 1}{\tau c F_D}, \\ a_{2C} &= \frac{\gamma+\nu+cv[1+\tau(\gamma+\nu)] - c^2[1+\tau(\gamma+\mu+\nu)]}{\tau c^2 F_D}, \\ a_{1C} &= \frac{c\left[\gamma+\mu+\nu-\tau\mu(\gamma+\nu)\left(\mathcal{Q}_0-1\right)\right] - v(\gamma+\nu)}{\tau c^2 F_D}, \\ a_{0C} &= \frac{\mu(\gamma+\nu)}{\tau c^2 F_D}\left(\mathcal{Q}_0-1\right). \end{aligned} \tag{4.4.5}$$

Owing to the biological meaning of A, M and J, we cannot expect any temporally oscillating solution around $\mathbf{E}_0$, then all solutions of (4.4.4) must be real. Thus, following [90], the following quantities are defined

$$\begin{aligned} &H = 8a_{2C} - 3a_{3C}^2, && F = 16a_{2C}^2 + 3a_{3C}^4 - 16a_{2C}a_{3C}^2 - 64a_{0C} + 16a_{3C}a_{1C}, \\ &I = a_{2C}^2 + 12a_{0C} - 3a_{1C}a_{3C}, && J = 72a_{2C}a_{0C} + 9a_{1C}a_{2C}a_{3C} - 2a_{2C}^3 - 27a_{1C}^2 - 27a_{0C}a_{3C}^2, \\ &\Delta = 4I^3 - J^2. \end{aligned} \tag{4.4.6}$$

The solutions of equation (4.4.4) are real iff [90]

$$H(c) < 0, \quad F(c) > 0, \quad \Delta(c) \geq 0. \tag{4.4.7}$$

Simply noting that, the leading coefficients of the above quantities are given by:

$$\begin{aligned} &lc(H(c)) = -3\tau^2 < 0, \\ &lc(F(c)) = 3\tau^4 > 0, \\ &lc(\Delta(c)) = 27\tau^2\left[\gamma^2 + (\mu-\nu)^2 + 2\gamma\left(2-\mu+\nu\right)\right]\left[\tau\gamma\left(\tau\left(\mu-1\right)-1\right) + \left(\tau\mu-1\right)\left(\tau\nu-1\right)\right]^2 > 0, \end{aligned}$$

then, it is easy to deduce that

$$\lim_{c\longrightarrow\infty} H(c) = -\infty, \quad \lim_{c\longrightarrow\infty} F(c) = \infty, \quad \lim_{c\longrightarrow\infty} \Delta(c) = \infty.$$

Therefore, ecologically realistic traveling wave fronts are possible only for

$$c \geq c_{min}^C = \max\{c^{(1)}, c^{(2)}, c^{(3)}\}, \tag{4.4.8}$$

where

$$\begin{aligned} c^{(1)} &= \max_j \{c_j \in \mathbb{R} \mid H(c_j) = 0\}, \\ c^{(2)} &= \max_j \{c_j \in \mathbb{R} \mid F(c_j) = 0\}, \\ c^{(3)} &= \max_j \{c_j \in \mathbb{R} \mid \Delta(c_j) = 0\}. \end{aligned} \tag{4.4.9}$$

If the restriction $c \geq c_{min}^C$ for the speed c is satisfied, a travelling wave solution of velocity c connecting equilibrium $\mathbf{E}_1$ and equilibrium $\mathbf{E}_0$ may exist $\forall\, c \in [c_{min}^C, +\infty[$, i.e. solutions of equations (4.4.2) on the real line $]-\infty, +\infty[$ satisfying conditions (4.4.3) of the form $a(x-ct)$, $m(x-ct)$ and $j(x-ct)$ may exist.

Thus a possible range of speeds due to linearization at the stationary point is given. Note that Volpert *et al* [162] demonstrated for parabolic systems without advection that monotone waves exist for a right interval of speed value, in monostable case. Even for the combined case (4.2.10), monotone waves can exist for a right interval of speed values. As with parabolic systems, the speed of waves can be infinite for the combined model. The existence of this type of solutions is supported by extensive numerical simulations.

The numerical solution of model (4.2.10) is shown in Figure 4.4, obtained choosing as initial data a bounded support function that link the two singular points. Note that each trace evolve in time as an advancing wave front and the shape is unchanged during the propagation. The speed of these waves is exactly the minimal. In Figure 4.5 the possible behaviour of the minimal wave speed c^C_{min} (defined in (4.4.8))

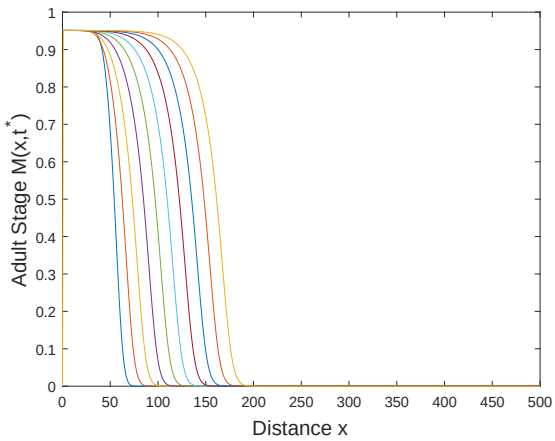

(a)

Figure 4.4: Wave propagation for Adult Mosquitoes $M(x,t)$ for system (4.2.10) at different time steps. Parameters value listed in Fig. 4.2(b) with $F_D = 0.5$ and $v = 5.2 \cdot 10^{-2}$ with minimal speed $c^C_{min} = 0.455716$.

is shown as function of coefficient F_D and velocity v, while in Figure 4.6 the speed c^C_{min} is a function of the diffusion coefficients $\widetilde{D}_0$ and $\widetilde{D}_1$. For small values of v there is a sudden increase in the value of c^C_{min}. If v and F_D increase simultaneously, c^C_{min} also increases. From the graphs (a) and (b) in Figure 4.6 we can deduce that the minimum velocity c^C_{min} decreases (very slowly) as the diffusion coefficients $\widetilde{D}_0$, $\widetilde{D}_1$ increase.

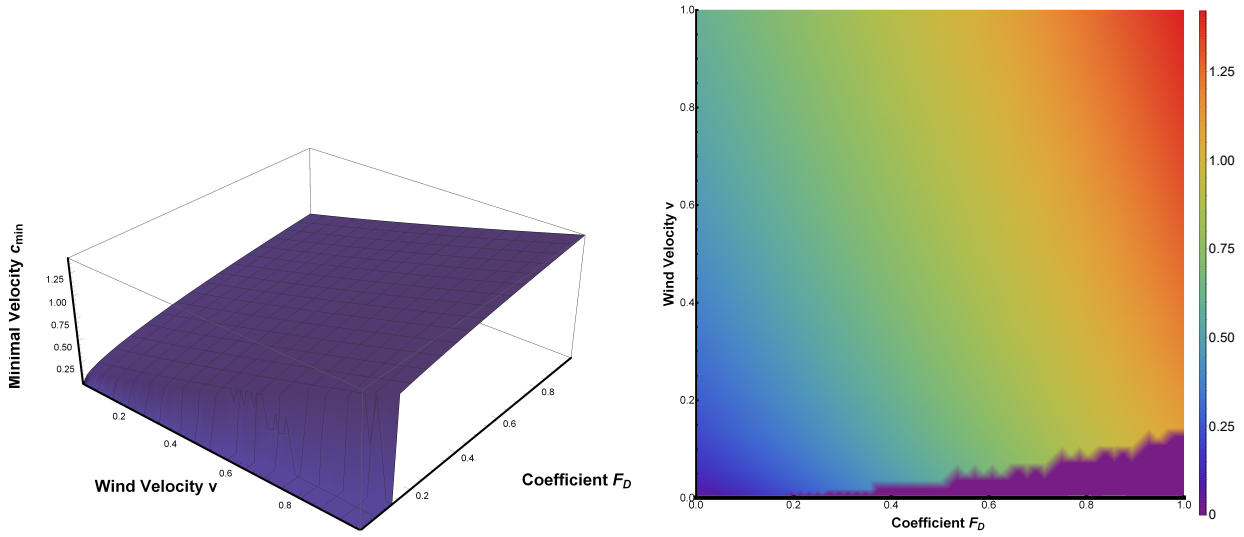

(a) (b)

Figure 4.5: Possible representation of minimal traveling wave speed c^C_{min} given in (4.4.8) as function of v and F_D. Parameters value are listed in in Fig. 4.2(b).

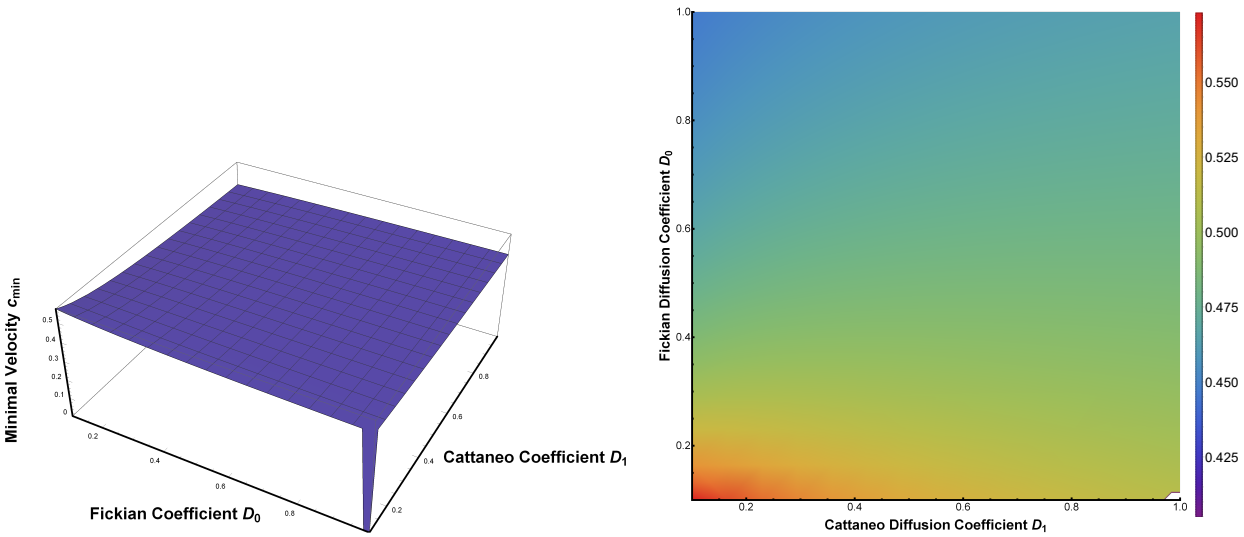

(a) (b)

Figure 4.6: Possible representation of minimal traveling wave speed c^C_{min} given in (4.4.8) as function of $\widetilde{D}_0$ and $\widetilde{D}_1$. Parameters value are listed in Fig. 4.2(b) with $v = 5.2 \cdot 10^{-2}$.

4.5 The classical parabolic model

In this section, the limit case of system (4.2.10) in which $F_D \to 1$ and $\tau \to 0$ is analyzed: as already observed in section 4.2, the total diffusive flux obeys at Fick's law, according to the main idea of Classical Thermodynamics.

The resulting parabolic model

$$\begin{aligned} \partial_t A &= k\,(1-A)\,M - (\nu+\gamma)A, \\ \partial_t M + v\partial_x M &= \nabla^2 M + \frac{\gamma}{k}\,(1-M)\,A - \mu M. \end{aligned} \tag{4.5.1}$$

was studied by Takahashi et al. [151] Of course, the linear stability analysis of the corresponding spatially omogeneous system of (4.5.1) has already been carried out in the section 4.3. Indeed, the numerical simulations in Figure 4.7 show that the numerical solutions of system (4.5.1) approach the equilibrium state $\mathbf{E}_1$ when $\mathcal{Q}_0 > 1$. For both aquatic and adult phases, the initial conditions are function with a bounded support, while zero Neumann condition at the boundary were taken for adult stage and flux. In particular three wind situations are considered.

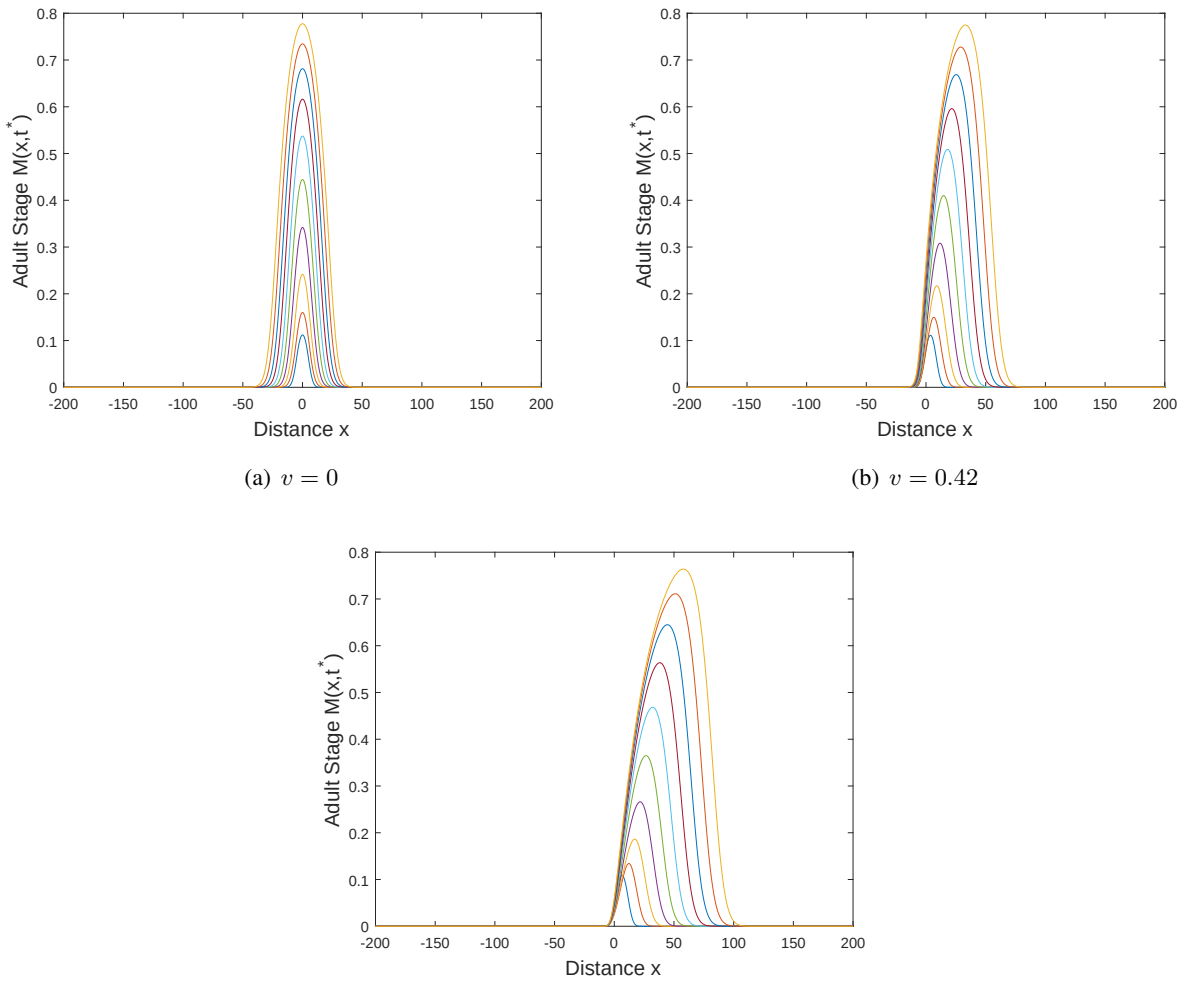

(a) $v = 0$

(b) $v = 0.42$

(c) $v = 0.73$

Figure 4.7: Numerical solutions of system (4.5.1) for adult mosquitoes $M(x,t)$ at different time steps. Parameters value used are listed in Figure 4.2 with $\tau = 0$ and $F_D = 1$ ($\widetilde{D}_1 = 0$).

In this section, possible heteroclinic connections between $\mathbf{E}_0$ and $\mathbf{E}_1$ are searched for the parabolic system (4.5.1). Substituting Eq. (4.4.1) into (4.5.1), the following system of ordinary differential equations is obtained:

$$\begin{aligned} ca' + k(1-a)m - (\nu+\gamma)a &= 0, \\ F_D m'' + (c-v)m' + \frac{\gamma}{k}(1-m)\,a - \mu m &= 0, \end{aligned} \tag{4.5.2}$$

(4.5.3)

Note that the system (4.5.2) just written can be obtained from the system (4.4.2) by placing $F_D = 1$ and $\tau = 0$.

At the origin $\mathbf{E}_0$, Takahashi et al. in [151] found the characteristic polynomial of the appropriate Jacobian matrix, that is given by the following c-family of λ polynomials

$$p_P(\xi, c) = -\xi^3 + a_{2P}\xi^2 + a_{1P}\xi + a_{0P}, \tag{4.5.4}$$

where

$$\begin{aligned} a_{2P} &= \frac{\gamma+\nu}{c} + v - c, \\ a_{1P} &= \mu - (v-c)\frac{\gamma+\mu}{c}, \\ a_{0P} &= \frac{\gamma}{c} - \mu\frac{\gamma+\nu}{c}. \end{aligned} \tag{4.5.5}$$

Note that both the polynomial (4.5.4) and the coefficients (4.5.5) just written turn out to be the special case of (4.4.4) and (4.4.5) respectively, when $F_D = 1$ and $\tau = 0$. Indeed, from the characteristic polynomial (4.4.4), we can write:

$$\tau c F_D p_C(\xi, c) = \tau c F_D \xi^4 + \tau c F_D a_{3C}\xi^3 + \tau c F_D a_{2C}\xi^2 + \tau c F_D a_{1C}\xi + \tau c F_D a_{0C} \tag{4.5.6}$$

Therefore, in the limit $F_D \to 1$ and $\tau \to 0$, it follows that:

$$p_P(\xi, c) = \lim_{F_D\to 0, \tau\to 0} \tau c F_D p_C(\xi, c) = a_{3P}\xi^3 + a_{2P}\xi^2 + a_{1P}\xi + a_{0P}, \tag{4.5.7}$$

with

$$\begin{aligned} \lim_{F_D\to 0, \tau\to 0} \tau c F_D &= 0 \\ a_{3P} = \lim_{F_D\to 0, \tau\to 0} \tau c F_D a_{3C} &= -1, \\ a_{2P} = \lim_{F_D\to 0, \tau\to 0} \tau c F_D a_{2C} &= \frac{\gamma+\nu}{c} + v - c, \\ a_{1P} = \lim_{F_D\to 0, \tau\to 0} \tau c F_D a_{1C} &= \mu - (v-c)\frac{\gamma+\mu}{c}, \\ a_{0P} = \lim_{F_D\to 0, \tau\to 0} \tau c F_D a_{0C} &= \frac{\gamma}{c} - \mu\frac{\gamma+\nu}{c} = \mu\frac{\gamma+\nu}{c}\left(\mathcal{Q}_0 - 1\right). \end{aligned} \tag{4.5.8}$$

Through geometric methods, Takahashi et al. [151] provide an estimate of the minimal speed associated with waves, solutions of the system (4.5.2).
By imposing that the polynomial (4.5.4) has all real roots, in particular one positive and two negative (from $a_{0P} > 0$) , they define as the minimal speed (denoted by c_m in their work and c^P_{min} in this paper) the smallest root (if it exists) of the second degree polynomial obtained by (4.5.4) deriving with respect to c. If c is greater than this value, then may exist waves that do not oscillate around $\mathbf{E}_0$ and that bind the two equilibria (as reported in Figure 4.8).

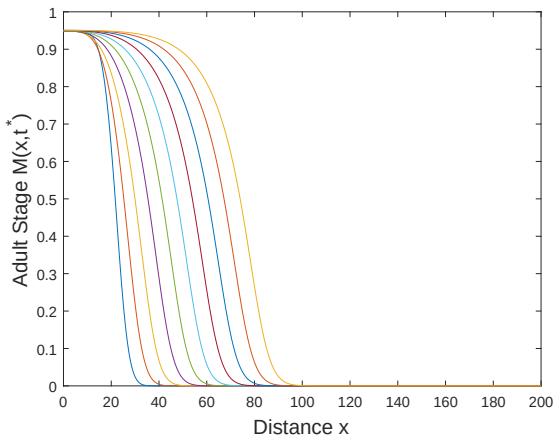

(a)

Figure 4.8: Wave propagation for Adult Mosquitoes $M(x,t)$ for system (4.5.2) at different time steps. Parameters value listed in Fig. 4.2 with $v = 5.2 \cdot 10^{-2}$, $F_D = 0.5$ and minimal speed $c^P_{min} = 0.491748$.

4.6 The Limiting Hyperbolic Model

In this section, the limit case of system (4.2.10) in which $F_D \to 0$ is analyzed: as already observed in section 4.2, the diffusive flux J is a new field variable satisfying a transport equation of Cattaneo type, according to the main idea of ET [120] and EIT [97]. The Fickian propagation is completely negleted and the only contribution to the diffusion flow is given by the equation of evolution assigned for J.
The resulting model obtained is:

$$\begin{aligned} \partial_t A &= k(1-A)M - (\nu+\gamma)A, \\ \partial_t M + v\partial_x M + \partial_x J &= \frac{\gamma}{k}(1-M)A - \mu M, \\ \tau\partial_t J + \partial_x M &= -J, \end{aligned} \tag{4.6.1}$$

with $t > 0$, $x \in \Omega = [-L, L]$, $L > 0$ and Neumann boundary conditions as defined in (4.2.11). The model can be recast in the compact form

$$\mathbf{U}_t + G\mathbf{U}_x = \mathbf{B}(\mathbf{U}), \tag{4.6.2}$$

where

$$\mathbf{U} = \begin{pmatrix} A \\ M \\ J \end{pmatrix}, \quad G = \begin{pmatrix} 0 & 0 & 0 \\ 0 & v & 1 \\ 0 & \frac{1}{\tau} & 0 \end{pmatrix}, \quad \mathbf{B}(\mathbf{U}) = \begin{pmatrix} k(1-A)M - (\nu+\gamma)A \\ \frac{\gamma}{k}(1-M)A - \mu M \\ -\frac{1}{\tau}J \end{pmatrix}. \tag{4.6.3}$$

The characteristic velocities associated to the system (4.6.2) are given by:

$$\lambda_{1,3} = \frac{1}{2\tau}\left(\tau v \mp \sqrt{\tau(\tau v^2 + 4)}\right), \ \lambda_2 = 0, \tag{4.6.4}$$

whose reality is ensured, while the corresponding right and left eigenvectors associated are:

$$\mathbf{d}_{1,3} = \begin{pmatrix} 0 \\ \tau\lambda_{1,3} \\ 1 \end{pmatrix}, \quad \mathbf{d}_2 = \mathbf{l}_2^T = \begin{pmatrix} 1 \\ 0 \\ 0 \end{pmatrix}, \quad \mathbf{l}_{1,3}^T = \begin{pmatrix} 0 \\ \lambda_{1,3} \\ 1 \end{pmatrix}, \tag{4.6.5}$$

so the model (4.6.2) is strictly hyperbolic.
Of course, the linear stability analysis of the corresponding spatially omogeneous system of (4.6.2) has already been carried out in the section 4.3. Indeed, the numerical simulations in Figure 4.9 show that the numerical solutions of system (4.6.2) approach the equilibrium state $\mathbf{E}_1$ when $\mathcal{Q}_0 > 1$. For both aquatic and adult phase, the initial conditions are function with a bounded support, while zero Neumann condition at the boundary were taken for adult stage and and flux. In particular three wind situations are considered. The comparison between Figure 4.3 and Figure 4.9 is shown in Figure 4.10.

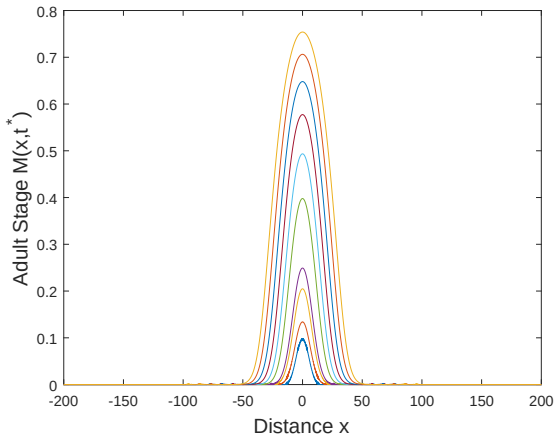

(a) $v = 0$

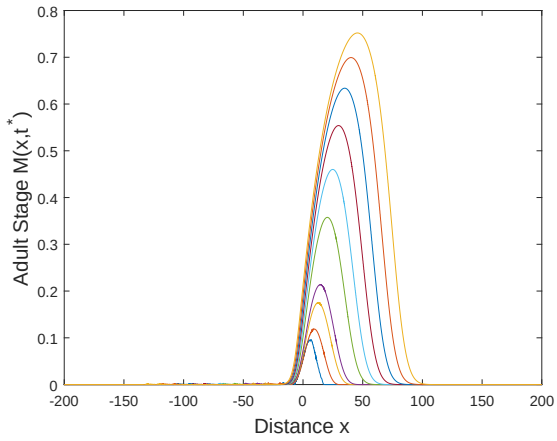

(b) $v = 0.42$

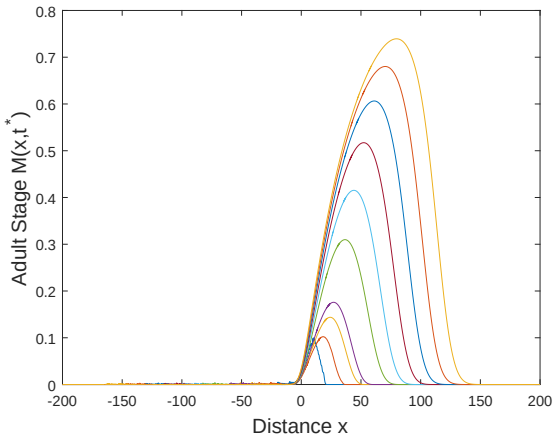

(c) $v = 0.73$

Figure 4.9: Numerical solutions of system (4.6.2) for adult mosquitoes $M(x,t)$ at different time steps. Parameters value used are listed in Figure 4.2 with $F_D = 0$ ($\widetilde{D}_0 = 0$).

4.6.1 Traveling Waves in the Limiting Hyperbolic Model

Now, possible heteroclinic connections between $\mathbf{E}_0$ and $\mathbf{E}_1$ are searched for the hyperbolic system (4.6.1). Substituting Eq. (4.4.1) into (4.6.1), the following system of ordinary differential equations is obtained:

$$\begin{aligned} ca' + k(1-a)m - (\nu+\gamma)a &= 0, \\ (c-v)m' - j' + \frac{\gamma}{k}(1-m)\,a - \mu m &= 0, \\ c\tau j' - m' - j &= 0. \end{aligned} \tag{4.6.6}$$

Note that the system (4.6.6) just written can be obtained directly from the system (4.4.2) by placing $F_D = 0$. If c is different from the characteristic velocities defined in (4.6.4), the system (4.6.6) can be recast in the compact form

$$\mathbf{U}'(z) = (\nabla\mathbf{F} - cI)^{-1}\,\mathbf{B}\left(\mathbf{U}(z)\right), \tag{4.6.7}$$

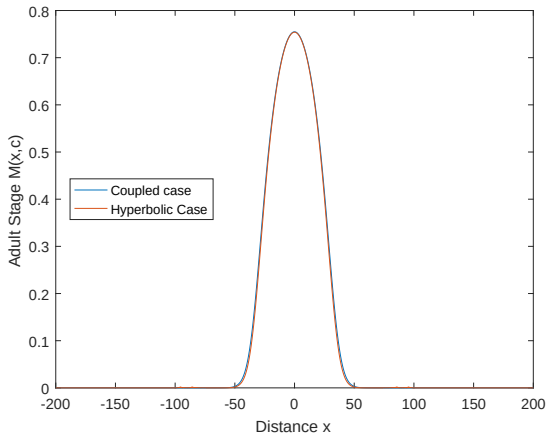

(a) $v = 0$

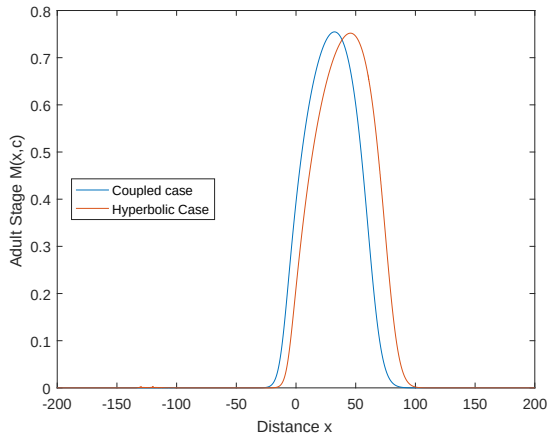

(b) $v = 0.42$

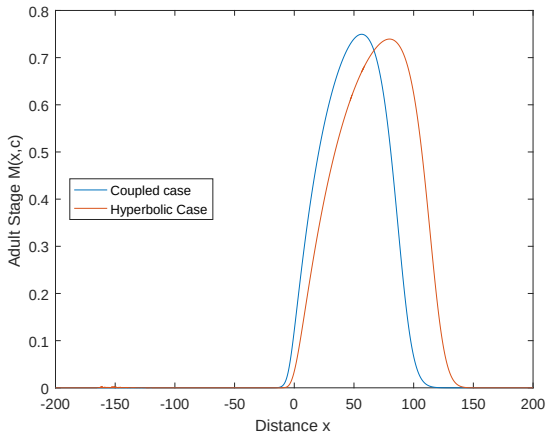

(c) $v = 0.73$

Figure 4.10: Numerical solutions of combined model (4.2.10) (blue line) and hyperbolic model (4.6.2) (brown line) for $M(x,t)$ at fixed time step. Comparison between Figure 4.3 and Figure 4.9.

where I is the identity matrix, $\mathbf{F}(z) = G\mathbf{U}(z)$, $\nabla = \partial_{\mathbf{U}}$, with the boundary conditions

$$\lim_{z\to-\infty} \mathbf{U}(z) = \mathbf{E}_1, \quad \lim_{z\to+\infty} \mathbf{U}(z) = \mathbf{E}_0, \tag{4.6.8}$$

$$\lim_{z\to-\infty} \mathbf{U}'(z) = 0, \quad \lim_{z\to+\infty} \mathbf{U}'(z) = 0. \tag{4.6.9}$$

The equation

$$\phi(c) \equiv det\,(\nabla\mathbf{F} - cI) = \frac{c[\tau c(c-v)-1]}{\tau} = 0, \tag{4.6.10}$$

defines a locus of irregular singular points usually named *singular barrier* [57], along which the solutions of (4.6.7) exhibit singularities. A smooth traveling wave connecting two equilibria may exist if they lie in the interior of the region bounded by the singular barrier [23, 57]. Indeed, since

$$\phi(c)\,|_{\mathbf{E}_0}\phi(c)|_{\mathbf{E}_1} = \left(\frac{c[\tau c(c-v)-1]}{\tau}\right)^2 > 0,$$

it can never happen that the barrier $\phi(c)$ lies between the equilibria $\mathbf{E}_0$ and $\mathbf{E}_1$ [23, 57]. Therefore, the equilibria are always on the same side with respect to the barrier $\phi(c)$. They lie in the inner region if $\phi(c) < 0$, i.e. if the speed c is lies between the characteristic speeds λ_2 and λ_3 defined in (4.6.4), while the two equilibria lie in the outer region if $\phi(c) > 0$, i.e. c is larger than λ_3. In addition, if λ^{max} is the greatest of the characteristic velocities of the system (4.6.1), Boillat and Ruggeri [23] proved that a continous traveling wave with velocity $c > \lambda^{max}$ does not exist. So that, a continous shock wave structure propagating with velocity c greater than the maximum characteristic speed λ_3 defined in (4.6.4) cannot exist, i.e. smooth solutions may exist only if $c \leq \lambda_3$.

Thus, a C^1 traveling wave solution may exist for system (4.6.7) with boundary conditions (4.6.9) only if c is less than the characteristic speed λ_3 defined in (4.6.4). Therefore, the value λ_3 defines the range of validity of the hyperbolic model (4.6.1), so we assume $c < \lambda_3$.

Now, the minimal speed such that may exist a monotone traveling wave connecting equilibria $\mathbf{E}_0$ and $\mathbf{E}_1$, is estimated. At the origin $\mathbf{E}_0$, the characteristic polynomial of the appropriate Jacobian matrix is given by the following c-family of λ polynomials

$$p_H(\xi, c) = \xi^3 + a_{2H}\xi^2 + a_{1H}\xi + a_{0H}, \tag{4.6.11}$$

where

$$\begin{aligned} a_{2H} &= \frac{\gamma + \nu + cv[1 + \tau(\gamma + \nu)] - c^2[1 + \tau(\gamma + \mu + \nu)]}{\tau\phi(c)}, \\ a_{1H} &= \frac{c[\gamma + \mu + \nu - \tau\mu(\gamma + \nu)(\mathcal{Q}_0 - 1)] - v(\gamma + \nu)}{\tau\phi(c)}, \\ a_{0H} &= \mu(\gamma + \nu)\frac{\mathcal{Q}_0 - 1}{\tau\phi(c)}. \end{aligned} \tag{4.6.12}$$

Note that both the polynomial (4.6.11) and the coefficients (4.6.12) just written turn out to be the special case of (4.4.4) and (4.4.5) respectively, when $F_D = 0$. Indeed, from the characteristic polynomial (4.4.4), we can write:

$$\begin{aligned} \frac{F_D c^2}{\phi(c)} p_C(\xi, c) &= \frac{F_D c^2}{\phi(c)}\xi^4 + \frac{c}{\tau\phi(c)}\left\{c\tau(c - v) - 1 - \tau(\gamma + \nu)F_D\right\}\xi^3 \\ &+ \frac{(\gamma + \nu) + cv[1 + \tau(\gamma + \nu)] - c^2[1 + \tau(\gamma + \nu + \mu)]}{\tau\phi(c)}\xi^2 \\ &+ \frac{c[\gamma + \nu + \mu - \tau\mu(\gamma + \nu)(\mathcal{Q}_0 - 1)] - v(\gamma + \nu)}{\tau\phi(c)}\xi \\ &+ \frac{\mu(\gamma + \nu)}{\tau\phi(c)}(\mathcal{Q}_0 - 1). \end{aligned} \tag{4.6.13}$$

Therefore, in the limit $F_D \to 0$ and $DF_D \to 1$, it follows that:

$$\begin{aligned}
\lim_{F_D\to 0} \frac{F_D c^2}{\phi(c)} p_C(\xi, c) &= p_H(\xi, c), \\
\lim_{F_D\to 0} \frac{F_D c^2}{\phi(c)} &= 0, \\
\lim_{F_D\to 0} \frac{c}{\tau\phi(c)} \{c\tau(c-v) - 1 - \tau(\gamma+\nu)F_D]\} = \lim_{F_D\to 0} \frac{F_D c^2 a_{3C}}{\phi(c)} &= 1, \\
\lim_{F_D\to 0} \frac{(\gamma+\nu) + cv[1+\tau(\gamma+\nu)] - c^2[1+\tau(\gamma+\nu+\mu)]}{\tau\phi(c)} = \lim_{F_D\to 0} \frac{F_D c^2 a_{2C}}{\phi(c)} &= a_{2H}, \\
\lim_{F_D\to 0} \frac{c[\gamma+\nu+\mu-\tau\mu(\gamma+\nu)(\mathcal{Q}_0-1)] - v(\gamma+\nu)}{\tau\phi(c)} = \lim_{F_D\to 0} \frac{F_D c^2 a_{1C}}{\phi(c)} &= a_{1H}, \\
\lim_{F_D\to 0} \frac{\mu(\gamma+\nu)}{\tau\phi(c)}(\mathcal{Q}_0-1) = \lim_{F_D\to 0} \frac{F_D c^2 a_{0C}}{\phi(c)} &= a_{0H}.
\end{aligned}$$

Owing to the biological meaning of A, M and J, we cannot expect any temporally oscillating solution around $\mathbf{E}_0$, then all solutions of (4.6.11) must be real and this is ensured iff [159]

$$\Delta(c) = a_{2H}^2 a_{1H}^2 + 18 a_{1H} a_{2H} a_{0H} - 4a_{1H}^3 - 4a_{0H} a_{2H}^3 - 27 a_{0H}^2 \geq 0. \tag{4.6.14}$$

Since the leading coefficient of the above discriminant, i.e.

$$lc(\Delta(c)) = \left[\gamma^2 + (\mu-\nu)^2 + \gamma(4-2\mu+2\nu)\right]\left[\gamma\tau(-1+(-1+\mu)\tau) + (-1+\ \mu\tau)(-1+\nu\tau)\right]^2 > 0,$$

is always positive, it can be easily deduced that $\lim_{c\to\infty} \Delta(c) = \infty$. Therefore, ecologically realistic traveling wave fronts are possible only for

$$c \geq c_{min}^H = \max_j \{c_j \in \mathbb{R}^+ \mid \Delta(c_j) = 0\}. \tag{4.6.15}$$

Later simulations suggest that the value just deduced c_{min}^H is a special case of the value c_{min}^C defined in (4.4.8) when $F_D \longrightarrow 0$.

Thus, a travelling wave solution of velocity c may exist, $\forall\ c \in [c_{min}^H, \lambda_3[$, connecting equilibrium $\mathbf{E}_1$ and equilibrium $\mathbf{E}_0$, i.e. functions $a(x-ct)$, $m(x-ct)$ and $j(x-ct)$ solutions of equation (4.6.6) on the real line $]-\infty, +\infty[$ and satisfying equation (4.4.3).
The hyperbolic structure of the system (4.6.2) allows to avoid the paradox of wave propagation at infinite speed.
Figure 4.11 shows the numerical solution of model (4.6.1) obtained as initial data a function with bounded support that link the two singular points. Propagation of monotone continuous waves at minimal speed can be seen. Figure 4.12 shows the possible behaviour of the minimal wave speed c_{min}^H defined in (4.6.15) as function of relaxation time τ and velocity v. It is clear that c_{min}^H is an increasing function of τ, while if τ is fixed, it seems that c_{min}^H is a constant function in v.

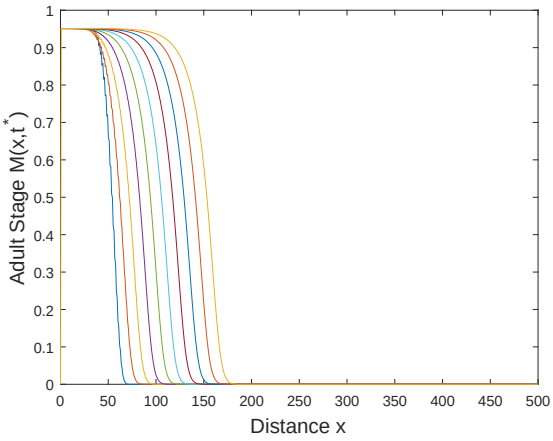

(a)

Figure 4.11: Numerical solutions of system (4.6.1) for adult mosquitoes $M(x,t)$ at different time steps. Parameters value are listed in Fig. 4.2 with $v = 5.2 \cdot 10^{-2}$ and $F_D = 0.5$. Propagation of waves at minimal velocity $c^H_{min} = 0.421655$.

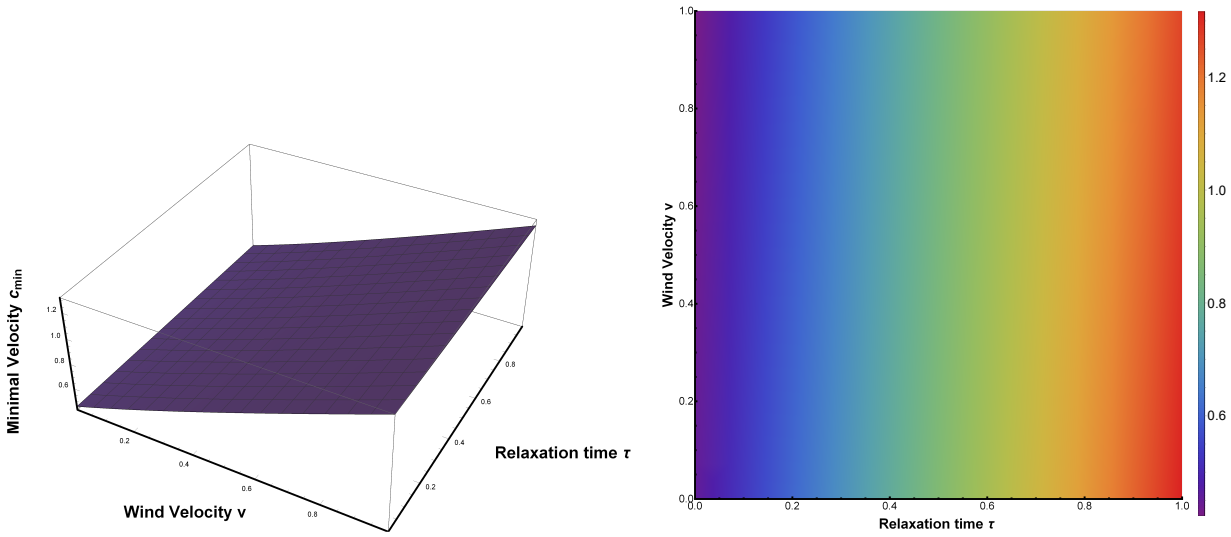

(a) (b)

Figure 4.12: Possible representation of minimal traveling wave speed c^H_{min} given in (4.6.15) as function of v and τ. Parameters value are listed in Fig. 4.2 ($F_D = 0$).

4.7 Numerical Comparison

We now show the numerical solution obtained from the integration of system (4.2.10) for different values of the parameter F_D.

The main feature of our model is the capability of reproducing both Fickian and non-Fickian behavior according to the values of F_D: indeed both the numerical solution of the hyperbolic model corresponding to the system (4.6.1) and the solution of the classical parabolic model ([151]) corresponding to the system (4.5.1)

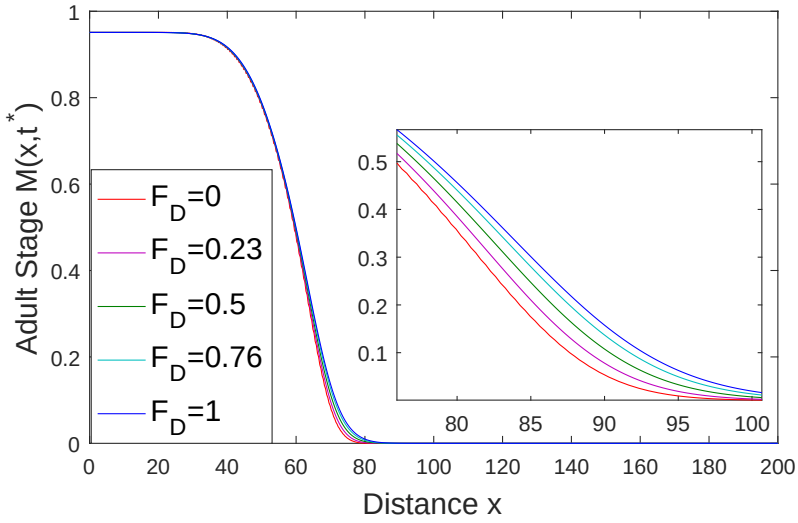

(a)

Figure 4.13: Comparison between numerical solutions of system (4.2.10) for the variable $M(x,t)$ at fixed time step with $F_D = 0$ (red line - hyperbolic limiting model corresponding to system (4.6.1)), $F_D = 0.26$ (magenta line), $F_D = 0.5$ (green line), $F_D = 0.76$ (cyan line) and $F_D = 1$ (blue line - classical parabolic model correspoding to (4.5.1)). Parameters value are listed in Fig. 4.2(b) with $v = 5.2 \cdot 10^{-2}$.

can be obtained as limiting cases. As can be seen from Figure 4.13, when F_D is very small a non-Fickian transport phenomenon is actually observed: slow diffusion process and relaxation appear. In this case, the solution of the model (4.2.10) approaches the solution of the limiting hyperbolic model corresponding to the system (4.6.1). For intermediate values of F_D, the model (4.2.10) represented a compromise between the classical parabolic model and the limiting hyperbolic model, since both diffusion processes coexist and overlap simultaneously. When the parameter F_D reaches its maximum value ($F_D = 1$) the model reproduces Fickian diffusion. In this case, the solution of the model (4.2.10) is very close to the solution of the parabolic system in literature [151].

Figure 4.14 shows the numerical comparison between the minimal speed in the combined model c^C_{min} obtained in (4.4.8), the minimal speed in the hyperbolic model c^H_{min} deduced in (4.6.15) and the minimal speed in the parabolic model (that in this dissertation is denoted by c^P_{min}), deduced in [151], as function of the wind velocity v in (a) panel, of adult mosquitoes maturation rate γ in (b) panel and of diffusion coeffient $\widetilde{D}_1$ in (c) panel. The simulations suggest that, once all the other parameters have been set, these speeds are increasing functions of both v and γ and decreasing of $\widetilde{D}_1$. It seems that the minimal speeds always retain their order of magnitude given by $c^H_{min} \leq c^C_{min} \leq c^P_{min}$.

As we have already observed in the previous figure in the case of trajectories, even the minimal speed c^C_{min} (for which can exist monotone traveling wave solutions of system (4.2.10)) has the characteristic of reproducing, for appropriate values of the parameter F_D, the classic parabolic case c^P_{min} given in [151] and the hyperbolic limit case c^H_{min} given in (4.6.15). The minimal speed c^C_{min} deduced for the combined case (4.4.8)

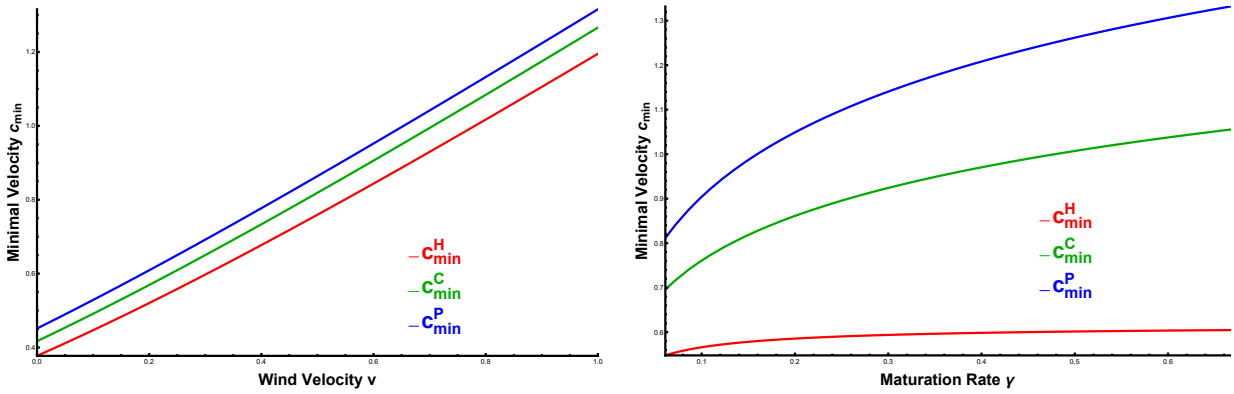

(a)

(b)

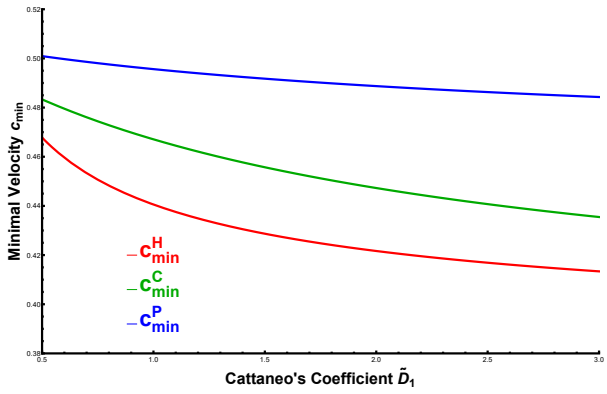

(c)

Figure 4.14: Numerical comparison among minimal traveling wave speeds given in (4.6.15) (hyperbolic model - red line - $F_D = 0$), in (4.4.8) (combined model - green line - $F_D = 0.5$) and in [151] (parabolic model - blue line - $F_D = 1$) as functions of v ((a) panel), of γ ((b) panel) and $\widetilde{D}_1$ ((c) panel). Parameters value are listed in Fig. 4.2 with $v = 5.2 \cdot 10^{-2}$ for (b) graph.

seems to recover the two minimal speeds c^H_{min} (defined in (4.6.15)) and c^P_{min} (present in literarure [151]) deduced for the hyperbolic and classical cases, respectively. In fact, in Figure 4.15, in the case in which F_D is very small, the velocity in the non-Fickian case is recovered (c^H_{min}), while when F_D reaches its maximum value, the minimal speed c^C_{min} reproduces the speed c^P_{min} valid in the Fickian propagation.
The numerical results found on the minimal speeds c^C_{min} and c^H_{min} extend those deduced by Takahashi *et al.* [151] for the parabolic case.

Finally, in Figure 4.16, the plan is divided into 5 regions identified by the minimal speed in the three models considered, using the values listed in Fig. 4.2 with $v = 5.2 \cdot 10^{-2}$. Moreover we plot the particular case in which $F_D = 0.5$ ($\widetilde{D}_0 = \widetilde{D}_1$) for system (4.2.10).

- Region I: $c < c^H_{min} < c^C_{min} < c^P_{min}$. There are no monotone waves in any of the three models.
- Region II: $c^H_{min} < c < c^C_{min} < c^P_{min}$. There are monotone waves in the hyperbolic model but they do not exist in the other two cases.

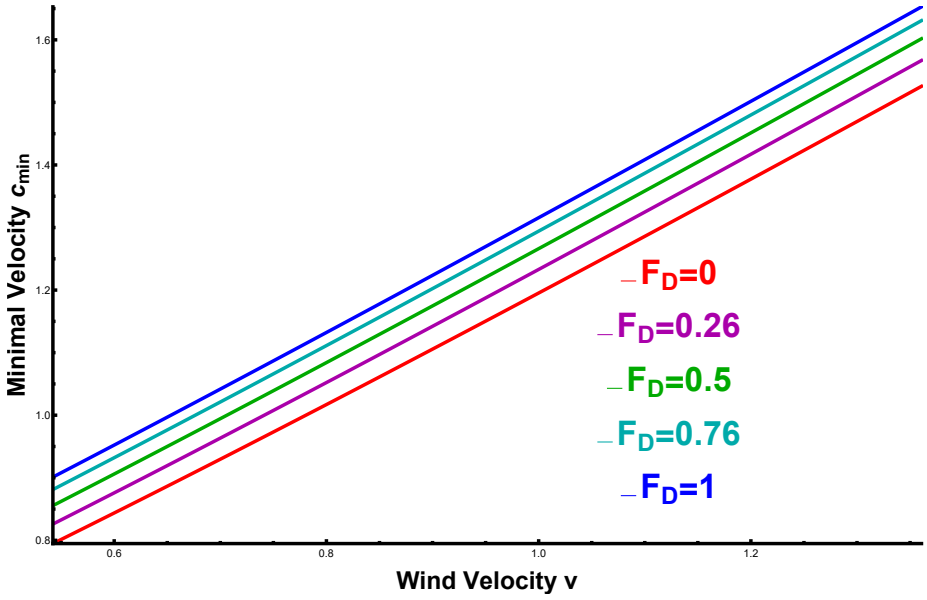

(a)

Figure 4.15: Representation of minimal traveling wave speed given in (4.4.8) as function of v with $F_D = 0$ (red line) corresponding to the limiting hyperbolic system (4.6.1), $F_D = 0.26$ (magenta line), $F_D = 0.5$ (green line), $F_D = 0.76$ (cyan line) and $F_D = 1$ (blue line) corresponding to the classical parabolic model (4.5.1) ([151]). Parameters value are listed in Fig. 4.2 with $v = 5.2 \cdot 10^{-2}$.

- Region III:$c^H_{min} < c^C_{min} < c < c^P_{min}$. There are monotone waves in the hyperbolic model and in the combined model but they do not exist in the classical parabolic model.
- Region IV: $c^H_{min} < c^C_{min} < c^P_{min} < c < \lambda_3$ with λ_3 the greatest characteristic velocity of hyperbolic model defined in (4.6.4). There are monotone waves in all three cases.
- Region V: $c^H_{min} < c^C_{min} < c^P_{min} < \lambda_3 < c$. There are no monotone and continuous waves for the hyperbolic model while they continue to exist for the combined and classical and parabolic models.

4.8 Conclusion

Mathematical modeling of biological phenomena provides an efficient tool for describing many type of invasive behaviour, such as the spread of epidemics. Biological invasion has a major impact on public health and vaccinations are the most effective way to combact many serious and potentially deadly infectious diseases. In the absence of vaccines, any other control policy to minimize the effects of the infestation can be taken into consideration. The novel mathematical model presented in this paper deals with the dispersal population of yellow fever mosquito A. aegypti, divided into two coupled sub-populations: the adult stage (that can spread diseases) and the aquatic stage which includes egg, pupa, larva. The life cycle of this mosquito is usually described through advection-reaction-diffusion equations [151], in which the diffusion mechanism is expressed by Fick-type law. This assumption leads to parabolic models with consequent diffusion of mosquito population at an infinite speed.

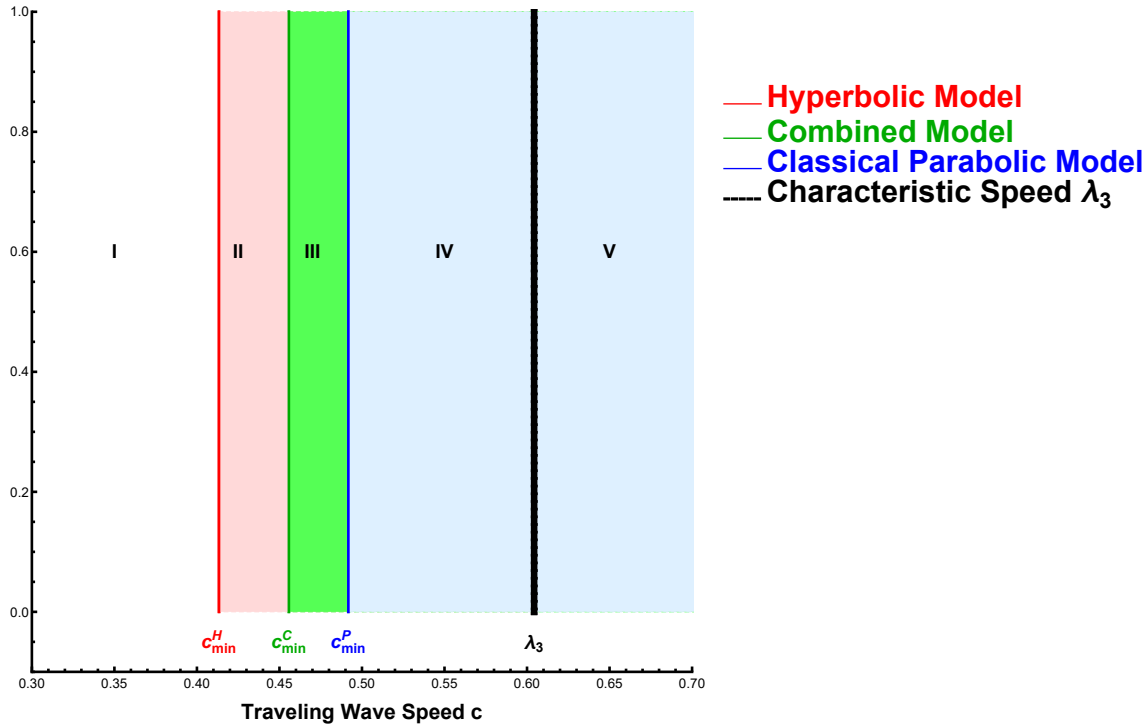

(a)

Figure 4.16: Set of values of c for which there are monotone waves in the hyperbolic model (red color), combined model (green color), and in the classical parabolic model (blue color). Parameters value are listed in Fig. 4.2 with $v = 5.2 \cdot 10^{-2}$. Moreover $F_D = 0.5$ for system (4.2.10).

The motivation of this work is to provide a more realistic description of diffusion phenomena of the mosquito population. The model presented here was deduced assuming that Fick-type fast processes, which have infinite speed of propagation, and Cattaneo-type slow processes, which have finite speed of propagation, simultaneously and independently coexist in the adult mosquitoes diffusion process. This hypothesis suggests to express the total diffusion flux as the sum of the fluxes corresponding to the fast and slow processes. The resulting system is still of parabolic type but the speed of propagation is limited superiorly by that obtained in [151] and represents a generalization of the classical parabolic model and the limiting hyperbolic model deduced. The different type of behavior is due to the values assumed by a parameter, F_D, expressed in terms of the two fast and slow diffusion coefficients. After analyzing the spatially homogeneous case, we moved on to the study of traveling wave solutions. It has been deduced that monotone waves can exist for a right interval of velocity values. An estimate of the minimum wavefront value has been provided. Several numerical simulations confirm analytical results. The special case was then studied in which $F_D \to 0$: the system appears to be hyperbolic. Also in this case traveling wave solutions have been studied, but unlike the previous case, it has been proved that continuous type solutions exist only for a right and finite range of speed values. The simulations confirmed these results. The minimum speeds were plotted in terms of biological parameters. Finally simulations have been conducted in order to compare the three models deduced in different contexts: it always results that the combined model proposed is a compromise between the limiting hyperbolic model obtained and the classical parabolic model. This also applies to the respective

speeds since $c^H_{min} \leq c^C_{min} \leq c^P_{min}$. A possible and important goal to be achieved in this study will be to demonstrate the result of the existence and uniqueness of traveling waves, both in the hyperbolic model and in the combined model and to provide an analytical expression of the respective minimal speeds, which will be the subject of a future work.

DISCUSSION AND CONCLUSION

The fundamental theme of this Ph.D. thesis was to model some infectious diseases and related aspects, such as vaccination or prevention methods, through the construction of ODE and PDE systems. The basic concept developed in the 4 chapters is the use of mathematical modeling approaches in the epidemiological field.
In Chapter 1, we study the interaction between the spatial mobility of individuals (based on classical diffusion), the effects of three different information structures and the dynamics of vaccine intake in the absence of infection. Evidence exists that there have been diseases that have been eradicated by the introduction of the vaccine long ago, but it is necessary to maintain a high-coverage immunization policy in the post-elimination period to prevent the risk of re-emergence of the infection. The mathematical analysis is the classical one, and allowed to test the establishment of the homogeneous solution in correspondence with particular types of kernel, the existence of generalized traveling waves. The study also focused on the influence of memory and campaigns in favor of vaccination on the phenomenon. The model is completely new and extends those in literature.
Chapter 2 deals with a novel ecology-epidemiology-hydrology model for the cholera transmission dynamics in a human host population having an interconnected pond-river water network. The novelty of the model consists in subdividing bacteria in subpopulation (in pond and river) and taking into account the water exchange between the two water reservoirs. We include the use of a nonlinear logistic growth rate for bacteria in the pond (and no such growth is considered for *V. cholerae* dynamics in the river) and accounting for the temporal evolution of the volume of water in the pond. The global stability of DFE was proved and four possible expressions of $\mathcal{R}_0$ are computed, showing the sensitivity of the model to different interpretations of the role of the environment. The problem was overcome by introducing the Type Reproduction Number $\mathcal{T}$ which is always unique. The model has been extended to the spatial case: for it an estimate of $\mathcal{R}_0^{PDE}$ (comparing it to the time case) was provided and the traveling waves were investigated.
The model proposed in Chapter 3 brings together some of the main features of vector-borne infectious disease models, including vertical transmission in mosquitoes, incubation period and recovery period in both host populations (reservoir and dead-end), a maximum capacity tolerable by the environment for the growth of mosquitoes. The boundedness and positiveness of solutions have been demonstrated, in addition to the local stability of the DFE, explicitly determining the expression of the threshold parameter. The existence of a backward bifurcation has been proven, determining the critical value. The number provides is a threshold value in the spatial case for the local and asymptotic stability of the homogeneous solution.

The first 3 chapters deal with parabolic systems and spatial approximations assuming that the diffusion flow obeys Fick's law, in agreement with the main ideas of Classical Thermodynamics. In order to give a description of the population dynamics of mosquitoes of the species *Aedes Aegypti*, in order to control their growth and provide a prevention method against vector-borne diseases, it is assumed that the diffusion flow is the sum of two contributions, one fast obedient to the laws of Classical Thermodynamics and one slow, considered as a new variable of the model and satisfying an equation of evolution of the Cattaneo type. This hypothesis is obtained in the literature as a result. After testing the global asymptotic stability of the MSE, traveling waves were numerically investigated, providing an estimate of the minimum velocity for which there are monotone waves for the proposed generalized model and for its boundary case (hyperbolic) obtained by setting the special parameter F_D null.The generalized model, the hyperbolic limit case and the parabolic limit case (obtained by setting $F_D = 1$) have been compared numerically, showing that the speed linked to the waves of the generalized model, even if parabolic, is limited superiorly by the speed of the corresponding waves to the classic parabolic case, showing that the presence of the slow flow limits the diffusion process of the population.
In conclusion, this thesis wanted to show different models related to the epidemiological field and related techniques to be able to predict the outbreak or limit the damages related to a disease.

APPENDICES

Appendix A: Reduction to two differential equations of the information model with memory (system (1.8.4))

Here, it is shown that the integro–differential information model (1.8.2) is equivalent to the differential system (1.8.4) with the delaying kernel $W(\tau)$ defined in (1.8.3). First, consider the function

$$Z(x,t) = be^{-bt}\int_{-\infty}^{t} e^{b\tau}P(x,\tau)d\tau, \tag{A-1}$$

which is clearly the solution of the following linear differential equation:

$$\partial_t Z + bZ = bP. \tag{A-2}$$

Given $W(\tau)$ defined in (1.8.3), consider

$$M(x,t) = \int_{-\infty}^{t} W(t-\tau)P(x,\tau)d\tau, \tag{A-3}$$

i.e.

$$M(x,t) = \frac{bd}{d-b}\left(e^{-bt}\int_{-\infty}^{t} e^{b\tau}P(x,\tau)d\tau - e^{-dt}\int_{-\infty}^{t} e^{d\tau}P(x,\tau)d\tau\right). \tag{A-4}$$

Therefore,

$$\partial_t M + dM = dbe^{-bt}\int_{-\infty}^{t} e^{b\tau}P(x,\tau)d\tau, \tag{A-5}$$

i.e.

$$\partial_t M + dM = dZ. \tag{A-6}$$

□

Appendix B

B1: Proof of Routh-Hurwitz Condition for the Cubic in Equation (2.3.5)

It should be recalled from Equation (2.3.6) that the coefficient, b_1, is given by:

$$b_1 = (a_3 + a_4)(\mu_B - 1) + a_3(a_4 + \lambda_p) + \mu_B\lambda_p - \beta_r\theta_r - \frac{\beta_p\theta_p}{k_p},$$

which can be re-written as:

$$b_1 = a_4(\mu_B - 1) + \lambda_p\mu_B + a_3(a_4 + \lambda_p + \mu_B - 1) - \frac{\beta_p\theta_p V_r\mu_B + \beta_r\theta_r k_p V_r\mu_B}{k_p V_r\mu_B}. \tag{B-1}$$

Further, it follows from Equation (2.3.4) that:

$$\begin{aligned}\beta_p\theta_p V_r\mu_B + \beta_r\theta_r k_p V_r\mu_B &= \mathcal{R}_0^{(1)} a_3 k_p V_r[a_4(\mu_B - 1) + \lambda_p\mu_B] - V_r\beta_p[V_r\theta_r\lambda_r + \theta_p\lambda_r] \\ &- k_p\beta_r[\theta_p\lambda_p + V_r\theta_r(\lambda_p - 1)].\end{aligned} \tag{B-2}$$

Substituting (B-2) into (B-1) gives:

$$\begin{aligned}b_1 &= \frac{1}{k_p V_r\mu_B}\{a_3 k_p V_r\mu_B(a_4 + \lambda_p)\left(1 - \mathcal{R}_0^{(1)}\right) + (a_4 + a_3)\, k_p V_r\mu_B(\mu_B - 1) \\ &+ k_p V_r\left(\mu_B^2\lambda_p + a_3 a_4\mathcal{R}_0^{(1)}\right) + V_r\beta_p(V_r\theta_r\lambda_r + \theta_p\lambda_r) \\ &+ k_p\beta_r[\theta_p\lambda_p + V_r\theta_r(\lambda_p - 1)]\}.\end{aligned} \tag{B-3}$$

Recalling the assumption that $\lambda_p \geq 1$, it follows from (B-3) that $b_1 > 0$ whenever $\mathcal{R}_0^{(1)} < 1$. Thus, the associated Routh-Hurwitz condition, $b_1 b_2 - b_0$, can be re-written as:

$$\begin{aligned}b_2 b_1 - b_0 &= \frac{a_3 + a_4 + \lambda_p + \mu_B - 1}{k_p V_r\mu_B}\{a_3 k_p V_r\mu_B(a_4 + \lambda_p)\left(1 - \mathcal{R}_0^{(1)}\right) \\ &+ (a_4 + a_3)\, k_p V_r\mu_B(\mu_B - 1) + k_p V_r\left(\mu_B^2\lambda_p + a_3 a_4\mathcal{R}_0^{(1)}\right) \\ &+ V_r\beta_p(V_r\theta_r\lambda_r + \theta_p\lambda_r) + k_p\beta_r[\theta_p\lambda_p + V_r\theta_r(\lambda_p - 1)]\} \\ &- a_3[a_4(\mu_B - 1) + \lambda_p\mu_B]\left(1 - \mathcal{R}_0^{(1)}\right) \\ &> 0.\end{aligned} \tag{B-4}$$

Hence, it follows from (B-4) and the expressions for the coefficients b_2 and b_0 in (2.3.6), that the Routh-Hurwitz condition $b_2 b_1 - b_0 > 0$ if and only if:

$$\begin{aligned}&\{(a_3 + a_4 + \lambda_p + \mu_B - 1)a_3(a_4 + \lambda_p) - a_3[a_4(\mu_B - 1) + \lambda_p\mu_B]\}\left(1 - \mathcal{R}_0^{(1)}\right) \\ > \; &-\frac{a_3 + a_4 + \lambda_p + \mu_B - 1}{k_p V_r\mu_B}\{(a_4 + a_3)\, k_p V_r\mu_B(\mu_B - 1) \\ + \; &k_p V_r\left(\mu_B^2\lambda_p + a_3 a_4\mathcal{R}_0^{(1)}\right) + V_r\beta_p[V_r\theta_r\lambda_r + \theta_p\lambda_r] + k_p\beta_r[\theta_p\lambda_p + V_r\theta_r(\lambda_p - 1)]\}.\end{aligned} \tag{B-5}$$

It should be noted from (B-5) that the right-hand side of the inequality is automatically negative (since all the parameters of the model are nonnegative). The left-hand side of the inequality (B-5) can be written as

$$a_3\left[a_4(a_3 + a_4) + \lambda_p(a_3 + a_4 + \lambda_p) + \lambda_p(\lambda_r + \mu_B - 1)\right]\left(1 - \mathcal{R}_0^{(1)}\right), \tag{B-6}$$

which is always positive whenever $\mathcal{R}_0^{(1)} < 1$ (noting that $\mu_B - 1 \geq 0$). Hence, the Routh-Hurwitz condition $b_1 b_2 - b_0 > 0$ always holds when $\mathcal{R}_0^{(1)} < 1$ (since the left-hand side of the inequality is always positive, and the right-hand side of the same inequality is always negative). □

B2: Positivity of the Discriminant of Equation (2.3.16)

Recall that the discriminant of Equation (2.3.16) is given by:

$$\Delta_p = d_2^2 d_1^2 + 18 d_1 d_2 d_0 - 4 d_1^3 - 4 d_0 d_2^3 - 27 d_0^2, \tag{B-7}$$

with d_2, d_1 and d_0 as defined in Equation (2.3.17). The expression (B-7) (with (2.3.17)) can be simplified to:

$$\begin{aligned}
\Delta_p \;=\; & \frac{1}{a_3^3 k_p^3 V_r^3 \mu_B^4 (\lambda_p + a_4)^4} \{4\, a_3^2 k_p^3 V_r^3 \beta_r \theta_r a_4^3 + 4\mu_B(\lambda_p + a_4)[k_p \beta_r\, (\theta_p \lambda_p + V_r \theta_r (\lambda_p + \mu_B)) \\
+ \;& V_r \beta_p (V_r \theta_r \lambda_r + \theta_p (\lambda_r + \;\mu_B))]^3 + a_3 k_p V_r [V_r^2 \beta_p^2 a_4^2 (V_r \theta_r\, \lambda_r + \theta_p a_4)^2 \\
+ \;& 2 k_p V_r \beta_p \beta_r a_4 (V_r \theta_r \lambda_r + \theta_p a_4)(\theta_p \lambda_p a_4 + V_r \theta_r (10\mu_B a_4 + \lambda_p (\;\lambda_r + 10\mu_B))) \\
+ \;& k_p^2 \beta_r^2 [\theta_p^2 \lambda_p^2 a_4^2 + 2 V_r \theta_p \theta_r \lambda_p a_4\, (10\mu_B a_4 + \lambda_p(\lambda_r + 10\mu_B)) + V_r^2 \theta_r^2 (-8\mu_B^2 a_4^2 \\
+ \;& \lambda_p^2 (\lambda_r^2 + 20\lambda_r \mu_B - 8\mu_B^2) + 4\lambda_p \mu_B (5\lambda_r^2 + \lambda_r \mu_B - 4\mu_B^2)))]]\} > 0.
\end{aligned}$$

□

Appendix C: Proof of Theorem 2.4.3

Proof. Consider the normalized model (2.2.3) with $v_p(t)$ at its maximum value ($v_p(t) = 1$) for all t in $\mathcal{D}$. Further, let $\mathcal{R}_0^{(1)} = \left(\mathcal{R}_0^{(3)}\right)^2 \leq 1$. Consider the following Lyapunov function (noting that, since $\mu_B - 1 \geq 0$, all coefficients of the Lyapunov function are positive):

$$\mathcal{L}(i, b_p, b_r) = \mathcal{R}_0^{(3)} i + \frac{\beta_p a_4 V_r + \beta_r k_p \lambda_p}{k V_r [a_4(\mu_B - 1) + \lambda_p \mu_B]} b_p + \frac{\beta_p \lambda_r V_r + \beta_r k_p (\mu_B - 1 + \lambda_p)}{k_p [a_4(\mu_B - 1) + \lambda_p \mu_B]} b_r, \tag{C-1}$$

with Lyapunov derivative given by:

$$
\begin{aligned}
\dot{\mathcal{L}} &= \mathcal{R}_0^{(3)}\dot{i} + \frac{\beta_p a_4 V_r + \beta_r k_p \lambda_p}{k_p V_r[a_4(\mu_B - 1) + \lambda_p \mu_B]}\dot{b}_p + \frac{\beta_p \lambda_r V_r + \beta_r k_p(\mu_B - 1 + \lambda_p)}{k_p[a_4(\mu_B - 1) + \lambda_p \mu_B]}\dot{b}_r \\
&= \mathcal{R}_0^{(3)}\left[\left(\frac{\beta_p}{k_p + b_p}b_p + \frac{\beta_r}{1 + b_r}b_r\right)s - a_3 i\right] \\
&+ a_3\frac{\left(\mathcal{R}_0^{(3)}\right)^2(\beta_p a_4 V_r + \beta_r k_p \lambda_p)}{V_r\beta_p a_1 + k_p\beta_r\left[(\theta_p + V_r\theta_r)\lambda_p + V_r\theta_r(\mu_B - 1)\right]}\left[\theta_p i + b_p(1 - b_p) - \mu_B b_p + \lambda_r V_r b_r - \lambda_p b_p\right] \\
&+ a_3\frac{V_r\left(\mathcal{R}_0^{(3)}\right)^2(\beta_p \lambda_r V_r + \beta_r k_p(\mu_B - 1 + \lambda_p))}{V_r\beta_p a_1 + k_p\beta_r\left[(\theta_p + V_r\theta_r)\lambda_p + V_r\theta_r(\mu_B - 1)\right]}\left[\theta_r i - \mu_B b_r - \lambda_r b_r + \lambda_p\frac{b_p}{V_r}\right] \qquad \text{(C-2)} \\
&= a_3(\mathcal{R}_0^{(3)} - 1)\left(\mathcal{R}_0^{(3)} i + \frac{\beta_p b_p}{k_p a_3} + \frac{\beta_r b_r}{a_3}\right) \\
&- \mathcal{R}_0^{(3)}\left[\frac{\beta_p b_p}{k_p}\left(1 - \frac{k_p s}{k_p + b_p}\right) + \beta_r b_r\left(1 - \frac{s}{1 + b_r}\right)\right] \\
&- \frac{a_3\left(\mathcal{R}_0^{(3)}\right)^2(\beta_p a_4 V_r + \beta_r k_p \lambda_p)}{V_r\beta_p a_1 + k_p\beta_r\left[(\theta_p + V_r\theta_r)\lambda_p + V_r\theta_r(\mu_B - 1)\right]}b_p^2.
\end{aligned}
$$

Since $s(t) \leq 1$ for all $t > 0$ in $\mathcal{D}$, it follows from (C-2) that $\frac{k_p s}{k_p + b_p} \leq 1$ and $\frac{s}{1 + b_r} \leq 1$. Hence,

$$
\dot{\mathcal{L}} \leq (\mathcal{R}_0^{(3)} - 1)\left(\mathcal{R}_0^{(3)} i + \frac{\beta_p}{k_p a_3}b_p + \frac{\beta_r}{a_3}b_r\right). \qquad \text{(C-3)}
$$

It follows from (C-3) that $\dot{\mathcal{L}} < 1$ whenever $\mathcal{R}_0^{(3)} < 1$. Furthermore, it follows from (C-2) and (C-3) that $\dot{\mathcal{L}} = 0$ if and only if:

(a) $\mathcal{R}_0^{(3)} = 1$ and $s(t) = 1$, or

(b) $i(t) = b_p(t) = b_r(t) = 0$.

In either of the above two cases, the largest compact invariant subset of the set

$$
\mathcal{G} = \{(s, i, b_p, b_r, v_p) \in \mathcal{D} : \dot{\mathcal{L}} = 0\}
$$

is the singleton $\{\mathbf{E}_0\}$. In fact, suppose $\mathcal{M}$ is the largest compact invariant subset of $\mathcal{G}$. To check for Case (a), we need to require that $s(t) = 1$ is the solution of the human component of the normalized model given by:

$$
\begin{cases}
\dot{s} = \mu(1 - s) - \left(\frac{\beta_p b_p}{k_p + b_p} + \frac{\beta_r b_r}{1 + b_r}\right)s + \gamma i, \\
\dot{i} = \left(\frac{\beta_p b_p}{k_p + b_p} + \frac{\beta_r b_r}{1 + b_r}\right)s - a_3 i,
\end{cases} \qquad \text{(C-4)}
$$

from which it follows (by adding the two equations, and recalling that $n(t) = s(t) + i(t)$)) that:

$$
\dot{n} = \mu(1 - s) - (\delta + \mu)i. \qquad \text{(C-5)}
$$

Substituting $s(t) = 1$ in (C-5) (and noting that, for solution of the form $s(t) = 1$, $\dot{s} = 0$) gives:

$$\dot{i} = -(\delta + \mu)i, \tag{C-6}$$

so that $\lim_{t\to\infty} i(t) = 0$. Substituting $s(t) = 1$ and $i(t) = 0$ into the normalized model (2.2.3) shows that $\lim_{t\to\infty} (b_p(t), b_r(t)) = (0, 0)$. Hence, it follows from the above analyses that, for Case (a), $\lim_{t\to 0}(s(t), i(t), b_p(t), b_r(t)) = (1, 0, 0, 0)$. Thus, for Case (a), $\mathcal{M} = \{\mathbf{E}_0\}$ and all solutions in $\mathcal{D}$ converge to the disease-free equilibrium ($\mathbf{E}_0$) of the normalized model.

Similarly, for Case (b), requiring each solution in $\mathcal{M}$ to satisfy $i(t) = b_p(t) = b_r(t) = 0$ leads to:

$$\dot{s} = \mu(1 - s), \tag{C-7}$$

whose solution is (where $s_0 = s(0) > 0$ and $0 < s_0 \leq 1$)

$$s(t) = 1 - (1 - s_0)\, e^{-\mu t}. \tag{C-8}$$

Since $\mu > 0$ and $0 < s_0 \leq 1$, it follows from (C-8) that $\lim_{t\to\infty} s(t) = 1$. That is, in Case (b) (where $i(t) = b_p(t) = b_r(t) = 0$), like in Case (a), the largest compact invariant subset where $\dot{\mathcal{L}} = 0$ is the singleton $\{\mathbf{E}_0\}$. Thus, it follows from the LaSalle's Invariance Principle [96] that the disease-free equilibrium of the normalized model ($\{\mathbf{E}_0\}$) is globally-asymptotically stable in $\mathcal{D}$ whenever $\mathcal{R}_0^{(3)} \leq 1$. □

It is worth mentioning that the above proof also works for the special case where $v_p(t) \neq 1$, if the associated water balance condition, $k_p \leq \frac{b_p(t)}{1-v_p(t)}$, holds (for all time $t \geq 0$).

Appendix D: Coefficients of quartic (2.6.4)

$$
\begin{aligned}
a &= -V_r\theta_r a_4[(\beta_p+\beta_r)(\delta+\mu)+\mu a_3] < 0,\\
\\
b &= -\lambda_p\theta_p a_4[(\beta_p+\beta_r)(\delta+\mu)+\mu a_3] - V_r\theta_r\{\beta_p(\delta+\mu)[2\mu_B a_6+\lambda_r(2(\mu_B-1)+\lambda_p)]+\\
&+ (\beta_r(\delta+\mu)+\mu a_3)[\lambda_r(2(\mu_B-1)+k_p+\lambda_p)+\mu_B(2a_6+k_p))]\} < 0,\\
\\
c &= a_4^2\beta_p\gamma V_r\theta_p - \lambda_r[(\beta_p+\beta_r)(V_r^2\theta r^2\mu-\gamma\theta_p\lambda_p^2) - V_r\gamma\theta_r\lambda_p(\beta_p a_6+\beta_r(a_6+k_p))]+\\
&- a_3\{a_4^2V_r\theta_p(\beta_p+\mu)-\lambda_r\lambda_p[\theta_p\lambda_p(\beta_p+\beta_r+\mu)+V_r\theta_r(\beta_p a_6+(\beta_r+\mu)(a_6+k_p))]+\\
&+ a_4[V_r^2\theta_r\lambda_r(\beta_p+\mu)+(\theta_p\lambda_p+V_r\theta_r a_6)(\beta_p a_6+(\beta_r+\mu)(a_6+k_p))]\}+a_4\{V_r^2\beta_p\gamma\theta_r\lambda_r+\\
&+ \gamma\theta_p\lambda_p[\beta_p a_6+\beta_r(a_6+k_p)]+V_r\theta_r[\beta_p(\theta_p\mu+\gamma a_6^2)+\beta_r(\theta_p+\mu a_6(a_6+k_p))]\},\\
\\
d &= a_4^2V_r\beta_p\gamma\theta_p a_6+a_4\{\theta_p^2\lambda_p\mu(\beta_p+\beta_r)+V_r^2\beta_p\gamma\theta_r\lambda_r a_6+V_r\theta_p[\beta_r\theta_r\mu a_6+\beta_p(\theta_r\mu a_6+\\
&- \gamma\lambda_r\lambda_p)]+k_p\beta_r[\gamma\theta_p\lambda_p a_6+V_r\theta_r(\theta_p+\gamma a_6^2)]\}-a_3\{a_4^2V_r^2\theta_p[\beta_p a_6+\mu(a_6+k_p)]+\\
&- \lambda_p\lambda_r[V_r^2\theta_r\lambda_r(\beta_p+\mu)+k_p(\beta_r+\mu)(\theta_p\lambda_p+V_r\theta_r a_6)]+a_4[V_r\lambda_r(\beta_p+\mu)(V_r\theta_r a_6-\theta_p\lambda_p)+\\
&+ k_p(V_r^2\theta_r\lambda_r\mu+\theta_p\lambda_p a_6(\beta_r+\mu)+V_r\theta_r a_6^2(\beta_r+\mu))]\}+\lambda_r\{k_p\beta_r[V_r^2\theta_r^2\mu-\gamma\theta_p\lambda_p^2+\\
&- V_r\gamma\theta_r\lambda_p a_6]+V_r\theta_r[\theta_p\lambda_p\mu(\beta_p+\beta_r)+V_r(\beta_r\theta_r\mu a_6+\beta_p(\theta_r\mu a_6-\gamma\lambda_r\lambda_p))]\},\\
\\
e &= -\mu a_1[a_4(\mu_B-1)+\lambda_p\mu_B]\left(1-\mathcal{R}_0^{(1)}\right),
\end{aligned}
$$

where $a_6=\lambda_p+\mu_B-1$.

Appendix E: Proof of Theorem 2.9.2

Proof. If $a_3 \ll D_I$, $v_p + (\mu_B - 1) \ll 1$ and $v_r + \mu_B \ll D_B$, one obtains

(1) $$\int_0^x \sinh\left[\sqrt{\frac{a_3}{D_I}}(x-\tau)\right]\phi_1(\tau)d\tau \doteq \int_0^x \sqrt{\frac{a_3}{D_I}}(x-\tau)\phi_1(\tau)d\tau \doteq 0$$

(2) $$\cosh\left[\sqrt{\frac{a_3}{D_I}}x\right]\int_0^1 \cosh\left[\sqrt{\frac{a_3}{D_I}}(1-\tau)\right]\phi_1(\tau)d\tau \doteq \int_0^1 \phi_1(\tau)d\tau$$

(3) $$e^{\frac{v_p}{2}(x-\tau)}\sinh\left[\varepsilon(x-\tau)\right] \doteq \varepsilon(x-\tau) \doteq 0$$

(4) $$k_{i4}e^{-\frac{v_p}{2D_{\mathrm{B}_p}}(1-x)}\left(\cosh\left[\varepsilon x\right] - \frac{v_p}{2D_{\mathrm{B}_p}\varepsilon}\sinh\left[\varepsilon x\right]\right)\int_0^1 e^{\frac{v_p}{2D_{\mathrm{B}_p}}(1-\tau)}\{\frac{v_p}{2D_{\mathrm{B}_p}}\sinh\left[\varepsilon(1-\tau)\right]$$

$$+\varepsilon\cosh\left[\varepsilon(1-\tau)\right]\}\phi_2(\tau)d\tau \tag{E-1}$$

$$\doteq \frac{\beta_p}{k_p(\mu_B-1)\varepsilon}\left(1-\frac{v_p}{2D_{\mathrm{B}_p}}\right)\int_0^1\left(\frac{v_p}{2D_{\mathrm{B}_p}}\varepsilon(1-\tau)+\varepsilon\right)\phi_2(\tau)d\tau \doteq \frac{\beta_p}{k_p(\mu_B-1)}\int_0^1\phi_2(\tau)d\tau$$

(5) $$e^{\frac{v_r}{2D_{\mathrm{B}_r}}(x-\tau)}\sinh\left[\omega(x-\tau)\right] \doteq \omega(x-\tau) \doteq 0$$

(6) $$k_{i6}e^{-\frac{v_p}{2D_{\mathrm{B}_r}}(1-x)}\left(\cosh\left[\omega x\right] - \frac{v_r}{2D_{\mathrm{B}_r}\omega}\sinh\left[\omega x\right]\right)\int_0^1 e^{\frac{v_p}{2D_{\mathrm{B}_r}}(1-\tau)}\{\frac{v_r}{2D_{\mathrm{B}_r}}\sinh\left[\omega(1-\tau)\right]$$

$$+\omega\cosh\left[\omega(1-\tau)\right]\}\phi_3(\tau)d\tau$$

$$\doteq \frac{\beta_r}{\mu_B\omega}\left(1-\frac{v_r}{2D_{\mathrm{B}_r}}\right)\int_0^1\left(\frac{v_r}{2D_{\mathrm{B}_r}}\omega(1-\tau)+\omega\right)\phi_3(\tau)d\tau \doteq \frac{\beta_r}{\mu_B}\int_0^1\phi_3(\tau)d\tau.$$

Substituting (E-1) to (2.9.20) yields

$$\begin{aligned}
\frac{\beta_p}{k_p(\mu_B-1)}\int_0^1\phi_2(\tau)d\tau + \frac{\beta_r}{\mu_B}\int_0^1\phi_3(\tau)d\tau &= \lambda\phi_1(x),\\
\frac{\theta_w}{a_3}\int_0^1\phi_1(\tau)d\tau &= \lambda\phi_2(x),\\
\frac{\theta_r}{a_3}\int_0^1\phi_1(\tau)d\tau &= \lambda\phi_3(x).
\end{aligned} \tag{E-2}$$

These equations imply that $\phi_1(x) \equiv c_1$, $\phi_2(x) \equiv c_2$ anf $\phi_3(x) \equiv c_3$ for some constants $c_1 \neq 0$, $c_2 \neq 0$ and $c_3 \neq 0$ [165]. Let $z_1 = \frac{c_2}{c_1}$ and $z_2 = \frac{c_3}{c_1}$. Thus, equations (E-2) give

$$\lambda = \frac{\beta_p}{k_p(\mu_B-1)}z_1 + \frac{\beta_r}{\mu_B}z_2 = \frac{\theta_w}{a_3}\frac{1}{z_1} = \frac{\theta_r}{a_3}\frac{1}{z_2}. \tag{E-3}$$

Solving it directly, one finds that

$$z_1 = \pm\theta_p\sqrt{\frac{k_p\mu_B(\mu_B-1)}{a_3[\beta_p\theta_p\mu_B + k_p\beta_r\theta_r(\mu_B-1)]}}. \tag{E-4}$$

Plugging (E-4) into (E-3) yields

$$\lambda_{1,2} = \pm\sqrt{\frac{\beta_p\theta_p\mu_B + k_p\beta_r\theta_r(\mu_B - 1)}{a_3 k_p\mu_B(\mu_B - 1)}}. \tag{E-5}$$

Thus

$$\mathcal{R}_0^{PDE} \doteq \sup\{\lambda_1, \lambda_2\} = \mathcal{R}_0^{ODE}. \tag{E-6}$$

□

Appendix F: Proof of Theorem 3.5.2

Proof. If $v_M^2 + 4D_M\alpha_M \ll 1$ and $nu_B \ll D_B$, one obtains

$$\begin{aligned}
&(1) \quad e^{\frac{v_M}{2D_M}(x-\tau)}\sinh[\lambda(x-\tau)] \doteq \sinh[\lambda(x-\tau)] \doteq \lambda(x-\tau) \doteq 0\\
&(2) \quad \sinh\left[\sqrt{\frac{\nu_B}{D_B}}(x-\tau)\right] \doteq \sqrt{\frac{\nu_B}{D_B}}(x-\tau) \doteq 0\\
&(3) \quad \cosh\left[\sqrt{\frac{\nu_B}{D_B}}x\right]\int_0^1 \cosh\left[\sqrt{\frac{\nu_B}{D_B}}(1-\tau)\right]\phi_3(\tau)d\tau \doteq \int_0^1 \phi_3(\tau)d\tau \qquad \text{(F-1)}\\
&(4) \quad k_{i3}e^{-\frac{v_M}{2D_M}(1-x)}\left(\cosh[\lambda x] - \frac{v_M}{2D_M\lambda}\sinh[\lambda x]\right)\int_0^1 e^{\frac{v_M}{2D_M}(1-\tau)}\left\{\frac{v_M}{2D_M}\sinh[\lambda(1-\tau)] + \lambda\cosh[\lambda(1-\tau)]\right\}\phi_1(\tau)d\tau\\
&\quad \doteq \frac{c_{i3}}{\lambda}\left(1 - \frac{v_M}{2D_M}\right)\int_0^1 [\frac{v_M}{2D_M}\lambda(1-\tau) + \lambda]\phi_1(\tau)d\tau \doteq c_{i3}\int_0^1 \phi_1(\tau)d\tau\\
&(5) \quad k_{i4}e^{-\frac{v_M}{2D_M}(1-x)}\left(\cosh[\lambda x] - \frac{v_M}{2D_M\lambda}\sinh[\lambda x]\right)\int_0^1 e^{\frac{v_M}{2D_M}(1-\tau)}\left\{\frac{v_M}{2D_M}\sinh[\lambda(1-\tau)] + \lambda\cosh[\lambda(1-\tau)]\right\}\phi_2(\tau)d\tau\\
&\quad \doteq c_{i4}\int_0^1 \phi_2(\tau)d\tau, \quad i = 1,2,3
\end{aligned}$$

where

$$\begin{aligned}
c_{13} &= \frac{qr\gamma}{\alpha_M\alpha_A}\left(1 - \frac{A_0}{k_A}\right)\left(1 - \frac{M_0}{k_M}\right), \quad c_{23} = 0, \quad c_{33} = \frac{a_B\beta_{MB}\gamma}{\alpha_A\alpha_M}\left(1 - \frac{M_0}{k_M}\right),\\
c_{14} &= \frac{qr}{\alpha_M}\left(1 - \frac{A_0}{k_A}\right), \qquad\qquad c_{24} = 0, \quad c_{34} = \frac{a_B\beta_{MB}}{\alpha_M}.
\end{aligned}$$

Substituting (F-1) to (3.5.13) yields

$$\begin{aligned}
c_{13}\int_0^1 \phi_1(\tau)d\tau + c_{14}\int_0^1 \phi_1(\tau)d\tau &= \lambda\phi_1(x),\\
k_{26}\int_0^1 \phi_2(\tau)d\tau &= \lambda\phi_2(x),\\
c_{33}\int_0^1 \phi_1(\tau)d\tau + c_{34}\int_0^1 \phi_2(\tau) &= \lambda\phi_3(x).
\end{aligned} \tag{F-2}$$

These equations imply that $\phi_1(x) \equiv b_1$, $\phi_2(x) \equiv b_2$ and $\phi_3(x) \equiv b_3$ for some constants $b_1 \neq 0$, $b_2 \neq 0$ and $b_3 \neq 0$. Let $z_1 = \frac{b_2}{b_1}$ and $z_2 = \frac{b_3}{b_2}$. Thus, equations (F-2) give

$$\lambda = c_{13} + c_{14}z_1 = k_{26}z_2 = \frac{c_{33}}{z_1 z_2} + \frac{c_{34}}{z_2}. \tag{F-3}$$

After algebraic manipulations, one finds that z_1 satisfies the following cubic polynomial

$$p(z_1) = -\frac{1}{\alpha_A^2 \alpha_M^2 k_A^2 k_M^2} \left[\alpha_A k_M z_1 + \gamma\left(k_M - M_0\right)\right] \left[z_1^2 + \frac{\gamma\left(k_M - M_0\right)}{k_M \alpha_M} z_1 - \frac{a_B \alpha_M \beta_{MB} k_{26} k_A^2}{q^2 r^2 \left(A_0 - k_A\right)^2}\right].$$

Solving it directly, it gives

$$z_1 = \frac{\gamma\left(M_0 - k_M\right)}{\alpha_A k_M}, \quad z_{2,3} = \frac{1}{2}\left(\frac{\gamma(M_0 - k_M)}{\alpha_A k_M} \pm \sqrt{\left(\frac{\gamma(M_0 - k_M)}{\alpha_A k_M}\right)^2 + 4\frac{a_B \beta_{MB} k_A^2 \alpha_M k_{26}}{q^2 r^2 \left(A_0 - k_A\right)}}\right). \tag{F-4}$$

Plugging (F-4) into (F-3) yields

$$\lambda_1 = 0, \quad \lambda_{2,3} = \frac{1}{2}\left(q \pm \sqrt{q^2 + 4\frac{a_B \beta_{MB} \beta_{BM} M_0}{\gamma_B \nu_B \alpha_M}}\right). \tag{F-5}$$

Thus

$$\mathcal{R}_0^{PDE} \doteq \sup\{\lambda_1, \lambda_2, \lambda_3\} = \mathcal{R}_0^{ODE}. \tag{F-6}$$

□

BIBLIOGRAPHY

[1] H. Abboubakar, J. C. Kamgang, N. L. Nkamba, D. Tieudjo, and L. Emini. Modeling the dynamics of arboviral diseases with vaccination perspective. *Biomath*, 4(1):1507241, 2015.

[2] H. Abboubakar, J. C. Kamgang, and D. Tieudjo. Backward bifurcation and control in transmission dynamics of arboviral diseases. *Mathematical Biosciences*, 278:100–129, 2016.

[3] B. Adams and D. D. Kapan. Man bites mosquito: understanding the contribution of human movement to vector-borne disease dynamics. *PloS One*, 4(8):e6763, 2009.

[4] F.B. Agusto, S. Bewick, and W.F. Fagan. Mathematical model of zika virus with vertical transmission. *Infectious Disease Modelling*, 2(2), 2017.

[5] M. Ali, A. R. Nelson, A. L. Lopez, and D. A. Sack. Updated global burden of cholera in endemic countries. *PLoS Neglected Tropical Diseases*, 9(6):e0003832, 2015.

[6] R. P.P. Almeida. Ecology of emerging vector-borne plant diseases. In *Institute of Medicine forum on Vector-borne diseases: understanding the environmental, human health, and ecological connections. National Academies Press, Washington, DC*, 2008.

[7] R. M. Anderson and R. M. May. Population biology of infectious diseases: Part i. *Nature*, 280(5721):361, 1979.

[8] N. Apreutesei, N. Bessonov, V. Volpert, and V. Vougalter. Spatial structures and generalized travelling waves for an integro-differential equation. *Discrete Contin. Dyn. Syst. Ser. B*, 13(3):537–557, 2010.

[9] A. Asmaidi, P. Sianturi, and Endar H. Nugrahani. A sir mathematical model of dengue transmission and its simulation. *Indonesian Journal of Electrical Engineering and Computer Science*, 12(11), 2014.

[10] G. A.J. Ayliffe, B.J. Collins, L. J. Taylor, et al. *Hospital-acquired infection: principles and prevention.* Bristol, UK; John Wright & Sons Ltd., 1982.

[11] N.T.J. Bailey. *The mathematical theory of infectious diseases and its applications (2nd edition).* Charles Griffin & Company Ltd, 1975.

[12] W.B. Baine, M. Mazzotti, D. Greco, E. Izzo, A. Zampieri, G. Angioni, M. Di Gioia, E.J. Gangarosa, and F. Pocchiari. Epidemiology of cholera in italy in 1973. *The Lancet*, 304(7893):1370–1374, 1974.

[13] D. Balcan and A. Vespignani. Phase transitions in contagion processes mediated by recurrent mobility patterns. *Nature Physics*, 7(7):581, 2011.

[14] M. Bani-Yaghoub, R. Gautam, Z. Shuai, P. Van Den Driessche, and R. Ivanek. Reproduction numbers for infections with free-living pathogens growing in the environment. *Journal of Biological Dynamics*, 6(2):923–940, 2012.

[15] S. Barve, T.B. Javadekar, S. Nanda, C. Pandya, A. Pathan, and P. Chavda. Isolation of vibrio cholera o1 during an outbreak of acute gastroenteritis in dahod district, gujarat. *Nat J Community Med*, 3:104–7, 2012.

[16] F. M. Bass. A new product growth for model consumer durables. *Management Science*, 15(5):215–227, 1969.

[17] C. T Bauch. Imitation dynamics predict vaccinating behaviour. *Proc. R. Soc. Lond. B Biol. Sci.*, 272(1573):1669–1675, 2005.

[18] E. Bertuzzo, S. Azaele, A. Maritan, M. Gatto, I. Rodriguez-Iturbe, and A. Rinaldo. On the space-time evolution of a cholera epidemic. *Water Resources Research*, 44(1), 2008.

[19] E. Bertuzzo, R. Casagrandi, M. Gatto, I. Rodriguez-Iturbe, and A. Rinaldo. On spatially explicit models of cholera epidemics. *Journal of the Royal Society Interface*, 7(43):321–333, 2009.

[20] E. Bertuzzo, L. Mari, L. Righetto, M. Gatto, R. Casagrandi, M. Blokesch, I. Rodriguez-Iturbe, and A. Rinaldo. Prediction of the spatial evolution and effects of control measures for the unfolding Haiti cholera outbreak. *Geophysical Research Letters*, 38(6), 2011.

[21] E. Bertuzzo, L. Mari, L. Righetto, M. Gatto, R. Casagrandi, I. Rodriguez-Iturbe, and A. Rinaldo. Hydroclimatology of dual-peak annual cholera incidence: insights from a spatially explicit model. *Geophysical Research Letters*, 39(5), 2012.

[22] K. W. Blayneh. Vertically transmitted vector-borne diseases and the effects of extreme temperature. *International Journal of Applied Mathematics*, 30(2), 2017.

[23] G. Boillat and T. Ruggeri. On the shock structure problem for hyperbolic system of balance laws and convex entropy. *Continuum Mechanics and Thermodynamics*, 10(5):285–292, 1998.

[24] J. P. Boto and N. Stollenwerk. Fractional calculus and Levy flights: modelling spatial epidemic spreading. *Computational and Mathematical Methods in Science and Engineering*, 2009.

[25] L. Bourouiba, A. Teslya, and J. Wu. Highly pathogenic avian influenza outbreak mitigated by seasonal low pathogenic strains: Insights from dynamic modeling. *Journal of Theoretical Biology*, 271(1):181–201, 2011.

[26] C. Bowman, A.B. Gumel, P. Van den Driessche, J. Wu, and H. Zhu. A mathematical model for assessing control strategies against west nile virus. *Bulletin of Mathematical Biology*, 67(5), 2005.

[27] J. M Boyce, G. Potter-Bynoe, C. Chenevert, and T. King. Environmental contamination due to methicillin-resistant Staphylococcus aureus possible infection control implications. *Infection Control & Hospital Epidemiology*, 18(9):622–627, 1997.

[28] D. Brockmann and L. Hufnagel. Front propagation in reaction-superdiffusion dynamics: Taming LÃ©vy flights with fluctuations. *Physical Review Letters*, 98(17):178301, 2009.

[29] H. A. Buchdahl. The concepts of classical thermodynamics. *The Concepts of Classical Thermodynamics, by HA Buchdahl, Cambridge, UK: Cambridge University Press, 2009*, 2009.

[30] R. Bueno-Marí and R. Jiménez-Peydró. Global change and human vulnerability to vector-borne diseases. *Front Physiol*, 4:158, 2013.

[31] B. Buonomo, G. Carbone, and A. d'Onofrio. Effect of seasonality on the dynamics of an imitation–based vaccination model with public health intervention. *Math. Biosci. Eng.*, 15(1):299–321, 2018.

[32] B. Buonomo, P. Manfredi, and A. d'Onofrio. Optimal time–profiles of public health intervention to shape voluntary vaccination for childhood diseases. *J. Math. Biol.*, Nov 2018.

[33] B. Buonomo, P. Manfredi, and A. d'Onofrio. Optimal time-profiles of public health intervention to shape voluntary vaccination for childhood diseases. *Journal of mathematical biology*, 78(4):1089–1113, 2019.

[34] G. Camera-Roda and G. C. Sarti. Mass transport with relaxation in polymers. *AIChE Journal*, 36(6):851–860, 1990.

[35] V. Capasso and V. Capasso. *Mathematical structures of epidemic systems*, volume 88. Springer, 1993.

[36] V. Capasso, A. Di Liddo, and L. Maddalena. A nonlinear model for the geographical spread of innovations. *Dynamic Systems and Applications*, 3:207–220, 1994.

[37] V. Capasso and S.L. Paveri-Fontana. A mathematical model for the 1973 cholera epidemic in the european mediterranean region. *Revue d'épidémiologie et de Santé Publiqué*, 27(2):121–132, 1979.

[38] V. Capasso and G. Serio. A generalization of the Kermack-McKendrick deterministic epidemic model. *Math. Biosci.*, 42(1-2):43–61, 1978.

[39] V. Capasso and M. Zonno. Mathematical Models for the Diffusion of Innovations. In *Proceedings of the Fourth European Conference on Mathematics in Industry*, pages 225–233. Springer, 1991.

[40] R. Casiday, T. Cresswell, D. Wilson, and C. Panter-Brick. A survey of UK parental attitudes to the MMR vaccine and trust in medical authority. *Vaccine*, 24(2):177–184, 2006.

[41] C. Castillo-Chavez and B. Song. Dynamical models of tuberculosis and their applications. *Mathematical Biosciences and Engineering*, 1(2), 2004.

[42] C. Cattaneo. Sulla conduzione del calore. *Atti Sem. Mat. Fis. Univ. Modena*, 3:83–101, 1948.

[43] P. P. Chapagain, J.S. Van Kessel, J.S. Karns, D.R. Wolfgang, E. Hovingh, K.A. Nelen, Y.H. Schukken, and Y.T. Grohn. A mathematical model of the dynamics of salmonella cerro infection in a us dairy herd. *Epidemiology & Infection*, 136(2):263–272, 2008.

[44] J. Chen, J. Huang, J. C. Beier, R. S. Cantrell, C. Cosner, D. O. Fuller, G. Zhang, and S. Ruan. Modeling and control of local outbreaks of west nile virus in the united states. *Discrete & Continuous Dynamical Systems-B*, 21(8), 2016.

[45] N. Chitnis, J. M. Hyman, and C. A. Manore. Modelling vertical transmission in vector-borne diseases with applications to rift valley fever. *Journal of Biological Dynamics*, 7(1), 2013.

[46] V. Ciancio, A. Lupica, and A. Palumbo. A thermodynamical model for population growth with relaxation phenomena. *Preprint*, 2019.

[47] V. Ciancio and A. Palumbo. A Thermodynamical Theory with Internal Variables Describing Thermal Effects in Viscous Fluids. *Journal of Non-Equilibrium Thermodynamics*, 43(2):171–184, 2018.

[48] V. Ciancio and A. Palumbo. A thermodynamic theory with hidden vectorial variables on possible interactions among heat conduction, diffusion phenomena, viscous flow and chemical reactions in fluid mixtures. *Atti della Accademia Peloritana dei Pericolanti-Classe di Scienze Fisiche, Matematiche e Naturali*, 97(S1):4, 2019.

[49] M. Ciddio. Sviluppo di un modello spazialmente esplicito di diffusione del colera e sua applicazione al caso endemico del Bangladesh. *Thesis*, 2012.

[50] C. T. Codeço. Endemic and epidemic dynamics of cholera: the role of the aquatic reservoir. *BMC Infectious Diseases*, 1(1):1, 2001.

[51] R. R. Colwell. Global climate and infectious disease: the cholera paradigm. *Science*, 274(5295):2025–2031, 1996.

[52] R. R Colwell and A. Huq. Environmental reservoir of vibrio cholerae the causative agent of cholera. *Annals of the New York Academy of Sciences*, 740(1):44–54, 1994.

[53] R. R Colwell, J. Kaper, and S.W. Joseph. Vibrio cholerae, vibrio parahaemolyticus, and other vibrios: occurrence and distribution in chesapeake bay. *Science*, 198(4315):394–396, 1977.

[54] C. Cosner, J. C Beier, R. S. Cantrell, D. Impoinvil, L. Kapitanski, M. D. Potts, A. Troyo, and S. Ruan. The effects of human movement on the persistence of vector-borne diseases. *Journal of Theoretical Biology*, 258(4):550–560, 2009.

[55] A. Cozad and R. D. Jones. Disinfection and the prevention of infectious disease. *American Journal of Infection Control*, 31(4):243–254, 2003.

[56] G. Cruz-Pacheco, L. Esteva, and C. Vargas. Seasonality and outbreaks in west nile virus infection. *Bulletin of Mathematical Biology*, 71(6), 2009.

[57] C. Currò and D. Fusco. Discontinuous travelling wave solutions for a class of dissipative hyperbolic models. *Atti della Accademia Nazionale dei Lincei. Classe di Scienze Fisiche, Matematiche e Naturali. Rendiconti Lincei. Matematica e Applicazioni*, 16(1):61–71, 2005.

[58] D. Danforth, L.E. Nicolle, K. Hume, N. Alfieri, and H. Sims. Nosocomial infections on nursing units with floors cleaned with a disinfectant compared with detergent. *Journal of Hospital Infection*, 10(3):229–235, 1987.

[59] F. Daschner and A. Schuster. Disinfection and the prevention of infectious disease: No adverse effects? *American Journal of Infection Control*, 32(4):224–225, 2004.

[60] DengueVirusNet.com. Life cycle of aedes aegypti, webpage: http://www.denguevirusnet.com/life-cycle-of-aedes-aegypti.html, accessed: August 2019.

[61] O. Diekmann and J. A. P. Heesterbeek. *Mathematical epidemiology of infectious diseases: model building, analysis and interpretation*, volume 5. John Wiley & Sons, 2000.

[62] O. Diekmann, J. A. P. Heesterbeek, and J. A.J. Metz. On the definition and the computation of the basic reproduction ratio r 0 in models for infectious diseases in heterogeneous populations. *Journal of Mathematical Biology*, 28(4):365–382, 1990.

[63] O. Domarle, R. Razakandrainibe, E. Rakotomalala, L. Jolivet, R. V. Randremanana, F. Rakotomanana, C. E. Ramarokoto, J.-L. Soares, and F. Ariey. Seroprevalence of malaria in inhabitants of the urban zone of Antananarivo, Madagascar. *Malaria Journal*, 5(1):106, 2006.

[64] A. d'Onofrio, P. Manfredi, and P. Poletti. The impact of vaccine side effects on the natural history of immunization programmes: an imitation–game approach. *J. Theor. Biol.*, 273(1):63–71, 2011.

[65] A. d'Onofrio, P. Manfredi, and P. Poletti. The interplay of public intervention and private choices in determining the outcome of vaccination programmes. *PLoS ONE*, 7(10):e45653, 2012.

[66] A. d'Onofrio, P. Manfredi, and E. Salinelli. Vaccinating behaviour, information, and the dynamics of SIR vaccine preventable diseases. *Theor. Popul. Biol.*, 71(3):301–317, 2007.

[67] A. d'Onofrio, P. Manfredi, and E. Salinelli. Vaccinating behaviour and the dynamics of vaccine preventable infections. In *Modeling the Interplay Between Human Behavior and the Spread of Infectious Diseases*, pages 267–287. Springer, 2013.

[68] E. Dubé, C. Laberge, M. Guay, P. Bramadat, R. Roy, and J. A. Bettinger. Vaccine hesitancy: an overview. *Human Vaccin. Immunother.*, 9(8):1763–1773, 2013.

[69] A. Ducrot and T. Giletti. Convergence to a pulsating travelling wave for an epidemic reaction-diffusion system with non-diffusive susceptible population. *Journal of Mathematical Biology*, 69(3):533–552, 2014.

[70] S. R. Dunbar and H. G. Othmer. On a nonlinear hyperbolic equation describing transmission lines, cell movement, and branching random walks. In *Nonlinear Oscillations in Biology and Chemistry*, pages 274–289. Springer, 1986.

[71] M. C. Eisenberg, S. L. Robertson, and J. H. Tien. Identifiability and estimation of multiple transmission pathways in cholera and waterborne disease. *Journal of Theoretical Biology*, 324:84–102, 2013.

[72] B. Ermentrout and M. Lewis. Pattern formation in systems with one spatially distributed species. *Bulletin of Mathematical Biology*, 59(3):533–549, 1997.

[73] R. Feachem, D. D. Mara, and D.J. Bradley. *Sanitation and disease*. John Wiley & Sons Washington DC, USA:, 1983.

[74] C. P. Ferreira, P. Pulino, H. Yang, and L. T. Takahashi. Controlling dispersal dynamics of Aedes aegypti. *Mathematical Population Studies*, 13(4):215–236, 2006.

[75] R. A. Fisher. The wave of advance of advantageous genes. *Annals of Eugenics*, 7(4):355–369, 1937.

[76] W. E. Fitzgibbon, J. J. Morgan, G. F Webb, and Y. Wu. A vector–host epidemic model with spatial structure and age of infection. *Nonlinear Analysis: Real World Applications*, 41:692–705, 2018.

[77] J. Fort and V. Méndez. Wavefronts in time-delayed reaction-diffusion systems. Theory and comparison to experiment. *Reports on Progress in Physics*, 65(6):895, 2002.

[78] E. Frey. Evolutionary game theory: Theoretical concepts and applications to microbial communities. *Physica A: Statistical Mechanics and its Applications*, 389(20):4265–4298, 2010.

[79] I. C.H. Fung, D. L. Fitter, R. H. Borse, M. I. Meltzer, and J. W. Tappero. Modeling the effect of water, sanitation, and hygiene and oral cholera vaccine implementation in haiti. *The American Journal of Tropical Medicine and Hygiene*, 89(4):633–640, 2013.

[80] S. Funk, E. Gilad, C. Watkins, and V. A.A. Jansen. The spread of awareness and its impact on epidemic outbreaks. *Proceedings of the National Academy of Sciences*, 106(16):6872–6877, 2009.

[81] N. H. Gaffga, R. V. Tauxe, and E. D. Mintz. Cholera: a new homeland in africa? *The American Journal of Tropical Medicine and Hygiene*, 77(4):705–713, 2007.

[82] K.T. Goh, S.H. Teo, S. Lam, and M.K. Ling. Person-to-person transmission of cholera in a psychiatric hospital. *Journal of Infection*, 20(3):193–200, 1990.

[83] M. C. Gonzalez, C. A. Hidalgo, and A.-L. Barabasi. Understanding individual human mobility patterns. *Nature*, 453(7196):779, 2008.

[84] D. M. Hartley, J. G. Morris Jr., and D. L. Smith. Hyperinfectivity: a critical element in the ability of V. cholerae to cause epidemics? *PLoS Medicine*, 3(1):e7, 2005.

[85] J.A.P. Heesterbeek and M.G. Roberts. The type-reproduction number t in models for infectious disease control. *Mathematical Biosciences*, 206(1):3–10, 2007.

[86] H. W. Hethcote. The mathematics of infectious diseases. *SIAM Review*, 42(4):599–653, 2000.

[87] L. K. Jackson and K. W. Schrader. Comparison theorems for nonlinear differential equations. *Journal of Differential Equations*, 3(2):248–255, 1967.

[88] V. A.A. Jansen, N. Stollenwerk, H. J. Jensen, M.E. Ramsay, W.J. Edmunds, and C.J. Rhodes. Measles outbreaks in a population with declining vaccine uptake. *Science*, 301(5634):804–804, 2003.

[89] M. A. Jensen, S. M. Faruque, J. J. Mekalanos, and B. R. Levin. Modeling the role of bacteriophage in the control of cholera outbreaks. *Proceedings of the National Academy of Sciences*, 103(12):4652–4657, 2006.

[90] E. Jury and M. Mansour. Positivity and nonnegativity conditions of a quartic equation and related problems. *IEEE Transactions on Automatic Control*, 26(2):444–451, 1981.

[91] W. Just, J. Saldaña, and Y. Xin. Oscillations in epidemic models with spread of awareness. *Journal of Mathematical Biology*, 76(4):1027–1057, 2018.

[92] M. J. Keeling and P. Rohani. *Modeling infectious diseases in humans and animals*. Princeton University Press, 2011.

[93] M. Kitaoka, S. T. Miyata, D. Unterweger, and S. Pukatzki. Antibiotic resistance mechanisms of Vibrio cholerae. *Journal of Medical Microbiology*, 60(4):397–407, 2011.

[94] A. N. Kolmogorov, I. N. Petrovsky, and N. S. Piskunov. Étude de l'équation de la diffusion avec croissance de la quantité de matière et son application à un problème biologique. *Bull. Univ. Moskow, Ser. Internat., Sec. A*, 1:1–25, 1937.

[95] B.V.S. Krishna, A.B. Patil, and M.R. Chandrasekhar. Fluoroquinolone-resistant vibrio cholerae isolated during a cholera outbreak in india. *Transactions of the Royal Society of Tropical Medicine and Hygiene*, 100(3):224–226, 2006.

[96] J. P. LaSalle. *The stability of dynamical systems*, volume 25. Siam, 1976.

[97] G. Lebon, D. Jou, and J. Casas-Vázquez. *Understanding non-equilibrium thermodynamics*, volume 295. Springer, 2008.

[98] S. A. Levin. Descartes' rule of signs - how hard can it be? 2002.

[99] E. K. Lipp, A. Huq, and R. R. Colwell. Effects of global climate on infectious disease: the cholera model. *Clinical Microbiology Reviews*, 15(4):757–770, 2002.

[100] J. Liu-Helmersson, Å. Brännström, M. O. Sewe, J. C. Semenza, and J. Rocklöv. Estimating Past, Present, and Future Trends in the Global Distribution and Abundance of the Arbovirus Vector Aedes aegypti Under Climate Change Scenarios. *Frontiers in Public Health*, 7, 2019.

[101] R. Löfstedt. *Risk management in post-trust societies*. Palgrave–McMillan, 2005.

[102] P. Magal, G. F. Webb, and Y. Wu. Spatial spread of epidemic diseases in geographical settings: seasonal influenza epidemics in Puerto Rico. *arXiv preprint arXiv:1801.01856*, 2018.

[103] P. Magal, G. F. Webb, and Y. Wu. On the basic reproduction number of reaction-diffusion epidemic models. *SIAM Journal on Applied Mathematics*, 79(1):284–304, 2019.

[104] V. Mahajan and R. A. Peterson. *Models for innovation diffusion*. Sage, 1985.

[105] N. A. Maidana and H. M. Yang. Describing the geographic spread of dengue disease by traveling waves. *Mathematical Biosciences*, 215(1), 2008.

[106] N. A. Maidana and H. M. Yang. Dynamic of west nile virus transmission considering several coexisting avian populations. *Mathematical and Computer Modelling*, 53(5-6), 2011.

[107] N. A. Maidana and M. Yang, H. Assessing the spatial propagation of west nile virus. *Biophysical Reviews and Letters*, 3(01n02), 2008.

[108] D. G. Maki, C. J. Alvarado, C. A. Hassemer, and M. A. Zilz. Relation of the inanimate hospital environment to endemic nosocomial infection. *New England Journal of Medicine*, 307(25):1562–1566, 1982.

[109] H. Malchow, S. V Petrovskii, and E. Venturino. *Spatiotemporal patterns in ecology and epidemiology: theory, models, and simulation*. Chapman and Hall/CRC, 2007.

[110] P. Manfredi and A. d'Onofrio. *Modeling the Interplay Between Human Behavior and the Spread of Infectious Diseases*. Springer, New York, 2013.

[111] L. Mari, E. Bertuzzo, L. Righetto, R. Casagrandi, M. Gatto, I. Rodriguez-Iturbe, and A. Rinaldo. Modelling cholera epidemics: the role of waterways, human mobility and sanitation. *Journal of the Royal Society Interface*, 9(67):376–388, 2011.

[112] V. Méndez and J. Camacho. Dynamics and thermodynamics of delayed population growth. *Physical Review E*, 55(6):6476, 1997.

[113] V. Méndez and J. E. Llebot. Hyperbolic reaction-diffusion equations for a forest fire model. *Physical Review E*, 56(6):6557, 1997.

[114] J. P. Messina, O. J. Brady, N. Golding, M. U.G. Kraemer, G.R. W. Wint, S. E. Ray, D.M. Pigott, F. M. Shearer, K. Johnson, L. Earl, et al. The current and future global distribution and population at risk of dengue. *Nature Microbiology*, page 1, 2019.

[115] C. Metcalf, E. Jessica, W.J. Edmunds, and J. Lessler. Six challenges in modelling for public health policy. *Epidemics*, 10(2):93—96, 2015.

[116] M. Mincheva and M. R. Roussel. Turing-hopf instability in biochemical reaction networks arising from pairs of subnetworks. *Mathematical Biosciences*, 240(1):1–11, 2012.

[117] D. Moulay, M.A. Aziz-Alaoui, and M. Cadivel. The chikungunya disease: modeling, vector and transmission global dynamics. *Mathematical Biosciences*, 229(1):50–63, 2011.

[118] Z. Mukandavire, S. Liao, J. Wang, H. Gaff, D. L. Smith, and J. G. Morris. Estimating the reproductive numbers for the 2008–2009 cholera outbreaks in zimbabwe. *Proceedings of the National Academy of Sciences*, 108(21):8767–8772, 2011.

[119] R. Mukherjee, D. Halder, S. Saha, R. Shyamali, C. Subhranshu, R. Ramakrishnan, M. V. Murhekar, and Y. J. Hutin. Five pond-centred outbreaks of cholera in villages of west bengal, india: evidence for focused interventions. *Journal of Health, Population, and Nutrition*, 29(5):421, 2011.

[120] I. Müller and T. Ruggeri. *Rational extended thermodynamics*, volume 37. Springer Science & Business Media, 2013.

[121] L. Multerer, T. Smith, and N. Chitnis. Modeling the impact of sterile males on an Aedes aegypti population with optimal control. *Mathematical Biosciences*, 311:91–102, 2019.

[122] J. D. Murray. *Mathematical biology. II Spatial models and biomedical applications*. Springer-Verlag New York Incorporated New York, 2001.

[123] J. D. Murray. *Mathematical biology I: an introduction*. Springer New York, 2002.

[124] R. S Nasci, R. A. Wirtz, and W. G. Brogdon. Protection against mosquitoes, ticks, and other arthropods. *CDC Health Information for International Travel*, pages 94–9, 2016.

[125] J. V. Noble. Geographic and temporal development of plagues. *Nature*, 250(5469):726, 1974.

[126] S. B. Omer, D. A Salmon, W. A. Orenstein, M. P. Dehart, and N. Halsey. Vaccine refusal, mandatory immunization, and the risks of vaccine-preventable diseases. *N. Engl. J. Med.*, 360(19):1981–1988, 2009.

[127] L. Osorio, J. Todd, and D. J. Bradley. Travel histories as risk factors in the analysis of urban malaria in Colombia. *The American Journal of Tropical Medicine and Hygiene*, 71(4):380–86, 2004.

[128] M. Pascual, M. J. Bouma, and A. P. Dobson. Cholera and climate: revisiting the quantitative evidence. *Microbes and Infection*, 4(2):237–245, 2002.

[129] R. Peres, E. Muller, and V. Mahajan. Innovation diffusion and new product growth models: A critical review and research directions. *International Journal of Research in Marketing*, 27(2):91–106, 2010.

[130] A. D Polyanin and V. F. Zaitsev. *Handbook of ordinary differential equations: exact solutions, methods, and problems*. Chapman and Hall/CRC, 2017.

[131] Z. Rahman, M. Rahman, M. Rashid, S. Monira, F.T. Johura, M. Mustafiz, S. I. Bhuyian, F. Zohura, T. Parvin, K. Hasan, et al. Vibrio cholerae transmits through water among the household contacts of cholera patients in cholera endemic coastal villages of bangladesh, 2015-2016 (chobi7 trial). *Frontiers in Public Health*, 6:238, 2018.

[132] L. Righetto, R. Casagrandi, E. Bertuzzo, L. Mari, M. Gatto, I. Rodriguez-Iturbe, and A. Rinaldo. The role of aquatic reservoir fluctuations in long-term cholera patterns. *Epidemics*, 4(1):33–42, 2012.

[133] M.G. Roberts and J.A.P. Heesterbeek. A new method for estimating the effort required to control an infectious disease. *Proceedings of the Royal Society of London. Series B: Biological Sciences*, 270(1522):1359–1364, 2003.

[134] S. D. Rodriguez, L. L. Drake, D. P. Price, J. I. Hammond, and I. A. Hansen. The efficacy of some commercially available insect repellents for Aedes aegypti (Diptera: Culicidae) and Aedes albopictus (Diptera: Culicidae). *Journal of Insect Science*, 15(1), 2015.

[135] L. A Ronald, S. L. Kenny, E. Klinkenberg, A. O. Akoto, I. Boakye, G. Barnish, and M. J. Donnelly. Malaria and anaemia among children in two communities of Kumasi, Ghana: a cross-sectional survey. *Malaria Journal*, 5(1):105, 2006.

[136] D. A. Sack, R.B. Sack, B. Nair, and A.K. Siddique. Cholera. *The Lancet*, 363, 2004.

[137] D.A. Sack, R.B. Sack, and L.C. Chaignat. Getting serious about cholera. *The New England Journal of Medicine*, 355(7):649, 2006.

[138] M. A. Safi, D. Y. Melesse, and A. B. Gumel. Dynamics analysis of a multi-strain cholera model with an imperfect vaccine. *Bulletin of Mathematical Biology*, 75(7):1104–1137, 2013.

[139] R. P. Sanches, C. P. Ferreira, and R. A. Kraenkel. The role of immunity and seasonality in cholera epidemics. *Bulletin of Mathematical Biology*, 73(12):2916–2931, 2011.

[140] E. Scott and S. F. Bloomfield. The survival and transfer of microbial contamination via cloths, hands and utensils. *Journal of Applied Bacteriology*, 68(3):271–278, 1990.

[141] Z. Shuai, J.A.P. Heesterbeek, and P. van Den Driessche. Extending the type reproduction number to infectious disease control targeting contacts between types. *Journal of Mathematical Biology*, 67(5):1067–1082, 2013.

[142] Z. Shuai, J.A.P. Heesterbeek, and P. van den Driessche. Erratum to: Extending the type reproduction number to infectious disease control targeting contacts between types. *Journal of Mathematical Biology*, 71(1):255–257, 2015.

[143] A.K. Siddique, K. Zaman, A.H. Baqui, K. Akram, P. Mutsuddy, A. Eusof, K. Haider, S. Islam, and R.B. Sack. Cholera epidemics in bangladesh: 1985-1991. *Journal of Diarrhoeal Diseases Research*, pages 79–86, 1992.

[144] U. Skwara, J. Martins, P. Ghaffari, M. Aguiar, J. Boto, and N. Stollenwerk. Applications of fractional calculus to epidemiological models. In *AIP Conference Proceedings*, volume 1479, pages 1339–1342. AIP, 2012.

[145] U. Skwara, J. Martins, P. Ghaffari, M. Aguiar, J. Boto, and N. Stollenwerk. Fractional calculus and superdiffusion in epidemiology: shift of critical thresholds. In *Proceedings of the 12th International Conference on Computational and Mathematical Methods in Science and Engineering, La Manga*, 2012.

[146] U. Skwara, L. Mateus, R. Filipe, F. Rocha, M. Aguiar, and N. Stollenwerk. Superdiffusion and epidemiological spreading. *Ecological complexity*, 36:168–183, 2018.

[147] W.M. Spira, M. U. Khan, Y.A. Saeed, and M.A. Sattar. Microbiological surveillance of intra-neighbourhood el tor cholera transmission in rural bangaldesh. *Bulletin of the World Health Organization*, 58(5):731, 1980.

[148] B. Straughan. *Heat waves*, volume 177. Springer Science & Business Media, 2011.

[149] B. Straughan. Gene–culture shock waves. *Physics Letters A*, 377(38):2531–2534, 2013.

[150] L. T. Takahashi et al. Modelos matemáticos de epidemiologia com vetores: simulaçao da propagaçao urbana e geográfica da dengue. *Repositório da Produção Científica e Intelectual da Unicamp*, 2004.

[151] L. T. Takahashi, N. A. Maidana, W. C. Ferreira, P. Pulino, and H. M. Y. Mathematical models for the aedes aegypti dispersal dynamics: travelling waves by wing and wind. *Bulletin of Mathematical Biology*, 67(3):509–528, 2005.

[152] A.J. Tatem, Z. Huang, A. Das, Q. Qi, J. Roth, and Y. Qiu. Air travel and vector-borne disease movement. *Parasitology*, 139(14):1816–1830, 2012.

[153] C. F. Teixeira, L. G. d. S. Augusto, and T. C. Morata. Hearing health of workers exposed to noise and insecticides. *Revista de Saude Publica*, 37(4):417–423, 2003.

[154] THEENDFUND. Schistosomiasis. webpage: https://end.org/ntds-in-focus/schistosomiasis/ (accessed july 2018).

[155] J. H. Tien and D. J.D. Earn. Multiple transmission pathways and disease dynamics in a waterborne pathogen model. *Bulletin of Mathematical Biology*, 72(6):1506–1533, 2010.

[156] The New York Times. Poor sanitation persisted at u.n. missions long after haiti cholera crisis. webpage: https://www.nytimes.com/2016/08/20/world/americas/haiti-cholera-sanitation-un-peacekeepers.html (accessed may 2019).

[157] A. R. Tuite, J. Tien, M. Eisenberg, D. J.D. Earn, J. Ma, and D. N. Fisman. Cholera epidemic in Haiti, 2010: using a transmission model to explain spatial spread of disease and identify optimal control interventions. *Annals of Internal Medicine*, 154(9):593–601, 2011.

[158] A. M. Turing. The chemical basis of morphogenesis. *Phil. Trans. R. Soc. Lond. B*, 237(641):37–72, 1952.

[159] H.W. Turnbull. *THEORY OF EQUATIONS*. OLIVER AND BOYD, 1947.

[160] S. Vakulenko and V. Volpert. Generalized travelling waves for perturbed monotone reaction-diffusion systems. *Nonlinear Analysis TMA*, 6(46):757–776, 2001.

[161] P. Van den Driessche and J. Watmough. Reproduction numbers and sub-threshold endemic equilibria for compartmental models of disease transmission. *Mathematical Biosciences*, 180(1-2), 2002.

[162] A. I. Volpert, V. A. Volpert, and V. A. Volpert. *Traveling wave solutions of parabolic systems*, volume 140. American Mathematical Soc., 1994.

[163] V. Volpert. *Elliptic Partial Differential Equations: Volume 2: Reaction-Diffusion Equations*, volume 104. Springer, 2014.

[164] W. Wang and X.Q. Zhao. Basic reproduction numbers for reaction-diffusion epidemic models. *SIAM Journal on Applied Dynamical Systems*, 11(4):1652–1673, 2012.

[165] X. Wang, D. Posny, and J. Wang. A reaction-convection-diffusion model for cholera spatial dynamics. *Discrete Contin. Dyn. Syst. Ser. B*, 21:2785–2809, 2016.

[166] X. Wang and J. Wang. Analysis of cholera epidemics with bacterial growth and spatial movement. *Journal of Biological Dynamics*, 9(sup1):233–261, 2015.

[167] Z. Wang, C. T. Bauch, S. Bhattacharyya, A. d'Onofrio, P. Manfredi, M. Perc, N. Perra, M. Salathé, and D. Zhao. Statistical physics of vaccination. *Phys. Rep.*, 664:1–113, 2016.

[168] R. A Weinstein and B. Hota. Contamination, disinfection, and cross-colonization: are hospital surfaces reservoirs for nosocomial infection? *Clinical Infectious Diseases*, 39(8):1182–1189, 2004.

[169] Wikipedia. Aedes aegypti. accessed: August 2019. webpaege https://en.wikipedia.org/wiki/aedes-aegypti.

[170] Wikipedia. Cholera. accessed: May 2019. webpaege https://en.wikipedia.org/wiki/cholera.

[171] M. J Wonham, T. de Camino-Beck, and M. A. Lewis. An epidemiological model for west nile virus: invasion analysis and control applications. 271(1538).

[172] Health Organization World. African health ministers commit to ending cholera outbreaks by 2030. website: https://www.afro.who.int/news/african-health-ministers-commit-ending-cholera-outbreaks-2030. accessed: March 2019.

[173] Health Organization World. Cholera: Key facts, 2019. webpage: https://www.who.int/news-room/fact-sheets/detail/cholera (accessed march 2019).

[174] Health Organization World. Global task force on cholera control webpage: https://www.who.int/cholera/publications/global-roadmap.pdf (accessed june 2019).

[175] Health Organization World. Largest cholera vaccine drive in history to target spike in outbreaks. 2018. website: https://www.who.int/news-room/detail/07-05-2018-largest-cholera-vaccine-drive-in-history-to-target-spike-in-outbreaks. accessed: March 2019.

[176] Health Organization World. Mosquito-borne diseases, webpage: https://www.who.int/neglected-diseases/vector-ecology/mosquito-borne-diseases/en/ , accessed: August 2019.

[177] Health Organization World. The treatment of diarrhoea, a manual for physicians and other senior health workers webpage: https://www.who.int/news-room/fact-sheets/detail/cholera (archived 2011-10-19 at the wayback machine), 2005, chapter 5: "management of suspected cholera".

[178] Health Organization World. Vector-borne diseases, webpage: https://www.who.int/news-room/fact-sheets/detail/vector-borne-diseases , accessed: August 2019.

[179] L. Yakob, L. Alphey, and M. B. Bonsall. Aedes aegypti control: the concomitant role of competition, space and transgenic technologies. *Journal of Applied Ecology*, 45(4):1258–1265, 2008.

[180] H.M. Yang, C.P. Ferreira, and S. Ternes. Dinâmica populacional do vetor transmissor da dengue. *Trends in Applied and Computational Mathematics*, 4(2):287–296, 2003.

[181] M. Zhang and Z. Lin. The diffusive model for Aedes aegypti mosquito on a periodically evolving domain. *Discrete & Continuous Dynamical Systems-B*, pages 1–20, 2019.

[182] L. Zhao, Z.-C. Wang, and S. Ruan. Traveling wave solutions in a two-group sir epidemic model with constant recruitment. *Journal of Mathematical Biology*, 77(6-7):1871–1915, 2018.

[183] X. Zhou, K. K Tamma, and C. V.D.R. Anderson. On a new c-and f-processes heat conduction constitutive model and the associated generalized theory of dynamic thermoelasticity. *Journal of Thermal Stresses*, 24(6):531–564, 2001.

[184] J. N. Zuckerman, L. Rombo, and A. Fisch. The true burden and risk of cholera: implications for prevention and control. *The Lancet Infectious Diseases*, 7(8):521–530, 2007.